

Beta human papillomavirus 8 E6 deregulates double strand break repair

by

Changkun Hu

B.S., Dalian Medical University, 2015

M.S., Emporia State University, 2017

AN ABSTRACT OF A DISSERTATION

submitted in partial fulfillment of the requirements for the degree

DOCTOR OF PHILOSOPHY

Division of Biology
College of Arts and Sciences

KANSAS STATE UNIVERSITY
Manhattan, Kansas

2022

Abstract

Beta human papillomaviruses are hypothesized to promote nonmelanoma skin cancer by deregulating DNA repair pathways. Most of the molecular evidence that β -HPV impairs DNA repair has been gained via characterization of the E6 protein from β -HPV 8 (8E6). By reducing p300 availability, 8E6 attenuates a major double-strand DNA break (DSB) repair pathway, homologous recombination. We show that 8E6 impairs another DSB repair pathway, non-homologous end joining (NHEJ). HR and NHEJ are not thought to occur in the same cell at the same time. HR is restricted to cells in phases of the cell cycle where homologous templates are available, while NHEJ occurs primarily during G1. We found that 8E6 causes colocalization of HR factors (RPA70 and RAD51) with an NHEJ factor (activated DNA-PKcs or pDNA-PKcs) at persistent DSBs. 8E6 also causes RAD51 foci to form during G1. Further, we used next-generation sequencing of the 200kb surrounding a CAS9-induced DSB to show that 8E6 caused a 21-fold increase in deletions. Chemical and genetic inhibition of p300 as well as an 8E6 mutant that is incapable of destabilizing p300 demonstrated that 8E6 is acting via p300 destabilization. More specific chemical inhibitors of DNA repair provided mechanistic insight by mimicking 8E6-induced dysregulation of DNA repair in a virus-free system. Specifically, inhibition of NHEJ causes RAD51 foci to form in G1 and colocalization of RAD51 with pDNA-PKcs. Finally, we show that 8E6 promotes a backup DSB repair pathway, alternative end-joining (Alt-EJ). Using CAS9 and transfection-based reporters, we found that 8E6 promotes both DNA resection-dependent and independent Alt-EJ. Together, these studies expand the knowledge that β -HPV deregulate DNA repair pathways and increases genomic instability. Moreover, we provide novel methods and tools for fundamental research in DNA repair fields.

Beta human papillomavirus 8 E6 deregulates double strand break repair

by

Changkun Hu

B.S., Dalian Medical University, 2015

M.S., Emporia State University, 2017

A DISSERTATION

submitted in partial fulfillment of the requirements for the degree

DOCTOR OF PHILOSOPHY

Division of Biology
College of Arts and Sciences

KANSAS STATE UNIVERSITY
Manhattan, Kansas

2022

Approved by:

Major Professor
Dr. Nicholas Wallace

Copyright

© Changkun Hu 2022.

Abstract

Beta human papillomaviruses are hypothesized to promote nonmelanoma skin cancer by deregulating DNA repair pathways. Most of the molecular evidence that β -HPV impairs DNA repair has been gained via characterization of the E6 protein from β -HPV 8 (8E6). By reducing p300 availability, 8E6 attenuates a major double-strand DNA break (DSB) repair pathway, homologous recombination. We show that 8E6 impairs another DSB repair pathway, non-homologous end joining (NHEJ). HR and NHEJ are not thought to occur in the same cell at the same time. HR is restricted to cells in phases of the cell cycle where homologous templates are available, while NHEJ occurs primarily during G1. We found that 8E6 causes colocalization of HR factors (RPA70 and RAD51) with an NHEJ factor (activated DNA-PKcs or pDNA-PKcs) at persistent DSBs. 8E6 also causes RAD51 foci to form during G1. Further, we used next-generation sequencing of the 200kb surrounding a CAS9-induced DSB to show that 8E6 caused a 21-fold increase in deletions. Chemical and genetic inhibition of p300 as well as an 8E6 mutant that is incapable of destabilizing p300 demonstrated that 8E6 is acting via p300 destabilization. More specific chemical inhibitors of DNA repair provided mechanistic insight by mimicking 8E6-induced dysregulation of DNA repair in a virus-free system. Specifically, inhibition of NHEJ causes RAD51 foci to form in G1 and colocalization of RAD51 with pDNA-PKcs. Finally, we show that 8E6 promotes a backup DSB repair pathway, alternative end-joining (Alt-EJ). Using CAS9 and transfection-based reporters, we found that 8E6 promotes both DNA resection-dependent and independent Alt-EJ. Together, these studies expand the knowledge that β -HPV deregulate DNA repair pathways and increases genomic instability. Moreover, we provide novel methods and tools for fundamental research in DNA repair fields.

Table of Contents

List of Figures	x
List of Tables	xii
Acknowledgements	xiii
Glossary	xiv
Introduction	xv
Chapter 1 - Beta HPV Deregulates Double-Strand Break Repair	1
Abstract	1
1. Introduction	2
2. Beta HPV and Genomic Instability	3
3. Approaches to Study DSB Repair	9
4. Summary and Discussions	18
References	18
Chapter 2 - Beta Human Papillomavirus 8E6 Attenuates Non-Homologous End Joining by Hindering DNA-PKcs Activity	29
Abstract	29
1. Introduction	30
2. Results	32
2.1. β -HPV 8E6 decreases NHEJ efficiency.	32
2.2. β -HPV 8E6 attenuates DNA-PKcs phosphorylation.	34
2.3. β -HPV 8E6 attenuates DNA-PKcs-dependent signaling.	36
2.4. p300 is required for robust DNA-PKcs signaling.	38
3. Discussion	39
4. Materials and Methods	41
4.1. Cell Culture and Reagents	41
4.2. Immunoblotting	42
4.3. Immunofluorescence Microscopy	42
4.4. End joining Reporter Assay	43
4.5. Statistical Analysis	43
5. Conclusions	43

References.....	44
Chapter 2 supplemental figures	62
Chapter 3 - Using Next Generation Sequencing to Identify Mutations Associated with Repair of a CAS9-induced Double Strand Break Near the CD4 Promoter	70
ABSTRACT.....	71
INTRODUCTION	72
PROTOCOL	74
1. Cell plating.....	74
2. Transfection	75
4. Nucleic acid extraction and amplicon generation	77
5. PCR clean-up	78
6. Library preparation	81
7. Data analysis	82
REPRESENTATIVE RESULTS.....	83
DISCUSSION.....	84
ACKNOWLEDGMENTS	86
REFERENCES	86
Chapter 4 - Beta human papillomavirus 8E6 allows colocalization of non-homologous end joining and homologous recombination repair factors	96
Abstract.....	96
Introduction.....	98
Results.....	100
8E6 promotes the recruitment of HR factors to sites of stalled NHEJ.	100
p300 catalytic activity prevents colocalization of HR factors with persistent pDNA-PKcs repair complexes.	103
8E6 allows RAD51 foci formation in G1 by binding to p300.....	104
NHEJ inhibition leads to HR initiation in G1 and colocalization of RAD51 and pDNA- PKcs.	105
8E6 increases genomic instability during DSB repair.	106
Discussion.....	106
Materials and Methods.....	110

Cell Culture and Reagents.....	110
Immunofluorescence Microscopy	110
Flow Cytometry	111
Immunoblotting.....	112
SgRNA/CAS9 Transfection.....	112
Next-generation sequencing.....	113
Sequencing Analyses	113
Statistical Analysis	114
References.....	115
Chapter 4 supplemental figures	133
Chapter 5 - Beta Human papillomavirus 8 E6 promotes alternative end-joining.....	144
Abstract.....	145
1. Introduction.....	145
2. Material and methods.....	147
2.1 Cell culture and Reagents	147
2.2 Immunofluorescence Microscopy.....	148
2.3 Flow Cytometry	149
2.4 Immunoblotting.....	149
2.5 Transfection and Alt-EJ assay.....	150
2.6 Statistical Analysis.....	150
3. Results.....	150
3.1 8E6 promotes DSB repair by Alt-EJ.....	150
3.2 DNA-PK inhibition forces 8E6 expressing cells to use Alt-EJ more frequently.....	151
3.3. DNA-PKcs inhibition prevents 8E6 from causing RAD51 foci to form during G1....	153
3.4 DNA-PKcs inhibition does not promote HR in cells with 8E6	153
3.5 8E6 promotes Alt-EJ by destabilizing p300	154
3.6 DNA-PKcs inhibition prevents the formation of RAD51 foci in G1 that is caused by loss of p300.	155
4. Discussion.....	155
References.....	157
Chapter 6-Conclusion and future directions	181

Conclusion	181
Future directions	183
References.....	185

List of Figures

Figure 2-1. β -HPV 8E6 decreases NHEJ efficiency using CD4 expression as a readout.	51
Figure 2-2. β -HPV 8E6 attenuates DNA-PKcs phosphorylation.....	53
Figure 2-3. β -HPV 8E6 increases pDNA-PKcs foci size but decreases frequency in untreated cells.	54
Figure 2-4. β -HPV 8E6 increases pDNA-PKcs foci persistence.....	55
Figure 2-5. β -HPV 8E6 decreases pDNA-PKcs target proteins pArtemis abundance and XRCC4 foci formation.....	57
Figure 2-6. HCT116 P300 knockout decreases NHEJ efficiency.....	59
Figure 2-7. NHEJ in Cells with and without β-HPV 8E6.	61
Figure 3-1. Representative image of immunoblot comparing CAS9 expression in untransfected and transfected HFK cells.	89
Figure 3-2. Representative immunofluorescence image of phosphorylated histone H2AX (S139) in sgRNA/CAS9 transfected cell and untransfected control.....	90
Figure 3-3. β -HPV8E6 increases genomic instability during DSB repair.	91
Figure 4-1. 8E6 allows RAD51:pDNA-PKcs colocalization.	117
Figure 4-2. By binding p300, 8E6 allows RAD51 and RPA70 foci to colocalize with persistent pDNA-PKcs foci.	120
Figure 4-3. p300 reduces co-localization of RAD51 and RPA70 foci with pDNA-PKcs foci. .	121
Figure 4-4. 8E6 allows RAD51 foci formation in G1.	123
Figure 4-5. p300 restricts RAD51 foci formation in G1.....	125
Figure 4-6. DNA-PKcs inhibition increases RAD51 foci in G1.	127
Figure 4-7. β -HPV8E6 increases genomic instability during DSB repair.....	129
Figure 4-8. Summary figure of DSB repair in G1 phase.	131
Figure 5-1. 8E6 promotes Alt-EJ frequency.	160
Figure 5-2. Olaparib abrogates Alt-EJ frequency and increases persistent pH2AX.....	162
Figure 5-3. NU7441 promotes Alt-EJ.....	164
Figure 5-4. Nu7441 increases DSB repair in cells with 8E6.	166
Figure 5-5. NU7441 abrogates RAD51 in G1 induced by 8E6.	167

Figure 5-6. NU7441 does not increase HR in cells with 8E6. 169
Figure 5-7. Losing p300 activity promotes Alt-EJ frequency. 171
Figure 5-8. NU7441 abrogates RAD51 in G1 induced by losing p300 activity..... 172

List of Tables

Table 1-1. Reporters to measure specific DSB repair pathway. Reporter column lists common names for different DSB repair reporters. DSB induction column lists enzymes used to induce DSBs for each reporter. Pathway and Readout column lists the DSB repair pathway(s) measured by each reporter and the signal activated the pathway(s). Reference column lists the original publications where the reporters are described.	28
Table 3-1. PCR Master mix components.	93
Table 3-2. PCR Program settings.	93
Table 3-3. Trouble shooting.	94

Acknowledgements

I would like to express my sincere gratitude to my advisor, Dr. Nicholas Wallace, for his continuous support, patience, encouragement, and friendship throughout my graduate study. I could not have imagined having a better advisor and mentor for my future study.

My thanks also go to the members of my committee, Dr. Rolie Clem, Dr. Zhilong Yang, Dr. Anna Zolkiewska, and Dr. Sherry Fleming for their kindness to serve on this committee and for their constructive comments on my project and my career development.

I would like to thank my lab mates and friends for their assistance in the lab and their understanding throughout my graduate study. I owe special thanks to Dalton Dacus, Sebastian Wendel, and Taylor Bugbee who not only help with my research but also makes me a better scientist.

I want my parents and my grandparents to receive my deepest gratitude for their education, dedication, encouragement, and endless love. Thanks to my sister for taking on the responsibility of taking care of the family after middle school. Without my wonderful sister, studying abroad is impossible for me.

Finally, thanks to my wife Shuangshuang Liang for her love and company since we were teenagers. Shuangshuang, thank you for being my best friend. I own you with everything. I love you!

Glossary

8E6: Human papillomavirus type 8 protein E6

Alt-EJ: A backup DNA double strand break repair pathway.

Artemis: A non-homologous end joining nuclease that is required for DNA end processing

CCS1477: a p300 inhibitor

Colocalization: two or more DNA repair complex locate at the same position detected by microscopy

DNA-PKcs: a major non-homologous end joining kinase that active multiple DNA repair proteins

HR: a major double strand break repair pathway that occurs in S/G2 phase

Ku80: a non-homologous end joining upstream protein

Ligase IV: a downstream non-homologous protein

NHEJ: a major double strand break repair protein that occurs mainly in G1 phase

NU7441: a DNA-PK inhibitor used to inhibit NHEJ

Olaparib: a PAPR1 inhibitor used to inhibit Alt-EJ

P300: an acetyltransferase that regulates transcription by chromosome remodeling

PARP1: a major protein that is involved in Alt-EJ

pDNA-PKcs: phosphorylated DNA-PKcs, an active form of DNA-PKcs

pH2AX: a standard double strand break marker

RAD51: a major downstream protein in HR that facilitate homologous searching

RPA70: a major protein in HR that protect single stranded DNA from degradation

SCR7: a ligase IV inhibitor that inhibit downstream step of NHEJ

XRCC4: a protein form downstream NHEJ.

Introduction

Skin cancer is more common than all other cancers combined [1,2]. Nonmelanoma skin cancer (NMSC) contributes to the majority of skin malignancy [2–4]. Over 5 million NMSCs are diagnosed in the US each year, which cost more than \$4.5 billion for treatment [5]. Discovering potential factors that promote the formation of this disease will contribute to the development of therapies to mitigate the physical and economic burden of patients. Beta human papillomavirus (β -HPV) infections are common, occurring in up to 90% of adults [4,6,7]. Certain β -HPVs are known to promote cutaneous squamous cell carcinoma (cSCC) in organ transplant recipients (OTR) and in people with a genetic disorder called epidermodysplasia verruciformis (EV) [3,6,8–10,10].

The oncogenic risk associated with β -HPV in the general population is unclear. Some have proposed that β -HPV promotes tumorigenesis, while others suggest that β -HPV protects against skin cancer [3,4,11,12]. In the immunocompetent population, β -HPVs cause transient infection in cutaneous epithelia. β -HPVs have been hypothesized to increase the risk of skin cancer by increasing genomic instability [13–17]. Particularly, it is hypothesized that β -HPVs disrupt DNA repair pathways, making UV-induced DNA damage more mutagenic [18,19].

Most evidence supporting this hypothesis is based on the study of β -HPV type 8 protein E6 (8E6). Previous studies showed that by degrading an important transcription regulator p300, 8E6 makes UV-induced damage more persistent [20,21]. Persistent UV-damage leads to DNA replication fork collapse and double strand breaks (DSBs) [22–24]. Two major DSB repair pathways are nonhomologous end joining (NHEJ) and homologous recombination (HR) [25–28].

It was known that 8E6 disrupts HR pathway by decreasing major HR proteins [29]. Mechanistic details show that this disruption depends on p300 degradation [21,29]. This

dissertation shows to what extent that β -HPV disrupts two major DSB repair pathways (NHEJ and HR), causing cells to use more mutagenic mechanisms of repair. Chapter 1 reviews β -HPV biology and DSB repair. Growing approaches and models that can be adapted to study the effect of β -HPV on DSB repair are summarized. Chapter 2 describes the effect of 8E6 on NHEJ. 8E6 attenuates NHEJ by decreasing the activity of a key protein of NHEJ (pDNA-PKcs), leading to persistent repair complexes following DSB induction. Chapter 3 is a protocol we developed to identify mutations that occur during the repair of a DSB induced by sgRNA/CAS9. This protocol can be adapted to any transfectable cell line. Chapter 4 shows that 8E6 allows NHEJ and HR to initiate at the same break site and cause multiple types of mutations including up to a 20-fold in deletions. Chapter 5 elucidates our most recent results showing that 8E6 increases a backup DSB repair pathway called alternative end joining (Alt-EJ). This is an intrinsically mutagenic pathway and helps cell survival [30–32]. Chapter 6 is the conclusion of this dissertation with a summary of outstanding questions in this field.

Chapter 1 - Beta HPV Deregulates Double-Strand Break Repair

Changkun Hu and Nicholas Wallace *

Division of Biology, Kansas State University, Manhattan, KS 66506, USA; chu1@ksu.edu

* Correspondence: nwallac@ksu.edu

Citation: Hu, C.; Wallace, N. Beta HPV Deregulates Double-Strand Break Repair. *Viruses* 2022, 14, 948. <https://doi.org/10.3390/v14050948>

Copyright: © 2022 by the authors. Licensee MDPI, Basel, Switzerland. This article is an open access article distributed under the terms and conditions of the Creative Commons Attribution (CC BY) license (<https://creativecommons.org/licenses/by/4.0/>).

Abstract

Beta human papillomavirus (beta HPV) infections are common in adults. Certain types of beta HPVs are associated with nonmelanoma skin cancer (NMSC) in immunocompromised individuals. However, whether beta HPV infections promote NMSC in the immunocompetent population is unclear. They have been hypothesized to increase genomic instability stemming from ultraviolet light exposure by disrupting DNA damage responses. Implicit in this hypothesis is that the virus encodes one or more proteins that impair DNA repair signaling. Fluorescence-based reporters, next-generation sequencing, and animal models have been used to test this primarily in cells expressing beta HPV E6/E7. Of the two, beta HPV E6 appears to have the

greatest ability to increase UV mutagenesis, by attenuating two major double-strand break (DSB) repair pathways, homologous recombination, and non-homologous end-joining. Here, we review this dysregulation of DSB repair and emerging approaches that can be used to further these efforts.

1. Introduction

The human papillomavirus (HPV) family is big, with over 450 HPV types already identified [1,2]. This virus family is subdivided into five genera (alpha, beta, gamma, nu, and mu) based on the sequence of the L1 capsid gene [3,4]. Alpha HPVs are most extensively studied, as a “high risk” subset of this genus can persistently infect mucosal epithelia leading to cervical, vulvar, vaginal, oropharyngeal, anal, and penile cancers [5–8]. Thanks to these efforts, life-saving vaccines against tumor-promoting HPVs have been developed and are widely available [6,9,10].

Unlike tumorigenic “high risk” alpha genus HPVs, beta genus HPV (beta HPV) infections occur in cutaneous epithelia [11,12]. In patients with a rare genetic disorder, epidermodysplasia verruciformis or EV, beta HPV infections persist and promote non-melanoma skin cancer (NMSC) [13–16]. In EV patients, HPV5 and HPV8 are enriched in cutaneous squamous cell carcinoma (cSCC), which frequently occurs in sunlight exposed areas [16,17]. Infection with these viruses also increases the risk of cSCC in organ trans-plant recipients (OTRs) who are receiving immunosuppression treatment [4–7]. High beta HPV viral loads in OTRs result in >100-fold higher risk of cSCC [18,19].

Beta HPV infections are also common in the general population [20–23]. However, the fact that viral loads plummet to less than a copy per cell in cSCCs makes the extent to which they promote NMSC unclear [11,15,16,24]. It is clear however that beta HPV infections cannot

promote tumors like known human oncogenic viruses, (i.e., by causing tumors that are dependent on continued viral oncogene expression). Further, higher beta HPV viral loads are found in precancerous skin lesions, such as actinic keratosis, but the amount of beta HPV dissipates to very low levels (<1 copy per cell) in cSCC [25,26]. It has been suggested that beta HPV increases mutations that drive tumorigenesis without continued viral gene expression being required for tumor maintenance or progression [25,27]. This would mean that beta HPV infections in the general population have their greatest impact on the cellular environment before transformation [15,28,29]. Epidemi-ological, animal, and cell culture systems support this hypothesis [15,16,25,30,31].

Here, we focus our discussion on the current understanding of how beta HPV hinders the repair of double-strand breaks in DNA (DSBs). The concentration on DSBs is based on the consensus that they are the most mutagenic type of DNA lesion. Further, failure to repair DSBs increases genomic instability and would be consistent with the hypothesized manner in which beta HPV infections promote NMSC formation. We also provide a survey of novel approaches that could be used to expand this knowledge base.

2. Beta HPV and Genomic Instability

2.1. Beta HPV Attenuates the Cellular Response to UV-Induced Damages

Because beta HPV infections occur in the skin, ultraviolet radiation or UV is the most biologically relevant source of DNA lesions. The cellular response to UV-induced DNA damage is well characterized [32]. The most frequent lesions caused directly by UV are the cyclobutane pyrimidine dimers (CPDs) that form at two adjacent thymine bases [33]. CPDs stall replication forks/replicative polymerases, but do not impact replicative helicase activity. The uncoupling of polymerase from helicases generates a growing stretch of unstable single-stranded DNA

(ssDNA). To prevent replication fork collapse, ssDNA is covered with an RPA trimer (RPA70, RPA32, and RPA14) [34]. With the help of TOPBP1 and ATRIP, the RPA trimer recruits ATR, the kinase that is largely responsible for co-ordinating the cellular response to stalled replication forks [35]. ATR activates itself by autophosphorylation [35]. Activated ATR phosphorylates downstream targets to initiate signaling cascades that turn on DNA repair and cell cycle arrest. Specifically, activated ATR phosphorylates CHK1 [32]. Phosphorated CHK1 phosphorylates and inactivates CDC25A and CDC25C, which are required for CDK2-mediated G1/S transition and CDK1-mediated G2/M transition, respectively [35]. ATR also activates a repair pathway known as nucleotide excision repair (NER) by phosphorylating XPA [36]. XPA abundance is rate-limiting for NER and its phosphorylation by ATR increases its stability [36]. This allows NER to remove UV lesions. ATR also facilitates translesion synthesis (TLS) by phosphorylating REV1 and DNA polymerase eta [35]. TLS is not directly responsible for repairing UV-lesions, but it helps prevent these lesions from causing replication fork collapse by allowing the replication fork to bypass these lesions. Finally, in response to UV damage, multiple kinases (ATR, CHK1, and casein kinase 2) induce further responses by phosphorylating and stabilizing p53 [32,35,37]. This leads to cell cycle arrest, apoptosis, and/or senescence.

High-risk alpha HPV encodes two primary oncogenes (E6 and E7) that facilitate extensive manipulation of the host cell environment. Studies of beta HPV biology often focus on the homologs of oncogenes [38]. This work primarily examines these homologs from only the subset of beta HPVs most closely linked to clinical manifestations (beta HPV5, 8, 20, 27, 38, and 49). Beta HPV studies have been performed in vitro using its natural host human keratinocytes. Human foreskin keratinocytes (HFKs) isolated from neonatal are frequently used because it has fewer mutations and are relatively easy to grow due to their young age. In human keratinocytes

E6 from multiple beta HPV types contributes to the evasion of UV-induced apoptosis [39–41]. In HFKs, HPV5 and 8 E6 disrupt DNA repair pathways to make UV-induced CDPs more mutagenic [27,42–44]. HPV8 E6 leads to decreased ATR expression and activation in response to UV [42,43]. Further HPV8 E6 decreases downstream proteins of ATR in cells exposed to UV. This includes phosphorylated CHK1, phosphorylated XPA, total XPA, and total DNA polymerase eta (TLS) [43]. Moreover, HPV5 and 8 E6 bind to p300, a histone acetyltransferase that acetylates p53 in response to UV [42,45]. HPV38 attenuates p53 signaling and allows the proliferation of cells with UV damage [46].

The E6 and/or E7 from these beta HPVs also show transforming properties *in vivo* following UV radiation [47–53]. Particularly, HPV5 and 8 E7 expressing xenograft on humanized mice promote pretumor or tumorous skin lesions [51,54,55]. HPV8 E7 increases α 3-integrin which promotes keratinocyte invasion [54]. HPV5 and 8 E7 also up-regulate beta-catenin, which may contribute to the oncogenic potential of the virus [55]. Transgenic mice expressing HPV8 early genes develop cSCC, which can be enhanced by UV light [39,47,48,56,57]. Associated with these skin lesions, HPV8 E6 reduces phosphorylation of DNA damage sensing factors (ATR, CHK1, and ATM) [31]. HPV8 E6 and E7 work together to decrease CHK1 protein levels [58]. HPV8 complete early region (CER) also increases cancer-associated proteins including metalloproteinase, StefinA, and Sprr2 [59,60]. HPV8 CER also upregulates oncogenic miRNAs (17-5p, 21, and 106a) and downregulates tumor-suppressive miRNAs (155 and 206) [61]. Transgenic mice expressing HPV20, 27, 38, and 49 E6/E7 develop cSCC following UV radiation [29,43,49,52,53]. In support of the “hit and runs” mutagenesis hypothesis, deletion of E6/E7 after these lesions form did not affect cancer growth [29]. Rodent papillomaviruses resembling beta HPV were used to aid the study of cutaneous HPV biology in

vivo [62–65]. *Mastomys natalensis* papilloma virus (MnPV) promotes cSCC in immunodeficient rats following UVB exposure [57]. Mouse papillomavirus type 1 (MmuPV1) induces papilloma in immunocompetent mice following UVB exposure [66].

2.2. Beta HPV Deregulates Double-Strand Break Repair Pathways

The interference with UV damage repair by HPV5 and HPV8 E6 causes a more frequent collapse of replication forks into mutagenic DSBs. Erroneous DSB repair can cause the loss of large regions of DNA, chromosome translocation/rearrangements, and aneuploidy [67,68]. Two major pathways, homologous recombination (HR) and non-homologous end-joining (NHEJ) have evolved to repair DSBs with high fidelity. In addition, alternative end-joining (Alt-EJ) serves as a more mutagenic backup DSB repair pathway should HR and/or NHEJ fail [69].

2.2.1. Beta HPV Disrupts HR

Homologous recombination is an error-free DNA-repair pathway. It occurs in S/G2 phase so that a sister chromatid can be used as a homologous template. HR is dependent on DNA resection. ATM kinase and its targets are responsible for DSB sensing, cell cycle arrest, and DNA resection [70–73]. The MRE11, Rad50, and Nbs1 (MRN) complex together with CtIP to initiate minor DNA resection to generate 3' short (~100 nt) ssDNA [74–76]. After short ssDNA is generated by the CtIP/MRN complex, downstream nucleases, and helicases such EXO1, DNA2, and BLM make extensive resection to reveal longer ssDNA [75,75,77]. With the help of mediator proteins BRCA1 and BRCA2, RPA and then RAD51 is recruited to the ssDNA to protect it from degradation [78–82]. RAD51-DNA filaments also facilitate homologous searching and strand invasion, which resolve the DSB [81,83].

A GFP-based HR reporter demonstrated that HPV5, 8, and 38 E6 decrease HR efficiency [84,85]. The mechanistic details of how this inhibition occurs have largely been worked

out. By degrading transcription regulator p300, beta HPV 5 and 8 E6 decrease BRCA1 and BRCA2 at both mRNA and protein levels [84]. HPV5 and 8 E6 similarly reduce ATM protein abundance [84]. HPV8 E6 can also decrease ATM activation via phosphorylation [43]. Further, HPV5 and 8 E6 decrease the formation of BRCA1 and BRCA2 repair complexes. However, HPV5 and 8 E6 do not decrease RAD51 foci formation that is believed to depend on BRCA1 and BRCA2. Instead, they delay the resolution of RAD51 foci, suggesting that the repair complexes that form may be non-functional [84]. Supporting this idea, some of the RAD51 foci that form in cells expressing HPV8 E6 occur in G1 phase, when they are unlikely to be efficiently resolved due to the lack of a ho-mologous template [86]. HPV38 E6 that weakly binds to p300 did not significantly de-crease BRCA1 or BRCA2 expression. It also did not significantly alter HR repair complex formation or resolution.

2.2.2. Beta HPV Attenuates NHEJ

NHEJ is responsible for DSB repair throughout interphase and G1 when homologous templates are not available. NHEJ initiates with localization of 53BP1 to the DSB. This helps prevent HR factors from promoting DNA resection [87–89]. Next, the Ku70/Ku80 dimer binds to DSB ends and recruits DNA-dependent protein kinase catalytic subunit (DNA-PKcs) [90–92]. Ku70/Ku80 and DNA-PKcs together form DNA-PK holoenzyme that facilitates NHEJ by phosphorylating downstream targets including Artemis [93–95]. Artemis has both endonuclease and exonuclease activity that helps to process the DNA end [93,95–97]. This end processing often includes the removal of overhangs and results in deletions. The resulting gap surrounding the blunt-ended DNA is resolved by XRCC4/XLF/ and DNA ligase IV repair complex [94,98].

HPV5 and 8 E6 delay 53BP1 repair complex resolution [84]. Further, a CAS9-based NHEJ reporter showed that endogenous NHEJ was decreased in HPV8 E6 expressing cells [99,100]. The mechanistic analysis demonstrated that HPV8 E6 attenuated NHEJ by reducing the phosphorylation of DNA-PKcs and its downstream target Artemis. HPV8 E6 also impaired the resolution of pDNA-PKcs complexes to persistent [99]. These phenotypes were linked to HPV8 E6 mediated destabilization of p300. However, the viral protein decreased XRCC4 foci independent of p300 destabilization. These data confirmed that deletion of the p300 binding residues (amino acids 132–136) does not globally impair 8E6 activity.

2.2.3. Beta HPV Promotes Mutagenic DSB Repair Pathway

It should be noted that neither HPV5 E6 nor HPV8 E6 completely abrogates DSB repair. Rather, these viral proteins delay DSB repair. This suggests that DSB repair is still occurring and motivated ongoing efforts to identify the pathway(s) by which it was happening. To address this knowledge gap, a recent effort tracked the persistent HR and NHEJ foci found in earlier work [84,99]. This work found that HPV8 E6 caused HR factors (RPA70 and RAD51) to be recruited to sites of stalled NHEJ repair [86]. NHEJ and HR are intrinsically incompatible. HR requires ssDNA while NHEJ removes it. The colocalization of NHEJ and HR factors at the same DSB suggests that in cells expressing HPV8 E6, some DSBs are being repaired through an unusual, combined effort of the two pathways. This is expected to lead to increased mutations, especially deletions. Next-generation sequencing targeted at 200 kb surrounding a CAS9-induced DSB supports this idea, by showing a 20-fold increase in deletions in cells with HPV8 E6 compared to vector control cells [86]. Our unpublished data show that HPV8 E6 increases the use of a backup DSB repair pathway, known as alternative end-joining (Alt-EJ). Alt-EJ is intrinsically mutagenic and frequently detected in cancers [101]. Notably, Alt-EJ also results in deletions. These

alterations in DSB repair suggest that HPV8 E6 makes DSBs more mutagenic. This may be a common property of cutaneous papillomaviruses as a recent study shows that MmuPV1 uses Alt-EJ to integrate DNA into the host genome in benign tumors [63].

3. Approaches to Study DSB Repair

3.1. Outstanding Questions

At least some beta HPV proteins abrogate correct DSB repair. However, outstanding questions remain. Many studies of beta HPV and DSB repair are conducted in cells expressing the E6 gene in isolation. While HPV8 E6 alone did not significantly decrease CHK1 protein levels, the combination of HPV8 E6 and E7 reduced CHK1 protein abundance in vitro and in vivo [58]. This suggests that HPV8 E7 augments HPV8 E6-mediated genome destabilization. To what extent, does co-expression of HPV8 E6 and E7 exacerbate the genome destabilization by HPV8 E6? More broadly, the most studied beta HPV proteins are HPV5, 8, 38, and 49 E6. Do other beta HPVs encode genes that hinder DSB repair? Do beta HPVs cause a unique enough pattern of mutations that they can be distinguished from mutations caused by other mutagens?

3.2. Induction of DSBs

DSBs can be induced by physical rays and chemical reagents. The source of these lesions is important to consider when studying DSB repair. UV and ionizing radiation (IR) are two types of radiation commonly used to generate DSBs in cells. Since UV relies on the collapse of replication forks, DSBs induced by UV do not occur in all cells at the same time [78,102]. Thus, the interpretation from kinetic studies becomes complicated. Moreover, UV especially UVA has low efficiency inducing DSBs [32,103]. Thus, only a fraction of cells will experience a DSB. In contrast, ionizing radiation (IR) efficiency induces DSBs by using high-energy particles to attack DNA strands directly [104,105]. This means that DSBs occur in nearly every cell at

approximately the same time. However, IR also induces reactive oxygen species (ROS) that cause DNA damage [106,107]. As a result, interrogation of cellular responses may be complicated by the induction of signaling by ROS. ROS may complicate strict kinetic analysis as they independently cause DSBs. There are also practical considerations, for example, not all laboratories have access to sources of ionizing radiation.

Chemicals can also be used to induce DSBs. For instance, radiation mimicking re-agents such as bleomycin can cleave DNA via intercalation [108,109]. Hydrogen peroxide can also induce DSBs by increasing ROS [110]. The limitation of chemical reagents is similar to those associated with DSB-induction via UV, in that they complicate kinetic studies by inducing damage over time. One way of addressing this problem is to use a short pulse of media containing a high concentration of the drug of interest, but this approach should be taken with caution to assure that a subset of cells is not faced with non-physiological levels of DSBs. Additionally, most chemicals require vigorous washing to remove the compounds for any kinetic study of DSB repair. There is at least one exception. The radiomimetic drug, neocarzinostatin can be used to induce DSBs without the need for extensive washes as it becomes inactive (via degradation) within five minutes of treatment [111].

All the physical rays or chemical reagents mentioned in the preceding paragraph cause genome-wide DSBs in a largely non-discriminative manner. This increases the challenge of dissecting the repair process at a single DSB site. To study the repair of a single DSB repair at a targeted locus, specified artificial endonuclease such as I-SceI can be used [112]. However, these rare-cutting endonucleases require the integration of their recognition site into the genome of interest. Thus, the genome context is somewhat artificial. Further, integrating the I-SceI recognition site into the locus of interest and then validating its integration can be labor-

intensive. The advent of sgRNA/CAS9 technology can subvert these restrictions allowing a DSB to be induced at a locus of interest without manipulation of the target cell beyond the transfection of the sgRNA and CAS9 expression plasmid [113].

IR and UV have been used to induce DSBs in cells with HPV5, 8, and 38 E6 [42,84]. Radiation mimic reagent zeocin was used to induce DSBs to study how HPV8 E6 de-regulates NHEJ [99]. sgRNA/CAS9 was used to induce DSB at a single genomic locus in cells expressing HPV8 E6 [86,114]. Their ability to cause DSBs in different manners can be used to examine alterations in DSB repair caused by beta HPVs. For instance, UV can be used as a physiological source of DSBs. IR/zeocin can be used to directly induce DSB, so that differences in repair are not masked/exacerbated by upstream responses to UV that can make it more or less likely to cause DSBs. Similarly, zeocin, IR, and UV induce genome-wide DSBs, while sgRNA/CAS9 can be used to create a DSB at a specific site. While the random distribution of lesions is more physiologically relevant, inducing a DSB via sgRNA/CAS9 allows for the evaluation of the genome contexts of lesions to be more readily evaluated.

3.3. Using Immunoblotting to Characterize DSB Repair Signaling

Activation of DNA repair is regulated by cellular signaling pathways [115–117]. Immunoblotting is a standard method to measure this activation in the form of altered protein abundance or post-translational modifications of signaling and repair factors. Phosphorylation and ubiquitination are common marks for the activation status of DNA repair proteins [118]. Immunoblotting together with densitometry can be used to measure the proportion of activated DNA repair proteins [99,119]. This is typically done following the induction of DSBs by one of the methods discussed in the preceding section. However, DNA repair is a complex, localized

process. Higher DNA repair protein abundance (or post-translational modifications associated with repair factor activation) does not necessarily indicate higher DNA repair activity. DNA repair factors should bind to the damage site or interact with other repair factors [120]. Co-immunoprecipitation together with immunoblotting can be used to detect DNA repair factors physically interacting with known DNA binding proteins such as the DSB marker described in the next section [121]. Subcellular fractionation may similarly help define changes in localization indicative of DSB repair activation.

Immunoblotting has been used to show that HPV5 and 8 E6 decrease major HR proteins including ATM, BRCA1, and BRCA2 [84]. The approach has also been used to show decreases in activation of NHEJ factors including pDNA-PKcs (S2056) and pArtemis (S516) [99].

Immunoblotting can be used to study how common these protein levels decrease in cells with beta HPVs or if these phenotypes change when E6 is expressed in the context of the whole viral genome or along with E7. Notably, HPV8 E6 decreases these DSB repair proteins above by destabilizing p300. Immunoblots can also be used to determine if HPV5 and 8 E6 make other DSB repair proteins are less abundant or less efficiently activated. Similarly, immunoblots can be used to determine if the expression of other beta HPV E6 genes decreases repair factor abundance.

3.4. Immunofluorescence Microscopy of DSB Repair Factors in Fixed Cells

As described above, DNA repair proteins should be recruited to the damaged site forming repair complexes, visible by microscopy as distinct foci. Immunofluorescence (IF) microscopy is often used together with DSB induction to examine the localization of repair factors to DSBs. In these analyses, phosphorylated H2AX (S139) or pH2AX is an established marker of DSBs that can be used to confirm the localization of repair factors to DSBs or define the overall rate of

DSB repair by fixing cells at intervals after DSB induction [122,123]. IF microscopy can also be used to characterize the kinetics by which other DSB repair complexes form and resolve, providing more detailed insight into repair [120]. Conjugated primary antibodies can be used to facilitate the detection of multiple protein targets in the sample. This can be used to detect the formation of multi-subunit repair complexes or combined with the detection of cyclin protein to determine when (regarding the cell cycle) repair complexes are forming [124–126].

IF microscopy has been used to detect repair kinetics of the HR pathway in cells expressing HPV5, 8, and 38 E6 [84]. The approach has also shown that HPV8 E6 delays the NHEJ pathway [99]. Future research can use IF microscopy to determine to what extent these changes in repair kinetics are induced by other beta HPVs and the impact of co-expressing E6 along with other beta HPV proteins. This approach can also be used to find more alterations in DSB repair kinetics, perhaps in other DSB repair pathways.

3.5. Immunofluorescence Microscopy of DSB Repair Complexes in Living Cells

IF microscopy of fixed cells does not allow tracking of a single cell through the course of repair. Although technically more challenging, IF microscopy of living cells can address this barrier. Following DSB induction as described above, the recruitment and resolution of DSB repair factors can be recorded by time-lapse microscopy. This approach was used to reveal that NHEJ occurs in the G1 phase and NHEJ to HR pathway switch occurs in the S phase [87,127]. This approach has been used in combination with laser microirradiation to characterize the recruitment of repair complexes to laser-induced DSBs [128]. As a further tool, different types of lasers (UV, visible, near-infrared) can be used to induce different types of damage and to investigate different repair pathways [129]. Caution should be exercised with this approach as lasers can induce localized DSBs at unphysiological levels. Another challenge for imaging living

cells is labeling DNA repair factors without altering their function. Typically, fluorescence tags are added to DNA repair proteins that are then transfected into cells. However, the increased abundance of certain DNA repair proteins may alter the DSB repair pathway choice. Further, the addition of the large fluorescence tag can impair protein function via steric hindrance [130]. One way of overcoming this challenge is to add smaller tags, (e.g., CLIP and SNAP) that self-label with fluorophores after repairing complex formation [131,132].

While live-cell imaging has been used to examine other aspects of beta HPV biology [46], it has not been used to study their impact on DSB repair. Thus, this approach has the most untapped potential of the techniques discussed in this review. One potential use would be to expand on our previous observation that HPV8 E6 promotes colocalization of NHEJ and HR factors [86]. Live-cell imaging would a definitive determination of how these abnormal complexes form and whether they are capable of resolving a DSB or marking cells for the death that is associated with an unrepaired DSB [133,134].

3.6. Reporters Constructs Can Measure Activity of Individual DSB Repair Mechanisms

To measure the frequency of a specific DSB repair pathway, specialized reporters have been developed. The general design of these reporters is that they contain a fluorescent protein (most often GFP) that is inactivated by insertions in the open reading frame [85]. I-SceI or sgRNA/CAS9 are used to induce DSBs [112,113]. Each reporter cassette is designed such that repair of the resulting DSB by a pathway of interest results in fluorophore expression. A recent adaptation of this approach uses CD4 expression as an alternative readout [100]. Using sgRNA/CAS9, two DSBs were induced at GAPDH and CD4 genes, if the DSBs are repaired by NHEJ it will result in deletion and rearrangement that will place the CD4 open reading frame just downstream of the GAPDH promoter. As a result, CD4 will be constitutively expressed. A

limitation of this assay is that it can only be used in cells not already expressing CD4. However, because it does not use a reporter cassette, it has the advantage of measuring NHEJ frequency at DSBs occurring in the unaltered host genome [114]. Further, all of these systems rely on non-physiological relevant mechanisms of inducing DSBs, (e.g., I-SceI or sgRNA/CAS9), producing lesions that are often “cleaner” than naturally occurring DSBs and thus do not represent the complex nature of naturally occurring DSBs [114]. Finally, reporter assays can only detect the type of repair that they are designed for, thus variations that produce unexpected DNA products will not be seen. DSB repair reporters and measurements are summarized in Table 1.

Reporter assays have been used to show that HPV5 and 8 E6 disrupt the HR pathway and that HPV8 E6 attenuates NHEJ [84,99]. Our unpublished data show that HPV8 E6 promotes Alt-EJ using the 4- μ HOM reporter [90,136]. These reporters can be used to screen other beta HPV expressing cell lines for the ability to alter these DSB repair pathways as well as to determine the extent that which co-expression of E6 along with other beta HPV genes changed E6-mediated alterations in DSB repair.

3.7. Flow Cytometry

IF microscopy allows the DNA repair process to be studied at a high resolution, but this benefit is offset by the time-consuming nature of image capturing and analysis to obtain robust data. The reporter constructs described above tend to result in fluorophore expression at levels too low (<5%) to be amenable to detection by IF microscopy. Instead, flow cytometry is more commonly used as a high throughput alternative with these assays. It can be used to detect GFP from fluorophore-based reporter constructs. Flow cytometry can also be used to determine the cell cycle position of the repair complex and offer valuable insight into the interplay between cell cycle position and DSB repair factor activation [137]. With these approaches, cell cycle stages

are most commonly determined by DNA content [138,139]. One weakness in this approach is that flow cytometry measures the total abundance or intensity of repair factors, which may or may not be equivalent to the detection of active repair complexes. Therefore, IF microscopy and flow cytometry should be used in tandem when investigating cell cycle-sensitive DNA repair factors.

Flow cytometry is used together with specified DSB reporters to measure the efficiency of different repair pathways [84]. It also has been used to determine how HPV8 E6 alters the cell cycle distribution of RAD51 repair complexes [86]. Flow cytometry could similarly be used to determine the extent that which beta HPV proteins change the cell cycle distribution of other DSB repair complexes, or whether expression of the whole viral genome also leads to the same changes in the cell cycle distribution of DSB repair factors caused by HPV8 E6 expression.

3.8. Next-Generation Sequencing

While the approaches above can be used to detect defects in DSB repair signaling, they do not measure the mutagenic impact of these defects (including increases in the number of changes in the types of mutations). Next-generation sequencing (NGS) is currently the best way to get this information. Whole-genome sequencing (WGS) is a type of NGS that offers an unbiased characterization of mutations by sequencing the entire genome. Whole exome sequencing (WES) focuses this analysis by allowing mutations in non-protein-coding regions to be ignored. Targeted NGS can provide a robust analysis of a small region of interest allowing deep sequencing at an affordable price [140]. Targeted NGS can be paired with sgRNA/CAS9 technology to induce a single DSB at a defined locus and then obtain an in-depth analysis of the mutations associated with repair at that locus under experimental conditions of interest [86,114]. There are limitations to NGS approaches. For example, WGS can be cost-prohibitive and

requires complex bioinformatics analysis. Perner et al. developed a sequencing strategy with reduced DNA quantity, which is more cost-effective than traditional WGS [141]. A random subset of the genome was obtained following double restriction enzyme digestion and size selection. However, this only yields data from areas where restriction ends are close enough together to facilitate sequencing and therefore be biased to certain regions.

NGS at a known region (CD4) around a single DSB induced by sgRNA/CAS9 shows that HPV8 E6 increases multiple types of mutations [86,114]. NGS could also be used to examine how common mutagenic events are in cells with beta HPVs, whether expressing the whole viral genome leads to similar mutations induced by HPV8 E6, and how the pattern of mutations changes with preexisting mutations in the host genome. Similarly, interesting questions that could be addressed with NGS include whether the same pattern of mutations that are seen at CAS9-induced DSB occurs after UV or IR induced DSBs and how common it is for the E6 from other members of the beta HPV genus to cause increased mutations during DSB repair. Computational analysis of these data may allow a unique mutational signature for DSB repair in HPV8 E6 expressing cells to be identified, which might allow mutations promoted by HPV8 E6 to be distinguished from those caused independent of the virus.

3.9. Approaches to Studying DSB Repair That Have Not Been Used to Study Beta HPVs

While most of the approaches described above have already been used to investigate beta HPV biology, their ability to ask other questions fundamental to cell biology allows them to remain useful. However, we are unaware of two of the approaches being used in this field, namely live imaging of repair complexes and WGS [86]. In addition to cell culture and rodent models, the organotypic raft can be a good model to simulate DNA damage response in

differentiating skin [142]. While organotypic is commonly used in the investigation of alpha HPVs, these studies are less commonly applied to beta HPVs.

4. Summary and Discussions

Established and cutting-edge techniques have been used to show that beta HPV E6 proteins disrupt DSB repair and in some cases cause striking increases in mutagens during DSB repair. While these results support the “hit and run” hypothesis, they fall well short of providing definitive support for the idea. Ultimately, addressing out-standing questions (Section 3) is critical regardless of the outcome. Demonstrating a novel mechanism of tumorigenesis would be significant, but there is also significant value in a better understanding of a viral genus that infects most adults.

Author Contributions: Conceptualization, C.H. and N.W.; writing—original draft preparation, C.H.; writing—review and editing, C.H. and N.W.; visualization, C.H.; supervision, N.W.; fund-ing acquisition, N.W. All authors have read and agreed to the published version of the manu-script.

Funding: This research was supported by the National Institute of General Medical Sciences (NIGMS) of the National Institutes of Health (NIH, P20GM130448); NIH Research Enhancement Award (NCI R15 CA242057 01A1); US department of defense (CMDRP PRCRP CA160224 (NW)); and Johnson Cancer Research Center of Kansas State University.

Acknowledgments: We thank Sebastian Wendel, Taylor Bugbee, and Rose Pollina for valuable insight and feedback on this manuscript.

Conflicts of Interest: The authors declare no conflicts of interest.

References

1. Van Doorslaer, K.; Li, Z.; Xirasagar, S.; Maes, P.; Kaminsky, D.; Liou, D.; Sun, Q.; Kaur, R.; Huyen, Y.; McBride, A.A. The Papillomavirus Episteme: A Major Update to the

- Papillomavirus Sequence Database. *Nucleic Acids Res.* **2017**, *45*, D499–D506. <https://doi.org/10.1093/nar/gkw879>.
2. McBride, A.A. Human Papillomaviruses: Diversity, Infection and Host Interactions. *Nat. Rev. Microbiol.* **2022**, *20*, 95–108. <https://doi.org/10.1038/s41579-021-00617-5>.
 3. Bernard, H.-U.; Burk, R.D.; Chen, Z.; van Doorslaer, K.; zur Hausen, H.; de Villiers, E.-M. Classification of Papillomaviruses (PVs) Based on 189 PV Types and Proposal of Taxonomic Amendments. *Virology* **2010**, *401*, 70–79. <https://doi.org/10.1016/j.virol.2010.02.002>.
 4. Kim, M.-J.; Kim, J.J.; Kim, S. Sequencing Analysis of HPV-Other Type on an HPV DNA Chip. *Obstet. Gynecol. Sci.* **2018**, *61*, 235–241. <https://doi.org/10.5468/ogs.2018.61.2.235>.
 5. Brianti, P.; De Flammineis, E.; Mercuri, S.R. Review of HPV-Related Diseases and Cancers. *New Microbiol.* **2017**, *40*, 80–85.
 6. Kombe Kombe, A.J.; Li, B.; Zahid, A.; Mengist, H.M.; Bounda, G.-A.; Zhou, Y.; Jin, T. Epidemiology and Burden of Human Papillomavirus and Related Diseases, Molecular Pathogenesis, and Vaccine Evaluation. *Front. Public Health* **2021**, *8*, 1003.
 7. Elrefaey, S.; Massaro, M.A.; Chiocca, S.; Chiesa, F.; Ansarin, M. HPV in Oropharyngeal Cancer: The Basics to Know in Clinical Practice. *Acta Otorhinolaryngol. Ital.* **2014**, *34*, 299–309.
 8. Grulich, A.E.; Poynten, I.M.; Machalek, D.A.; Jin, F.; Templeton, D.J.; Hillman, R.J. The Epidemiology of Anal Cancer. *Sex Health* **2012**, *9*, 504–508. <https://doi.org/10.1071/SH12070>.
 9. Cheng, L.; Wang, Y.; Du, J. Human Papillomavirus Vaccines: An Updated Review. *Vaccines* **2020**, *8*, 391. <https://doi.org/10.3390/vaccines8030391>.
 10. National Cancer Institute. Study Confirms HPV Vaccine Prevents Cervical Cancer. Available online: <https://www.cancer.gov/news-events/cancer-currents-blog/2020/hpv-vaccine-prevents-cervical-cancer-sweden-study> (accessed on 11 February 2022).
 11. Hasche, D.; Vinzón, S.E.; Rösl, F. Cutaneous Papillomaviruses and Non-Melanoma Skin Cancer: Causal Agents or Innocent Bystanders? *Front Microbiol.* **2018**, *9*, 874. <https://doi.org/10.3389/fmicb.2018.00874>.
 12. NISC Comparative Sequencing Program; Tirosh, O.; Conlan, S.; Deming, C.; Lee-Lin, S.-Q.; Huang, X.; Su, H.C.; Freeman, A.F.; Segre, J.A.; Kong, H.H. Expanded Skin Virome in DOCK8-Deficient Patients. *Nat. Med.* **2018**, *24*, 1815–1821. <https://doi.org/10.1038/s41591-018-0211-7>.
 13. Rollison, D.E.; Viariso, D.; Amorrortu, R.P.; Gheit, T.; Tommasino, M. An Emerging Issue in Oncogenic Virology: The Role of Beta Human Papillomavirus Types in the Development of Cutaneous Squamous Cell Carcinoma. *J. Virol.* **2019**, *93*, e01003-18. <https://doi.org/10.1128/JVI.01003-18>.
 14. Nichols, A.J.; Allen, A.H.; Shareef, S.; Badiavas, E.V.; Kirsner, R.S.; Ioannides, T. Association of Human Papillomavirus Vaccine With the Development of Keratinocyte Carcinomas. *JAMA Dermatol.* **2017**, *153*, 571–574. <https://doi.org/10.1001/jamadermatol.2016.5703>.
 15. Howley, P.M.; Pfister, H.J. Beta Genus Papillomaviruses and Skin Cancer. *Virology* **2015**, *0*, 290–296. <https://doi.org/10.1016/j.virol.2015.02.004>.
 16. Slichero, L.; Rollison, D.E.; Amorrortu, R.P.; Tommasino, M. Beta Human Papillomavirus and Associated Diseases. *Acta Cytol.* **2019**, *63*, 100–108. <https://doi.org/10.1159/000492659>.
 17. Dell’Oste, V.; Azzimonti, B.; De Andrea, M.; Mondini, M.; Zavattaro, E.; Leigheb, G.; Weissenborn, S.J.; Pfister, H.; Michael, K.M.; Waterboer, T.; et al. High β -HPV DNA Loads and Strong Seroreactivity Are Present in Epidermodysplasia Verruciformis. *J. Investig. Dermatol.* **2009**, *129*, 1026–1034. <https://doi.org/10.1038/jid.2008.317>.

18. Bavinck, J.N.B.; Feltkamp, M.C.W.; Green, A.C.; Fiocco, M.; Euvrard, S.; Harwood, C.A.; Nasir, S.; Thomson, J.; Proby, C.M.; Naldi, L.; et al. Human Papillomavirus and Posttransplantation Cutaneous Squamous Cell Carcinoma: A Multicenter, Prospective Cohort Study. *Am. J. Transplant.* **2018**, *18*, 1220–1230. <https://doi.org/10.1111/ajt.14537>.
19. Bouwes Bavinck, J.N.; Feltkamp, M.; Struijk, L.; ter Schegget, J. Human Papillomavirus Infection and Skin Cancer Risk in Organ Transplant Recipients. *J. Investig. Dermatol. Symp. Proc.* **2001**, *6*, 207–211. <https://doi.org/10.1046/j.0022-202x.2001.00048.x>.
20. Neale, R.E.; Weissenborn, S.; Abeni, D.; Bavinck, J.N.B.; Euvrard, S.; Feltkamp, M.C.W.; Green, A.C.; Harwood, C.; de Koning, M.; Naldi, L.; et al. Human Papillomavirus Load in Eyebrow Hair Follicles and Risk of Cutaneous Squamous Cell Carcinoma. *Cancer Epidemiol. Biomark. Prev.* **2013**, *22*, 719–727. <https://doi.org/10.1158/1055-9965.EPI-12-0917-T>.
21. Venuti, A.; Lohse, S.; Tommasino, M.; Smola, S. Cross-Talk of Cutaneous Beta Human Papillomaviruses and the Immune System: Determinants of Disease Penetrance. *Philos. Trans. R Soc. Lond. B Biol. Sci.* **2019**, *374*, 20180287. <https://doi.org/10.1098/rstb.2018.0287>.
22. Bzhalava, D.; Mühr, L.S.A.; Lagheden, C.; Ekström, J.; Forslund, O.; Dillner, J.; Hultin, E. Deep Sequencing Extends the Diversity of Human Papillomaviruses in Human Skin. *Sci. Rep.* **2015**, *4*, 5807. <https://doi.org/10.1038/srep05807>.
23. Winer, R.L.; Gheit, T.; Feng, Q.; Stern, J.E.; Lin, J.; Cherne, S.; Tommasino, M. Prevalence and Correlates of Beta and Gamma Human Papillomavirus Detection in Oral Samples from Mid-Adult Women. *J. Infect. Dis.* **2019**, *219*, 1067–1075. <https://doi.org/10.1093/infdis/jiy632>.
24. Strickley, J.D.; Messerschmidt, J.L.; Awad, M.E.; Li, T.; Hasegawa, T.; Ha, D.T.; Nabeta, H.W.; Bevins, P.A.; Ngo, K.H.; Asgari, M.M.; et al. Immunity to Commensal Papillomaviruses Protects against Skin Cancer. *Nature* **2019**, *575*, 519–522. <https://doi.org/10.1038/s41586-019-1719-9>.
25. Hufbauer, M.; Akgül, B. Molecular Mechanisms of Human Papillomavirus Induced Skin Carcinogenesis. *Viruses* **2017**, *9*, E187. <https://doi.org/10.3390/v9070187>.
26. Weissenborn, S.J.; Nindl, I.; Purdie, K.; Harwood, C.; Proby, C.; Breuer, J.; Majewski, S.; Pfister, H.; Wieland, U. Human Papillomavirus-DNA Loads in Actinic Keratoses Exceed Those in Non-Melanoma Skin Cancers. *J. Investig. Dermatol.* **2005**, *125*, 93–97. <https://doi.org/10.1111/j.0022-202X.2005.23733.x>.
27. Wendel, S.O.; Wallace, N.A. Loss of Genome Fidelity: Beta HPVs and the DNA Damage Response. *Front. Microbiol.* **2017**, *8*, 2250. <https://doi.org/10.3389/fmicb.2017.02250>.
28. Gheit, T. Mucosal and Cutaneous Human Papillomavirus Infections and Cancer Biology. *Front. Oncol.* **2019**, *9*, 355.
29. Viarisio, D.; Müller-Decker, K.; Accardi, R.; Robitaille, A.; Dürst, M.; Beer, K.; Jansen, L.; Flechtenmacher, C.; Bozza, M.; Harbottle, R.; et al. Beta HPV38 Oncoproteins Act with a Hit-and-Run Mechanism in Ultraviolet Radiation-Induced Skin Carcinogenesis in Mice. *PLoS Pathog.* **2018**, *14*, e1006783. <https://doi.org/10.1371/journal.ppat.1006783>.
30. Lambert, P.F.; Münger, K.; Rösl, F.; Hasche, D.; Tommasino, M. Beta Human Papillomaviruses and Skin Cancer. *Nature* **2020**, *588*, E20–E21. <https://doi.org/10.1038/s41586-020-3023-0>.
31. Hufbauer, M.; Cooke, J.; van der Horst, G.T.J.; Pfister, H.; Storey, A.; Akgül, B. Human Papillomavirus Mediated Inhibition of DNA Damage Sensing and Repair Drives Skin Carcinogenesis. *Mol. Cancer* **2015**, *14*, 183. <https://doi.org/10.1186/s12943-015-0453-7>.
32. Lee, J.W.; Ratnakumar, K.; Hung, K.-F.; Rokunohe, D.; Kawasumi, M. Deciphering UV-Induced DNA Damage Responses to Prevent and Treat Skin Cancer. *Photochem. Photobiol.* **2020**, *96*, 478–499. <https://doi.org/10.1111/php.13245>.

33. Schreier, W.J.; Schrader, T.E.; Koller, F.O.; Gilch, P.; Crespo-Hernández, C.E.; Swaminathan, V.N.; Carell, T.; Zinth, W.; Kohler, B. Thymine Dimerization in DNA Is an Ultrafast Photoreaction. *Science* **2007**, *315*, 625–629. <https://doi.org/10.1126/science.1135428>.
34. Maréchal, A.; Zou, L. RPA-Coated Single-Stranded DNA as a Platform for Post-Translational Modifications in the DNA Damage Response. *Cell Res.* **2015**, *25*, 9–23. <https://doi.org/10.1038/cr.2014.147>.
35. Saldivar, J.C.; Cortez, D.; Cimprich, K.A. The Essential Kinase ATR: Ensuring Faithful Duplication of a Challenging Genome. *Nat. Rev. Mol. Cell Biol.* **2017**, *18*, 622–636. <https://doi.org/10.1038/nrm.2017.67>.
36. Shell, S.M.; Li, Z.; Shkriabai, N.; Kvaratskhelia, M.; Brosey, C.; Serrano, M.A.; Chazin, W.J.; Musich, P.R.; Zou, Y. Checkpoint Kinase ATR Promotes Nucleotide Excision Repair of UV-Induced DNA Damage via Physical Interaction with Xeroderma Pigmentosum Group A. *J. Biol. Chem.* **2009**, *284*, 24213–24222. <https://doi.org/10.1074/jbc.M109.000745>.
37. Harris, S.L.; Levine, A.J. The P53 Pathway: Positive and Negative Feedback Loops. *Oncogene* **2005**, *24*, 2899–2908. <https://doi.org/10.1038/sj.onc.1208615>.
38. Yeo-Teh, N.S.L.; Ito, Y.; Jha, S. High-Risk Human Papillomaviral Oncogenes E6 and E7 Target Key Cellular Pathways to Achieve Oncogenesis. *Int. J. Mol. Sci.* **2018**, *19*, 1706. <https://doi.org/10.3390/ijms19061706>.
39. O’Shaughnessy, R.F.L.; Akgül, B.; Storey, A.; Pfister, H.; Harwood, C.A.; Byrne, C. Cutaneous Human Papillomaviruses Down-Regulate AKT1, Whereas AKT2 up-Regulation and Activation Associates with Tumors. *Cancer Res.* **2007**, *67*, 8207–8215. <https://doi.org/10.1158/0008-5472.CAN-07-0755>.
40. Tomlins, C.; Storey, A. Cutaneous HPV5 E6 Causes Increased Expression of Osteoprotegerin and Interleukin 6 Which Contribute to Evasion of UV-Induced Apoptosis. *Carcinogenesis* **2010**, *31*, 2155–2164. <https://doi.org/10.1093/carcin/bgq200>.
41. Jackson, S.; Harwood, C.; Thomas, M.; Banks, L.; Storey, A. Role of Bak in UV-Induced Apoptosis in Skin Cancer and Abrogation by HPV E6 Proteins. *Genes Dev.* **2000**, *14*, 3065–3073. <https://doi.org/10.1101/gad.182100>.
42. Wallace, N.A.; Robinson, K.; Howie, H.L.; Galloway, D.A. HPV 5 and 8 E6 Abrogate ATR Activity Resulting in Increased Persistence of UVB Induced DNA Damage. *PLoS Pathog.* **2012**, *8*, e1002807. <https://doi.org/10.1371/journal.ppat.1002807>.
43. Snow, J.A.; Murthy, V.; Dacus, D.; Hu, C.; Wallace, N.A. β -HPV 8E6 Attenuates ATM and ATR Signaling in Response to UV Damage. *Pathogens* **2019**, *8*, 267. <https://doi.org/10.3390/pathogens8040267>.
44. Giampieri, S.; Storey, A. Repair of UV-Induced Thymine Dimers Is Compromised in Cells Expressing the E6 Protein from Human Papillomaviruses Types 5 and 18. *Br. J. Cancer* **2004**, *90*, 2203–2209. <https://doi.org/10.1038/sj.bjc.6601829>.
45. Howie, H.L.; Koop, J.I.; Weese, J.; Robinson, K.; Wipf, G.; Kim, L.; Galloway, D.A. Beta-HPV 5 and 8 E6 Promote P300 Degradation by Blocking AKT/P300 Association. *PLoS Pathog.* **2011**, *7*, e1002211. <https://doi.org/10.1371/journal.ppat.1002211>.
46. Wallace, N.A.; Robinson, K.; Galloway, D.A. Beta Human Papillomavirus E6 Expression Inhibits Stabilization of P53 and Increases Tolerance of Genomic Instability. *J. Virol.* **2014**, *88*, 6112–6127. <https://doi.org/10.1128/JVI.03808-13>.
47. Marcuzzi, G.P.; Hufbauer, M.; Kasper, H.U.; Weißenborn, S.J.; Smola, S.; Pfister, H. Spontaneous Tumour Development in Human Papillomavirus Type 8 E6 Transgenic Mice and Rapid Induction by UV-Light Exposure and Wounding. *J. Gen. Virol.* **2009**, *90*, 2855–2864. <https://doi.org/10.1099/vir.0.012872-0>.

48. Schaper, I.D.; Marcuzzi, G.P.; Weissenborn, S.J.; Kasper, H.U.; Dries, V.; Smyth, N.; Fuchs, P.; Pfister, H. Development of Skin Tumors in Mice Transgenic for Early Genes of Human Papillomavirus Type 8. *Cancer Res.* **2005**, *65*, 1394–1400. <https://doi.org/10.1158/0008-5472.CAN-04-3263>.
49. Michel, A.; Kopp-Schneider, A.; Zentgraf, H.; Gruber, A.D.; de Villiers, E.-M. E6/E7 Expression of Human Papillomavirus Type 20 (HPV-20) and HPV-27 Influences Proliferation and Differentiation of the Skin in UV-Irradiated SKH-Hr1 Transgenic Mice. *J. Virol.* **2006**, *80*, 11153–11164. <https://doi.org/10.1128/JVI.00954-06>.
50. Viarisio, D.; Mueller-Decker, K.; Kloz, U.; Aengeneyndt, B.; Kopp-Schneider, A.; Gröne, H.-J.; Gheit, T.; Flechtenmacher, C.; Gissmann, L.; Tommasino, M. E6 and E7 from Beta Hpv38 Cooperate with Ultraviolet Light in the Development of Actinic Keratosis-Like Lesions and Squamous Cell Carcinoma in Mice. *PLoS Pathog.* **2011**, *7*, e1002125. <https://doi.org/10.1371/journal.ppat.1002125>.
51. Buitrago-Pérez, Á.; Hachimi, M.; Dueñas, M.; Lloveras, B.; Santos, A.; Holguín, A.; Duarte, B.; Santiago, J.L.; Akgül, B.; Rodríguez-Peralto, J.L.; et al. A Humanized Mouse Model of HPV-Associated Pathology Driven by E7 Expression. *PLoS ONE* **2012**, *7*, e41743. <https://doi.org/10.1371/journal.pone.0041743>.
52. Viarisio, D.; Robitaille, A.; Müller-Decker, K.; Flechtenmacher, C.; Gissmann, L.; Tommasino, M. Cancer Susceptibility of Beta HPV49 E6 and E7 Transgenic Mice to 4-Nitroquinoline 1-Oxide Treatment Correlates with Mutational Signatures of Tobacco Exposure. *Virology* **2019**, *538*, 53–60. <https://doi.org/10.1016/j.virol.2019.09.010>.
53. Viarisio, D.; Müller-Decker, K.; Zanna, P.; Kloz, U.; Aengeneyndt, B.; Accardi, R.; Flechtenmacher, C.; Gissmann, L.; Tommasino, M. Novel SS-HPV49 Transgenic Mouse Model of Upper Digestive Tract Cancer. *Cancer Res.* **2016**, *76*, 4216–4225. <https://doi.org/10.1158/0008-5472.CAN-16-0370>.
54. Heuser, S.; Hufbauer, M.; Steiger, J.; Marshall, J.; Sterner-Kock, A.; Mauch, C.; Zigrino, P.; Akgül, B. The Fibronectin/A3β1 Integrin Axis Serves as Molecular Basis for Keratinocyte Invasion Induced by BHPV. *Oncogene* **2016**, *35*, 4529–4539. <https://doi.org/10.1038/onc.2015.512>.
55. Heuser, S.; Hufbauer, M.; Marx, B.; Tok, A.; Majewski, S.; Pfister, H.; Akgül, B. The Levels of Epithelial Anchor Proteins β-Catenin and Zona Occludens-1 Are Altered by E7 of Human Papillomaviruses 5 and 8. *J. Gen. Virol.* **2016**, *97*, 463–472. <https://doi.org/10.1099/jgv.0.000363>.
56. Hufbauer, M.; Lazić, D.; Akgül, B.; Brandsma, J.L.; Pfister, H.; Weissenborn, S.J. Enhanced Human Papillomavirus Type 8 Oncogene Expression Levels Are Crucial for Skin Tumorigenesis in Transgenic Mice. *Virology* **2010**, *403*, 128–136. <https://doi.org/10.1016/j.virol.2010.04.013>.
57. Hasche, D.; Stephan, S.; Braspenning-Wesch, I.; Mikulec, J.; Niebler, M.; Gröne, H.-J.; Flechtenmacher, C.; Akgül, B.; Rösl, F.; Vinzón, S.E. The Interplay of UV and Cutaneous Papillomavirus Infection in Skin Cancer Development. *PLoS Pathog.* **2017**, *13*, e1006723. <https://doi.org/10.1371/journal.ppat.1006723>.
58. Akgül, B.; Kirschberg, M.; Storey, A.; Hufbauer, M. Human Papillomavirus Type 8 Oncoproteins E6 and E7 Cooperate in Downregulation of the Cellular Checkpoint Kinase-1. *Int. J. Cancer* **2019**, *145*, 797–806. <https://doi.org/10.1002/ijc.32223>.
59. Akgül, B.; Pfefferle, R.; Marcuzzi, G.P.; Zigrino, P.; Krieg, T.; Pfister, H.; Mauch, C. Expression of Matrix Metalloproteinase (MMP)-2, MMP-9, MMP-13, and MT1-MMP in Skin Tumors of Human Papillomavirus Type 8 Transgenic Mice. *Exp. Dermatol.* **2006**, *15*, 35–42. <https://doi.org/10.1111/j.0906-6705.2005.00387.x>.

60. Lazić, D.; Alborzi, F.; Marcuzzi, G.P.; Angel, P.; Hess, J.; Pfister, H.; Akgül, B. Enhanced StefinA and Sprr2 Expression during Papilloma Formation in HPV8 Transgenic Mice. *J. Dermatol. Sci.* **2011**, *62*, 84–90. <https://doi.org/10.1016/j.jdermsci.2011.02.006>.
61. Hufbauer, M.; Lazić, D.; Reinartz, M.; Akgül, B.; Pfister, H.; Weissenborn, S.J. Skin Tumor Formation in Human Papillomavirus 8 Transgenic Mice Is Associated with a Deregulation of Oncogenic MiRNAs and Their Tumor Suppressive Targets. *J. Dermatol. Sci.* **2011**, *64*, 7–15. <https://doi.org/10.1016/j.jdermsci.2011.06.008>.
62. Uberoi, A.; Lambert, P.F. Rodent Papillomaviruses. *Viruses* **2017**, *9*, E362. <https://doi.org/10.3390/v9120362>.
63. Yu, L.; Majerciak, V.; Xue, X.-Y.; Uberoi, A.; Lobanov, A.; Chen, X.; Cam, M.; Hughes, S.H.; Lambert, P.F.; Zheng, Z.-M. Mouse Papillomavirus Type 1 (MmuPV1) DNA Is Frequently Integrated in Benign Tumors by Microhomology-Mediated End-Joining. *PLoS Pathog.* **2021**, *17*, e1009812. <https://doi.org/10.1371/journal.ppat.1009812>.
64. Meyers, J.M.; Uberoi, A.; Grace, M.; Lambert, P.F.; Munger, K. Cutaneous HPV8 and MmuPV1 E6 Proteins Target the NOTCH and TGF- β Tumor Suppressors to Inhibit Differentiation and Sustain Keratinocyte Proliferation. *PLoS Pathog.* **2017**, *13*, e1006171. <https://doi.org/10.1371/journal.ppat.1006171>.
65. Xue, X.-Y.; Majerciak, V.; Uberoi, A.; Kim, B.-H.; Gotte, D.; Chen, X.; Cam, M.; Lambert, P.F.; Zheng, Z.-M. The Full Transcription Map of Mouse Papillomavirus Type 1 (MmuPV1) in Mouse Wart Tissues. *PLoS Pathog.* **2017**, *13*, e1006715. <https://doi.org/10.1371/journal.ppat.1006715>.
66. Uberoi, A.; Yoshida, S.; Frazer, I.H.; Pitot, H.C.; Lambert, P.F. Role of Ultraviolet Radiation in Papillomavirus-Induced Disease. *PLoS Pathog.* **2016**, *12*, e1005664. <https://doi.org/10.1371/journal.ppat.1005664>.
67. Chang, H.H.Y.; Pannunzio, N.R.; Adachi, N.; Lieber, M.R. Non-Homologous DNA End Joining and Alternative Pathways to Double-Strand Break Repair. *Nat. Rev. Mol. Cell Biol.* **2017**, *18*, 495–506. <https://doi.org/10.1038/nrm.2017.48>.
68. Dacus, D.; Wallace, N.A. Beta-Genus Human Papillomavirus 8 E6 Destabilizes the Host Genome by Promoting P300 Degradation. *Viruses* **2021**, *13*, 1662. <https://doi.org/10.3390/v13081662>.
69. Iliakis, G.; Murmann, T.; Soni, A. Alternative End-Joining Repair Pathways Are the Ultimate Backup for Abrogated Classical Non-Homologous End-Joining and Homologous Recombination Repair: Implications for the Formation of Chromosome Translocations. *Mutat. Res./Genet. Toxicol. Environ. Mutagenesis* **2015**, *793*, 166–175. <https://doi.org/10.1016/j.mrgentox.2015.07.001>.
70. Beucher, A.; Birraux, J.; Tchouandong, L.; Barton, O.; Shibata, A.; Conrad, S.; Goodarzi, A.A.; Krempler, A.; Jeggo, P.A.; Löbrich, M. ATM and Artemis Promote Homologous Recombination of Radiation-induced DNA Double-strand Breaks in G2. *EMBO J.* **2009**, *28*, 3413–3427. <https://doi.org/10.1038/emboj.2009.276>.
71. Lee, J.-H.; Paull, T.T. ATM Activation by DNA Double-Strand Breaks through the Mre11-Rad50-Nbs1 Complex. *Science* **2005**, *308*, 551–554. <https://doi.org/10.1126/science.1108297>.
72. Bakr, A.; Oing, C.; Köcher, S.; Borgmann, K.; Dornreiter, I.; Petersen, C.; Dikomey, E.; Mansour, W.Y. Involvement of ATM in Homologous Recombination after End Resection and RAD51 Nucleofilament Formation. *Nucleic Acids Res.* **2015**, *43*, 3154–3166. <https://doi.org/10.1093/nar/gkv160>.
73. Zellweger, R.; Dalcher, D.; Mutreja, K.; Berti, M.; Schmid, J.A.; Herrador, R.; Vindigni, A.; Lopes, M. Rad51-Mediated Replication Fork Reversal Is a Global Response to Genotoxic

- Treatments in Human Cells. *J. Cell Biol.* **2015**, *208*, 563–579. <https://doi.org/10.1083/jcb.201406099>.
74. Cai, M.-Y.; Dunn, C.E.; Chen, W.; Kochupurakkal, B.S.; Nguyen, H.; Moreau, L.A.; Shapiro, G.I.; Parmar, K.; Kozono, D.; D'Andrea, A.D. Cooperation of the ATM and Fanconi Anemia/BRCA Pathways in Double-Strand Break End Resection. *Cell Rep.* **2020**, *30*, 2402–2415.e5. <https://doi.org/10.1016/j.celrep.2020.01.052>.
 75. Zhao, F.; Kim, W.; Kloeber, J.A.; Lou, Z. DNA End Resection and Its Role in DNA Replication and DSB Repair Choice in Mammalian Cells. *Exp. Mol. Med.* **2020**, *52*, 1705–1714. <https://doi.org/10.1038/s12276-020-00519-1>.
 76. Lamarche, B.J.; Orazio, N.I.; Weitzman, M.D. The MRN Complex in Double-Strand Break Repair and Telomere Maintenance. *FEBS Lett.* **2010**, *584*, 3682–3695. <https://doi.org/10.1016/j.febslet.2010.07.029>.
 77. Liu, T.; Huang, J. DNA End Resection: Facts and Mechanisms. *Genom. Proteom. Bioinform.* **2016**, *14*, 126–130. <https://doi.org/10.1016/j.gpb.2016.05.002>.
 78. Pathania, S.; Nguyen, J.; Hill, S.J.; Scully, R.; Feunteun, J.; Livingston, D.M. BRCA1 Is Required for Post-Replication Repair after UV-Induced DNA Damage. *Mol. Cell* **2011**, *44*, 235–251. <https://doi.org/10.1016/j.molcel.2011.09.002>.
 79. Prakash, R.; Zhang, Y.; Feng, W.; Jasin, M. Homologous Recombination and Human Health: The Roles of BRCA1, BRCA2, and Associated Proteins. *Cold Spring Harb. Perspect. Biol.* **2015**, *7*, a016600. <https://doi.org/10.1101/cshperspect.a016600>.
 80. Godin, S.K.; Sullivan, M.R.; Bernstein, K.A. Novel Insights into RAD51 Activity and Regulation during Homologous Recombination and DNA Replication. *Biochem. Cell Biol.* **2016**, *94*, 407–418. <https://doi.org/10.1139/bcb-2016-0012>.
 81. Rossi, M.J.; Mazin, A.V. Rad51 Protein Stimulates the Branch Migration Activity of Rad54 Protein. *J. Biol. Chem.* **2008**, *283*, 24698–24706. <https://doi.org/10.1074/jbc.M800839200>.
 82. Bhat, K.P.; Cortez, D. RPA and RAD51: Fork Reversal, Fork Protection, and Genome Stability. *Nat. Struct. Mol. Biol.* **2018**, *25*, 446–453. <https://doi.org/10.1038/s41594-018-0075-z>.
 83. Tavares, E.M.; Wright, W.D.; Heyer, W.-D.; Le Cam, E.; Dupaigne, P. In Vitro Role of Rad54 in Rad51-SsDNA Filament-Dependent Homology Search and Synaptic Complexes Formation. *Nat. Commun.* **2019**, *10*, 4058. <https://doi.org/10.1038/s41467-019-12082-z>.
 84. Wallace, N.A.; Robinson, K.; Howie, H.L.; Galloway, D.A. β -HPV 5 and 8 E6 Disrupt Homology Dependent Double Strand Break Repair by Attenuating BRCA1 and BRCA2 Expression and Foci Formation. *PLoS Pathog.* **2015**, *11*, e1004687. <https://doi.org/10.1371/journal.ppat.1004687>.
 85. Pierce, A.J.; Johnson, R.D.; Thompson, L.H.; Jasin, M. XRCC3 Promotes Homology-Directed Repair of DNA Damage in Mammalian Cells. *Genes Dev.* **1999**, *13*, 2633–2638.
 86. Hu, C.; Bugbee, T.; Dacus, D.; Palinski, R.; Wallace, N.A. Beta Human Papillomavirus 8 E6 Allows Colocalization of Non-Homologous End Joining and Homologous Recombination Repair Factors. *PLoS Pathog.* **2022**, *18*, e1010275. <https://doi.org/10.1371/journal.ppat.1010275>.
 87. Sollazzo, A.; Brzozowska, B.; Cheng, L.; Lundholm, L.; Scherthan, H.; Wojcik, A. Live Dynamics of 53BP1 Foci Following Simultaneous Induction of Clustered and Dispersed DNA Damage in U2OS Cells. *Int. J. Mol. Sci.* **2018**, *19*, 519. <https://doi.org/10.3390/ijms19020519>.
 88. Bunting, S.F.; Callén, E.; Wong, N.; Chen, H.-T.; Polato, F.; Gunn, A.; Bothmer, A.; Feldhahn, N.; Fernandez-Capetillo, O.; Cao, L.; et al. 53BP1 Inhibits Homologous Recombination in Brca1-Deficient Cells by Blocking Resection of DNA Breaks. *Cell* **2010**, *141*, 243–254. <https://doi.org/10.1016/j.cell.2010.03.012>.

89. Daley, J.M.; Sung, P. 53BP1, BRCA1, and the Choice between Recombination and End Joining at DNA Double-Strand Breaks. *Mol. Cell. Biol.* **2014**, *34*, 1380–1388. <https://doi.org/10.1128/MCB.01639-13>.
90. Bhargava, R.; Sandhu, M.; Muk, S.; Lee, G.; Vaidehi, N.; Stark, J.M. C-NHEJ without Indels Is Robust and Requires Synergistic Function of Distinct XLF Domains. *Nat. Commun.* **2018**, *9*, 2484. <https://doi.org/10.1038/s41467-018-04867-5>.
91. Davis, A.J.; Chen, B.P.C.; Chen, D.J. DNA-PK: A Dynamic Enzyme in a Versatile DSB Repair Pathway. *DNA Repair* **2014**, *17*, 21–29. <https://doi.org/10.1016/j.dnarep.2014.02.020>.
92. Pierce, A.J.; Hu, P.; Han, M.; Ellis, N.; Jasin, M. Ku DNA End-Binding Protein Modulates Homologous Repair of Double-Strand Breaks in Mammalian Cells. *Genes Dev.* **2001**, *15*, 3237–3242. <https://doi.org/10.1101/gad.946401>.
93. Goodarzi, A.A.; Yu, Y.; Riballo, E.; Douglas, P.; Walker, S.A.; Ye, R.; Härer, C.; Marchetti, C.; Morrice, N.; Jeggo, P.A.; et al. DNA-PK Autophosphorylation Facilitates Artemis Endonuclease Activity. *EMBO J.* **2006**, *25*, 3880–3889. <https://doi.org/10.1038/sj.emboj.7601255>.
94. Drouet, J.; Delteil, C.; Lefrançois, J.; Concannon, P.; Salles, B.; Calsou, P. DNA-Dependent Protein Kinase and XRCC4-DNA Ligase IV Mobilization in the Cell in Response to DNA Double Strand Breaks. *J. Biol. Chem.* **2005**, *280*, 7060–7069. <https://doi.org/10.1074/jbc.M410746200>.
95. Soubeyrand, S.; Pope, L.; De Chasseval, R.; Gosselin, D.; Dong, F.; de Villartay, J.-P.; Haché, R.J.G. Artemis Phosphorylated by DNA-Dependent Protein Kinase Associates Preferentially with Discrete Regions of Chromatin. *J. Mol. Biol.* **2006**, *358*, 1200–1211. <https://doi.org/10.1016/j.jmb.2006.02.061>.
96. Li, S.; Chang, H.H.; Niewolik, D.; Hedrick, M.P.; Pinkerton, A.B.; Hassig, C.A.; Schwarz, K.; Lieber, M.R. Evidence That the DNA Endonuclease ARTEMIS Also Has Intrinsic 5'-Exonuclease Activity. *J. Biol. Chem.* **2014**, *289*, 7825–7834. <https://doi.org/10.1074/jbc.M113.544874>.
97. Niewolik, D.; Peter, I.; Butscher, C.; Schwarz, K. Autoinhibition of the Nuclease ARTEMIS Is Mediated by a Physical Interaction between Its Catalytic and C-Terminal Domains. *J. Biol. Chem.* **2017**, *292*, 3351–3365. <https://doi.org/10.1074/jbc.M116.770461>.
98. Francis, D.B.; Kozlov, M.; Chavez, J.; Chu, J.; Malu, S.; Hanna, M.; Cortes, P. DNA Ligase IV Regulates XRCC4 Nuclear Localization. *DNA Repair* **2014**, *21*, 36–42. <https://doi.org/10.1016/j.dnarep.2014.05.010>.
99. Hu, C.; Bugbee, T.; Gamez, M.; Wallace, N.A. Beta Human Papillomavirus 8E6 Attenuates Non-Homologous End Joining by Hindering DNA-PKcs Activity. *Cancers* **2020**, *12*, 2356. <https://doi.org/10.3390/cancers12092356>.
100. Bhargava, R.; Lopezcolorado, F.W.; Tsai, L.J.; Stark, J.M. The Canonical Non-Homologous End Joining Factor XLF Promotes Chromosomal Deletion Rearrangements in Human Cells. *J. Biol. Chem.* **2020**, *295*, 125–137. <https://doi.org/10.1074/jbc.RA119.010421>.
101. Patterson-Fortin, J.; D'Andrea, A.D. Exploiting the Microhomology-Mediated End-Joining Pathway in Cancer Therapy. *Cancer Res.* **2020**, *80*, 4593–4600. <https://doi.org/10.1158/0008-5472.CAN-20-1672>.
102. He, H.; Wang, J.; Liu, T. UV-Induced RPA1 Acetylation Promotes Nucleotide Excision Repair. *Cell Rep.* **2017**, *20*, 2010–2025. <https://doi.org/10.1016/j.celrep.2017.08.016>.
103. Rapp, A.; Greulich, K.O. After Double-Strand Break Induction by UV-A, Homologous Recombination and Nonhomologous End Joining Cooperate at the Same DSB If Both Systems Are Available. *J. Cell Sci.* **2004**, *117*, 4935–4945. <https://doi.org/10.1242/jcs.01355>.

104. Borrego-Soto, G.; Ortiz-López, R.; Rojas-Martínez, A. Ionizing Radiation-Induced DNA Injury and Damage Detection in Patients with Breast Cancer. *Genet. Mol. Biol.* **2015**, *38*, 420–432. <https://doi.org/10.1590/S1415-475738420150019>.
105. Labay, E.; Efimova, E.V.; Quarshie, B.K.; Golden, D.W.; Weichselbaum, R.R.; Kron, S.J. Ionizing Radiation-Induced Foci Persistence Screen to Discover Enhancers of Accelerated Senescence. *Int. J. High Throughput Screen.* **2011**, *2*, 1–13. <https://doi.org/10.2147/IJHTS.S17076>.
106. Cooke, M.S.; Evans, M.D.; Dizdaroglu, M.; Lunec, J. Oxidative DNA Damage: Mechanisms, Mutation, and Disease. *FASEB J.* **2003**, *17*, 1195–1214. <https://doi.org/10.1096/fj.02-0752rev>.
107. Azzam, E.I.; Jay-Gerin, J.-P.; Pain, D. Ionizing Radiation-Induced Metabolic Oxidative Stress and Prolonged Cell Injury. *Cancer Lett.* **2012**, *327*, 48–60. <https://doi.org/10.1016/j.canlet.2011.12.012>.
108. Tsukuda, M.; Miyazaki, K. DNA Fragmentation Caused by an Overdose of Zeocin. *J. Biosci. Bioeng.* **2013**, *116*, 644–646. <https://doi.org/10.1016/j.jbiosc.2013.05.004>.
109. Chen, J.; Ghorai, M.K.; Kenney, G.; Stubbe, J. Mechanistic Studies on Bleomycin-Mediated DNA Damage: Multiple Binding Modes Can Result in Double-Stranded DNA Cleavage. *Nucleic Acids Res.* **2008**, *36*, 3781–3790. <https://doi.org/10.1093/nar/gkn302>.
110. Driessens, N.; Versteijhe, S.; Ghaddhab, C.; Burniat, A.; Deken, X.D.; Sande, J.V.; Dumont, J.-E.; Miot, F.; Corvilain, B. Hydrogen Peroxide Induces DNA Single- and Double-Strand Breaks in Thyroid Cells and Is Therefore a Potential Mutagen for This Organ. *Endocr.-Relat. Cancer* **2009**, *16*, 845–856. <https://doi.org/10.1677/ERC-09-0020>.
111. Shiloh, Y.; van der Schans, G.P.; Lohman, P.H.; Becker, Y. Induction and Repair of DNA Damage in Normal and Ataxia-Telangiectasia Skin Fibroblasts Treated with Neocarzinostatin. *Carcinogenesis* **1983**, *4*, 917–921. <https://doi.org/10.1093/carcin/4.7.917>.
112. Bellaïche, Y.; Mogila, V.; Perrimon, N. I-SceI Endonuclease, a New Tool for Studying DNA Double-Strand Break Repair Mechanisms in Drosophila. *Genetics* **1999**, *152*, 1037–1044.
113. Janssen, J.M.; Chen, X.; Liu, J.; Gonçalves, M.A.F.V. The Chromatin Structure of CRISPR-Cas9 Target DNA Controls the Balance between Mutagenic and Homology-Directed Gene-Editing Events. *Mol. Ther.-Nucleic Acids* **2019**, *16*, 141–154. <https://doi.org/10.1016/j.omtn.2019.02.009>.
114. Hu, C.; Doerksen, T.; Bugbee, T.; Wallace, N.; Palinski, R. Using Next Generation Sequencing to Identify Mutations Associated with Repair of a CAS9-Induced Double Strand Break Near the CD4 Promoter|Protocol. *JoVE J. Vis. Exp.* **2022**, *181*, e62583, <https://doi.org/10.3791/62583>.
115. Chen, J.-J.; Silver, D.; Cantor, S.; Livingston, D.M.; Scully, R. BRCA1, BRCA2, and Rad51 Operate in a Common DNA Damage Response Pathway. *Cancer Res.* **1999**, *6* (Suppl. S7), 1752s–1756s.
116. Polo, S.E.; Jackson, S.P. Dynamics of DNA Damage Response Proteins at DNA Breaks: A Focus on Protein Modifications. *Genes Dev.* **2011**, *25*, 409–433. <https://doi.org/10.1101/gad.2021311>.
117. Pilié, P.G.; Tang, C.; Mills, G.B.; Yap, T.A. State-of-the-Art Strategies for Targeting the DNA Damage Response in Cancer. *Nat. Rev. Clin. Oncol.* **2019**, *16*, 81–104. <https://doi.org/10.1038/s41571-018-0114-z>.
118. Al-Hakim, A.; Escribano-Diaz, C.; Landry, M.-C.; O'Donnell, L.; Panier, S.; Szilard, R.K.; Durocher, D. The Ubiquitous Role of Ubiquitin in the DNA Damage Response. *DNA Repair* **2010**, *9*, 1229–1240. <https://doi.org/10.1016/j.dnarep.2010.09.011>.

119. Butler, T.A.J.; Paul, J.W.; Chan, E.-C.; Smith, R.; Tolosa, J.M. Misleading Westerns: Common Quantification Mistakes in Western Blot Densitometry and Proposed Corrective Measures. *BioMed. Res. Int.* **2019**, *2019*, e5214821. <https://doi.org/10.1155/2019/5214821>.
120. Murthy, V.; Dacus, D.; Gamez, M.; Hu, C.; Wendel, S.O.; Snow, J.; Kahn, A.; Walterhouse, S.H.; Wallace, N.A. Characterizing DNA Repair Processes at Transient and Long-Lasting Double-Strand DNA Breaks by Immunofluorescence Microscopy. *JoVE J. Vis. Exp.* **2018**, *136*, e57653. <https://doi.org/10.3791/57653>.
121. Yang, X.; Zou, P.; Yao, J.; Yun, D.; Bao, H.; Du, R.; Long, J.; Chen, X. Proteomic Dissection of Cell Type-Specific H2AX-Interacting Protein Complex Associated with Hepatocellular Carcinoma. *J. Proteome Res.* **2010**, *9*, 1402–1415. <https://doi.org/10.1021/pr900932y>.
122. Kuo, L.J.; Yang, L.-X. γ -H2AX—A Novel Biomarker for DNA Double-Strand Breaks. *In Vivo.* **2008**, *22*, 305–309.
123. Rogakou, E.P.; Pilch, D.R.; Orr, A.H.; Ivanova, V.S.; Bonner, W.M. DNA Double-Stranded Breaks Induce Histone H2AX Phosphorylation on Serine 139. *J. Biol. Chem.* **1998**, *273*, 5858–5868. <https://doi.org/10.1074/jbc.273.10.5858>.
124. Gudas, J.M.; Payton, M.; Thukral, S.; Chen, E.; Bass, M.; Robinson, M.O.; Coats, S. Cyclin E2, a Novel G1 Cyclin That Binds Cdk2 and Is Aberrantly Expressed in Human Cancers. *Mol. Cell Biol.* **1999**, *19*, 612–622.
125. Perkins, N.D.; Felzien, L.K.; Betts, J.C.; Leung, K.; Beach, D.H.; Nabel, G.J. Regulation of NF-KappaB by Cyclin-Dependent Kinases Associated with the P300 Coactivator. *Science* **1997**, *275*, 523–527. <https://doi.org/10.1126/science.275.5299.523>.
126. Yam, C.H.; Fung, T.K.; Poon, R.Y.C. Cyclin A in Cell Cycle Control and Cancer. *Cell Mol. Life Sci.* **2002**, *59*, 1317–1326. <https://doi.org/10.1007/s00018-002-8510-y>.
127. Shahar, O.D.; Raghu Ram, E.V.S.; Shimshoni, E.; Hareli, S.; Meshorer, E.; Goldberg, M. Live Imaging of Induced and Controlled DNA Double-Strand Break Formation Reveals Extremely Low Repair by Homologous Recombination in Human Cells. *Oncogene* **2012**, *31*, 3495–3504. <https://doi.org/10.1038/onc.2011.516>.
128. Kong, X.; Wakida, N.M.; Yokomori, K. Application of Laser Microirradiation in the Investigations of Cellular Responses to DNA Damage. *Front. Phys.* **2021**, *8*, 597866.
129. Gassman, N.R.; Wilson, S.H. Micro-Irradiation Tools to Visualize Base Excision Repair and Single-Strand Break Repair. *DNA Repair* **2015**, *31*, 52–63. <https://doi.org/10.1016/j.dnarep.2015.05.001>.
130. Kobayashi, W.; Sekine, S.; Machida, S.; Kurumizaka, H. Green Fluorescent Protein Fused to the C Terminus of RAD51 Specifically Interferes with Secondary DNA Binding by the RAD51-SsDNA Complex. *Genes Genet. Syst.* **2014**, *89*, 169–179. <https://doi.org/10.1266/ggs.89.169>.
131. Cole, N.B. Site-Specific Protein Labeling with SNAP-Tags. *Curr. Protoc. Protein Sci.* **2013**, *73*, 30.1.1–30.1.16. <https://doi.org/10.1002/0471140864.ps3001s73>.
132. Erdmann, R.S.; Baguley, S.W.; Richens, J.H.; Wissner, R.F.; Xi, Z.; Allgeyer, E.S.; Zhong, S.; Thompson, A.D.; Lowe, N.; Butler, R.; et al. Labeling Strategies Matter for Super-Resolution Microscopy: A Comparison between HaloTags and SNAP-Tags. *Cell Chem. Biol.* **2019**, *26*, 584–592.e6. <https://doi.org/10.1016/j.chembiol.2019.01.003>.
133. Vitor, A.C.; Huertas, P.; Legube, G.; de Almeida, S.F. Studying DNA Double-Strand Break Repair: An Ever-Growing Toolbox. *Front. Mol. Biosci.* **2020**, *7*, 24. <https://doi.org/10.3389/fmolb.2020.00024>.
134. Smith, B.A.; Smith, B.D. Biomarkers and Molecular Probes for Cell Death Imaging and Targeted Therapeutics. *Bioconjug. Chem.* **2012**, *23*, 1989–2006. <https://doi.org/10.1021/bc3003309>.

135. Bennardo, N.; Cheng, A.; Huang, N.; Stark, J.M. Alternative-NHEJ Is a Mechanistically Distinct Pathway of Mammalian Chromosome Break Repair. *PLoS Genet.* **2008**, *4*, e1000110. <https://doi.org/10.1371/journal.pgen.1000110>.
136. Tsai, L.J.; Lopezcolorado, F.W.; Bhargava, R.; Mendez-Dorantes, C.; Jahanshir, E.; Stark, J.M. RNF8 Has Both KU-Dependent and Independent Roles in Chromosomal Break Repair. *Nucleic Acids Res.* **2020**, *48*, 6032–6052. <https://doi.org/10.1093/nar/gkaa380>.
137. Hustedt, N.; Durocher, D. The Control of DNA Repair by the Cell Cycle. *Nat. Cell Biol.* **2017**, *19*, 1–9. <https://doi.org/10.1038/ncb3452>.
138. Forment, J.V.; Walker, R.V.; Jackson, S.P. A High-Throughput, Flow Cytometry-Based Method to Quantify DNA-End Resection in Mammalian Cells. *Cytom. A* **2012**, *81A*, 922–928. <https://doi.org/10.1002/cyto.a.22155>.
139. Wallace, N.A.; Khanal, S.; Robinson, K.L.; Wendel, S.O.; Messer, J.J.; Galloway, D.A. High-Risk Alphas Papillomavirus Oncogenes Impair the Homologous Recombination Pathway. *J. Virol.* **2017**, *91*, e01084-17. <https://doi.org/10.1128/JVI.01084-17>.
140. Behjati, S.; Tarpey, P.S. What Is next Generation Sequencing? *Arch. Dis. Child. Educ. Pract. Ed.* **2013**, *98*, 236–238. <https://doi.org/10.1136/archdischild-2013-304340>.
141. Perner, J.; Abbas, S.; Nowicki-Osuch, K.; Devonshire, G.; Eldridge, M.D.; Tavaré, S.; Fitzgerald, R.C. The MutREAD Method Detects Mutational Signatures from Low Quantities of Cancer DNA. *Nat. Commun.* **2020**, *11*, 3166. <https://doi.org/10.1038/s41467-020-16974-3>.
142. Banerjee, N.S.; Moore, D.; Parker, C.J.; Broker, T.R.; Chow, L.T. Targeting DNA Damage Response as a Strategy to Treat HPV Infections. *Int. J. Mol. Sci.* **2019**, *20*, 5455. <https://doi.org/10.3390/ijms20215455>.

Table 1-1. Reporters to measure specific DSB repair pathway. Reporter column lists common names for different DSB repair reporters. DSB induction column lists enzymes used to induce DSBs for each reporter. Pathway and Readout column lists the DSB repair pathway(s) measured by each reporter and the signal activated the pathway(s). Reference column lists the original publications where the reporters are described.

Reporter	DSB induction	Pathway and readout	Reference
DR-GFP	I-SCE1	HR restores GFP	[80]
EJ2-GFP	I-SCE1	Alt-EJ restores GFP	[128]
EJ5-GFP	I-SCE1	NHE/Alt-EJ restores GFP	[4]
EJ7-GFP	sgRNA/CAS9	NHEJ restores GFP	[5]
4- μ HOM	sgRNA/CAS9	Alt-EJ restores GFP	[5,6]
EJ-CD4	sgRNA/CAS9	NHEJ activates CD4	[7]

Chapter 2 - Beta Human Papillomavirus 8E6 Attenuates Non-Homologous End Joining by Hindering DNA-PKcs Activity

Changkun Hu 1, Taylor Bugbee 1, Monica Gamez 2 and Nicholas A. Wallace 1,*

1. Division of Biology, Kansas State University, Manhattan, Kansas, USA;

2. Bristol Medical School, Translational Health Sciences, University of Bristol, Bristol,

BS1 3NY United Kingdom

* Correspondence: nwallac@ksu.edu

Published: Hu C, Bugbee T, Gamez M, Wallace NA. Beta Human Papillomavirus 8E6 Attenuates Non-Homologous End Joining by Hindering DNA-PKcs Activity. *Cancers*. 2020; 12(9):2356. <https://doi.org/10.3390/cancers12092356>

Abstract

Cutaneous viral infections occur in a background of near continual exposure to environmental genotoxins, like the UV radiation in sunlight. Failure to repair damaged DNA is an established driver of tumorigenesis and substantial cellular resources are devoted to repairing DNA lesions. Beta-human papillomaviruses (β -HPVs) attenuate DNA repair signaling. However, their role in human disease is unclear. Some have proposed that β -HPV promotes tumorigenesis, while others suggest that β -HPV protects against skin cancer. Most of the molecular evidence that β -HPV impairs DNA repair has been gained via characterization of the E6 protein from β -HPV 8 (β -HPV 8E6). β -HPV 8E6 hinders DNA repair by binding and destabilizing p300, a transcription factor for multiple DNA repair genes. By reducing p300 availability, β -HPV 8E6

attenuates a major double strand DNA break (DSB) repair pathway, homologous recombination. Here, β -HPV 8E6 impairs another DSB repair pathway, non-homologous end joining (NHEJ). Specifically, β -HPV 8E6 acts by attenuating DNA-dependent protein kinase (DNA-PK) activity, a critical NHEJ kinase. This includes DNA-PK activation and downstream of steps in the pathway associated with DNA-PK activity. Notably, β -HPV 8E6 inhibits NHEJ through p300 dependent and independent means. Together, these data expand the known genome destabilizing capabilities of β -HPV 8E6.

Keywords: Human Papillomavirus; HPV; DNA Repair; Double Strand Breaks; Non-Homologous End Joining

1. Introduction

Human papillomavirus (HPV) is a small double-stranded DNA virus family that infects mucosal and cutaneous epithelia. Currently, about 400 types of HPV have been identified [1]. This family is classified into five genera (alpha, beta, gamma, mu, and nu) based on the sequence of the L1 capsid gene [2–5]. Of these genera, the alpha genus of HPV has been most thoroughly characterized because members of this genus cause cervical cancer, head and neck cancer, and genital warts [2,4,6]. Despite their widespread presence in the skin, the contribution of members of the beta genus of HPV (β -HPV) to human disease is unclear. β -HPVs were first isolated from patients with a rare genetic disorder, epidermodysplasia verruciformis (EV) [5,7]. In these individuals and people receiving immunosuppressive drugs after organ transplants, β -HPVs appear to promote non-melanoma skin cancer (NMSC) [5,8]. An array of in vivo and in vitro studies also support the role of β -HPVs in promoting NMSC [9,10].

However, there are questions about the oncogenic potential of β -HPV in the general population. In most immunocompetent individuals, β -HPV infections are transient [11]. Further,

β -HPV genes are rarely expressed in tumor tissue [12,13]. This ruled out traditional methods of viral oncogenesis where the tumor becomes dependent on continued viral gene expression and led to the so called “hit and run” hypothesis [13]. This hypothesis proposes that β -HPVs promote early stages of tumorigenesis by destabilizing the host genome, leading to mutations that could drive oncogenesis without continued viral gene expression [14]. Although feasible, the model is difficult to test. As a result, it remains unclear if/how frequently β -HPV infections contribute to NMSC. The “hit and run” model faced further challenges when a recent report suggested β -HPV infections protected against NMSC [15]. The widespread nature of these infections and their contentious role in tumorigenesis are strong motivating factors for ongoing research into the basic biology of the virus and its gene products.

Among β -HPV proteins, the E6 or β -HPV E6 is best characterized. This report focuses on the E6 from β -HPV 8 (β -HPV 8E6) and its ability to disrupt DNA repair [16–19]. β -HPV 8E6 exerts its influence in part by binding and destabilizing the cellular histone acetyltransferase, p300[20]. p300 is a transcription factor necessary for robust expression of key DNA repair proteins (ATM, ATR, BRCA1, and BRCA2)[16–18]. When β -HPV 8E6 is present, the reduced availability of these repair factors makes UV-induced DNA lesions more persistent [17,18]. The inability to resolve these lesions increases the frequency of replication fork collapse and the generation of UV-induced double stranded DNA breaks (DSBs) [18]. These breaks occur during S and G2 phases of the cell cycle when homologous recombination (HR) is the principle mechanism of DSB repair [21–25]. Despite increasing the need for HR, β -HPV 8E6 impairs the pathway by decreasing BRCA1 and BRCA2 expression and foci formation [16].

When HR fails, non-homologous end joining (NHEJ) serves as a backup repair mechanism. NHEJ is not restricted to any portion of the cell cycle but tends to occur when HR is

not available (i.e. G1 and early S phases) [26–30]. It is an error-prone pathway that initiates with 53BP1 binding to the DSB [31,32]. This simultaneously promotes NHEJ while restricting HR [32–37]. After 53BP1 binding, a heterodimer of Ku70 and Ku80 is recruited to the damaged site, tethering at the exposed DNA ends [27]. Next, DNA-dependent protein kinase catalytic subunit (DNA-PKcs) binds to the Ku dimer to form a holoenzyme, known as DNA-PK. Then, DNA-PKcs becomes activated by auto-phosphorylation (pDNA-PKcs) [38–40]. Once activated, pDNA-PKcs facilitates NHEJ by phosphorylating/activating downstream targets, included Artemis, XRCC4, and DNA ligase IV (LIG4) [40–44]. Artemis has both exonuclease and endonuclease activity that process DNA single-strand overhangs into blunt end NHEJ-ready substrates [45–47]. When overhanging DNA ends have been removed, the XRCC4-XLF-Ligase IV complex links the two DNA ends together [48,49].

Since limitations in HR are addressed with increases in NHEJ, it was reasonable to hypothesize that β -HPV 8E6 increased repair by NHEJ. However, this report presents contrary evidence to this idea. β -HPV 8E6 reduced NHEJ repair at a defined genomic location and reduced DNA-PKcs autophosphorylation. This culminated in more persistent DNA-PKcs foci and diminished pDNA-PKcs-dependent signaling events (phosphorylation of Artemis and XRCC4 repair complex formation). Interestingly, β -HPV 8E6 appears to diminish NHEJ activity through both p300-dependent and -independent mechanisms.

2. Results

2.1. β -HPV 8E6 decreases NHEJ efficiency.

We have previously shown that β -HPV 8E6 disrupts HR by destabilizing p300, a transcription factor for two HR genes (BRCA1 and BRCA2) [16]. NHEJ competes with HR for access to DSBs [26,50,51], suggesting that NHEJ may occur more frequently in cells expressing

β -HPV 8E6. To test this, we measured NHEJ efficiency using a recently described end-joining assay that uses CD4 expression as a readout [28]. In this assay, CAS9 endonucleases are used to create breaks in the human genome downstream of the GAPDH promoter and upstream of the CD4 exon. These genes are oriented in the same direction and sit ~0.25 Mb apart. When NHEJ repairs the breaks, it results in a recombination event where CD4 expression is driven by the GAPDH promoter (Figure 2-1A). The CD4 promoter is typically inactive in cells outside of the immune system, which provides a low background in many cell types [52]. This assay was verified by measuring NHEJ efficiency in U2OS cells. CD4 expression was detected by immunoblot and normalized to the abundance of FLAG-tagged CAS9 as a control for transfection efficiency (Figure 2-1B-C). As previously reported, expression of CAS9 endonucleases targeting GAPDH and CD4 lead to CD4 expression. The assay was further verified by treating U2OS cells with 10 μ M ATM inhibitor (KU55933) and 10 μ M DNA-PKcs inhibitor (NU7441) that are known to increase and decrease NHEJ, respectively [28,38]. As expected, KU55933 increased CD4 expression, while NU7441 decreased it (Figure 2-1B, 1C). Next, the impact of β -HPV 8E6 on NHEJ was determined in previously described U2OS cells expressing β -HPV 8E6 (U2OS β -HPV 8E6) or vector control (U2OS LXSJ). Unexpectedly, β -HPV 8E6 significantly decreased CD4 compared to U2OS LXSJ cells (Figure 2-1D, 1E). The p300-dependence of this phenotype was also probed in U2OS cells expressing a mutant β -HPV 8E6 (β -HPV Δ 8E6), where 5 amino acids responsible for p300 binding (Residues 132-136) were deleted [20]. NHEJ frequency was also decreased in these cells (U2OS β -HPV Δ 8E6) (Figure 1D,1E). Neither inhibitor nor expression of wild type or mutant β -HPV 8E6 significantly altered transfection efficiency (Supplemental Figure 2-1). To determine if these results were reproducible in a more physiological relevant cell line, the assay was repeated in a pair of

previously described telomerase immortalized human foreskin keratinocytes (HFK) cell lines [53]. Again, β -HPV 8E6 expressing HFK cells (HFK β -HPV 8E6) had reduced NHEJ efficiency compared with vector control HFK cells (HFK LXS_N, Figure 2-1F and 1G). Together, these data indicate that β -HPV 8E6 hinders NHEJ, through p300-independent mechanisms. However, they cannot rule out a role the possibility that β -HPV 8E6 also acts through a p300-dependent mechanism.

for using FLAG abundance. (F) Representative immunoblots showing CD4 expression in HFK LXS_N and HFK β -HPV 8 E6 after transfection with control (UT), FLAG-tagged SgRNA-CAS9 targeting CD4 (CD4), and FLAG-tagged SgRNA-CAS9 targeting GAPDH and FLAG-tagged SgRNA-CAS9 targeting CD4 (GAP/CD4). (G) Densitometry of immunoblots (n=3) from panel F. CD4 was normalized to β -actin as a loading control. Transfection efficiency was accounted for using FLAG abundance. All values are represented as mean \pm standard error from at least three independent experiments. Statistical differences between groups were measured by using Student's T-test. * indicates P<0.05. ** indicates P<0.01. ! indicates significant difference between transfection with SgRNA-CAS9 targeting CD4 and co-transfection with SgRNA-CAS9 targeting CD4 and GAPDH.

2.2. β -HPV 8E6 attenuates DNA-PKcs phosphorylation.

β -HPV 8E6 prevents repair of UV lesions and completion of HR by reducing the abundance of key repair factors (ATM, ATR, BRCA1 and BRCA2) [16–18]. This suggests that β -HPV 8E6 may act through a similar mechanism to impair NHEJ. To assess this possibility, the abundance of canonical NHEJ proteins was determined in HFK. In untreated HFK cells, β -HPV 8E6 did not decrease Ku80, DNA-PKcs, Artemis, XRCC4, or Ligase IV abundance (Supplemental figure 2-2). These data suggest that β -HPV 8E6 exerted its influence in a post-

translational manner, so DNA-PKcs activation (via autophosphorylation at S2056) was assessed in cells exposed to Zeocin, a radiomimetic [54,55]. This modification was chosen because phosphorylated DNA-PKcs or pDNA-PKcs is a well characterized and early step in NHEJ [39,56]. Cells were treated with designated Zeocin concentrations for 24 hours (Figure 2-2). pDNA-PKcs increased in a Zeocin dose-dependent manner in HFK LXS_N. However, this response was attenuated in HFK β -HPV 8E6 (Figure 2-2A and 2B, Supplemental figure 2-3A). Similar results were observed when the experiment was repeated in U2OS LXS_N and U2OS β -HPV 8E6 cells. However, U2OS expressing β -HPV Δ 8E6 (U2OS β -HPV Δ 8E6) behaved like U2OS LXS_N cells by increasing the proportion of activated DNA-PKcs in response to Zeocin exposure (Figure 2-2C and 2D). These data suggest that β -HPV 8E6 impairs DNA-PKcs activation in a p300-dependent manner. pDNA-PKcs and total DNA-PKcs were separately normalized to GAPDH (Supplemental figure 2-3). Consistently, β -HPV 8E6 attenuated DNA-PKcs phosphorylation in both HFK and U2OS. Zeocin exposure consistently decreased total DNA-PKcs. However, β -HPV 8E6 did not statistically significantly change this decrease (Supplemental figure 2-3B and 3D).

To probe the breadth of DNA-PKcs inhibition, another genotoxic reagent (hydrogen peroxide or H₂O₂) was used to activate NHEJ in U2OS LXS_N, U2OS β -HPV 8E6 and U2OS β -HPV Δ 8E6 cells. Unlike Zeocin, which induces breaks by intercalating into base pairs and causing cleavage, H₂O₂ generates DSBs by generating reactive oxygen species (ROS) [54,55]. This represents a more physiological type of DSB as ROS are caused by cell metabolism [57]. β -HPV 8E6 and β -HPV Δ 8E6 blunted pDNA-PKcs in response to H₂O₂ (Supplemental figure 2-4A and 4B).

To facilitate repair, pDNA-PKcs must localize to a DSBs. This localization results in complexes that are detectable as foci by immunofluorescence (IF) microscopy. These foci are indicative of ongoing repair. pDNA-PKcs foci were readily detected in untreated HFK LXS cells, but less frequent in HFK β -HPV 8E6 cells (Figure 2-3A and 3B). Prior reports found that β -HPV 8E6 increased the frequency of DSBs in untreated cells, suggesting that the reduced pDNA-PKcs foci are unlikely to indicate genomic stabilization [16]. An alternative explanation consistent with the data shown in figure 1 is that β -HPV 8E6 reduced the frequency of NHEJ. When repair complexes are not resolved, the repair proteins spread along nearby chromatin producing larger/brighter foci [58–60]. As a result, foci intensity was used as an indicator of repair efficiency (brighter foci indicate more persistent lesions). Consistent with NHEJ inhibition, β -HPV E6 increased pDNA-PKcs foci intensity in HFKs (Figure 3A and 3C). Similar results were obtained in U2OS cells (Figure 2-3D, 3E, 3F). Interestingly, β -HPV Δ 8E6 did not alter pDNA-PKcs foci prevalence or intensity (Figure 3D, 3E, and 3F). Together, our data suggest that β -HPV 8E6 hinders DNA-PKcs activation in a p300-dependent manner (Figure 2-1-3), but also can impair NHEJ through an p300-independent mechanism(s) (Figure 2-1D-E).

2.3. β -HPV 8E6 attenuates DNA-PKcs-dependent signaling.

To further determine the ability of β -HPV 8E6 to alter pDNA-PKcs signaling, DSBs were induced with Zeocin (10 μ g/ml) then observed with immunofluorescence microscopy. pDNA-PKcs foci appeared rapidly in HFK LXS cells and reached their maxima approximately one hour after Zeocin exposure (Figure 2-4A-B). Twenty-four hours later, the pDNA-PKcs foci had returned to background levels. β -HPV 8E6 did not alter the initial induction of pDNA-PKcs foci by Zeocin. However, pDNA-PKcs foci were significantly more persistent in HFK β -HPV 8E6 cells. Similar results were obtained in U2OS LXS and U2OS β -HPV 8E6 cells (Figure 2-

4C, 4D). Consistent with a p300-dependent mechanism, pDNA-PKcs foci kinetics were similar in U2OS β -HPV Δ 8E6 and U2OS LXS cells after Zeocin exposure (100 μ g/ml). Supporting the idea that pDNA-PKcs foci represent active repair complexes, while pDNA-PKcs was detected in damage induced foci, total DNA-PKcs showed pan-nuclear staining in treated and untreated cells (Supplemental figure 2-5).

Having seen β -HPV 8E6 impair DNA-PKcs autophosphorylation and repair complex resolution, the ability of β -HPV 8E6 to hinder other DNA-PKcs-dependent steps in NHEJ was determined. Published reports indicated that Artemis is a DSB-induced target of DNA-PKcs phosphorylation at Serine 516 (pArtemis) [46,47]. This relationship was confirmed using immunoblots to detect pArtemis when DNA-PKcs activity was blocked with a small molecule inhibitor (1 μ M NU7441). While pArtemis levels rose in a Zeocin dose-dependent manner in wild type cells, pArtemis abundance was limited by the inhibitor (Supplemental figure 2-6). Having confirmed that Artemis phosphorylation depended on DNA-PKcs activity, the extent that β -HPV 8E6 reduced phosphorylation of Artemis in response to Zeocin was defined. β -HPV 8E6 blocked Artemis phosphorylation in HFKs (Figure 5A-B, Supplemental figure 2-7A). These results were also reproducible in U2OS (Figure 5C-D, Supplemental figure 2-7C and 7D). Notably, pArtemis levels rose in U2OS LXS and U2OS β -HPV Δ 8E6 cells in response to Zeocin. These data indicate that β -HPV 8E6's p300-dependent attenuation of DNA-PKcs-dependent signaling extended to Artemis activation.

To better understand the extent that NHEJ was impaired by β -HPV 8E6 hindered NHEJ, the ability of XRCC4 to localize to sites of damage was assessed. This occurs downstream of Artemis activation and is required for the DNA ligation step in NHEJ [49,61,62]. Like Artemis, XRCC4 is also a substrate of DNA-PKcs [27,28]. However the role of that phosphorylation is

poorly understood [63,64]. A study showed that DNA ligation fails without XRCC4 because it is required for LIG4 stabilization [65]. In HFK LXS cells, Zeocin induced XRCC4 foci (detected by IF microscopy) and were readily resolved (Figure 2-5E and 5F). However, β -HPV 8E6 prevented an induction of XRCC4 foci in response to Zeocin. These results were repeated in U2OS cells (Figure 2-5G and 5H). Interestingly, U2OS β -HPV Δ 8E6 also decreased XRCC4 recruitment, which may partially explain the p300-independent mechanism that β -HPV 8E6 diminish NHEJ efficiency. Together these data suggest that β -HPV 8E6 impairs XRCC4 recruitment to sites of damage.

2.4. p300 is required for robust DNA-PKcs signaling.

The data above suggest that p300 is required for DNA-PKcs-dependent NHEJ. To confirm this relationship, NHEJ and DNA-PKcs signaling was assessed in previously described p300 competent (p300 WT) and p300 knockout (p300 KO) HCT116 cells [66]. p300 KO HCT116 cells were notably less capable of initiating and completing the pathway. Specifically, the CD4 reporter assay (described in Figure 2-1A) found reduced NHEJ in p300 KO HCT116 cells (Figure 2-6A-B). While p300 knockout did not change basal DNA-PKcs phosphorylation (Supplemental figure 2-8), immunoblots indicate that it hindered DNA-PKcs activation (pDNA-PKcs) following Zeocin exposure (Figure 2-6C-D, Supplemental figure 2-9A and 9B). Loss of p300 also increased pDNA-PKcs foci persistence (Figure 2-6E and 6F). Finally, p300 knockout attenuated Artemis phosphorylation in response to DSB induction (Figure 2-6G-H, Supplemental figure 2-9C and 9D). These data demonstrate p300's requirement in NHEJ and DNA-PKcs-dependent signaling.

3. Discussion

Because β -HPV 8E6 attenuated the repair of DSBs by HR [16], we initially hypothesized that this would make cells more likely to use the NHEJ pathway. NHEJ is prone to mutations, because it requires blunt ends as a substrate for repair. Typically, when NHEJ initiates, a Ku70/Ku80/DNA-PKcs trimer localizes to the lesion (Figure 2-7A). Once becoming activated via autophosphorylation, DNA-PKcs then promotes the pathway's progression via phosphorylating downstream repair components. The phosphorylation of Artemis leads to resection of any overhanging DNA. Finally, XRCC4, XLF and LIG4 form a trimer at the newly blunted ends and ligate them together, fixing the break [48,49,67]. This was not the case in cells expressing β -HPV 8E6 (Figure 2-7B). β -HPV 8E6 reduced DNA-PKcs autophosphorylation (Figure 2-2) and increased the persistence of DNA-PKcs localized to DNA damage (Figure 3-4). In turn, DNA-PKcs's phosphorylation of Artemis was reduced and XRCC4 was less able to form repair complexes in response to DSB-induction (Figure 2-5). A reporter assay confirmed that these defects resulted in a reduced ability to repair DSBs via NHEJ.

β -HPV 8E6 hinders NHEJ, at least in part, by binding and destabilizing p300. p300 functions as a transcription factor for repair gene expression [68,69]. By reducing p300 availability, β -HPV 8E6 lowers the abundance of at least four DNA repair factors (BRCA1, BRCA2, ATR, and ATM) [16,18,17]. This manifests in a limited ability to respond to UV damage or to utilize the HR pathway. In contrast, p300 does not appear to be a transcription factor for canonical NHEJ genes (Supplemental Figure 2-5). Nevertheless, p300 is clearly required for robust NHEJ (Figure 2-6). Specifically, p300 promotes DNA-PKcs activity. Although the specific mechanistic explanation for our observations are not fully resolved, a prior study showed p300 is required for the recruitment of Ku70/80 [70]. This may explain our

observations, as Ku70/80 form a holoenzyme with DNA-PKcs to facilitate DNA-PKcs-mediated phosphorylation. However, our data rule out the possibility that p300 is needed for DNA-PKcs to localize to sites of damage. Instead, in the absence of p300, DNA-PKcs repair complexes become more persistent. DNA-PKcs activity requires acetylation, but the histone acetyltransferase was not determined [71]. Perhaps, p300 is responsible for the post-translational modification. Setting aside these unknowns, our data demonstrate that p300 is required for the completion rather than initiation of NHEJ. Interestingly, the NHEJ reporter assay indicates that β -HPV 8E6 also impairs NHEJ independently of p300 binding or reduced DNA-PKcs activity (Figure 2-1). Our data suggest a possible mechanism. β -HPV Δ 8E6 retains the ability to hinder XRCC4 foci formation (Figure 2-5G-H) which would limit NHEJ independent of p300 destabilization. Further, these data provide confirmation that the β -HPV Δ 8E6 mutant retains some functionality.

The evidence provided here show that β -HPV 8E6 diminishes essential NHEJ events including DNA-PKcs phosphorylation at S2056. However, our efforts fall well short of resolving the role of β -HPV in NMSC development. Granted, the reduced DNA repair potential associated with β -HPV 8E6 would not be desirable in cutaneous tissue as our skin protects against external mutagens. Supporting this assertion, previous studies have shown that pharmacological inhibition of DNA-PKcs increases mutagenesis [72]. Further, DNA-PKcs inhibitors and DNA-PKcs inactivating mutations sensitize in vitro and animal models to radiation [43,73,74]. Given the importance of DNA-PKcs in protecting genome fidelity, β -HPV infections could increase mutations in skin cells after UV exposure. However, given the typically transient nature of β -HPV infections, the increased mutational burden may not be particularly consequential. Further, others have suggested that β -HPV infections prime the immune system helping to prevent

NMSCs [15]. These positions are not mutually exclusive and should not be interpreted as being in conflict. Perhaps the oncogenic consequences of β -HPV associated repair inhibition are limited to specific circumstances (e.g. immune suppression). One other difference in the two studies is that Strickley and colleagues used a mouse papillomavirus that does not bind p300 [75].

Accumulating evidence shows that β -HPV E6 increases the mutagenic potential of UV. This includes increasing the frequency with which UV causes DSBs and hindering repair of these deleterious lesions. Both error-free HR and error-prone NHEJ are impaired when β -HPV 8E6 is expressed. However, β -HPV 8E6 does not appear to limit their initiation, as evidenced by the formation of both RAD51 [16] and pDNA-PKcs repair complexes (Figure 2-4). If initiation of NHEJ and HR were to occur at the same DSB, it would be problematic as the two pathways are intrinsically incompatible. HR begins by generating a large single-stranded DNA overhang, while NHEJ starts by removing any overhangs. This could result in large deletions as repair osculates between the two DSB repair pathways. Further, despite attenuated HR and NHEJ, β -HPV 8E6 expressing cells eventually resolve most DSBs. This suggests that β -HPV 8E6 could force DSB repair to occur by a less efficient and/or more mutagenic pathway. Our future directions include defining the dominant mechanisms of DSB repair in cells expressing β -HPV 8E6 and determining the mutagenic consequences of β -HPV 8E6 on DSB repair.

4. Materials and Methods

4.1. Cell Culture and Reagents

Immortalized human foreskin keratinocytes (HFK), provided by Michael Underbrink (University of Texas Medical Branch, Galveston, TX), were grown in EpiLife medium (Gibco) supplemented with 60 μ M calcium chloride (Gibco), human keratinocyte growth supplement

(Gibco), and 1% penicillin-streptomycin (Caisson). U2OS and HCT116 cells were maintained in DMEM supplemented with 10% FBS and 1% penicillin-streptomycin. Zeocin (Alfa Aesar) and H₂O₂ were used to induce DSBs. NU7441 (Selleckchem) was used to inhibit DNA-PKcs phosphorylation. KU55933 (Selleckchem) was used to inhibit ATM kinase activity.

4.2. Immunoblotting

After being washed with ice-cold PBS, cells were lysed with RIPA Lysis Buffer (VWR Life Science) supplemented with Phosphatase Inhibitor Cocktail 2 (Sigma) and Protease Inhibitor Cocktail (Bimake). The Pierce BCA Protein Assay Kit (Thermo Scientific) was used to determine protein concentration. Equal protein lysates were run on Novex 3-8% Tris-acetate 15 Well Mini Gels (Invitrogen) and transferred to Immobilon-P membranes (Millipore). Membranes were then probed with the following primary antibodies: GAPDH (Santa Cruz Biotechnologies), DNA-PKcs (abcam), phospho DNA-PKcs S2056 (abcam), Artemis (abcam), phospho Artemis S516 (abcam), XRCC4 (Santa Cruz Biotechnologies), Ligase IV (abcam), CD4 (abcam), and DYKDDDDK (FLAG) Tag (Invitrogen). After exposure to the matching HRP-conjugated secondary antibody, cells were visualized using SuperSignal West Femto Maximum Sensitivity Substrate (Thermo Scientific).

4.3. Immunofluorescence Microscopy

Cells were seeded onto either 96-well glass-bottom plates (Cellvis) or coverslips and grown overnight. Cells treated with Zeocin for specified time and concentration were fixed with 4% formaldehyde. Then 0.1% Triton-X solution in PBS was used to permeabilize the cells, followed by blocking with 3% bovine serum albumin in PBS for 30 minutes. Cell were then incubated with the following antibodies: phospho DNA-PKcs S2056 (abcam), XRCC4 (Santa Cruz Biotechnology). The cells were washed and stained with the appropriate secondary

antibodies: Alexa Fluor 594 goat anti-rabbit (Thermo Scientific A11012), Alexa Fluor 488 goat anti-mouse (Thermo Scientific A11001). After washing, the cells were stained with 30 μ M DAPI in PBS and visualized with the Zeiss LSM 770 microscope. Images were analyzed using ImageJ techniques previously described [3].

4.4. End joining Reporter Assay

The reporter assay used a previously described protocol [38] with the following modifications. Cells were seeded into 6-well plates. After transfection, CD4 expression was measured by immunoblotting.

4.5. Statistical Analysis

All values are represented as mean \pm Standard Error (SE) from at least three independent experiments. Statistical differences between groups were measured by using Student's T-test. P-values in all experiments were considered significant at less than 0.05.

5. Conclusions

Accumulating evidence shows that β -HPV 8E6 reduces genome stability by disrupting DNA damage response. Particularly, β -HPV 8E6 disrupts homologous recombination, which is a major DSB repair pathway in S phase and G2 phase of the cell cycle. The data presented here shows that β -HPV 8E6 diminishes NHEJ, which can occur throughout the cell cycle. This expands β -HPV 8E6's influence over DSB repair throughout the cell cycle. Finally, this work demonstrates that β -HPV 8E6 uses p300-dependent and p300-independent mechanisms to disrupt DNA repair. This suggests that there are considerable evolutionary forces driving β -HPV to hinder cellular responses to damaged DNA.

Supplementary Materials: The following are available online at www.mdpi.com/xxx/s1, Figure S1: Transfection efficiency represented by FLAG tagged SgRNA-CAS9 targeting CD4

and GAPDH., Figure S2: β -HPV 8 E6 does not decrease NHEJ protein in untreated cells., Figure S3: pDNA-PKcs and total DNA-PKcs normalized to GAPDH in HFK and U2OS. Figure S4: β -HPV 8 E6 decreases H₂O₂ induced DNA-PKcs phosphorylation., Figure S5. Total DNA-PKcs shows pan-nuclear expression in HFK cells. Figure S6: Inhibiting DNA-PK decreases Artemis phosphorylation., Figure S7: pArtemis and total Artemis normalized to GAPDH in HFK and U2OS cells. Figure S8: p300 knockout does not decrease major NHEJ proteins in untreated cells. Figure S9: pDNA-PKcs, total DNA-PKcs, pArtemis, and total Artemis normalized to GAPDH in HCT cells.

Author Contributions: Conceptualization, N.A.W.; methodology, C.H., M.G.; software, C.H.; validation, C.H., T.B.; investigation, C.H., M.G., T.B.; resources, N.A.W.; writing—original draft preparation, C.H., N.A.W.; writing—review and editing, C.H., T.B., N.A.W.; visualization, C.H.; supervision, N.A.W.; funding acquisition, N.A.W. All authors have read and agreed to the published version of the manuscript.

Funding: This study is funded by the U.S. Department of Defense (CMDRP PRCRP CA160224 (NW)) and Kansas State University Johnson Cancer Research Center.

Acknowledgments: We appreciate KSU-CVM Confocal Core for our immunofluorescence microscopy, Michael Underbrink for providing the TERT-immortalized HFKs, and Jeremy M. Stark for providing plasmids of end-joining reporter assay.

Conflicts of Interest: The authors declare no conflict of interest.

References

1. Bzhalava, D.; Mühr, L.S.A.; Lagheden, C.; Ekström, J.; Forslund, O.; Dillner, J.; Hultin, E. Deep sequencing extends the diversity of human papillomaviruses in human skin. *Scientific Reports* 2015, 4, doi:10.1038/srep05807.

2. Cubie, H.A. Diseases associated with human papillomavirus infection. *Virology* 2013, 445, 21–34, doi:10.1016/j.virol.2013.06.007.
3. Wendel, S.O.; Wallace, N.A. Loss of Genome Fidelity: Beta HPVs and the DNA Damage Response. *Frontiers in Microbiology* 2017, 8, doi:10.3389/fmicb.2017.02250.
4. Doorbar, J.; Egawa, N.; Griffin, H.; Kranjec, C.; Murakami, I. Human papillomavirus molecular biology and disease association: Human papillomavirus. *Reviews in Medical Virology* 2015, 25, 2–23, doi:10.1002/rmv.1822.
5. Pfister, H.; Nürnberg, F.; Gissmann, L.; Hausen, H.Z. Characterization of a human papillomavirus from epidermodysplasia verruciformis lesions of a patient from upper-volta. *International Journal of Cancer* 1981, 27, 645–650, doi:10.1002/ijc.2910270511.
6. Mudigonda et al. - 2010 - The Economic Impact of Non-Melanoma Skin Cancer A.pdf.
7. Kremsdorf, D.; Jablonska, S.; Favre, M.; Orth, G. Biochemical characterization of two types of human papillomaviruses associated with epidermodysplasia verruciformis. *J Virol* 1982, 43, 436–447.
8. Rollison, D.E.; Viarisio, D.; Amorrortu, R.P.; Gheit, T.; Tommasino, M. An Emerging Issue in Oncogenic Virology: the Role of Beta Human Papillomavirus Types in the Development of Cutaneous Squamous Cell Carcinoma. *Journal of Virology* 2019, 93, doi:10.1128/JVI.01003-18.
9. White, E.A.; Walther, J.; Javanbakht, H.; Howley, P.M. Genus Beta Human Papillomavirus E6 Proteins Vary in Their Effects on the Transactivation of p53 Target Genes. *J Virol* 2014, 88, 8201–8212, doi:10.1128/JVI.01197-14.
10. Howley, P.M.; Pfister, H.J. Beta Genus Papillomaviruses and Skin Cancer. *Virology* 2015, 0, 290–296, doi:10.1016/j.virol.2015.02.004.
11. Shanmugasundaram, S.; You, J. Targeting Persistent Human Papillomavirus Infection. *Viruses* 2017, 9, doi:10.3390/v9080229.
12. Tommasino, M. HPV and skin carcinogenesis. *Papillomavirus Research* 2019, 7, 129–131, doi:10.1016/j.pvr.2019.04.003.
13. Viarisio, D.; Müller-Decker, K.; Accardi, R.; Robitaille, A.; Dürst, M.; Beer, K.; Jansen, L.; Flechtenmacher, C.; Bozza, M.; Harbottle, R.; et al. Beta HPV38 oncoproteins act with a hit-and-run mechanism in ultraviolet radiation-induced skin carcinogenesis in mice. *PLoS Pathog* 2018, 14, doi:10.1371/journal.ppat.1006783.
14. Hufbauer, M.; Akgül, B. Molecular Mechanisms of Human Papillomavirus Induced Skin Carcinogenesis. *Viruses* 2017, 9, 187, doi:10.3390/v9070187.
15. Strickley, J.D.; Messerschmidt, J.L.; Awad, M.E.; Li, T.; Hasegawa, T.; Ha, D.T.; Nabeta, H.W.; Bevins, P.A.; Ngo, K.H.; Asgari, M.M.; et al. Immunity to commensal papillomaviruses protects against skin cancer. *Nature* 2019, 575, 519–522, doi:10.1038/s41586-019-1719-9.
16. Wallace, N.A.; Robinson, K.; Howie, H.L.; Galloway, D.A. β -HPV 5 and 8 E6 Disrupt Homology Dependent Double Strand Break Repair by Attenuating BRCA1 and BRCA2

- Expression and Foci Formation. *PLOS Pathogens* 2015, 11, e1004687, doi:10.1371/journal.ppat.1004687.
17. Wallace, N.A.; Gasior, S.L.; Faber, Z.J.; Howie, H.L.; Deininger, P.L.; Galloway, D.A. HPV 5 and 8 E6 expression reduces ATM protein levels and attenuates LINE-1 retrotransposition. *Virology* 2013, 443, 69–79, doi:10.1016/j.virol.2013.04.022.
 18. Wallace, N.A.; Robinson, K.; Howie, H.L.; Galloway, D.A. HPV 5 and 8 E6 Abrogate ATR Activity Resulting in Increased Persistence of UVB Induced DNA Damage. *PLoS Pathogens* 2012, 8, e1002807, doi:10.1371/journal.ppat.1002807.
 19. Snow, J.A.; Murthy, V.; Dacus, D.; Hu, C.; Wallace, N.A. β-HPV 8E6 Attenuates ATM and ATR Signaling in Response to UV Damage. 2019, doi:10.20944/preprints201909.0338.v1.
 20. Howie, H.L.; Koop, J.I.; Weese, J.; Robinson, K.; Wipf, G.; Kim, L.; Galloway, D.A. β -HPV5 and 8 E6 Promote p300 Degradation by Blocking AKT/p300 Association. *PLOS Pathogens* 2011, 7, e1002211, doi:10.1371/journal.ppat.1002211.
 21. Ceccaldi, R.; Rondinelli, B.; D'Andrea, A.D. Repair Pathway Choices and Consequences at the Double-Strand Break. *Trends in Cell Biology* 2016, 26, 52–64, doi:10.1016/j.tcb.2015.07.009.
 22. Ahmed, K.M.; Pandita, R.K.; Singh, D.K.; Hunt, C.R.; Pandita, T.K. β 1-Integrin Impacts Rad51 Stability and DNA Double-Strand Break Repair by Homologous Recombination. *Mol Cell Biol* 2018, 38, doi:10.1128/MCB.00672-17.
 23. Pierce, A.J.; Johnson, R.D.; Thompson, L.H.; Jasin, M. XRCC3 promotes homology-directed repair of DNA damage in mammalian cells. *Genes Dev* 1999, 13, 2633–2638.
 24. Bakr, A.; Oing, C.; Köcher, S.; Borgmann, K.; Dornreiter, I.; Petersen, C.; Dikomey, E.; Mansour, W.Y. Involvement of ATM in homologous recombination after end resection and RAD51 nucleofilament formation. *Nucleic Acids Res* 2015, 43, 3154–3166, doi:10.1093/nar/gkv160.
 25. Schwartz, M.; Zlotorynski, E.; Goldberg, M.; Ozeri, E.; Rahat, A.; Sage, C. le; Chen, B.P.C.; Chen, D.J.; Agami, R.; Kerem, B. Homologous recombination and nonhomologous end-joining repair pathways regulate fragile site stability. *Genes Dev* 2005, 19, 2715–2726, doi:10.1101/gad.340905.
 26. Lieber, M.R. The Mechanism of Double-Strand DNA Break Repair by the Nonhomologous DNA End Joining Pathway. *Annu Rev Biochem* 2010, 79, 181–211, doi:10.1146/annurev.biochem.052308.093131.
 27. Weterings, E.; van Gent, D.C. The mechanism of non-homologous end-joining: a synopsis of synopsis. *DNA Repair* 2004, 3, 1425–1435, doi:10.1016/j.dnarep.2004.06.003.
 28. Bhargava, R.; Lopezcolorado, F.W.; Tsai, L.J.; Stark, J.M. The canonical non-homologous end joining factor XLF promotes chromosomal deletion rearrangements in human cells. *J. Biol. Chem.* 2020, 295, 125–137, doi:10.1074/jbc.RA119.010421.
 29. Zhang, Y.; Hefferin, M.L.; Chen, L.; Shim, E.Y.; Tseng, H.-M.; Kwon, Y.; Sung, P.; Lee, S.E.; Tomkinson, A.E. Role of Dnl4-Lif1 in nonhomologous end-joining repair complex

- assembly and suppression of homologous recombination. *Nat. Struct. Mol. Biol.* 2007, 14, 639–646, doi:10.1038/nsmb1261.
30. Patel, A.G.; Sarkaria, J.N.; Kaufmann, S.H. Nonhomologous end joining drives poly(ADP-ribose) polymerase (PARP) inhibitor lethality in homologous recombination-deficient cells. *PNAS* 2011, 108, 3406–3411, doi:10.1073/pnas.1013715108.
 31. Gunn, A.; Bennardo, N.; Cheng, A.; Stark, J.M. Correct End Use during End Joining of Multiple Chromosomal Double Strand Breaks Is Influenced by Repair Protein RAD50, DNA-dependent Protein Kinase DNA-PKcs, and Transcription Context. *Journal of Biological Chemistry* 2011, 286, 42470–42482, doi:10.1074/jbc.M111.309252.
 32. Gupta, A.; Hunt, C.R.; Chakraborty, S.; Pandita, R.K.; Yordy, J.; Ramnarain, D.B.; Horikoshi, N.; Pandita, T.K. Role of 53BP1 in the Regulation of DNA Double-Strand Break Repair Pathway Choice. *Radiat Res* 2014, 181, 1–8, doi:10.1667/RR13572.1.
 33. A chromatin-based signalling mechanism directs the switch from mutagenic to error-free repair of DNA double strand breaks: *Molecular & Cellular Oncology: Vol 6, No 4* Available online: <https://www.tandfonline.com/doi/full/10.1080/23723556.2019.1605820> (accessed on Nov 27, 2019).
 34. Sollazzo, A.; Brzozowska, B.; Cheng, L.; Lundholm, L.; Scherthan, H.; Wojcik, A. Live Dynamics of 53BP1 Foci Following Simultaneous Induction of Clustered and Dispersed DNA Damage in U2OS Cells. *International Journal of Molecular Sciences* 2018, 19, 519, doi:10.3390/ijms19020519.
 35. Daley, J.M.; Sung, P. 53BP1, BRCA1, and the Choice between Recombination and End Joining at DNA Double-Strand Breaks. *Molecular and Cellular Biology* 2014, 34, 1380–1388, doi:10.1128/MCB.01639-13.
 36. Dimitrova, N.; Chen, Y.-C.M.; Spector, D.L.; de Lange, T. 53BP1 promotes non-homologous end joining of telomeres by increasing chromatin mobility. *Nature* 2008, 456, 524–528, doi:10.1038/nature07433.
 37. Bunting, S.F.; Callén, E.; Wong, N.; Chen, H.-T.; Polato, F.; Gunn, A.; Bothmer, A.; Feldhahn, N.; Fernandez-Capetillo, O.; Cao, L.; et al. 53BP1 Inhibits Homologous Recombination in Brca1-Deficient Cells by Blocking Resection of DNA Breaks. *Cell* 2010, 141, 243–254, doi:10.1016/j.cell.2010.03.012.
 38. Zhen, Y.; Li, S.; Zhu, Y.; Wang, X.; Zhou, X.; Zhu, L. Identification of DNA-PKcs as a primary resistance factor of salinomycin in osteosarcoma cells. *Oncotarget* 2016, 7, 79417–79427, doi:10.18632/oncotarget.12712.
 39. Jiang, W.; Crowe, J.L.; Liu, X.; Nakajima, S.; Wang, Y.; Li, C.; Lee, B.J.; Dubois, R.L.; Liu, C.; Yu, X.; et al. Differential phosphorylation of DNA-PKcs regulates the interplay between end-processing and end-ligation during non-homologous end-joining. *Mol Cell* 2015, 58, 172–185, doi:10.1016/j.molcel.2015.02.024.
 40. Uematsu, N.; Weterings, E.; Yano, K.; Morotomi-Yano, K.; Jakob, B.; Taucher-Scholz, G.; Mari, P.-O.; van Gent, D.C.; Chen, B.P.C.; Chen, D.J. Autophosphorylation of DNA-PKcs regulates its dynamics at DNA double-strand breaks. *J Cell Biol* 2007, 177, 219–229, doi:10.1083/jcb.200608077.

41. Smith, G.C.M.; Jackson, S.P. The DNA-dependent protein kinase. *Genes Dev.* 1999, 13, 916–934.
42. Veuger, S.J.; Curtin, N.J.; Richardson, C.J.; Smith, G.C.M.; Durkacz, B.W. Radiosensitization and DNA Repair Inhibition by the Combined Use of Novel Inhibitors of DNA-dependent Protein Kinase and Poly(ADP-Ribose) Polymerase-1. *Cancer Res* 2003, 63, 6008–6015.
43. Zhao, Y.; Thomas, H.D.; Batey, M.A.; Cowell, I.G.; Richardson, C.J.; Griffin, R.J.; Calvert, A.H.; Newell, D.R.; Smith, G.C.M.; Curtin, N.J. Preclinical Evaluation of a Potent Novel DNA-Dependent Protein Kinase Inhibitor NU7441. *Cancer Res* 2006, 66, 5354–5362, doi:10.1158/0008-5472.CAN-05-4275.
44. Mamo, T.; Mladek, A.C.; Shogren, K.L.; Gustafson, C.; Gupta, S.K.; Riester, S.M.; Maran, A.; Galindo, M.; van Wijnen, A.J.; Sarkaria, J.N.; et al. Inhibiting DNA-PKCS Radiosensitizes Human Osteosarcoma Cells. *Biochem Biophys Res Commun* 2017, 486, 307–313, doi:10.1016/j.bbrc.2017.03.033.
45. Beucher, A.; Birraux, J.; Tchouandong, L.; Barton, O.; Shibata, A.; Conrad, S.; Goodarzi, A.A.; Krempler, A.; Jeggo, P.A.; Löbrich, M. ATM and Artemis promote homologous recombination of radiation-induced DNA double-strand breaks in G2. *The EMBO Journal* 2009, 28, 3413–3427, doi:10.1038/emboj.2009.276.
46. Soubeyrand, S.; Pope, L.; De Chasseval, R.; Gosselin, D.; Dong, F.; de Villartay, J.-P.; Haché, R.J.G. Artemis phosphorylated by DNA-dependent protein kinase associates preferentially with discrete regions of chromatin. *J. Mol. Biol.* 2006, 358, 1200–1211, doi:10.1016/j.jmb.2006.02.061.
47. Li, S.; Chang, H.H.; Niewolik, D.; Hedrick, M.P.; Pinkerton, A.B.; Hassig, C.A.; Schwarz, K.; Lieber, M.R. Evidence That the DNA Endonuclease ARTEMIS also Has Intrinsic 5'-Exonuclease Activity. *J Biol Chem* 2014, 289, 7825–7834, doi:10.1074/jbc.M113.544874.
48. Mari, P.-O.; Florea, B.I.; Persengiev, S.P.; Verkaik, N.S.; Bruggenwirth, H.T.; Modesti, M.; Giglia-Mari, G.; Bezstarosti, K.; Demmers, J.A.A.; Luiders, T.M.; et al. Dynamic assembly of end-joining complexes requires interaction between Ku70/80 and XRCC4. *Proceedings of the National Academy of Sciences* 2006, 103, 18597–18602, doi:10.1073/pnas.0609061103.
49. Normanno, D.; Négre, A.; de Melo, A.J.; Betzi, S.; Meek, K.; Modesti, M. Mutational phospho-mimicry reveals a regulatory role for the XRCC4 and XLF C-terminal tails in modulating DNA bridging during classical non-homologous end joining. *eLife* 6, doi:10.7554/eLife.22900.
50. Hustedt, N.; Durocher, D. The control of DNA repair by the cell cycle. *Nature Cell Biology* 2017, 19, 1–9, doi:10.1038/ncb3452.
51. Heyer, W.-D.; Ehmsen, K.T.; Liu, J. Regulation of homologous recombination in eukaryotes. *Annu. Rev. Genet.* 2010, 44, 113–139, doi:10.1146/annurev-genet-051710-150955.
52. Salmon, P.; Giovane, A.; Wasylyk, B.; Klatzmann, D. Characterization of the human CD4 gene promoter: transcription from the CD4 gene core promoter is tissue-specific and is activated by Ets proteins. *Proc Natl Acad Sci U S A* 1993, 90, 7739–7743.

53. Underbrink, M.P.; Howie, H.L.; Bedard, K.M.; Koop, J.I.; Galloway, D.A. E6 proteins from multiple human betapapillomavirus types degrade Bak and protect keratinocytes from apoptosis after UVB irradiation. *J. Virol.* 2008, 82, 10408–10417, doi:10.1128/JVI.00902-08.
54. Delacôte, F.; Deriano, L.; Lambert, S.; Bertrand, P.; Saintigny, Y.; Lopez, B.S. Chronic exposure to sublethal doses of radiation mimetic Zeocin™ selects for clones deficient in homologous recombination. *Mutation Research/Fundamental and Molecular Mechanisms of Mutagenesis* 2007, 615, 125–133, doi:10.1016/j.mrfmmm.2006.11.028.
55. Tsukuda, M.; Miyazaki, K. DNA fragmentation caused by an overdose of Zeocin. *Journal of Bioscience and Bioengineering* 2013, 116, 644–646, doi:10.1016/j.jbiosc.2013.05.004.
56. Davis, A.J.; Chi, L.; So, S.; Lee, K.-J.; Mori, E.; Fattah, K.; Yang, J.; Chen, D.J. BRCA1 modulates the autophosphorylation status of DNA-PKcs in S phase of the cell cycle. *Nucleic Acids Res* 2014, 42, 11487–11501, doi:10.1093/nar/gku824.
57. Greinert, R.; Volkmer, B.; Henning, S.; Breitbart, E.W.; Greulich, K.O.; Cardoso, M.C.; Rapp, A. UVA-induced DNA double-strand breaks result from the repair of clustered oxidative DNA damages. *Nucleic Acids Research* 2012, 40, 10263–10273, doi:10.1093/nar/gks824.
58. Lee, C.-S.; Lee, K.; Legube, G.; Haber, J.E. Dynamics of yeast histone H2A and H2B phosphorylation in response to a double-strand break. *Nat. Struct. Mol. Biol.* 2014, 21, 103–109, doi:10.1038/nsmb.2737.
59. Polo, S.E.; Jackson, S.P. Dynamics of DNA damage response proteins at DNA breaks: a focus on protein modifications. *Genes Dev* 2011, 25, 409–433, doi:10.1101/gad.2021311.
60. Murthy, V.; Dacus, D.; Gamez, M.; Hu, C.; Wendel, S.O.; Snow, J.; Kahn, A.; Walterhouse, S.H.; Wallace, N.A. Characterizing DNA Repair Processes at Transient and Long-lasting Double-strand DNA Breaks by Immunofluorescence Microscopy. *JoVE (Journal of Visualized Experiments)* 2018, e57653, doi:10.3791/57653.
61. Drouet, J.; Delteil, C.; Lefrançois, J.; Concannon, P.; Salles, B.; Calsou, P. DNA-dependent Protein Kinase and XRCC4-DNA Ligase IV Mobilization in the Cell in Response to DNA Double Strand Breaks. *J. Biol. Chem.* 2005, 280, 7060–7069, doi:10.1074/jbc.M410746200.
62. KOIKE, M.; YUTOKU, Y.; KOIKE, A. Cloning, localization and focus formation at DNA damage sites of canine XRCC4. *J Vet Med Sci* 2016, 78, 1865–1871, doi:10.1292/jvms.16-0381.
63. Collis, S.J.; DeWeese, T.L.; Jeggo, P.A.; Parker, A.R. The life and death of DNA-PK. *Oncogene* 2005, 24, 949–961, doi:10.1038/sj.onc.1208332.
64. Davis, A.J.; Chen, B.P.C.; Chen, D.J. DNA-PK: a dynamic enzyme in a versatile DSB repair pathway. *DNA Repair (Amst)* 2014, 17, 21–29, doi:10.1016/j.dnarep.2014.02.020.
65. Ghezraoui, H.; Piganeau, M.; Renouf, B.; Renaud, J.-B.; Sallmyr, A.; Ruis, B.; Oh, S.; Tomkinson, A.; Hendrickson, E.A.; Giovannangeli, C.; et al. Chromosomal translocations in human cells are generated by canonical nonhomologous end-joining. *Mol Cell* 2014, 55, 829–842, doi:10.1016/j.molcel.2014.08.002.
66. Iyer, N.G.; Chin, S.-F.; Ozdag, H.; Daigo, Y.; Hu, D.-E.; Cariati, M.; Brindle, K.; Aparicio, S.; Caldas, C. p300 regulates p53-dependent apoptosis after DNA damage in colorectal cancer

- cells by modulation of PUMA/p21 levels. *Proc. Natl. Acad. Sci. U.S.A.* 2004, 101, 7386–7391, doi:10.1073/pnas.0401002101.
67. Francis, D.B.; Kozlov, M.; Chavez, J.; Chu, J.; Malu, S.; Hanna, M.; Cortes, P. DNA Ligase IV regulates XRCC4 nuclear localization. *DNA Repair (Amst)* 2014, 21, 36–42, doi:10.1016/j.dnarep.2014.05.010.
 68. Goodman, R.H.; Smolik, S. CBP/p300 in cell growth, transformation, and development. *Genes Dev.* 2000, 14, 1553–1577, doi:10.1101/gad.14.13.1553.
 69. Chen, J.; Halappanavar, S.S.; St-Germain, J.R.; Tsang, B.K.; Li, Q. Role of Akt/protein kinase B in the activity of transcriptional coactivator p300. *CMLS, Cell. Mol. Life Sci.* 2004, 61, 1675–1683, doi:10.1007/s00018-004-4103-9.
 70. Ogiwara, H.; Ui, A.; Otsuka, A.; Satoh, H.; Yokomi, I.; Nakajima, S.; Yasui, A.; Yokota, J.; Kohno, T. Histone acetylation by CBP and p300 at double-strand break sites facilitates SWI/SNF chromatin remodeling and the recruitment of non-homologous end joining factors. *Oncogene* 2011, 30, 2135–2146, doi:10.1038/onc.2010.592.
 71. Mori, E.; Davis, A.J.; Hasegawa, M.; Chen, D.J. Lysines 3241 and 3260 of DNA-PKcs are important for genomic stability and radioresistance. *Biochem Biophys Res Commun* 2016, 477, 235–240, doi:10.1016/j.bbrc.2016.06.048.
 72. Jette, N.; Lees-Miller, S.P. The DNA-dependent protein kinase: a multifunctional protein kinase with roles in DNA double strand break repair and mitosis. *Prog Biophys Mol Biol* 2015, 117, 194–205, doi:10.1016/j.pbiomolbio.2014.12.003.
 73. Eccles, L.J.; Bell, A.C.; Powell, S.N. Inhibition of non-homologous end joining in Fanconi Anemia cells results in rescue of survival after interstrand crosslinks but sensitization to replication associated double-strand breaks. *DNA Repair* 2018, 64, 1–9, doi:10.1016/j.dnarep.2018.02.003.
 74. Dong, J.; Zhang, T.; Ren, Y.; Wang, Z.; Ling, C.C.; He, F.; Li, G.C.; Wang, C.; Wen, B. Inhibiting DNA-PKcs in a non-homologous end-joining pathway in response to DNA double-strand breaks. *Oncotarget* 2017, 8, 22662–22673, doi:10.18632/oncotarget.15153.
 75. Meyers, J.M.; Uberoi, A.; Grace, M.; Lambert, P.F.; Munger, K. Cutaneous HPV8 and MmuPV1 E6 Proteins Target the NOTCH and TGF- β Tumor Suppressors to Inhibit Differentiation and Sustain Keratinocyte Proliferation. *PLOS Pathogens* 2017, 13, e1006171, doi:10.1371/journal.ppat.1006171.

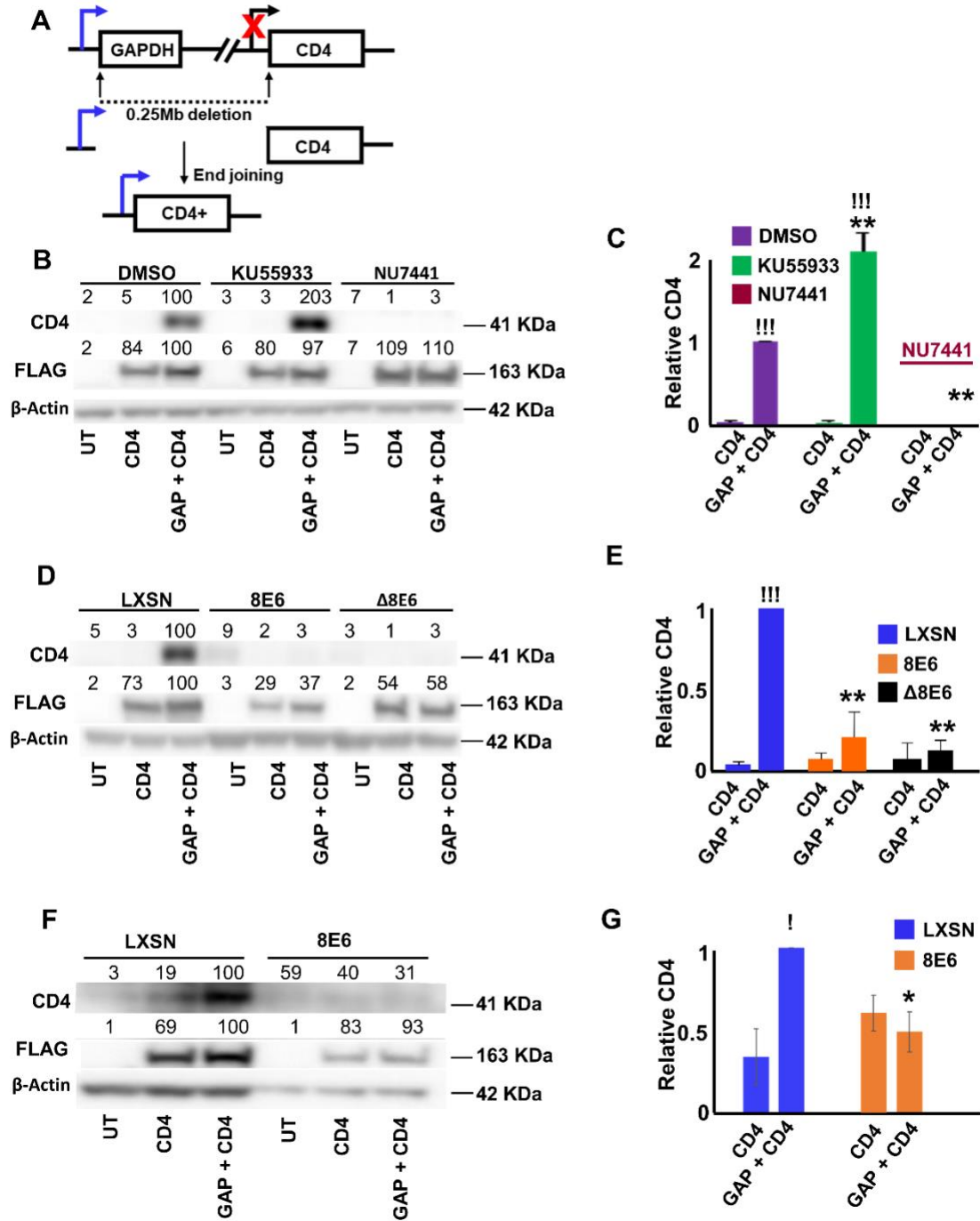


Figure 2-1. β -HPV 8E6 decreases NHEJ efficiency using CD4 expression as a readout.

(A) Schematic of end-joining reporter assay. FLAG-tagged SgRNA-CAS9 induced double strand breaks in GAPDH and CD4 on chromosome 12 in U2OS cells. Rearrangement leads to CD4 expression driven by the promoter of GAPDH. Red “X” represents that CD4 expression is

naturally inactivated. (B) Representative immunoblots showing CD4 expression in U2OS cells treated with control, ATM inhibitor (KU55933), and DNA-PK inhibitor (NU7441) after transfection with control (UT), FLAG-tagged SgRNA-CAS9 targeting CD4 (CD4), and FLAG-tagged SgRNA-CAS9 targeting GAPDH together with FLAG-tagged SgRNA-CAS9 targeting CD4 (GAP/CD4). (C) Densitometry of immunoblots (n=3) from panel B. CD4 was normalized to β -actin as a loading control. Transfection efficiency was accounted for using FLAG abundance. (D) Representative immunoblots showing CD4 expression in U2OS LXS^N, β -HPV 8 E6, and β -HPV Δ 8E6 after transfection with control (UT), FLAG-tagged SgRNA-CAS9 targeting CD4 (CD4), and FLAG-tagged SgRNA-CAS9 targeting GAPDH and FLAG-tagged SgRNA-CAS9 targeting CD4 (GAP/CD4). (E) Densitometry of immunoblots (n=3) from panel D. CD4 was normalized to β -actin as a loading control. Transfection efficiency was accounted for using FLAG abundance. (F) Representative immunoblots showing CD4 expression in HFK LXS^N and HFK β -HPV 8 E6 after transfection with control (UT), FLAG-tagged SgRNA-CAS9 targeting CD4 (CD4), and FLAG-tagged SgRNA-CAS9 targeting GAPDH and FLAG-tagged SgRNA-CAS9 targeting CD4 (GAP/CD4). (G) Densitometry of immunoblots (n=3) from panel F. CD4 was normalized to β -actin as a loading control. Transfection efficiency was accounted for using FLAG abundance. All values are represented as mean \pm standard error from at least three independent experiments. Statistical differences between groups were measured by using Student's T-test. * indicates P<0.05. ** indicates P<0.01. ! indicates significant difference between transfection with SgRNA-CAS9 targeting CD4 and co-transfection with SgRNA-CAS9 targeting CD4 and GAPDH.

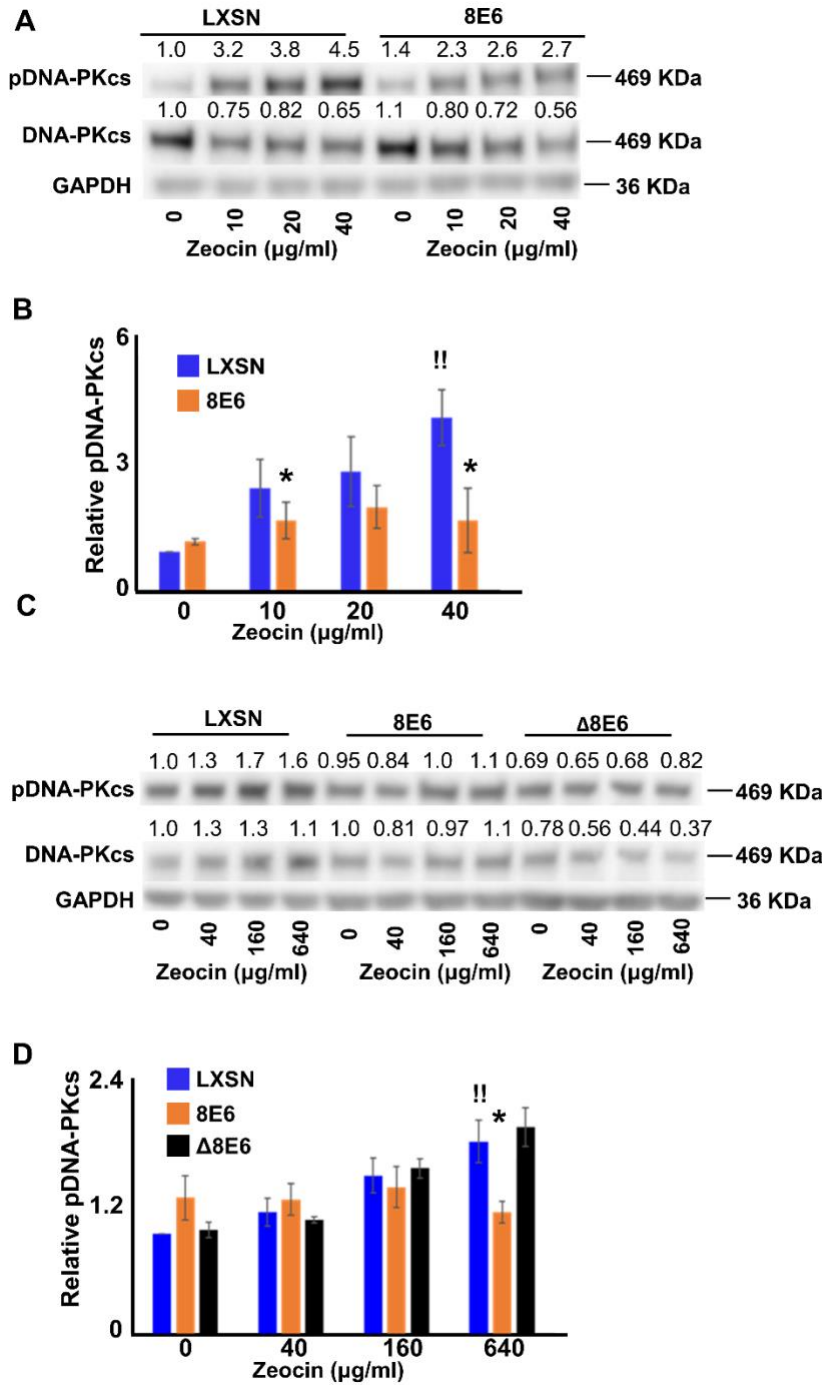


Figure 2-2. β -HPV 8E6 attenuates DNA-PKcs phosphorylation.

(A) Representative immunoblot showing phospho-DNA-PKcs (pDNA-PKcs) and total DNA-PKcs in HFK LXSN and HFK β -HPV 8 E6. (B) Densitometry of immunoblots of pDNA-PKcs normalized to total DNA-PKcs and GAPDH as a loading control. (C) Representative

immunoblot showing that pDNA-PKcs and DNA-PKcs in U2OS LXS_N, U2OS β -HPV 8 E6, and U2OS β -HPV Δ 8 E6. (D) Densitometry of immunoblots (n=4) of pDNA-PKcs normalized to total DNA-PKcs and GAPDH as a loading control. All values are represented as mean \pm standard error from at least three independent experiments. Statistical differences between groups were measured by using Student's T-test. * indicates P<0.05. ** indicates P<0.01. !! indicates significant difference between Zeocin treated and untreated group.

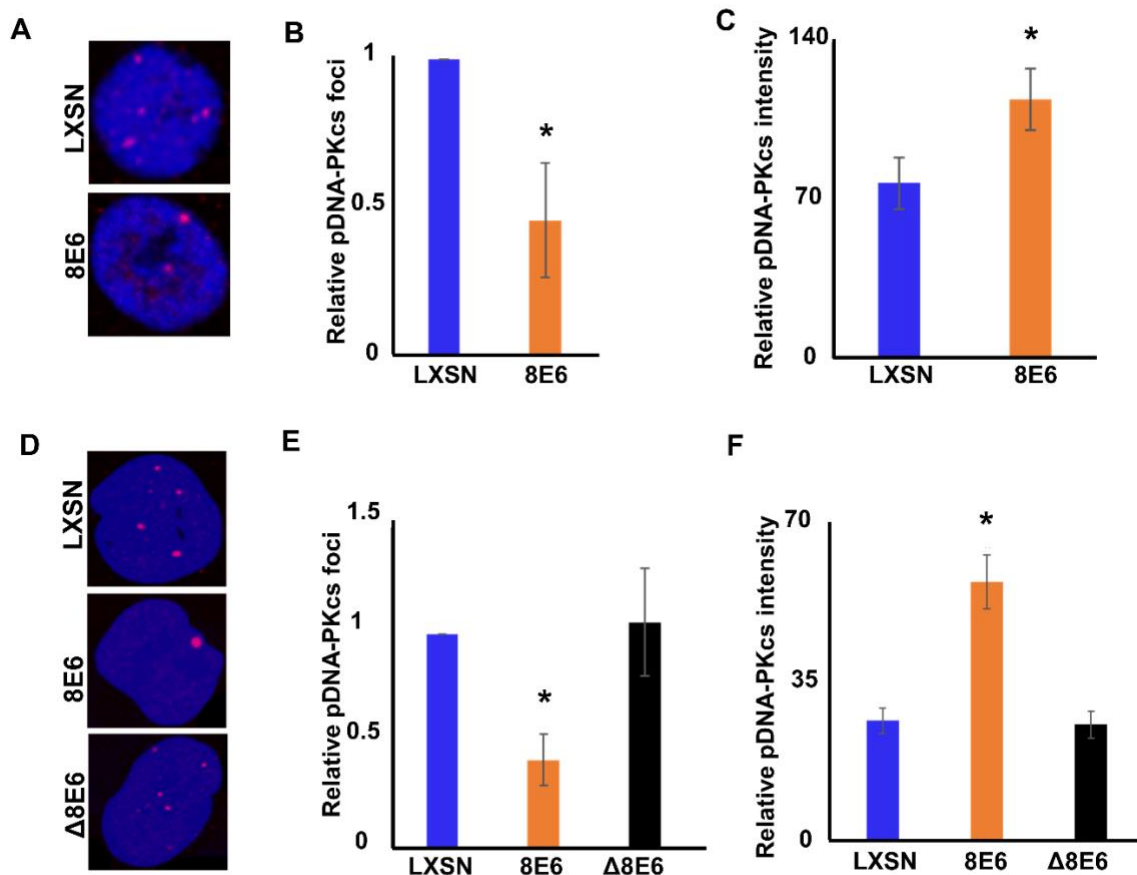


Figure 2-3. β -HPV 8E6 increases pDNA-PKcs foci size but decreases frequency in untreated cells.

(A) Representative images of pDNA-PKcs foci in HFK LXS_N and HFK β -HPV 8 E6. (B)

Percentages of cells with one or more pDNA-PKcs foci. (C) Average pDNA-PKcs foci intensity

of HFK cells. (D) Representative images of pDNA-PKcs foci in U2OS LXS^N, U2OS β -HPV 8E6, and U2OS β -HPV Δ 8E6. (E) Percentages of cells with one or more pDNA-PKcs foci. (F) Average pDNA-PKcs focus intensity in U2OS cells. All values are represented as mean \pm standard error from at least three independent experiments. Statistical differences between groups were measured by using Student's T-test. * indicates $P < 0.05$.

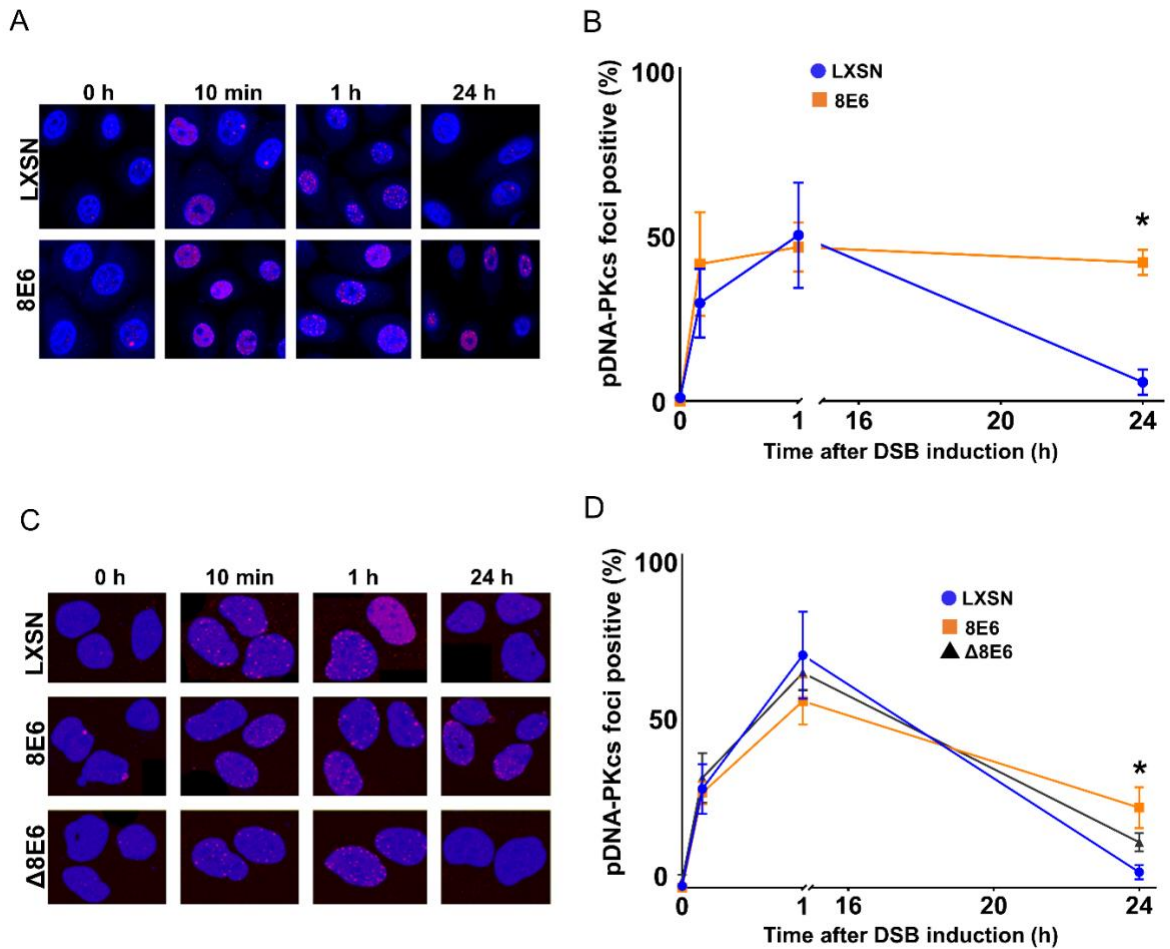


Figure 2-4. β -HPV 8E6 increases pDNA-PKcs foci persistence.

Immunofluorescence microscopy was used to detect pDNA-PKcs foci in cells that were treated with Zeocin. (A) Representative images of pDNA-PKcs foci in HFK cell lines following treatment with Zeocin for 10 mins. (B) Percentage of pDNA-PKcs foci positive (>2) cells following Zeocin exposure. (C) Representative images of pDNA-PKcs foci in U2OS cell lines

treatment with Zeocin for 1 hour then harvested 0 hours, 10 minutes, 1 hour, and 24 hours after Zeocin treatment. (D) Percentage of pDNA-PKcs foci positive (>4) U2OS cells following Zeocin exposure. All values are represented as mean \pm standard error from at least three independent experiments. Statistical differences between groups were measured by using Student's T-test. * indicates $P < 0.05$.

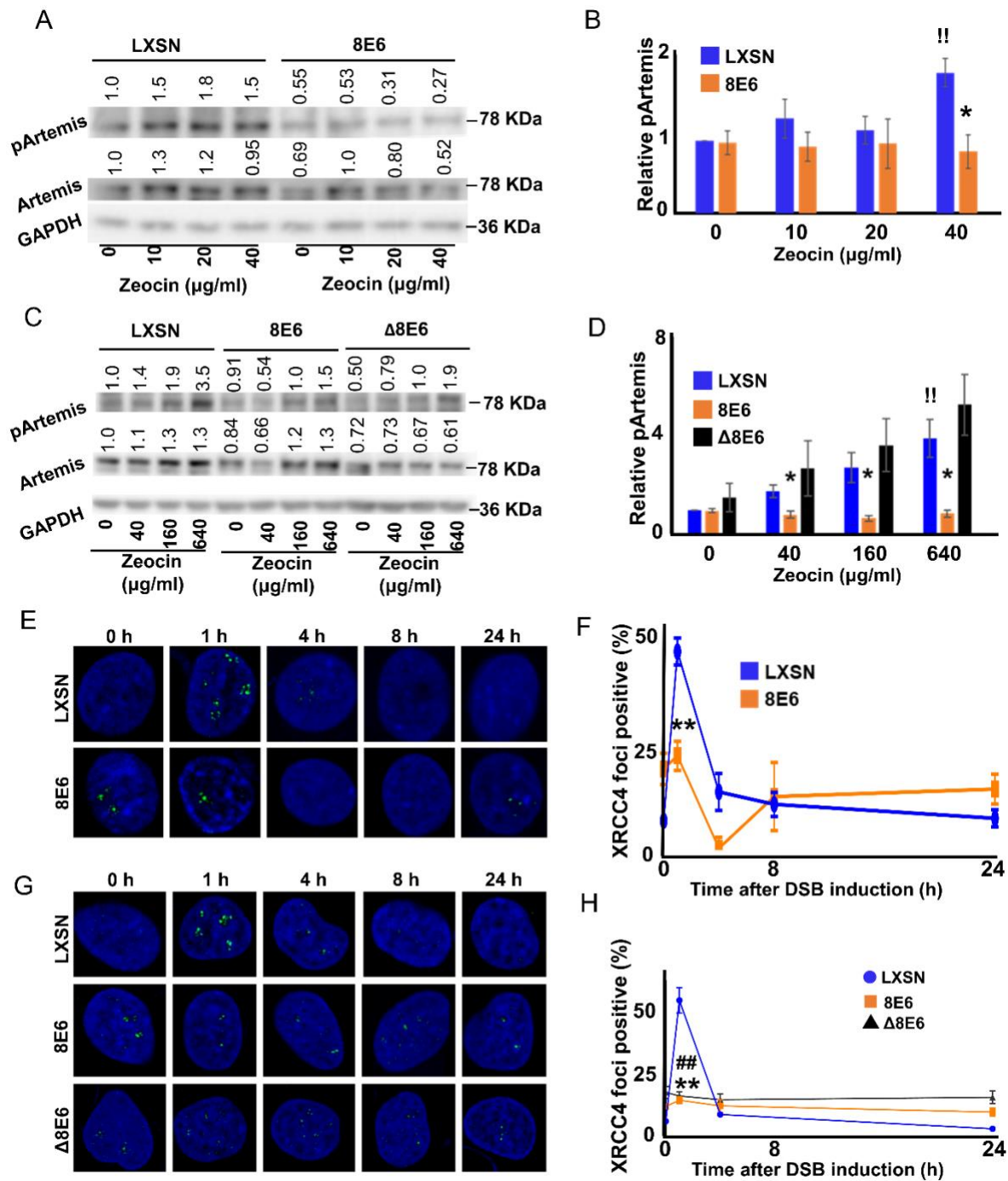


Figure 2-5. β -HPV 8E6 decreases pDNA-PKcs target proteins pArtemis abundance and XRCC4 foci formation.

(A) Representative immunoblot showing pArtemis and total Artemis in HFK LXSN and HFK β -HPV 8 E6. (B) Densitometry of immunoblots (n=4) of pArtemis normalized to total Artemis and to GAPDH as a loading control. (C) Representative immunoblot showing that pArtemis and total

Artemis in U2OS LXS^N, U2OS β -HPV 8 E6, or U2OS β -HPV Δ 8 E6. (D) Densitometry of immunoblots (n=4) of pArtemis normalized to total Artemis and to GAPDH as a loading control. (E) Representative images of XRCC4 foci in HFK cell lines 0-24 hours following Zeocin exposure. (F) Percentages of XRCC4 foci positive (>2) HFK cells following DSB induction. (G) Representative images of XRCC4 foci in U2OS cell lines 0-24 hours following Zeocin exposure. (H) Percentages of XRCC4 foci positive (>2) U2OS cells following DSB induction. All values are represented as mean \pm standard error from at least three independent experiments. Statistical differences between groups were measured by using Student's T-test. * indicates P<0.05. ** indicates P<0.01. !! indicates significant difference between Zeocin treated and untreated group. ## indicates significant difference between U2OS β -HPV Δ 8 E6 and control.

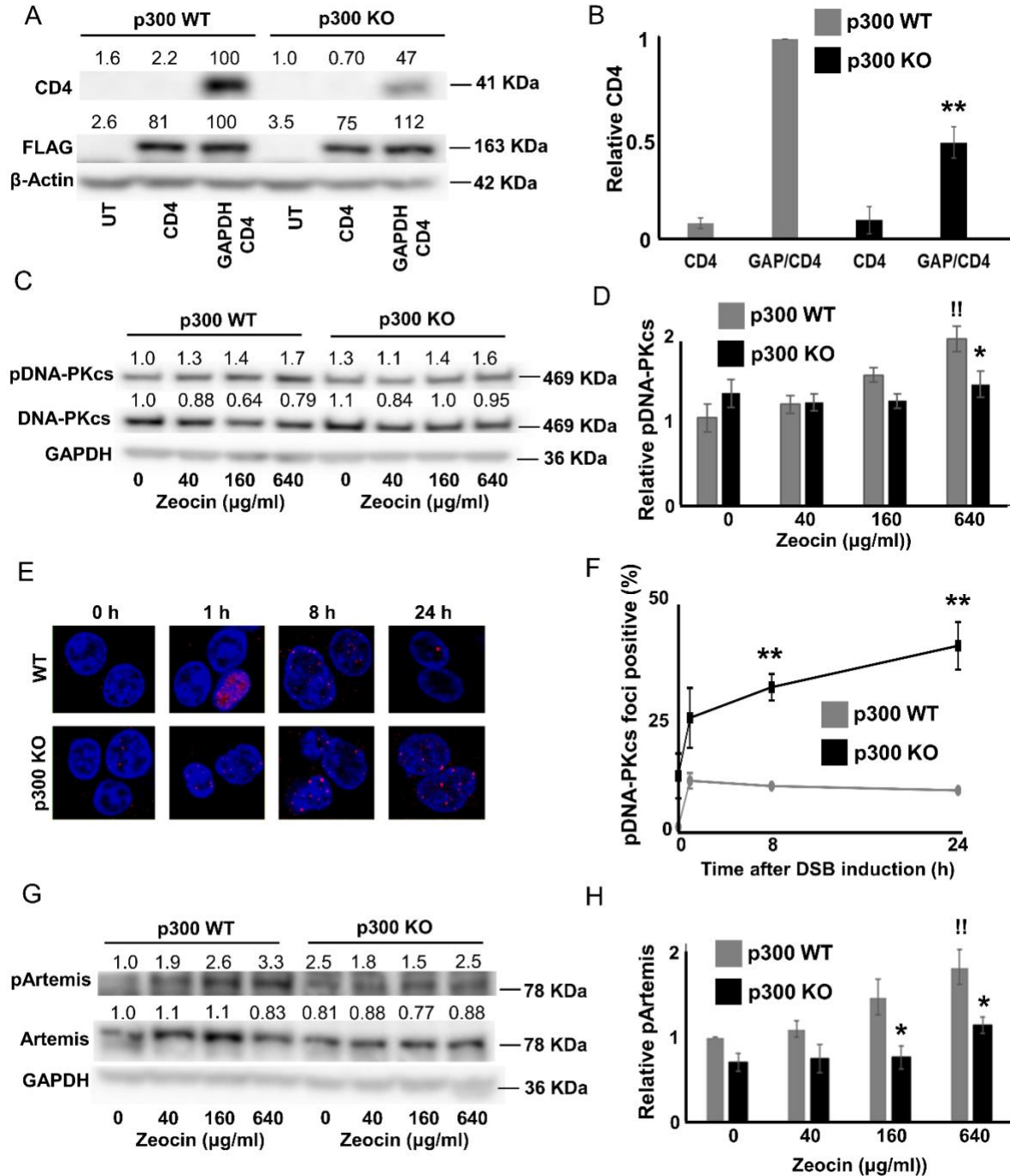


Figure 2-6. HCT116 P300 knockout decreases NHEJ efficiency.

(A) Representative immunoblots showing CD4 expression in HCT116 p300 WT and HCT116 p300 KO after transfection with control (UT), FLAG-tagged SgRNA-CAS9 targeting CD4 (CD4), and FLAG-tagged SgRNA-CAS9 targeting GAPDH and FLAG-tagged SgRNA-CAS9 targeting CD4 (GAP/CD4). (B) Densitometry of immunoblots (n=3) from panel A. CD4 was

normalized to β -actin as a loading control. Transfection efficiency was accounted for using FLAG abundance. (C) Representative images of immunoblot of pDNA-PKcs and total DNA-PKcs in HCT116 p300 WT and HCT116 p300 KO. (D) Densitometry of pDNA-PKcs normalized to total DNA-PKcs and GAPDH as a loading control. Data is shown relative HCT116 WT control. (E) Representative images of pDNA-PKcs foci following Zeocin exposure. (F) Percentages of pDNA-PKcs foci positive (>2) HCT116 cells following Zeocin exposure. (G) Representative immunoblot of pArtemis and total Artemis of HCT116 cells. (H). Densitometry of immunoblots (n=4) of pArtemis normalized to total Artemis and to GAPDH as a loading control. All values are represented as mean \pm standard error from at least three independent experiments. Statistical differences between groups were measured by using Student's T-test. * indicates $P < 0.05$. ** indicates $P < 0.01$. !! indicates significant difference between Zeocin treated and untreated group.

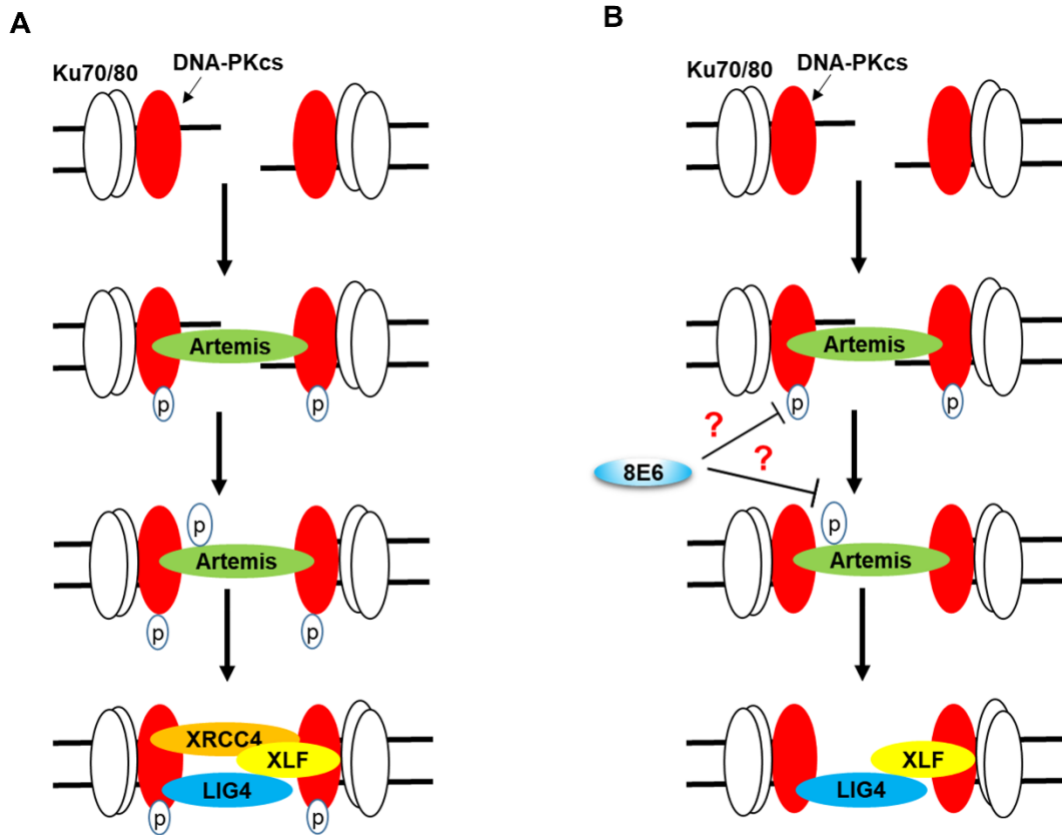
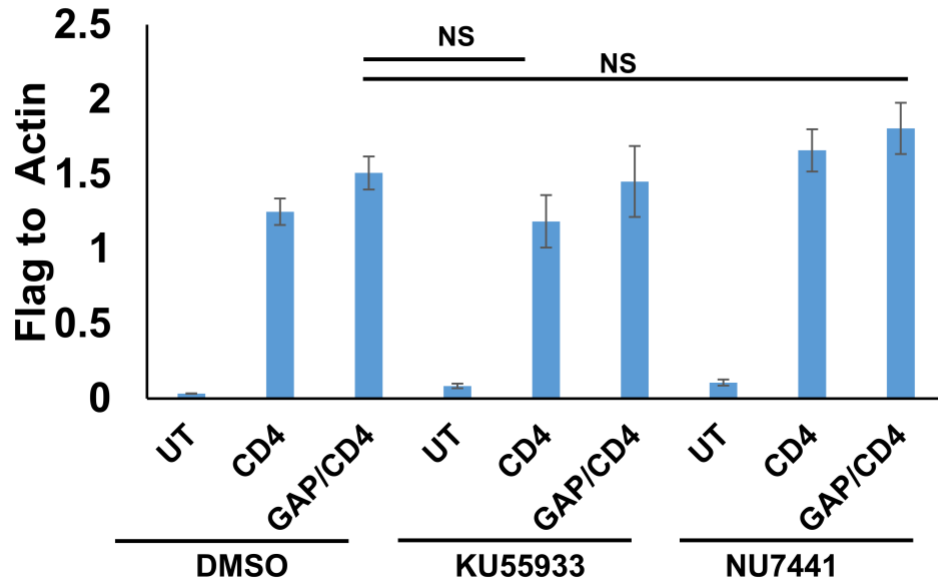


Figure 2-7. NHEJ in Cells with and without β -HPV 8E6.

(A) Schematic of canonical NHEJ pathway. DNA-PK holoenzyme (Ku70/80/DNA-PKcs) binds to DSB leading to DNA-PKcs autophosphorylation. Activated DNA-PK leads to Artemis phosphorylation and DNA end processing. Finally, the XRCC4/XLF/LIG complex repairs the break. (B) Schematic of β -HPV 8E6 alterations in canonical NHEJ. β -HPV 8E6 hinders DNA-PKcs autophosphorylation and activation, by which downstream steps including Artemis phosphorylation and XRCC4 recruitment were diminished. “?” represents unknown mechanism.

Chapter 2 supplemental figures

A



B

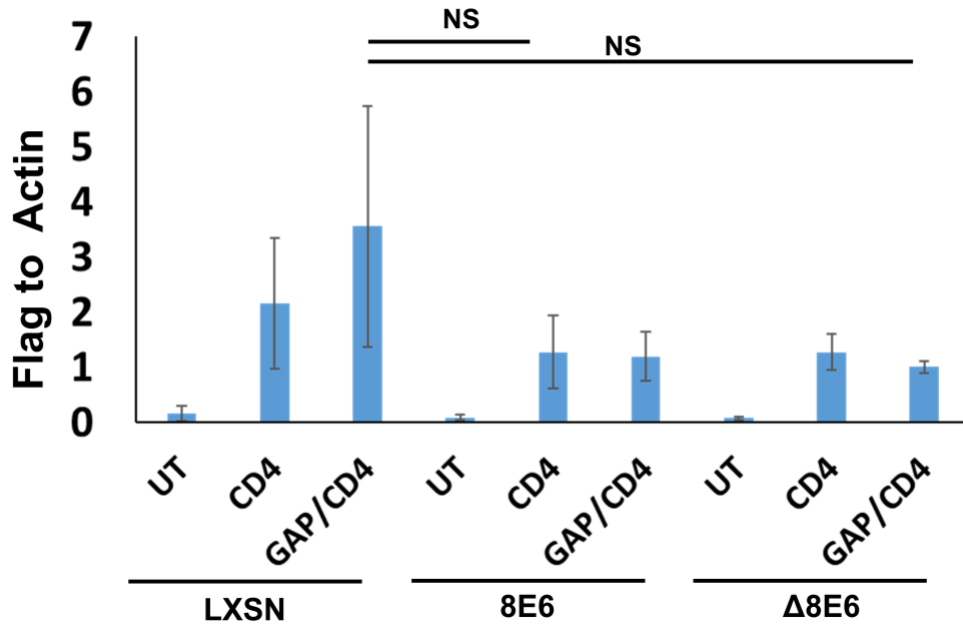


Figure S2-1. Transfection efficiency represented by FLAG tagged SgRNA-CAS9 targeting CD4 and GAPDH. NS: Not significant.

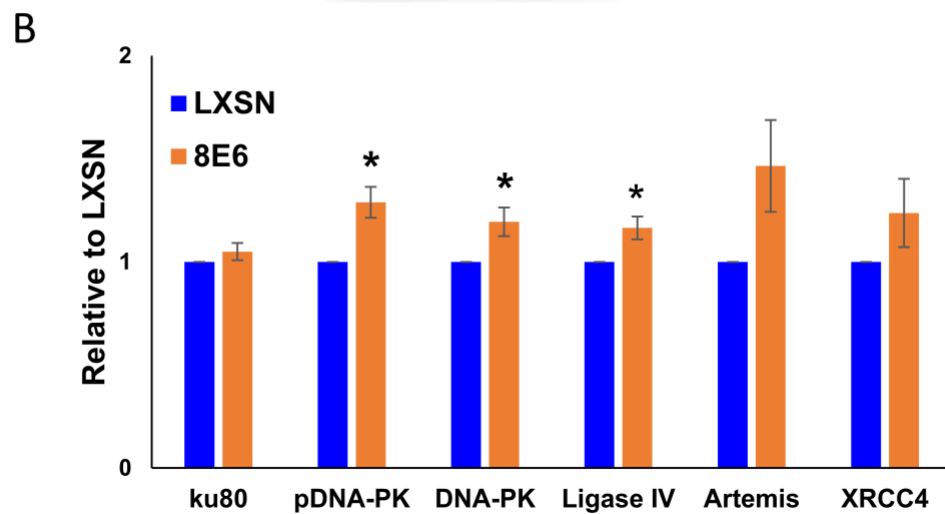
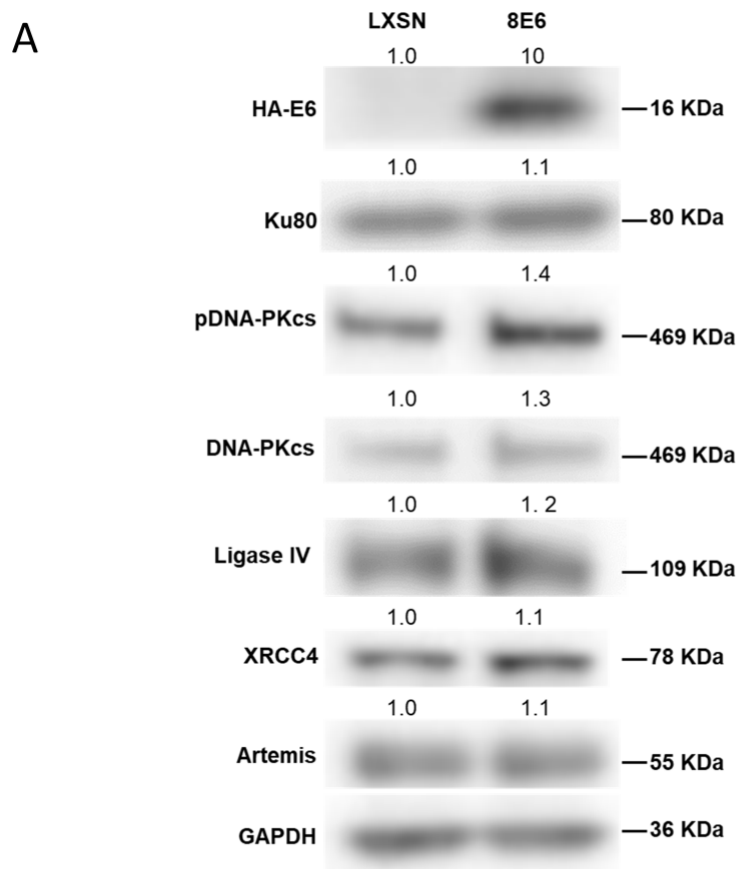


Figure S2-2. β -HPV 8 E6 does not decrease NHEJ protein in untreated cells. * indicates $p < 0.05$.

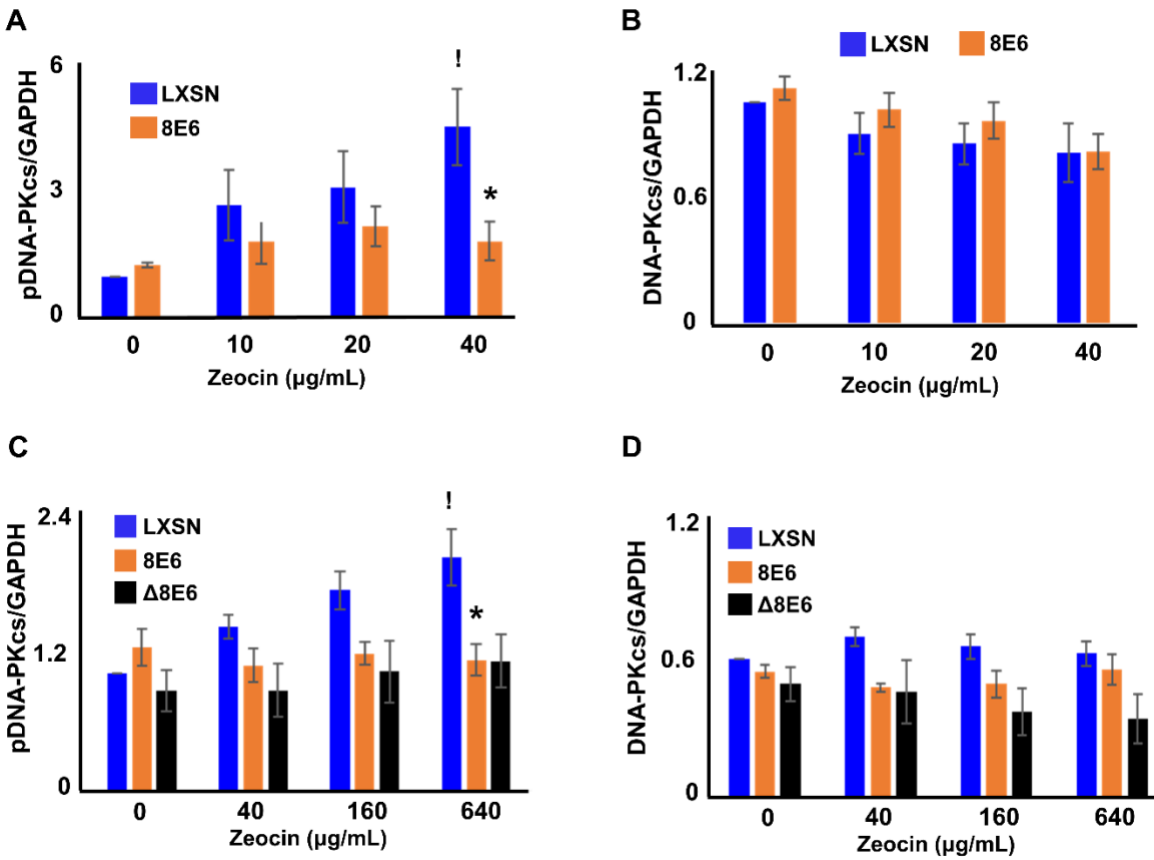


Figure S2-3. pDNA-PKcs and total DNA-PKcs normalized to GAPDH in HFK and U2OS. (A) HFK cells. (B) HFK cells. (C) U2OS cells. (D) U2OS cells. * indicates $p < 0.05$. ! indicates significant difference between Zeocin treated and untreated group.

Figure S2-3. pDNA-PKcs and total DNA-PKcs normalized to GAPDH in HFK and U2OS. (A) HFK cells. (B) HFK cells. (C) U2OS cells. (D) U2OS cells. * indicates $p < 0.05$. ! indicates significant difference between Zeocin treated and untreated group.

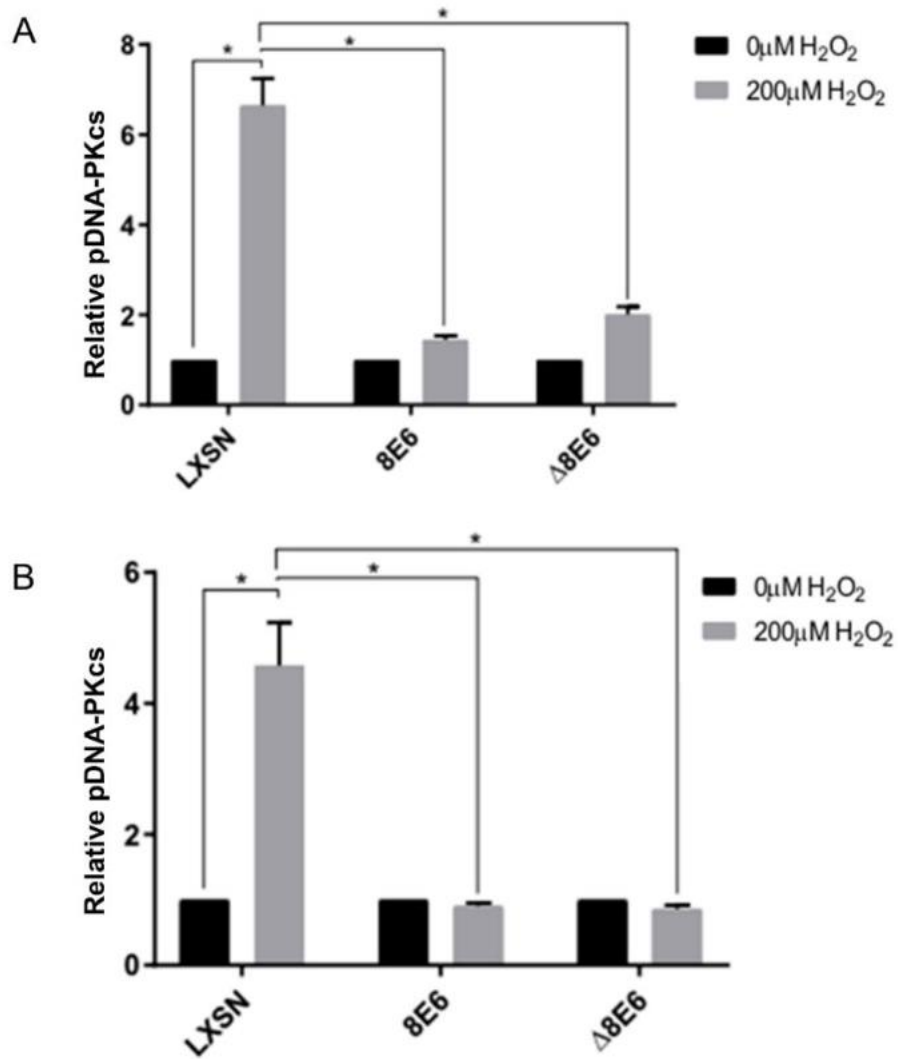


Figure S2-4. β -HPV 8 E6 decreases H₂O₂ induced DNA-PKcs phosphorylation. * indicates $p < 0.05$.

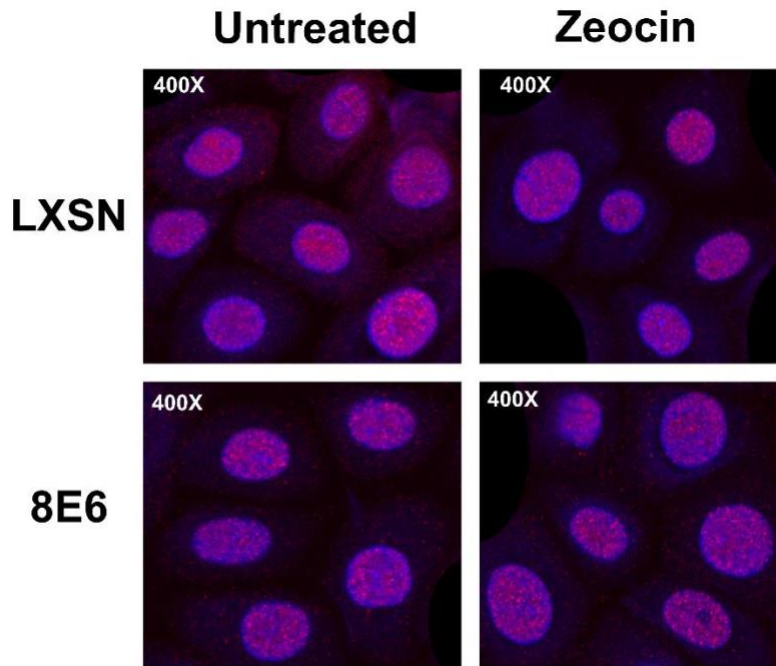


Figure S2-5. Total DNA-PKcs shows pan-nuclear expression in HFK cells. All microscopy images are 400X magnification.

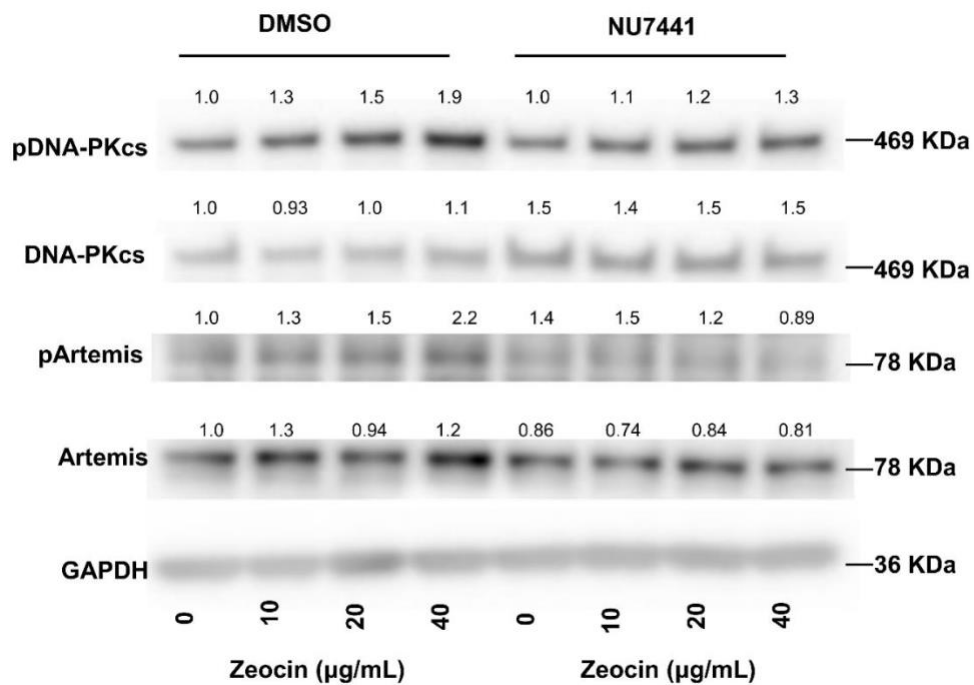


Figure S2-6. Inhibiting DNA-PK decreases Artemis phosphorylation.

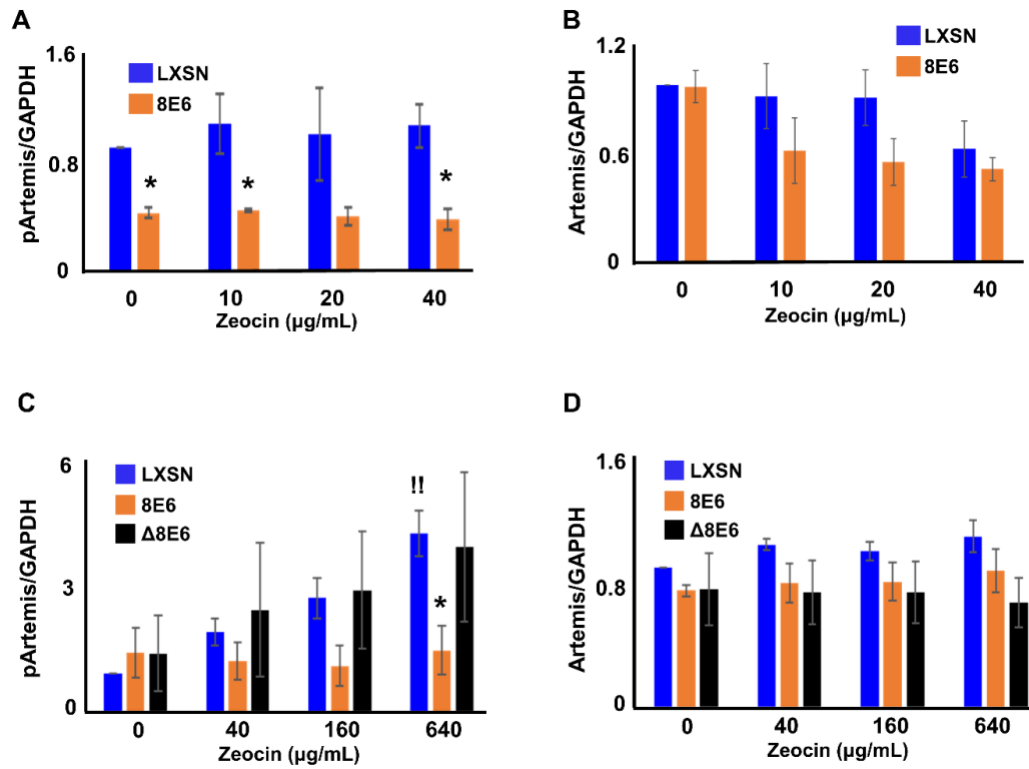


Figure S2-7. pArtemis and total Artemis normalized to GAPDH in HFK and U2OS cells. (A) HFK cells. (B) HFK cells. (C) U2OS cells. (D) U2OS cells. * indicates $p < 0.05$. !! indicates significant difference between Zeocin treated and untreated group ($p < 0.01$).

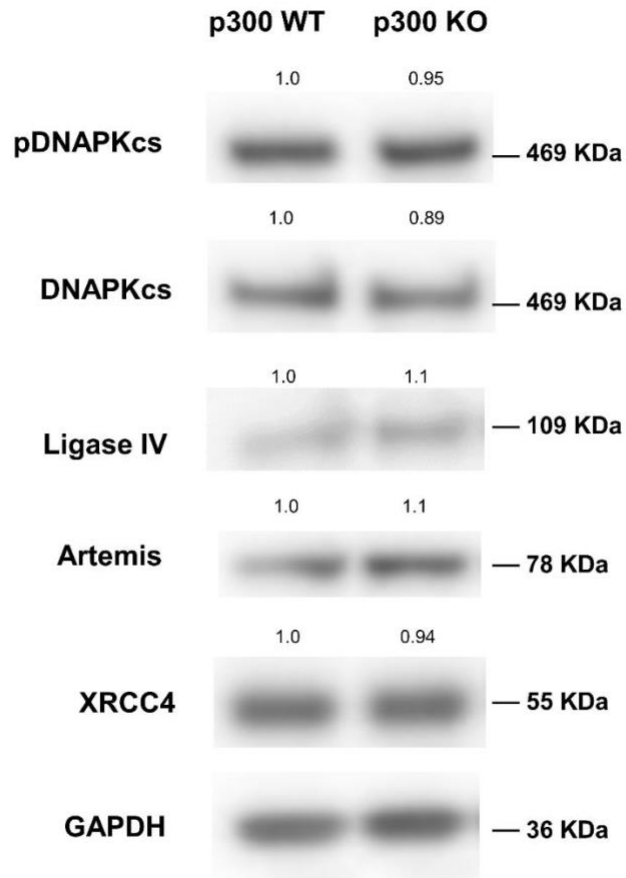


Figure S2-8. p300 knockout does not decrease major NHEJ proteins in untreated cells.

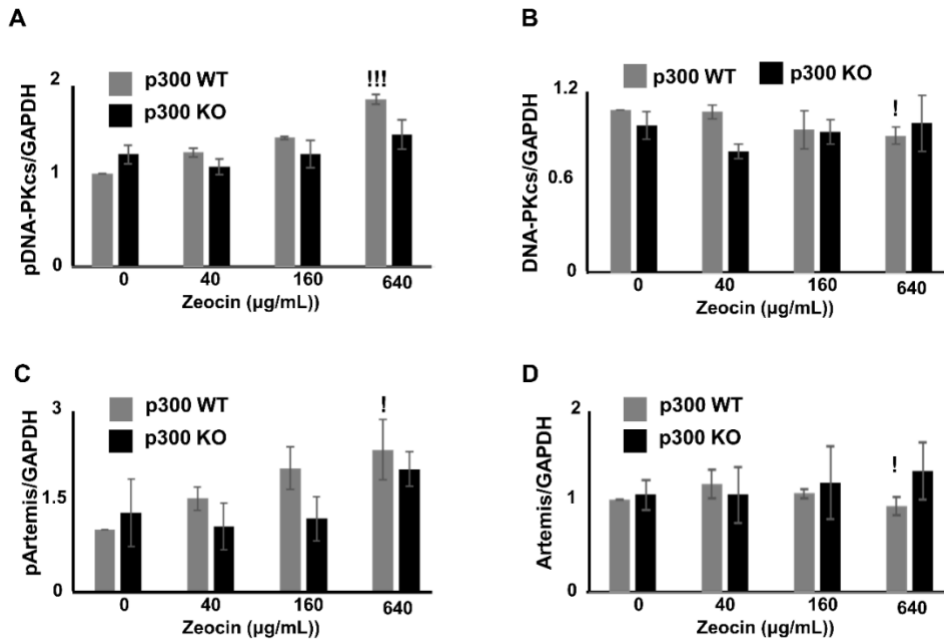


Figure S2-9. pDNA-PKcs, total DNA-PKcs, pArtemis, and total Artemis normalized to GAPDH in HCT cells. ! indicates significant difference between Zeocin treated and untreated group. !!! indicates significant difference between Zeocin treated and untreated group ($p < 0.001$).

Chapter 3 - Using Next Generation Sequencing to Identify Mutations Associated with Repair of a CAS9-induced Double Strand Break Near the CD4 Promoter

Changkun Hu^{1*}, Tyler Doerksen^{2*}, Taylor Bugbee¹, Nicholas A. Wallace¹, Rachel Palinski^{2,3}

¹Division of Biology, Kansas State University, Manhattan, KS 66506, USA

²Kansas State Veterinary Diagnostic Laboratory, Kansas State University, Manhattan, KS 66506, USA

³Department of Diagnostic Medicine/Pathobiology, Kansas State University, Manhattan, KS 66506, USA

*These authors contributed equally to this work.

Corresponding author: Rachel Palinski (rpalinski@vet.k-state.edu)

KEYWORDS:

DNA damage response, DSB, DSB repair, CAS9 induced DSB, Next-generation sequencing, genomics.

Published as: Hu, C., Doerksen, T., Bugbee, T., Wallace, N. A., Palinski, R. Using Next Generation Sequencing to Identify Mutations Associated with Repair of a CAS9-induced Double Strand Break Near the CD4 Promoter. *J. Vis. Exp.* (181), e62583, doi:10.3791/62583 (2022).

SUMMARY:

Presented here is sgRNA/CAS9 endonuclease and next-generation sequencing protocol that can be used to identify the mutations associated with double strand break repair near the CD4 promoter.

ABSTRACT

Double strand breaks (DSBs) in DNA are the most cytotoxic type of DNA damage. Because a myriad of insults can result in these lesions (e.g., replication stress, ionizing radiation, unrepaired UV damage), DSBs occur in most cells each day. In addition to cell death, unrepaired DSBs reduce genome integrity and the resulting mutations can drive tumorigenesis. These risks and the prevalence of DSBs motivate investigations into the mechanisms by which cells repair these lesions. Next generation sequencing can be paired with the induction of DSBs by ionizing radiation to provide a powerful tool to precisely define the mutations associated with DSB repair defects. However, this approach requires computationally challenging and cost prohibitive whole genome sequencing to detect the repair of the randomly occurring DSBs associated with ionizing radiation. Rare cutting endonucleases, like I-Sce1, provide the ability to generate a single DSB, but their recognition sites must be inserted into the genome of interest. As a result, the site of repair is inherently artificial. Recent advances allow guide RNA (sgRNA) to direct a Cas9 endonuclease to any genome locus of interest. This could be applied to the study of DSB repair making next generation sequencing more cost effective by allowing it to be focused on the DNA flanking the Cas9-induced DSB. The goal of the manuscript is to demonstrate the feasibility of this approach by presenting a protocol that can define mutations that stem from the repair of a DSB upstream of the CD4 gene. The protocol can be adapted to determine changes in the mutagenic potential of DSB associated with exogenous factors, such as repair inhibitors, viral

protein expression, mutations, and environmental exposures with relatively limited computation requirements. Once an organism's genome has been sequenced, this method can be theoretically employed at any genomic locus and in any cell culture model of that organism that can be transfected. Similar adaptations of the approach could allow comparisons of repair fidelity between different loci in the same genetic background.

INTRODUCTION

Maintaining genomic stability is critical for all living organisms. Accurate DNA replication and a robust DNA damage response (DDR) are necessary to faithfully propagate the genetic material^{1,2}. DNA damages occur regularly in most cells^{2,3}. When these damages are sensed, cell cycle progression is halted, and DNA repair mechanisms are activated. Double strand breaks in DNA or DSBs are the most toxic and mutagenic type of DNA damage^{3,4}.

While several DDR signaling pathways can repair these lesions, the most thoroughly studied DSB repair pathways are homologous recombination (HR) and non-homologous end joining (NHEJ). HR is a largely error-free pathway that repairs a DSB using a sister chromatid as a homologous template. This tends to happen in the S phase and G2 phase of a cell cycle⁵⁻⁷. NHEJ is more error-prone, but it can happen throughout the cell cycle^{8,9}. Various reporter assays have been developed to measure the efficiency of specific repair mechanisms¹⁰⁻¹². These assays tend to rely on flow cytometry for a high throughput measurements of DSB repair pathway activity using GFP or mCherry as a readout^{11,13}. While highly efficient, they rely on canonical repair occurring at an artificially introduced DSB.

There are a variety of other methods used to study DSB repair. Many of these rely on immunofluorescence (IF) microscopy^{1,14}. IF microscopy detects discreet nuclear foci

representative of repair complexes after DSBs are induced by exposure to genotoxic chemicals or ionizing radiation^{15,16}. Tracking the formation and resolution of these foci provides an indication of repair initiation and completion, respectively^{14,17}. However, these methods of DSB induction (i.e., chemicals or ionizing radiation) do not cause DSBs at defined locations in the genome. It is also functionally impossible to use them to consistently induce only a small number (e.g., 2-4) of DSBs. As a result, the most commonly used methods of inducing DSBs cause a multitude of lesions randomly distributed throughout the genome¹⁸. A small number of DSBs can be introduced by inserting the recognition site for a rare-cutting endonuclease and expressing the pertinent endonuclease, such as I-SceI¹⁹. Unfortunately, the required integration of a target site prevents the examination of DSB at endogenous genomic loci.

This manuscript describes a method to detect mutations associated with the repair of a DSB generated at a user-defined locus. We provide a representative example of the approach applied to assess the ability of a viral protein to increase the number of mutations associated with a DSB. Specifically, this manuscript describes the use of a single guide RNA (sgRNA) to direct a CAS9 endonuclease to induce a DSB at human CD4 open reading frame in human foreskin keratinocytes expressing vector control (HFK LXS_N) and HFK that expresses the E6 protein of human papilloma virus type 8 (HFK 8E6). Targeted next-generation sequencing (NGS) of the region surrounding the break allows mutations associated with the repair of the lesion to be rigorously defined. These data demonstrate that the viral protein causes an approximately 20-fold increase in mutations during DSB repair. It also provides an unbiased characterization of the mutagenic consequences of DSBs at a single locus without the need for whole-genome sequencing. In principle, the protocol could be readily adapted to compare the relative risk of mutations between genome loci or cell lines.

PROTOCOL

1. Cell plating

1.1 Grow HFK LXS_N and HFK 8E6 cells in 10 cm plates in keratinocyte culture media (10 mL/plate) with human keratinocyte growth supplement (HKGS) and 1% penicillin and streptomycin. Grow cells to about 80% confluence at 37 °C in a jacket incubator with 5% CO₂.

1.2 Replace culture media with 3 mL of trypsin-EDTA (0.05%, ethylenediamine tetraacetic acid). Incubate at 37 °C for 3 min. Neutralize trypsin with equal volume of fetal bovine serum (FBS) supplemented media and transfer cells to a 15 mL centrifuge tube.

Centrifuge at 300 x g for 5 min.

1.3 Resuspend cells with 10 mL of keratinocyte culture media with HKGS.

Determine the concentration of cells with a hemocytometer.

1.4 Plate 4 x 10⁵ cells/6-cm plates (seed two plates for HFK LXS_N and two plates for HFK 8E6) in 4mL of keratinocyte culture media with HKGS and 1% penicillin and streptomycin. Grow at 37 °C in a jacket incubator with 5% CO₂.

NOTE: Analysis of HFK cells was chosen for this protocol for two reasons. First, they are a difficulty to transfect cell line. Thus, by demonstrating that the protocol works in this cell line, evidence is provided that it will likely work in more commonly used and more readily transfected cells. Secondly, previously published data demonstrate that a viral protein (8E6) hinders the repair of double strand breaks in DNA^{20–22}. Thus, comparing HFK LXS_N and HFK

8E6 allows us to demonstrate the ability of the assay to detect increases in mutations associated with a reduction in cellular repair capacity.

2. Transfection

2.1. On the day of transfection (24 h after plating), replace media with 3 mL of antibiotic-free supplemented media. Incubate for 2 h at 37 °C in a jacket incubator.

2.2. Transfect cells with appropriate lipid-based transfection reagents according to the manufacturer's instructions.

2.2.1. Warm transfection reagents to room temperature and pipette gently before using.

2.2.2. For each cell line (HFK LXS and HFK 8E6), place appropriate amount of transfection buffer (as directed by manufacturer) in a sterile 1.5 mL centrifuge tube (Tube 1). Include another tube with same amount of transfection buffer (mock transfection or Tube 2).

2.2.3. Add 2 µg of plasmid DNA expressing CAS9/sgRNA targeting human CD4 (px330-CD4, 5' - GGCGTATCTGTGTGAGGACT) to Tube 1 from step 2.2.2. Pipette gently to mix completely. Add equal volume of sterile water to Tube 2.

2.2.4. Include a control plate with transfection reagents alone (no plasmid) for each cell line.

NOTE: The second plate serves as a negative control in the experiment, allowing the user to confirm that transfection with the CAS9/sgRNA are not responsible for any mutations.

2.2.5. Add appropriate amount transfection reagent (as directed by manufacturer) to the tube with DNA mixture (Tube 1) from step 2.2.3 and the mock transfection (Tube 2) from step

2.2.2. Pipette gently to mix completely. Incubate at room temperature for 15-30 min to allow sufficient time for complexes to form.

2.2.6. Add the transfection mixture drop-wise to the plate. Gently rock the culture for 1 min to evenly distribute the transfection mixture.

2.3. Wait 48 h after the transfection to allow CAS9 expression.

2.4. Harvest cells by trypsinization.

2.4.1. Replace culture media with 1 mL of trypsin-EDTA (0.05%, ethylenediamine tetraacetic acid). Incubate at 37 °C for 3 min. Neutralize trypsin with equal volume of FBS supplemented media.

2.4.2. For each plate of cells, transfer the cells suspension to two microcentrifuge tubes with equal aliquots. Centrifuge at 300 x g for 5 min.

2.4.3. Resuspend the cell pellet from one tube in step 2.4.2 in 1 mL of phosphate buffered saline (PBS) for sequencing. Resuspend the other tube from 2.4.2 with ice-cold PBS for immunoblot.

2.5. Harvest the whole cell lysates for immunoblot.

2.5.1. Centrifuge the tube at 300 x g for 5 min. Discard the supernatant.

2.5.2. Add 100 µL radioimmunoprecipitation assay buffer (RIPA lysis buffer) mixed with 1 % protease inhibitor and 1% phosphatase inhibitor into the tube, mix thoroughly with a pipette and incubate for 10 min on ice.

NOTE: RIPA lysis buffer contains 10 mM Tris-HCl, pH 8.0; 1 mM EDTA; 0.5 mM EGTA; 1% Triton X-100; 0.1% Sodium Deoxycholate; 0.1% SDS; 140 mM NaCl, and deionized water.

2.5.3. Centrifuge lysates at 13,000 x g for 10 min. Collect supernatants for immunoblot.

3. Measuring CAS9 expression via immunoblot

3.1. Determine the protein concentration with a bicinchoninic acid (BCA) assay according to the manufacturer's instructions.

3.2. Run 20 µg of protein of each sample in the wells of a 3-8% Tris-acetate gel for 150 min and semidry transfer (10 V for 30 min then 25 V for 12 min) to polyvinylidene difluoride membrane.

3.3. After blocking the membrane in 5% nonfat dry milk in PBS with 0.1% tween (PBST) for 1 h at room temperature, add anti-CAS9 (1:1000) and anti-GAPDH (1:1000) antibodies. Incubate at 4 °C overnight.

3.4. After washing the membrane with PBST, incubate the membrane with secondary antibody in 5% nonfat dry milk in PBST for 1 h at room temperature.

3.5. Image the blot and determine CAS9 level by densitometry²³. See Figure 1 for a representative blot.

NOTE: Detecting phosphorylated H2AX (S139) foci formation by immunofluorescence microscopy can be used to validate CAS9 activity¹⁴. A low number of distinct foci (typically 1-4 foci) are expected depending on the cell cycle position, whether mutations in the CAS9 target site prevent further cutting, and how many copies of the CAS9 cutting site exist in the genome of interest. A representative image is showed in Figure 3-2.

4. Nucleic acid extraction and amplicon generation

4.1. Extract DNA from cell samples from 2.4.3 using a high-molecular weight DNA extraction kit, as specified by the manufacturer.

4.2. Resuspend primers with indicated solvent according to datasheet. Dilute with the same reagent to 20 μ M and pool 20 μ M primers into the indicated pools.

NOTE: Primer pool is listed in Supplemental table 1.

4.3. Create a PCR Master mix using a long amplification Taq polymerase for each 20 μ M primer pool as specified in Table 1.

4.3.1. Add 21 μ L of the mastermixes to separate PCR tubes.

4.4. Add 4 μ L of the target sample (100 ng/ μ L) from step 4.1 to PCR assay tubes containing mastermix and cap assay tubes. Ensure separate reactions for each primer pool.

4.4.1. Vortex to mix PCR assay tubes and centrifuge (quick spin) to remove droplets from tube lids.

4.4.2. Place the PCR tubes on a conventional thermal cycler machine.

5.4.3. Program PCR machine as specified in Table 2.

4.4.4. Run the program on a thermal cycler.

5. PCR clean-up

5.1. Remove primers from PCR reactions using a bead-based PCR cleanup system.

5.1.1. Remove clean-up beads from the refrigerator 30 min prior to use.

5.1.2. Vortex beads well prior to use and ensure all beads are resuspended.

5.1.3. Add 30 μ L (1.2x) of resuspended beads to each well of a deep well 96-well plate.

5.1.4. Add 25 μ L of PCR reaction to wells containing beads.

5.1.5. Place the plate on a plate shaker at 2000 rpm for 2 min.

5.1.6. Allow the plate to remain at room temperature for 5 min following shaking.

- 5.1.7. Place the deep well plate on a 96-well plate magnet and incubate for 2 min.
- 5.1.8. Remove and discard the supernatant without disturbing beads.
- 5.1.9. While the plate remains on the magnet, add 180 μL of 80% ethanol and incubate for 30 s. Remove and discard supernatant.
- 5.1.10. Repeat step 5.1.9.
- 5.1.11. Using a 10 μL pipette, remove and discard any remaining liquid from wells.
- 5.1.12. Allow beads to dry at room temperature for 10 min.
- 5.1.13. Add 20 μL of nuclease free water to the wells containing beads and remove plate from magnet.
- 5.1.14. Shake the plate at 2000 rpm for 2 min at room temperature.
- 5.1.15. Incubate the plate at room temperature for 5 min.
- 5.1.16. Place the plate on a magnet stand and incubate for 2 min at room temperature.
- 5.1.17. Remove the supernatant into a second, labeled PCR plate. This contains the cleaned-up DNA.
- 5.2. Measure the concentration of each reaction with a Fluorometer.
- 5.2.1. Ensure dsDNA Fluorometer reagents are at room temperature.
- 5.2.2. Set up Fluorometric assay tubes plus two additional tubes for standards.
- 5.2.3. Add 199 μL of 1x dsDNA working solution to all but two tubes. Add 190 μL of the working solution to last two tubes.
- 5.2.4. Add 10 μL of the two standards (included in the material table) to separate assay tubes.

5.2.5. Add 1 μL of each PCR reaction to Fluorometer mastermix tubes.

5.2.6. Vortex tubes to mix and incubate at room temperature for 2 min.

5.2.7. On the home screen of the fluorometer, select the button with the assay kit in use (1x dsDNA) then 'Read Standards and run samples.

5.2.8. Insert standard 1 tube, select the 'read' button then repeat for standard 2.

5.2.9. Following 5.2.6, repeat for one sample, select a sample volume of 1 μL and the resulting concentration will be provided.

5.2.10. Repeat 5.2.7 for remaining samples

5.3. Calculate the projected molarity of all reactions and pool equal concentrations of reactions from each individual sample separately (one final pool per sample) using the equation below.

$$\text{Picomoles}/\mu\text{L} = (\text{DNA Concentration } (\mu\text{g}/\text{mL})) / (0.66 \times \text{DNA Size (bp}=1000))$$

5.3.1. Repeat steps 5.2.1 to 5.2.7 to obtain the final pool concentration.

5.4. Check the amplicon pool on a capillary electrophoresis machine/agarose gel as specified by the manufacturer.

5.4.1. Prepare capillary electrophoresis tubes for the appropriate number of samples.

5.4.1. Add 7 μL of DNA buffer as specified to the manufacturer.

5.4.2. Add 4 μL of the amplicon pool to the tube containing DNA buffer.

5.4.3. Place tubes on electrophoresis machine and run machine as specified by the manufacturer for dsDNA.

5.4.4. View the electrophoresis gel pictures ensuring the bands localize to ~5 kb (size of amplicons).

5.5. Calculate the projected molarity of all reactions and pool equal concentrations of reactions from each individual sample separately (one final pool per sample) using the equation below.

$$\text{Picomoles}/\mu\text{L} = (\text{DNA Concentration } (\mu\text{g}/\text{mL})) / (0.66 \times \text{DNA Size (bp}=1000))$$

6. Library preparation

6.1. Dilute sample pools from 5.3.1 to 0.2 ng/ μ L for library preparation.

6.1.1 Using a low-input library preparation kit compatible with short sequences (300bp) prepare libraries using unique index combinations for each sample pool created in step 5.3 following the manufacturer's instructions.

NOTE: Follow manufacturer's instructions to select index sequences. All indexes amenable to the library prep kit will work for the samples.

6.1.2. Following library preparation, pool all samples according to the manufacturer's instructions.

NOTE: Before creating the library pool, calculate the number of reads necessary for 250x coverage of your target sequence and ensure that the selected sequencing cartridge can provide adequate coverage for each included sample. For 0.5Mb total, this will equate to 1M reads.

6.2. Prepare the library pool for sequencing.

6.2.1. Thaw and prepare 300-cycle cartridge and sequencing reagents.

6.2.2. Denature and dilute sequencing pool created in step 5.1.1 according to the sequencer's manufacturer's instructions.

6.2.3. Add denatured and diluted library pool to sequencing reagents and Run the sequencing machine as specified by the manufacturer.

NOTE: See attached Table 3 for trouble shootings.

7. Data analysis

NOTE: All data steps are performed in genomic data analysis software. Parentheses indicate user input. Greater than sign indicates the order of mouse clicks for any given step (e.g. 1st mouse click>2nd mouse click)

7.1. Import the reads by clicking on Open software>Import>Illumina>Select files>Next>Select location to Save>Finish. The reads will now appear in the software.

7.2. Trim and filter the reads.

7.2.1. In the deep sequence data analysis software, trim the raw reads default parameters.

7.2.2. Highlight reads and click Toolbox>Prepare sequencing data>Trim reads>Next>Next>Next>Next>Save>Next>(Select location to save)>Finish

7.3. Map Trimmed reads to reference.

7.3.1. Map trimmed reads to the reference sequence used in 4.1 using a match score of 2, mismatch cost of 3 and insertion/deletion costs of 2. Ensure length fraction is above 0.7 and similarity fraction is at or above 0.8.

7.3.2. Highlight trimmed read file and click Toolbox>Resequencing analysis>Map reads to reference>Next>(Select reference sequence)>Next>(Ensure parameters are indicated as above)>Next>Save>(Select location to save)>Finish.

7.4. Extract variants and indels.

7.4.1. Using an appropriate indel caller, extract indels using a p-value threshold of 0.005 or lower and a maximum number of mismatches of 3.

7.4.2. Highlight mapped read file and click Toolbox>Resequencing analysis>Variant detection>Indels and Structural variants>Next>(Ensure required significance is input>Next>Save>(Select location to save)>Finish.

7.4.3. Using an appropriate variant caller, call variants from the read mapping using a significance of 5%.

7.4.4. Highlight mapped read file and click Toolbox>Resequencing analysis>Variant detection>Low frequency variant detection>Next>(Ensure required significance is input>Next>Next>Save>(Select location to save)>Finish

NOTE: Ensure to account for the ploidy of the host genome in the indel and variant callers. Do not extract mutants below 5%. This threshold accounts for PCR and sequencing errors associated with the assay. Normalization (based on immunoblot detection of CAS9) should be done by adjusting sequencing coverage. For example, if sample A has twice the transfection efficiency of sample B, then 50% of the reads from sample A should be used for analysis. This should be done by random sampling and not reduce the coverage for any sample below 100x.

REPRESENTATIVE RESULTS

Three representative results are presented for this protocol. Figure 3-1 is an immunoblot confirming expression of CAS9 in HFK control (LXSN) and HFK expressing β -HPV 8E6 (8E6). 48 h after transfection, whole cell lysates were harvested and subsequently probed with an anti-CAS9 antibody (or GAPDH as a loading control). The result shows that HFK LXSN and HFK 8E6 are expressing similar amount of CAS9 indicating that transfection efficiency is similar

between two cell lines. Figure 3-2 is an immunofluorescence microscopy image showing CAS9 induced DSBs using pH2AX foci, a standard marker for DSBs 24. This indicates two DSBs are induced by CAS9/sgRNA and thus confirms that DSB induction is occurring as expected. Figure 3 shows that 8E6 increases genomic variations within 200 Kb around the CAS9 induced DSB 22. This is consistent with the hypothesis that HPV8 E6 deregulates DSB repair and increases genomic instability. This figure shows one way in which data obtained from this approach can be displayed.

DISCUSSION

In addition to the depth of information provided, there are several advantages to this method. First, DSB repair, in theory, can be assessed at any genomic loci without modifying the genome of the cell of interest. Second, access to NGS analysis of repair is increased by the reduced cost and computational effort afforded by making and analyzing a single DSB targeted to a defined area. Finally, with the genomes of additional organisms routinely becoming available and multiple publications demonstrating successful transfection of diverse mammalian and non-mammalian cell lines, the utility of this approach is expected to be broad ^{10,23,24}.

This manuscript analyzed DSB repair in human foreskin keratinocytes as an illustrative example. Transfection efficiency tends to be lower in keratinocytes than other tissue types. Therefore, this protocol used a transfection approach optimized for these hard-to-transfect cells. The transfection approach should be optimized for the cell type analyzed. The ability of CAS9-induced DSB used in this protocol has been confirmed in osteosarcoma, colon cancer, lung cancer, fibroblast, embryonic kidney, and human keratinocyte cells ^{10,23}. However, before performing next generation sequencing, it is recommended that CAS9 expression and activity are confirmed.

A critical step in this protocol is when comparing between or among different samples to normalize the analysis to account for differences in CAS9 transfection efficiency. To do that, relative CAS9 protein level should be measured by immunoblotting and densitometry (Figure 3-1). It is also important to ensure the specificity of CAS9 cleavage as indicated by distinct pH2AX (S139) foci formation, detectable by IF microscopy¹⁴ (Figure 3-3). Alternately, T7 endonuclease assay can be used to examine CRISPR/Cas9 activity and sgRNA efficiency.

A notable limitation of this approach is that CAS9-induced DSB tend to be “cleaner” than DSB caused by radiation or similar physiological damage. Therefore, the method described here may underestimate the number or severity of the mutations associated with the repair of naturally occurring lesions. The use of other sequence specific nucleases that induce DSB with longer overhangs may help overcome this limitation²⁶. Moreover, it is not fully understood whether chromatin region (e.g., heterochromatin and euchromatin) affects CAS9 activity. Thus, the user should be careful to confirm equivalent CAS9 activity when comparing mutations at different sites.

The method described here can be used to define the relative mutagenic consequences of repairing DSBs in a variety of contexts. For example, it could facilitate examination of novel small molecule DNA repair inhibitors. This would allow inhibitors that are more mutagenic in transformed (compared to untransformed) cells to be prioritized for development as chemotherapeutic agents. This approach may also be useful to compare within the same genomic background to determine the frequency of mutations associated with DSB repair at different gene contexts (e.g., near a promoter, enhancer, or repressor), between cells with different mutations (e.g., signaling genes that are constitutively active or missense mutations), or other similar

permutations. The flexibility and affordability of the approach provides a powerful tool for future analyses.

ACKNOWLEDGMENTS

Research reported in this manuscript was supported by the National Institute of General Medical Sciences of the National Institutes of Health (P20GM130448) (NAW and RP); National Cancer Institute of the National Institutes of Health (NCI R15 CA242057 01A1); Johnson Cancer Research Center in Kansas State University; and the U.S. Department of Defense (CMDRP PRCRP CA160224 (NAW)). We appreciate KSU-CVM Confocal Core and Joel Sanneman for our immunofluorescence microscopy. The content is solely the responsibility of the authors and does not necessarily represent the official views of these funding agencies.

DISCLOSURES:

The authors have nothing to disclose.

REFERENCES

- [1] P. Brianti, E. De Flammineis, S.R. Mercuri, Review of HPV-related diseases and cancers, *New Microbiol.* 40 (2017) 80–85.
- [2] D. Hasche, S.E. Vinzón, F. Rösl, Cutaneous Papillomaviruses and Non-melanoma Skin Cancer: Causal Agents or Innocent Bystanders?, *Front Microbiol.* 9 (2018). <https://doi.org/10.3389/fmicb.2018.00874>.
- [3] A.J. Pierce, R.D. Johnson, L.H. Thompson, M. Jasin, XRCC3 promotes homology-directed repair of DNA damage in mammalian cells, *Genes Dev.* 13 (1999) 2633–2638.
- [4] N. Bennardo, A. Cheng, N. Huang, J.M. Stark, Alternative-NHEJ Is a Mechanistically Distinct Pathway of Mammalian Chromosome Break Repair, *PLoS Genet.* 4 (2008). <https://doi.org/10.1371/journal.pgen.1000110>.
- [5] R. Bhargava, M. Sandhu, S. Muk, G. Lee, N. Vaidehi, J.M. Stark, C-NHEJ without indels is robust and requires synergistic function of distinct XLF domains, *Nat Commun.* 9 (2018) 2484. <https://doi.org/10.1038/s41467-018-04867-5>.

- [6] L.J. Tsai, F.W. Lopezcolorado, R. Bhargava, C. Mendez-Dorantes, E. Jahanshir, J.M. Stark, RNF8 has both KU-dependent and independent roles in chromosomal break repair, *Nucleic Acids Research*. 48 (2020) 6032–6052. <https://doi.org/10.1093/nar/gkaa380>.
- [7] R. Bhargava, F.W. Lopezcolorado, L.J. Tsai, J.M. Stark, The canonical non-homologous end joining factor XLF promotes chromosomal deletion rearrangements in human cells, *J. Biol. Chem.* 295 (2020) 125–137. <https://doi.org/10.1074/jbc.RA119.010421>.
- [8] K.M. Bedard, M.P. Underbrink, H.L. Howie, D.A. Galloway, The E6 Oncoproteins from Human Betapapillomaviruses Differentially Activate Telomerase through an E6AP-Dependent Mechanism and Prolong the Lifespan of Primary Keratinocytes, *J Virol.* 82 (2008) 3894–3902. <https://doi.org/10.1128/JVI.01818-07>.
- [9] A. Kötter, K. Cornils, K. Borgmann, J. Dahm-Daphi, C. Petersen, E. Dikomey, W.Y. Mansour, Inhibition of PARP1-dependent end-joining contributes to Olaparib-mediated radiosensitization in tumor cells, *Mol Oncol.* 8 (2014) 1616–1625. <https://doi.org/10.1016/j.molonc.2014.06.008>.
- [10] M. Tsukuda, K. Miyazaki, DNA fragmentation caused by an overdose of Zeocin, *Journal of Bioscience and Bioengineering.* 116 (2013) 644–646. <https://doi.org/10.1016/j.jbiosc.2013.05.004>.
- [11] E.P. Rogakou, D.R. Pilch, A.H. Orr, V.S. Ivanova, W.M. Bonner, DNA Double-stranded Breaks Induce Histone H2AX Phosphorylation on Serine 139, *Journal of Biological Chemistry.* 273 (1998) 5858–5868. <https://doi.org/10.1074/jbc.273.10.5858>.
- [12] G. Iliakis, T. Murmann, A. Soni, Alternative end-joining repair pathways are the ultimate backup for abrogated classical non-homologous end-joining and homologous recombination repair: Implications for the formation of chromosome translocations, *Mutation Research/Genetic Toxicology and Environmental Mutagenesis.* 793 (2015) 166–175. <https://doi.org/10.1016/j.mrgentox.2015.07.001>.
- [13] J. Patterson-Fortin, A.D. D'Andrea, Exploiting the Microhomology-Mediated End-Joining Pathway in Cancer Therapy, *Cancer Res.* 80 (2020) 4593–4600. <https://doi.org/10.1158/0008-5472.CAN-20-1672>.
- [14] D. Simsek, M. Jasin, Alternative end-joining is suppressed by the canonical NHEJ component Xrcc4–ligase IV during chromosomal translocation formation, *Nature Structural & Molecular Biology.* 17 (2010) 410–416. <https://doi.org/10.1038/nsmb.1773>.
- [15] M. Wang, W. Wu, W. Wu, B. Rosidi, L. Zhang, H. Wang, G. Iliakis, PARP-1 and Ku compete for repair of DNA double strand breaks by distinct NHEJ pathways, *Nucleic Acids Res.* 34 (2006) 6170–6182. <https://doi.org/10.1093/nar/gkl840>.
- [16] C. Hu, T. Bugbee, M. Gamez, N.A. Wallace, Beta Human Papillomavirus 8E6 Attenuates Non-Homologous End Joining by Hindering DNA-PKcs Activity, *Cancers.* 12 (2020) 2356. <https://doi.org/10.3390/cancers12092356>.
- [17] C. Hu, T. Bugbee, D. Dacus, R. Palinski, N.A. Wallace, Beta human papillomavirus 8 E6 allows colocalization of non-homologous end joining and homologous recombination repair factors, *PLOS Pathogens.* 18 (2022) e1010275. <https://doi.org/10.1371/journal.ppat.1010275>.
- [18] A. Orthwein, S.M. Noordermeer, M.D. Wilson, S. Landry, R.I. Enchev, A. Sherker, M. Munro, J. Pinder, J. Salsman, G. Dellaire, B. Xia, M. Peter, D. Durocher, A mechanism for the suppression of homologous recombination in G1 cells, *Nature.* 528 (2015) 422–426. <https://doi.org/10.1038/nature16142>.

- [19] J.R. Chapman, M.R.G. Taylor, S.J. Boulton, Playing the End Game: DNA Double-Strand Break Repair Pathway Choice, *Molecular Cell*. 47 (2012) 497–510. <https://doi.org/10.1016/j.molcel.2012.07.029>.
- [20] S.F. Bunting, E. Callén, N. Wong, H.-T. Chen, F. Polato, A. Gunn, A. Bothmer, N. Feldhahn, O. Fernandez-Capetillo, L. Cao, X. Xu, C.-X. Deng, T. Finkel, M. Nussenzweig, J.M. Stark, A. Nussenzweig, 53BP1 Inhibits Homologous Recombination in *Brc1*-Deficient Cells by Blocking Resection of DNA Breaks, *Cell*. 141 (2010) 243–254. <https://doi.org/10.1016/j.cell.2010.03.012>.
- [21] N.A. Wallace, K. Robinson, H.L. Howie, D.A. Galloway, β -HPV 5 and 8 E6 Disrupt Homology Dependent Double Strand Break Repair by Attenuating BRCA1 and BRCA2 Expression and Foci Formation, *PLOS Pathogens*. 11 (2015) e1004687. <https://doi.org/10.1371/journal.ppat.1004687>.
- [22] T. Gheit, Mucosal and Cutaneous Human Papillomavirus Infections and Cancer Biology, *Frontiers in Oncology*. 9 (2019). <https://www.frontiersin.org/article/10.3389/fonc.2019.00355> (accessed February 9, 2022).
- [23] D. Kremsdorf, S. Jablonska, M. Favre, G. Orth, Biochemical characterization of two types of human papillomaviruses associated with epidermodysplasia verruciformis., *J Virol*. 43 (1982) 436–447.
- [24] H. Pfister, Chapter 8: Human Papillomavirus and Skin Cancer, *JNCI Monographs*. 2003 (2003) 52–56. <https://doi.org/10.1093/oxfordjournals.jncimonographs.a003483>.
- [25] L.N. Truong, Y. Li, L.Z. Shi, P.Y.-H. Hwang, J. He, H. Wang, N. Razavian, M.W. Berns, X. Wu, Microhomology-mediated End Joining and Homologous Recombination share the initial end resection step to repair DNA double-strand breaks in mammalian cells, *Proc Natl Acad Sci U S A*. 110 (2013) 7720–7725. <https://doi.org/10.1073/pnas.1213431110>.
- [26] L. Deriano, D.B. Roth, Modernizing the nonhomologous end-joining repertoire: alternative and classical NHEJ share the stage., *Annual Review of Genetics*. 47 (2013) 433–55. <https://doi.org/10.1146/annurev-genet-110711-155540>.
- [27] D. Viarisis, K. Müller-Decker, R. Accardi, A. Robitaille, M. Dürst, K. Beer, L. Jansen, C. Flechtenmacher, M. Bozza, R. Harbottle, C. Voegelé, M. Ardin, J. Zavadil, S. Caldeira, L. Gissmann, M. Tommasino, Beta HPV38 oncoproteins act with a hit-and-run mechanism in ultraviolet radiation-induced skin carcinogenesis in mice, *PLoS Pathog*. 14 (2018). <https://doi.org/10.1371/journal.ppat.1006783>.
- [28] S.O. Wendel, N.A. Wallace, Loss of Genome Fidelity: Beta HPVs and the DNA Damage Response, *Frontiers in Microbiology*. 8 (2017). <https://doi.org/10.3389/fmicb.2017.02250>.
- [29] M. Tommasino, HPV and skin carcinogenesis, *Papillomavirus Research*. 7 (2019) 129–131. <https://doi.org/10.1016/j.pvr.2019.04.003>.
- [30] J.E. Leeman, Y. Li, A. Bell, S.S. Hussain, R. Majumdar, X. Rong-Mullins, P. Blecua, R. Damerla, H. Narang, P.T. Ravindran, N.Y. Lee, N. Riaz, S.N. Powell, D.S. Higginson, Human papillomavirus 16 promotes microhomology-mediated end-joining, *Proc Natl Acad Sci USA*. 116 (2019) 21573–21579. <https://doi.org/10.1073/pnas.1906120116>.
- [31] A.N. Weaver, T.S. Cooper, M. Rodriguez, H.Q. Trummell, J.A. Bonner, E.L. Rosenthal, E.S. Yang, DNA double strand break repair defect and sensitivity to poly ADP-ribose polymerase (PARP) inhibition in human papillomavirus 16-positive head and neck squamous cell carcinoma, *Oncotarget*. 6 (2015). <https://doi.org/10.18632/oncotarget.4863>.

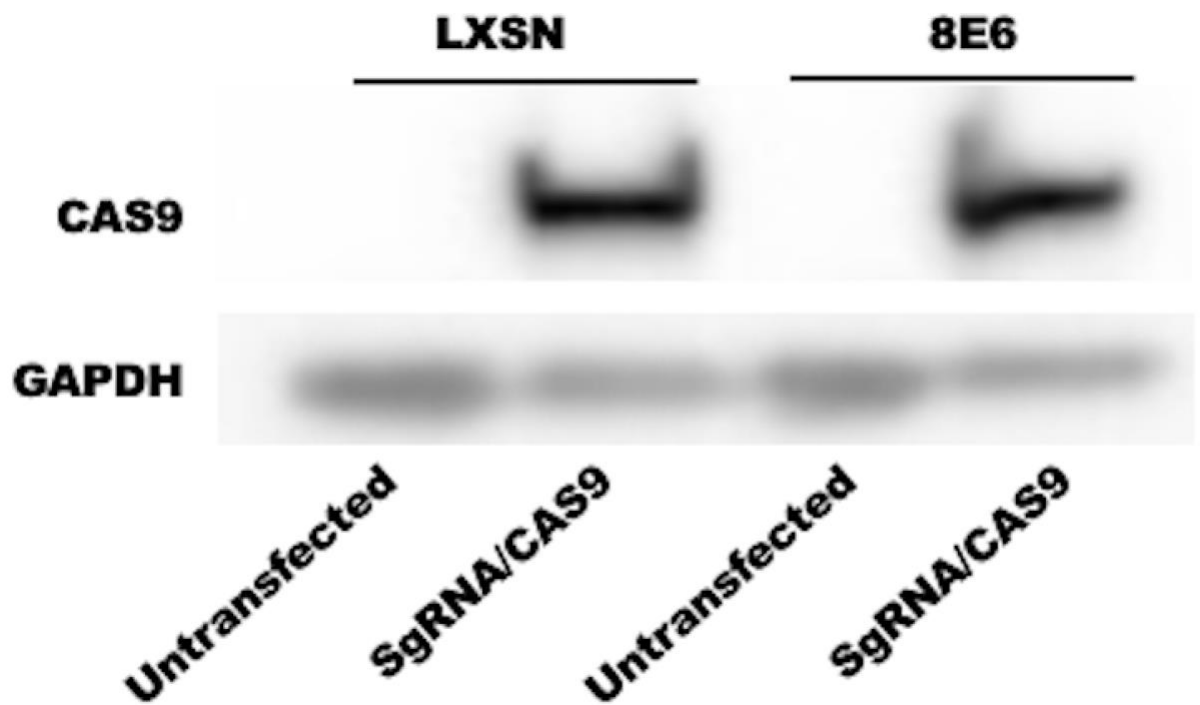


Figure 3-1. Representative image of immunoblot comparing CAS9 expression in untransfected and transfected HFK cells.

sgRNA/CAS9 plasmids were used to transfect HFK cells. Anti-CAS9 antibody was used to detect the CAS9 protein. GAPDH is used as a loading control.

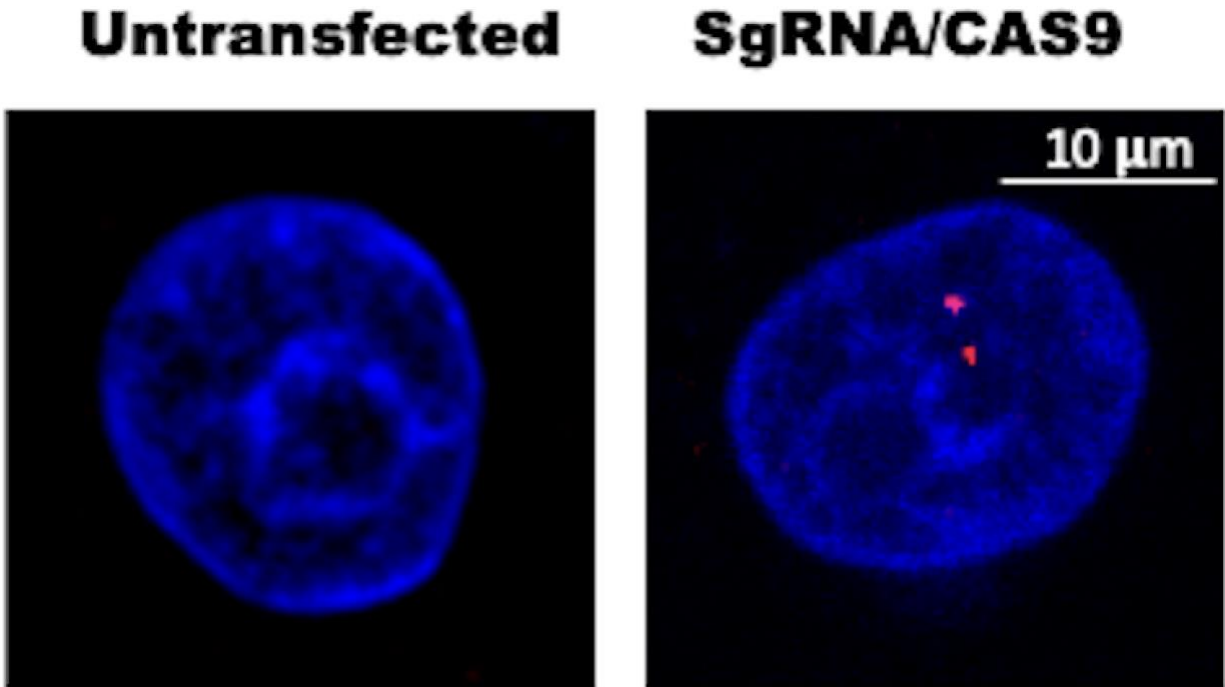


Figure 3-2. Representative immunofluorescence image of phosphorylated histone H2AX (S139) in sgRNA/CAS9 transfected cell and untransfected control.

DAPI was used to stain DNA (Blue). pH2AX (Red) is a marker for CAS9-induced DSB. This demonstrates that optimal CAS9 expression has been achieved by the absence of off-target cleavage. Depending on the number of targeted genome loci (altered by changes in ploidy of the cell, target site copy number variations, or cell cycle position), the number of foci could be higher. However, any increase should be predictable based on the cell type and target site analyzed.

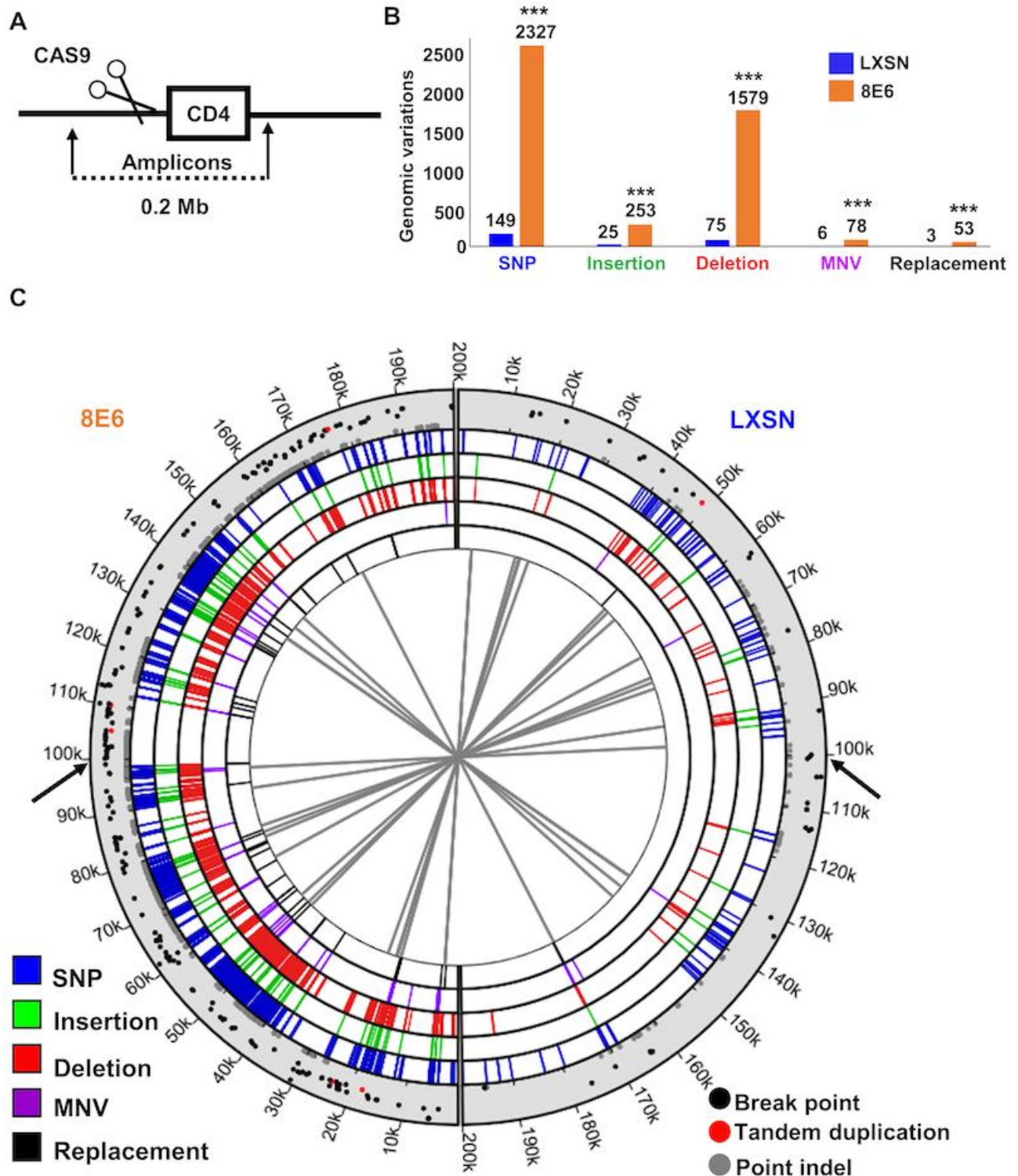


Figure 3-3. β -HPV8E6 increases genomic instability during DSB repair.

(A) Schematic of the placement of CAS9 induced DSB along the sequenced portion of the genome. (B) Genomic variations grouped by types of mutational events in HFK LXSN and HFK

8E6. Each group of genomic variations and total number of variations were compared between HFK LXS and HFK 8E6. (C) Circos plot of DNA mutations in HFK LXS (right side) and HFK 8E6 cells (left side). Black arrows indicate CAS9 cutting sites. The innermost circle displays connections between identical genomic rearrangements. The location of genomic rearrangements colored by types of genomic variations are shown in five concentric circles (blue represents SNP, green represents insertion, red represents deletion, purple represents MNV, and black represents replacement). Scatter plot in the outermost circle displays breakpoints (black), tandem duplications (red), and point indels (grey), in which proximity to the outer edge represents high variant ratio. SNP, single nucleotide polymorphism. MNV, multi-nucleotide variation. Statistical differences between cell lines were measured using a Student's T-test. *** indicates $p < 0.001$ ". This is adapted from a previously published reference with permission²².

Table 3-1. PCR Master mix components.

Component	Per 25μL reaction
PCR-grade water	7 μ L
2x Buffer	12.5 μ L
Primer pool X	1.5 μ L
Template DNA (25ng/ μ L)	4 μ L

Table 3-2. PCR Program settings.

Temperature	Time	Cycles
95°C	3 minutes	1
98°C	20 seconds	25
55-60°C	15 seconds	
72°C	5 minutes (or as calculated for amplicons in 4.1)	
72°C	5 minutes (or as calculated for amplicons in 4.1)	1

Table 3-3. Trouble shooting.

Step	Problem observed	Solution
1	Low transfection efficiency.	Be certain that you are using the optimal transfection reagent for the cell line of choice. Human keratinocytes tend to have lower transfection efficiency and require a specialized transfection reagent. This may be true for other cell lines as well. Alternatively, many transformed cell lines can be quite easily transfected using most lipid-based transfection reagents. Incubating the cells with antibiotic free but otherwise supplemented media for longer time before transfection can also increase transfection efficiency.
2	Incomplete or Uneven Immunoblot Transfer	Proteins with high molecular weight are hard to transfer. Use wet transfer will increase transfer quality for immunoblotting.
3	More pH2AX Foci Than Expected	Confirm that your sgRNA does not target multiple places in the genome. If this does not resolve the issue, reduce the amount of DNA transfected to lower off-target effects.
4	Contaminating sequence reads	If the first sequencing attempt results in many non-mapped reads, and the sequencing coverage of 250x is not achieved, check the primer specificity to other common mammalian and pathogen genomes in publically available websites. If the primers are similar to naturally occurring pathogen or mammalian sequences, revise and retry new primers. If contaminants cannot be removed from the samples, accounting for these read contaminants in your sequencing reads (i.e. using 2M reads per sample versus 1M) will allow for the 250x coverage threshold.

5	Lower than expected band sizes or laddering on electrophoresis gel	Laddering of shorter-than-expected bands may be a result of non-specific priming of sequences other than the target sequence. In this case, primer sequences may need to be reassessed for similarity to other potential components of the sample as in step 4.
6	Small fragment Sizes (below 100bp) following Capillary Electrophoresis	If a dark, low band appears on the gel following amplicon generation, the PCR cleanup was not successfully in removing primers from the PCR samples. In this case, rerunning the bead-based purification will remove remaining primers from the samples.
7	Resulting gel shows no bands or Fluorometer concentration is below 1 ng/ μ L	The primers created in 4.1 did not amplify the target region. Check primers to ensure adequate binding, recheck primer pools for dimerization and/or prepare additional primer pools containing fewer primers than previously used.

Chapter 4 - Beta human papillomavirus 8E6 allows colocalization of non-homologous end joining and homologous recombination repair factors

Changkun Hu¹, Taylor Bugbee¹, Rachel Palinski^{2,3}, Dalton Dacus, and Nicholas Wallace^{1,*}

¹ Division of Biology, Kansas State University, Manhattan, KS 66506, USA.

² Kansas State Veterinary Diagnostic Laboratory, Kansas State University, Manhattan, KS 66506, USA.

³ Department of Diagnostic Medicine/Pathobiology, Kansas State University, Manhattan, KS 66506, USA.

* To whom correspondence should be addressed. Tel: +1 785-532-6014; Fax: +1 785-532-6653; Email: nwallac@ksu.edu

Published as: Hu C, Bugbee T, Dacus D, Palinski R, Wallace N (2022) Beta human papillomavirus 8 E6 allows colocalization of non-homologous end joining and homologous recombination repair factors. PLoS Pathog 18(2): e1010275.

<https://doi.org/10.1371/journal.ppat.1010275>

Abstract

Beta human papillomavirus (β -HPV) are hypothesized to make DNA damage more mutagenic and potentially more carcinogenic. Double strand breaks (DSBs) are the most deleterious DNA lesion. They are typically repaired by homologous recombination (HR) or non-

homologous end joining (NHEJ). HR occurs after DNA replication while NHEJ can occur at any point in the cell cycle. HR and NHEJ are not thought to occur in the same cell at the same time. HR is restricted to cells in phases of the cell cycle where homologous templates are available, while NHEJ occurs primarily during G1. β -HPV type 8 protein E6 (8E6) attenuates both repair pathways. We use a series of immunofluorescence microscopy and flow cytometry experiments to better define the impact of this attenuation. We found that 8E6 causes colocalization of HR factors (RPA70 and RAD51) with an NHEJ factor (activated DNA-PKcs or pDNA-PKcs) at persistent DSBs. 8E6 also causes RAD51 foci to form during G1. The initiation of NHEJ and HR at the same lesion could lead to antagonistic DNA end processing. Further, HR cannot be readily completed in an error-free manner during G1. Both aberrant repair events would cause deletions. To determine if these mutations were occurring, we used next generation sequencing of the 200kb surrounding a CAS9-induced DSB. 8E6 caused a 21-fold increase in deletions. Chemical and genetic inhibition of p300 as well as an 8E6 mutant that is incapable of destabilizing p300 demonstrates that 8E6 is acting via p300 destabilization. More specific chemical inhibitors of DNA repair provided mechanistic insight by mimicking 8E6-induced dysregulation of DNA repair in a virus-free system. Specifically, inhibition of NHEJ causes RAD51 foci to form in G1 and colocalization of RAD51 with pDNA-PKcs.

Author Summary

Our previous work shows that a master transcription regulator, p300, facilitates two major DNA double strand break (DSB) repair pathways: non-homologous end joining (NHEJ) and homologous recombination (HR). By degrading p300, beta genus human papillomavirus 8 protein E6 (8E6) hinders pDNA-PKcs resolution, an essential step during NHEJ. NHEJ and HR are known to compete, with only one pathway initiating repair of a DSB. NHEJ tends to be used

in G1 and HR occurs in S/G2. Here, we show that 8E6 allows NHEJ and HR to initiate at the same break site. We show that 8E6 allows HR to initiate in G1, suggesting that NHEJ starts but fails before HR is initiated at the same DSB. Next generation sequencing of the region surrounding a CAS9-induced DSB supports our hypothesis that this dysregulation of DSB repair is mutagenic as 8E6 caused a 15- to 20-fold increase in mutations associated with a CAS9-induced DSB. These studies support the putative role of HPV8 infections in non-melanoma skin cancer development.

Introduction

Beta genus of human papillomaviruses (β -HPVs) are frequently found in human skin [1,2]. HPV replication requires actively proliferating cells and the replication machinery of the host cells. This puts β -HPV infections in conflict with the cell cycle arrest associated with the repair of UV photolesions that frequently occur in skin [3–6]. Potentially as a mechanism to counter cell cycle arrest, some β -HPVs hinder the cellular response to DNA damage [7–9]. The E6 protein from β -HPV type 8 (8E6) dysregulates the cellular response to DNA damage by binding and destabilizing p300, a histone acetyltransferase that regulates transcription by chromosome remodelling [10–12]. p300 destabilization decreases expression of at least four DNA repair genes (ATM, ATR, BRCA1, and BRCA2) [7,13–15]. 8E6 also reduces ATM and ATR activation in response to UV [8]. This hinders UV damage repair, making UV-induced pyrimidine dimers more persistent and UV more likely to cause double stranded DNA breaks (DSBs) [14].

These DSBs are primarily repaired by two pathways, non-homologous end joining (NHEJ) and homologous recombination (HR). NHEJ can happen throughout the cell cycle but tends to occur during G1 and early S phase [16–19]. NHEJ initiation occurs when a DSB is

sensed, and Ku70 and Ku80 bind DNA near the lesion [16,20]. DNA-dependent protein kinase catalytic subunit (DNA-PKcs) is then recruited to form a heterotrimer known as the DNA-PK holoenzyme. This allows autophosphorylation of DNA-PKcs at S2056 (pDNA-PKcs) and facilitates downstream steps in the pathway, including Artemis activation [21–23]. Artemis has both endonuclease and exonuclease activity that removes single stranded DNA, producing blunt ends [24–26]. Once processed, other NHEJ factors (e.g. XRCC4, XLF, and DNA ligase IV) ligate the gap to resolve the DSB [27–29].

HR uses a sister chromatid as a homologous template to provide error-free repair but is restricted to the S and G2 phases [19,30–32]. HR initiation includes the formation of a MRE11, RAD50, and NBS1 heterotrimer, known as the MRN complex [33]. The MRN complex together with CtIP, EXO1, and DNA-BLM complex resects DNA around the DSB, resulting in single stranded DNA overhangs [34–38]. An RPA trimer (RPA70, RPA32, and RPA14) coats and stabilizes this single stranded DNA [37,39]. Then BRCA1, BRCA2, and PALB2 facilitate the exchange of RPA trimers for RAD51 [19,40]. Finally, RAD51 facilitates a search for the homologous template, strand invasion, and resolution of the lesion [31,41,42].

8E6 attenuates both NHEJ and HR, by preventing the resolution of pDNA-PKcs (NHEJ) and RAD51 (HR) [7,9]. 8E6 also impairs DNA-PKcs activity. These repair defects are the result of 8E6 binding and destabilizing p300. These observations are consistent with the hypothesized ability of some β -HPV infections in promoting skin cancer, by making DNA damage more mutagenic [43,44]. Because β -HPV infections are generally transient, they are thought to induce mutations in premalignant lesion (actinic keratosis) that drive tumorigenesis independent of continued viral gene expression. This model is based in part on observations that β -HPV viral loads are higher in actinic keratosis than in cutaneous squamous cell carcinoma [45,46].

However, the feasibility of this “hit and run” model of tumorigenesis rest on the β -HPV expressing proteins (e.g., 8E6) that are sufficiently genotoxic to introduce tumorigenic mutations before the viral infection is cleared. Thus, to evaluate the potential pathogenicity of HPV8, our group has been characterizing the mutagenic potential of 8E6.

Here, we use immunoblotting, microscopy, and flow cytometry to characterize the persistent pDNA-PKcs and RAD51 repair complexes caused by 8E6 [7,9]. The DNA end processing during NHEJ and HR are mechanistically incompatible; therefore, NHEJ (pDNA-PKcs) and HR (RAD51) repair complexes are not often seen at the same break site [47]. We show that 8E6 promotes the colocalization of pDNA-PKcs and RAD51 foci. 8E6 also causes RAD51 foci to form during G1, when finding a homologous template will be unlikely. This dysregulated DSB repair is caused by the destabilization of p300. It can be phenocopied by chemical inhibition of the NHEJ pathway that mimics the NHEJ inhibition seen when p300 is destabilized. Finally, we developed an assay that combines the ability of a CAS9 endonuclease to be targeted to a specific genomic locus and next generation sequencing to define the extent to which 8E6 increased mutations during DSB repair. This approach demonstrated 8E6 caused a greater than 15-fold increase in overall mutations and a greater than 20-fold increase in deletions in the 200 kb surrounding a DSB.

Results

8E6 promotes the recruitment of HR factors to sites of stalled NHEJ.

To characterize the persistent NHEJ (pDNA-PKcs) and HR (RAD51) repair complexes associated with 8E6 expression, we used previously described vector control (HFK LXSJ) and 8E6 (HFK 8E6) expressing telomerase (N/TERT) immortalized human foreskin keratinocyte cell

lines [48]. 8E6 was HA-tagged and the expression was confirmed (S4-1A-B Fig). DSBs were induced by growth in media containing 10 $\mu\text{g}/\text{mL}$ of zeocin for 10 min, a water-soluble radiation mimetic [49]. While UV is the most common mutagen encountered by cutaneous keratinocytes, zeocin was used to induce DSBs because 8E6 doubles the amount and delays the onset of UV-induced DSBs [14]. Thus, direct comparisons between UV-induced DSB repair would have required normalization to account for the differences in the time for DSBs to occur and the quantity of DSBs induced.

Twenty-four hours after DSB-induction, RAD51 and pDNA-PKcs repair complexes were detected. Consistent with numerous reports that NHEJ and HR are employed at separate phases of the cell cycle [50–52], HFK LXS cells less frequently contained both RAD51 and pDNA-PKcs foci (S4-1C-D Fig). However, HFK 8E6 cells were more likely to have both RAD51 and pDNA-PKcs foci in the same cells (S4-1C-D Fig). Moreover, 8E6 significantly increased the colocalization of RAD51 and pDNA-PKcs repair complexes (Fig 4-1A-B). These colocalizations occur at DNA break sites, as evidenced by co-staining with phosphorylated H2AX (serine 139, pH2AX) foci, a standard marker for DSBs (S4-1E Fig).

To better characterize this colocalization, we observed the colocalization of RAD51 and pDNA-PKcs foci in HFK LXS and HFK 8E6 over a 32-hour period after DSB-induction. We also determined the extent to which another HR factor (RPA70) colocalized with pDNA-PKcs. RPA70 repair complex formation occurs immediately prior to RAD51 complex formation during HR. In LXS cells, the colocalization of RPA70 and RAD51 with pDNA-PKcs was rarely observed with or without damage (Fig 4-2A-D). In contrast, both RPA70:pDNA-PKcs and RAD51:pDNA-PKcs colocalization were significantly increased in HFK 8E6 cells compared to untreated controls and similarly treated HFK LXS cells (Fig 4-2A-D). If repair complexes are

not resolved, they increase in size with time, making them appear more intense when detected by microscopy [53]. Consistent with the idea that colocalized repair complexes represent difficult to repair DSBs, RAD51 and pDNA-PKcs foci were more intense when colocalized (S4-2 Fig). We also compared the kinetics of RPA70 and RAD51 colocalization. During canonical HR, RPA complexes are replaced by RAD51. Consistent with active progression through the canonical HR pathway, the peak for RPA70:pDNA-PKcs foci is followed by the peak for RAD51:pDNA-PKcs colocalization (Fig 4-2A-D). Supporting the biological relevance of our work, 8E6 increased RAD51:pDNA-PKcs colocalization in response to UV damage (S4-3 Fig).

Because we have previously reported that exogenous TERT expression can augment 8E6-associated genome destabilization [54], we measured colocalization in primary keratinocytes expressing 8E6 or vector control (primary HFK 8E6 and primary HFK LXS_N, respectively). p300 degradation by 8E6 (relative to LXS_N) was confirmed by immunoblot (S4-4A Fig). 8E6 continued to cause a significant increase in both RPA70 and RAD51 colocalization with pDNA-PKcs in these cells (Fig 4-2E-F). Because 8E6 has been reported to dysregulate DSB repair by destabilizing p300, we also expressed a previously described mutant of 8E6 that cannot destabilize p300 (8E6 Δ 132-136) in primary HFKs (primary HFK 8E6 Δ 132-136). The inability of 8E6 Δ 132-136 to reduce p300 levels (relative to LXS_N) was confirmed by immunoblot (S4A Fig). We did not detect elevated levels of RAD51 or RPA70 colocalization with pDNA-PKcs in primary HFK 8E6 Δ 132-136 (Fig 4-2E-F). S4-5 Fig describes the frequency of primary HFK LXS_N, 8E6, and 8E6 Δ 132-136 cells with no foci; just RPA70, RAD51, or pDNA-PKcs foci; with HR and NHEJ foci in the same cell but not colocalized, and cells with colocalization of HR and NHEJ factors. This analysis also demonstrated that the majority of RAD51 foci present in HFK 8E6 cells 24 hours after zeocin were colocalized with pDNA-PKcs. Together, our data

shows that 8E6 causes colocalization independently of exogenous TERT expression. They also suggest that 8E6 acts by destabilizing p300.

p300 catalytic activity prevents colocalization of HR factors with persistent pDNA-PKcs repair complexes.

Because deletion of the p300 binding domain has been reported to disrupt other functions of 8E6 [55], data obtained from 8E6 Δ 132-136 must be further verified. To this end, we used CRISPR/CAS9 technology to knock out p300 in telomerase-immortalized human foreskin keratinocyte cell lines (N/TERT HFKs) that we will refer to as HFK p300 KO. A non-targeting control was used to produce a control cell line (HFK p300 WT). The knockout of p300 was confirmed by immunoblot (S4-4B Fig). We detected RPA70:pDNA-PKcs and RAD51:pDNA-PKcs colocalization in these cells over a 32-hour period after DSB induction. Demonstrating a role for p300 in preventing colocalization of HR and NHEJ factors, there was a significant increase of both RPA70 and RAD51 colocalizing with pDNA-PKcs in HFK p300 KO compared to HFK p300 WT cells (Fig 4-3A-B).

p300 is a large protein (~300kDa) that can promote repair by acting as a scaffold for other repair factors and through its catalytic activity [56]. To determine whether p300 prevented HR:NHEJ colocalization by acting as a scaffold or through its catalytic activity, HFK LXS cells were grown in media containing a small molecule (1 μ M of CCS1477) that blocks p300 catalytic activity. Because our previous work demonstrated that p300 is required for ATM and ATR activation [8], damage-induced ATM and ATR phosphorylation were used as a positive control for p300 inhibition. Immunoblots demonstrated that CCS1477 reduced ATM and ATR phosphorylation (S4-6 Fig). CCS1477 significantly increased RPA70:pDNA-PKcs and RAD51:pDNA-PKcs colocalization (Fig 4-3C-D). Again, the colocalization of RPA70:pDNA-

PKcs peaked before colocalization of RAD51:pDNA-PKcs. CCS1477 also increased this colocalization in primary HFK LXS cells, demonstrating that the effect is independent of exogenous TERT expression (Fig 4-3E-F). As a further control that 8E6 was acting by reducing p300 activity, we measured colocalization in primary HFK 8E6 and 8E6 Δ 132-136 cells with CCS1477 (Fig 4-3E-F). Validating the p300-dependent mechanism of action, CCS1477 increased colocalization in primary HFK 8E6 Δ 132-136 but not primary HFK 8E6 cells. This also supports the specificity of CCS1477.

8E6 allows RAD51 foci formation in G1 by binding to p300.

The colocalization of pDNA-PKcs with HR factors (RPA70 and RAD51) associated with sequential steps in HR indicates that progression through the HR pathway occurs when NHEJ stalls. If this is the case, then 8E6 likely allows HR factors to form repair complexes during G1. To test this, we used cyclin E as a marker of G1 [57,58]. Twenty-four hours after DSB induction, co-staining of cyclin E and RAD51 foci were significantly more frequent in HFK 8E6 than in HFK LXS cells (Fig 4-4A-B). As cyclin E also occurs in early S, we used cyclin A as a marker of S/G2. HFK 8E6 increased the frequency of cyclin A negative cells with RAD51 foci compared to HFK LXS (S4-7 Fig). Similar results were obtained by using flow cytometry of DAPI stained cells to identify cells in G1 (Fig 4-4C-D and S8A Fig). The cut-off for RAD51 positivity was determined by measuring staining intensity after incubation with only the relevant secondary antibody (S4-8B Fig). Consistent with prior reports [59,60], RAD51 staining was infrequently detected in HFK LXS cells during the G1. The increased RAD51 in G1 cells seen in HFK 8E6 cells was dependent on CtIP (S4-9 Fig). This was expected based on prior reports that CtIP was required for RAD51 repair complex formation in G1 in 53BP1 depleted cells [61].

Of note, 8E6 also promoted RAD51 foci formation during G1 in primary HFK cells (Fig 4-4C-D).

Consistent with a p300-dependent mechanism of action, HFK 8E6 Δ 132-136 did not increase RAD51 complex staining in G1 cells (Fig 4-4E-F). Moreover, HFK p300 KO cells had increased RAD51 complex staining in G1 (Fig 4-5A-B). CCS1477 significantly increased the frequency of RAD51 staining in G1 in HFK LXSN, primary HFK LXSN, and primary HFK 8E6 Δ 132-136 cells (Fig 4-5C-F). However, CCS1477 was not able to further increase RAD51 staining in G1 in primary HFK 8E6 cells (Fig 4-5E-F). Together these data demonstrate that 8E6 promotes RAD51 repair complex formation during G1 by destabilizing p300.

NHEJ inhibition leads to HR initiation in G1 and colocalization of RAD51 and pDNA-PKcs.

8E6 impairs multiple DSB repair mechanisms. Our prior work demonstrated that 8E6 hindered DNA-PKcs activity. Our data also suggest that 8E6 caused HR factors to be recruited to sites of stalled NHEJ repair. As a result, we treated HFK LXSN cells with a DNA-PKcs inhibitor (1 μ M of NU7441) to mimic 8E6-mediated inhibition of NHEJ. We performed two controls to ensure that the DNA-PKcs inhibitor was working. As expected, the inhibitor blunted damage-induced autophosphorylation of DNA-PKcs and delayed the resolution of pH2AX foci (S4-10 Fig). DNA-PKcs inhibition also delayed the resolution of RAD51 foci and increased the frequency of RAD51 staining in G1 cells (Fig 4-6A-D). We turned to a DNA ligase IV inhibitor (1 μ M of SCR7) that impaired the pathway after pDNA-PKcs foci formed [18]. Treating cells with SCR7 resulted in a significant increase in RAD51:pDNA-PKcs colocalization (Fig 4-6E-F). The most parsimonious explanation of these data is that 8E6 increases the formation of aberrant

RAD51 foci (colocalized with pDNA-PKcs and present in G1) by causing NHEJ to stall.

However, it is possible that 8E6 promotes colocalization in another manner.

8E6 increases genomic instability during DSB repair.

To determine the extent to which 8E6 makes DSB repair more mutagenic, we transfected HFK LXSXN and HFK 8E6 cells with vectors that expressed CAS9 endonuclease and sgRNA designed to induce a DSB just upstream of the CD4 open reading frame. Our group and others have previously described and validated this method of DSB induction [9,62]. We confirmed that this transfection induced RAD51:pDNA-PKcs colocalization in HFK 8E6, but not in HFK LXSXN cells (S4-11A Fig). We designed a series of overlapping primers targeting the 100 kb region upstream and downstream of the CAS9 target site (Fig 4-7A). We then pooled the primers and used them to produce amplicons for next-generation sequencing. The resulting raw reads were trimmed for quality, mapped to the reference sequence, and assessed for mutations (SNPs, indels). As an additional control, 500 kb was sequenced surrounding the CAS9 cleavage site. Mutations within 100 kb of the CAS9 cleavage site were ~10-fold more common compared to sequences more distant from the CAS9 cleavage site (S4-11B Fig). These data showed a ~10-fold increase in mutations associated with a DSB in HFK 8E6 cells compared to HFK LXSXN cells (Fig 4-7B-C). This includes more replacements, insertions, deletions, multi-nucleotide variations, and single nucleotide polymorphisms (SNPs). Of these, deletions occur about 21-fold more often in HFK 8E6 than in HFK LXSXN cells.

Discussion

We have previously shown that 8E6 decreases the efficiency of HR and NHEJ [7,9]. This results in persistent pDNA-PKcs and RAD51 repair complexes and is dependent on 8E6 binding and destabilizing p300. Here, we demonstrate that 8E6 triggers HR repair factors (RPA70 and

RAD51) to be recruited to DSBs when pDNA-PKcs repair complexes do not efficiently repair the lesion. Further, 8E6 allows RAD51 repair complexes to form in G1. These abnormal repair events are the result of p300-destabilization by 8E6 and the resulting inhibition of NHEJ after pDNA-PKcs activation. Finally, we developed an assay that uses targeted next generation sequencing at a CAS9-induced DSB to demonstrate that 8E6 significantly increases the frequency of mutations associated with DSB repair. Here, we discuss our interpretation of these results.

We propose three ways in which 8E6-induced abrogation of DSB repair results in the increased mutations seen by our next generation sequencing analysis. They are depicted in Fig 8, described below, and notably are not mutually exclusive. Our data show that 8E6 does not prevent initiation of NHEJ as indicated by the formation of pDNA-PKcs repair complex formation. We have previously shown that 8E6 causes NHEJ to stall after pDNA-PKcs foci formation by destabilizing p300, hindering further DNA-PKcs activity and progression through the pathway [9]. The data presented here show that this results in progression through the HR pathway at sites of stalled NHEJ. Specifically, DNA near the DSB is resected (indicated by RPA70 foci formation) and RAD51 repair complexes form. This is expected to cause deletions in at least two ways. Since NHEJ occurs primarily during G1, the RAD51 foci that form in response to stalled NHEJ would be unlikely to find suitable homologous template to facilitate their resolution. As a result, the single stranded DNA (ssDNA) created by resection will be subject to degradation. Further, the initiation of NHEJ and HR at the same lesion is expected to result in antagonistic end processing that will result in deletions (NHEJ removes ssDNA, while HR generates ssDNA). Finally, the inability of cells to efficiently repair DSBs using HR and NHEJ likely shunts repair in more mutagenic tertiary repair pathways.

8E6 induced RAD51:pDNA-PKcs colocalization in response to low dose UV exposure. These data support our hypothesis that 8E6 leads to abnormal repair events in response to the levels of UV regularly encountered by cells infected with HPV8. We acknowledge that the reported RAD51:pDNA-PKcs could result from multiple DSBs occurring so close to each other that our microscopy cannot distinguish them as separate lesions. While we cannot formally exclude this possibility, it is unlikely. If the colocalization was the result of staining occurring at two separate DSBs, the maxima for colocalization would be expected when RAD51 and pDNA-PKcs staining is the highest. However, while RAD51 and pDNA-PKcs staining peak within a few hours of DSB induction, RAD51:pDNA-PKcs colocalization peaks 24 hours after DSB induction. Thus, we believe it is unlikely that the RAD51:pDNA-PKcs colocalization that we report is the result of staining of clustered DSBs.

There have been other reports of RAD51:pDNA-PKcs colocalization and resection in G1. One study found that RAD51:pDNA-PKcs colocalization occurs following a high dosage of UV radiation [63]. Another study found RAD51:pDNA-PKcs colocalization at common fragile sites in cells exposed to aphidicolin, a DNA polymerase inhibitor [64]. Given the complex nature of these lesions, the results are consistent with our hypothesis that co-localization of these factors occurs primarily at difficult to repair DSBs. However, unlike these studies we provide mechanistic insight into how RAD51:pDNA-PKcs colocalization occurs. Resection (indicated by RPA foci) has also been reported during G1 [38]. Biehs et al found that RPA complex formation during G1 can lead to Alt-EJ. Our data do not rule out that 8E6 may promote Alt-EJ. In fact, it seems likely that Alt-EJ plays a role in repairing DSBs in 8E6 expressing cells. However, some of our data were incongruent with other data reported by Biehs et al. Their study found that BRCA1 was required for robust RPA foci formation, while we have previously reported that

RPA foci levels are not altered by 8E6-mediated reduction of BRCA1 [7]. We believe that differences in cell culture models likely explain the inconsistencies. We used primary and TERT-immortalized keratinocytes, while Biehs et al used mouse embryonic fibroblasts (MEFs) and HeLa cells. HPV does not infect fibroblasts. Further, HeLa cells are immortalized by high-risk alpha-papillomavirus (HR- α HPV) oncogenes. These oncogenes have a well-documented ability to dysregulate both cell cycle and DSB repair [65]. Thus, the requirement of BRCA1 for RPA repair complex formation in cell systems relevant to β -HPV biology have has not been rigorously established elsewhere. Another relevant paper reported that extensive genetic manipulation (depletion of 53bp1 and KEAP1 along with the introduction of phospho-mimetic mutations in CtIP) was required for RAD51 foci to form during G1 [61]. This is consistent with our reports that 8E6 leads to extensive alteration of DSB repair [7,9].

The ability of high-risk alpha-papillomavirus (HR- α HPV) oncogenes to cause co-localization of HR and NHEJ factors has not been reported. However, the ability of these oncogenes to dysregulate DSB repair is an area of active investigation. Both HR- α HPV E6 and E7 have been shown to increase expression and post-translational modification of DSB repair proteins [66,67]. The additional repair factors facilitate the viral lifecycle as they are recruited away from damaged host DNA and to sites of viral replication [58,68]. HR- α HPV E7 has also been reported to decrease NHEJ [69]. Our data suggests that this reduction could result in the recruitment of HR factors to sites of failed NHEJ. Supporting this possibility, RAD51 foci have also been reported in G1 in Hela cells (transformed by HR- α HPV oncogenes) [70].

Our data are consistent with the proposed role of β -HPV infections in early stages of non-melanoma skin cancer development via genome destabilization. We show that 8E6 significantly increases the mutational burden of DSBs. However, we have only examined the E6 from HPV8.

The E6 from some other members of the β -HPV genus do not destabilize p300, but can immortalize primary cells in combination with expression of β -HPV E7 [55]. Thus, continued investigations into the diversity of β -HPV biology are needed to fully evaluate the oncogenic potential of the genus.

Materials and Methods

Cell Culture and Reagents

Immortalized human foreskin keratinocytes (N/TERT HFK) provided by Michael Underbrink (University of Texas Medical Branch) and primary HFK were grown in EpiLife medium (MEPICF500, Gibco), supplemented with 60 μ M calcium chloride (MEPICF500, Gibco), human keratinocyte growth supplement (MEPICF500, Gibco), and 1% penicillin-streptomycin (PSL02-6X100ML, Caisson). U2OS were maintained in DMEM supplemented with 10% FBS and 1% penicillin-streptomycin. Zeocin (J67140-XF, Alfa Aesar) was used to induce DSBs (10 μ g/mL, 10 min). NU7441 (S2638, Selleckchem) was used to inhibit DNA-PKcs phosphorylation (1 μ M) and verify the pDNA-PKcs antibody. SiRNA DNA-PKcs was used to further validate pDNA-PKcs antibody. KU55933 (Sigma-Aldrich, SML1109) was used to validate RAD51 antibody as previously described [71]. CCS1477 (CT-CCS1477, Chemietek) was used to inhibit p300 activity (1 μ M). sgRNA/CAS9 plasmids (#136938, Addgene) were used to generate a DSB for next-generation sequencing.

Immunofluorescence Microscopy

Cells were seeded onto either 96-well glass-bottom plates and grown overnight. Cells treated with zeocin for specified time and concentration were fixed with 4% formaldehyde. Then, 0.1% Triton-X was used to permeabilize the cells, followed by blocking with 3% bovine

serum albumin. Cells were then incubated with the following antibodies: phospho DNA-PKcs S2056 (ab18192, Abcam, 1:200), RAD51 (ab1837, Abcam, 1:200), RPA70 (ab176467, Abcam, 1:200), cyclin E (4132S, Cell Signalling), or HA-tag (#3724, Cell Signalling, 1:100). The cells were washed and stained with the appropriate secondary antibodies: Alexa Fluor 594 (red) goat anti-rabbit (A11012, Thermo Scientific), Alexa Fluor 488 (green) goat anti-mouse (A11001, Thermo Scientific). After washing, the cells were stained with 10 μ M DAPI in PBS and visualized with the Zeiss LSM 770 microscope. Images were analyzed using the ImageJ techniques previously described [72]. Cyclin E intensity was measured for each cell. Average cyclin E intensity of cells grown in media without growth factor for 4 hours was used to define the threshold of cyclin E positive. Colocalized foci appear yellow when green and red channels are merged in ImageJ.

Flow Cytometry

Cells were collected from 10 cm plates, at about 80-90% confluence, by using trypsinization. Cells were washed with cold PBS and fixed with 4% formaldehyde in PBS for 10 min. Then, cells were permeabilized with 0.5% Triton-X for 10 min at room temperature. Cells were stained with anti-RAD51 antibody (ab1837, Abcam, 1:100) and Alexa Fluor 488 goat anti-mouse (A11001, Thermo Scientific,). After washing, cells were resuspended in 200 μ L PBS and 30 μ M DAPI (4',6-diamidino-2-phenylindole), and incubated in the dark at room temperature for 15 min. Samples were analysed by a LSRFortessa X20 Flow Cytometer. Flowing software (v2.5.1) was used for data analysis.

Immunoblotting

After being washed with ice-cold PBS, cells were lysed with RIPA Lysis Buffer (VWRVN653-100ML, VWR Life Science), supplemented with Phosphatase Inhibitor Cocktail 2 (P5726-1ML, Sigma) and Protease Inhibitor Cocktail (B14001, Bimake). The Pierce BCA Protein Assay Kit (89167-794, Thermo Scientific) was used to determine protein concentration. Equal protein lysates were run on Novex 3–8% Tris-acetate 15 Well Mini Gels (EA03785BOX, Invitrogen) and transferred to Immobilon-P membranes (IPVH00010, Fisher Scientific). Membranes were then probed with the following primary antibodies: GAPDH (sc-47724, Santa Cruz Biotechnologies, 1:1000) and phospho DNA-PKcs S2056 (ab18192, Abcam). P300 (sc-48343, Santa Cruz Biotechnologies), pATM (13050S, Cell signaling), ATM (92356S, Cell Signaling), pATR (58014S, Cell signaling), and ATR (2790S, Cell signaling). After exposure to the matching HRP-conjugated secondary antibody, cells were visualized using SuperSignal West Femto Maximum Sensitivity Substrate (34095, Thermo Scientific).

SgRNA/CAS9 Transfection

The sequencing was performed 15 subcultures (passaged 1 to 3) after 8E6 expression in N/TERT immortalized HFKs. HFK cells were plated in 2 mL of complete growth medium in a 6-well plate. Cells were used at 80-90% confluency. 2 μ L of plasmid (#JS825, Addgene) was diluted in 200 μ L Xfect transfection reagent (631317, Takara). The mixture was incubated at room temperature for 15 min. The transfection mixture was added to each well drop-wise and incubated for 48 hours at 37 °C. Cells were harvested for DNA extraction and sequencing.

Next-generation sequencing

Specific primers were designed to cover 0.1 Mb on each side of the Cas9 target site (6689603-6889603 on Chromosome 12) resulting in a total of 42 primer sets each producing a ~5 Kb overlapping amplicon (S1 Table). Primer sets were pooled based on primer dimerization and annealing temperature compatibility. Genomic DNA was extracted using the MagAttract High Molecular Weight DNA kit (Qiagen) according to the manufacturers' instructions. The target regions were amplified for each sample using the primer pools coupled with KAPA HiFi Hotstart readymix (KAPA Biosystems) using 20 μ M primers as well as a 50/53 °C (Annealing temperature 1/2; Supplementary table 1) and a 5-minute extension time. Primers were removed from PCR amplicons using the Highprep PCR cleanup system (Magbio) as specified by the manufacturer. Libraries were prepared from amplicons with Nextera XT DNA library preparation kit (Illumina) and sequenced on a Nextseq 500 system. A minimum of 100x coverage was targeted for each of the tested samples.

Sequencing Analyses

Raw reads were trimmed for quality and mapped to the target region in CLC genomics workbench v21.0. Trimmed reads were normalized manually transfection efficiency. Normalized reads were assessed for indels and structural variants and normalized for paired read variations in CLC Genomics Workbench v 20.0.4 (Qiagen) using a variant threshold of 5 reads and 100 read coverage (5%). Next generation sequencing of mock transfected cells were used as a reference for determining mutations. Thus, only mutations that does not exist in mock transfected cells were reported. Breakpoints (sites of genomic instability), site-specific variant ratios, insertions,

deletions, replacements, inversions and complex (combination of 2 or more genomic changes) were compared between 8E6 and the vector control samples.

Statistical Analysis

All values are represented as mean \pm standard error (SE). Statistical differences between groups were measured by using Student's t-test. p-values in all experiments were considered significant at less than 0.05.

Acknowledgements

We appreciate KSU-CVM Confocal Core for our immunofluorescence microscopy, Michael Underbrink for providing the N/TERT-immortalized HFKs, and Jeremy M. Stark for providing plasmids of sgRNA/CAS9. This research was supported by the National Institute of General Medical Sciences (NIGMS) of the National Institutes of Health under award number P20GM130448.

Data Availability Statement

All relevant data are within the paper and its Supporting Information files.

Funding

This work was supported by the U.S. Department of Defense (CMDRP PRCRP CA160224); Kansas State University Johnson Cancer Research Center (No grant number); and National Institutes of Health (P20GM130448).

Competing Interests

The authors have declared that no competing interests exist.

Author Contributions

Conceived and designed the experiments: CH NAW RP. Performed the experiments:CH TB RP. Analyzed the data: CH TB RP. Wrote the paper: CH TB NAW RP.

References

- [1] P. Brianti, E. De Flammineis, S.R. Mercuri, Review of HPV-related diseases and cancers, *New Microbiol.* 40 (2017) 80–85.
- [2] D. Hasche, S.E. Vinzón, F. Rösl, Cutaneous Papillomaviruses and Non-melanoma Skin Cancer: Causal Agents or Innocent Bystanders?, *Front Microbiol.* 9 (2018). <https://doi.org/10.3389/fmicb.2018.00874>.
- [3] A.J. Pierce, R.D. Johnson, L.H. Thompson, M. Jasin, XRCC3 promotes homology-directed repair of DNA damage in mammalian cells, *Genes Dev.* 13 (1999) 2633–2638.
- [4] N. Bennardo, A. Cheng, N. Huang, J.M. Stark, Alternative-NHEJ Is a Mechanistically Distinct Pathway of Mammalian Chromosome Break Repair, *PLoS Genet.* 4 (2008). <https://doi.org/10.1371/journal.pgen.1000110>.
- [5] R. Bhargava, M. Sandhu, S. Muk, G. Lee, N. Vaidehi, J.M. Stark, C-NHEJ without indels is robust and requires synergistic function of distinct XLF domains, *Nat Commun.* 9 (2018) 2484. <https://doi.org/10.1038/s41467-018-04867-5>.
- [6] L.J. Tsai, F.W. Lopezcolorado, R. Bhargava, C. Mendez-Dorantes, E. Jahanshir, J.M. Stark, RNF8 has both KU-dependent and independent roles in chromosomal break repair, *Nucleic Acids Research.* 48 (2020) 6032–6052. <https://doi.org/10.1093/nar/gkaa380>.
- [7] R. Bhargava, F.W. Lopezcolorado, L.J. Tsai, J.M. Stark, The canonical non-homologous end joining factor XLF promotes chromosomal deletion rearrangements in human cells, *J. Biol. Chem.* 295 (2020) 125–137. <https://doi.org/10.1074/jbc.RA119.010421>.
- [8] K.M. Bedard, M.P. Underbrink, H.L. Howie, D.A. Galloway, The E6 Oncoproteins from Human Betapapillomaviruses Differentially Activate Telomerase through an E6AP-Dependent Mechanism and Prolong the Lifespan of Primary Keratinocytes, *J Virol.* 82 (2008) 3894–3902. <https://doi.org/10.1128/JVI.01818-07>.
- [9] A. Kötter, K. Cornils, K. Borgmann, J. Dahm-Daphi, C. Petersen, E. Dikomey, W.Y. Mansour, Inhibition of PARP1-dependent end-joining contributes to Olaparib-mediated radiosensitization in tumor cells, *Mol Oncol.* 8 (2014) 1616–1625. <https://doi.org/10.1016/j.molonc.2014.06.008>.
- [10] M. Tsukuda, K. Miyazaki, DNA fragmentation caused by an overdose of Zeocin, *Journal of Bioscience and Bioengineering.* 116 (2013) 644–646. <https://doi.org/10.1016/j.jbiosc.2013.05.004>.
- [11] E.P. Rogakou, D.R. Pilch, A.H. Orr, V.S. Ivanova, W.M. Bonner, DNA Double-stranded Breaks Induce Histone H2AX Phosphorylation on Serine 139, *Journal of Biological Chemistry.* 273 (1998) 5858–5868. <https://doi.org/10.1074/jbc.273.10.5858>.
- [12] G. Iliakis, T. Murmann, A. Soni, Alternative end-joining repair pathways are the ultimate backup for abrogated classical non-homologous end-joining and homologous recombination repair: Implications for the formation of chromosome translocations, *Mutation Research/Genetic Toxicology and Environmental Mutagenesis.* 793 (2015) 166–175. <https://doi.org/10.1016/j.mrgentox.2015.07.001>.

- [13] J. Patterson-Fortin, A.D. D'Andrea, Exploiting the Microhomology-Mediated End-Joining Pathway in Cancer Therapy, *Cancer Res.* 80 (2020) 4593–4600. <https://doi.org/10.1158/0008-5472.CAN-20-1672>.
- [14] D. Simsek, M. Jasin, Alternative end-joining is suppressed by the canonical NHEJ component Xrcc4–ligase IV during chromosomal translocation formation, *Nature Structural & Molecular Biology.* 17 (2010) 410–416. <https://doi.org/10.1038/nsmb.1773>.
- [15] M. Wang, W. Wu, W. Wu, B. Rosidi, L. Zhang, H. Wang, G. Iliakis, PARP-1 and Ku compete for repair of DNA double strand breaks by distinct NHEJ pathways, *Nucleic Acids Res.* 34 (2006) 6170–6182. <https://doi.org/10.1093/nar/gkl840>.
- [16] C. Hu, T. Bugbee, M. Gamez, N.A. Wallace, Beta Human Papillomavirus 8E6 Attenuates Non-Homologous End Joining by Hindering DNA-PKcs Activity, *Cancers.* 12 (2020) 2356. <https://doi.org/10.3390/cancers12092356>.
- [17] C. Hu, T. Bugbee, D. Dacus, R. Palinski, N.A. Wallace, Beta human papillomavirus 8 E6 allows colocalization of non-homologous end joining and homologous recombination repair factors, *PLOS Pathogens.* 18 (2022) e1010275. <https://doi.org/10.1371/journal.ppat.1010275>.
- [18] A. Orthwein, S.M. Noordermeer, M.D. Wilson, S. Landry, R.I. Enchev, A. Sherker, M. Munro, J. Pinder, J. Salsman, G. Dellaire, B. Xia, M. Peter, D. Durocher, A mechanism for the suppression of homologous recombination in G1 cells, *Nature.* 528 (2015) 422–426. <https://doi.org/10.1038/nature16142>.
- [19] J.R. Chapman, M.R.G. Taylor, S.J. Boulton, Playing the End Game: DNA Double-Strand Break Repair Pathway Choice, *Molecular Cell.* 47 (2012) 497–510. <https://doi.org/10.1016/j.molcel.2012.07.029>.
- [20] S.F. Bunting, E. Callén, N. Wong, H.-T. Chen, F. Polato, A. Gunn, A. Bothmer, N. Feldhahn, O. Fernandez-Capetillo, L. Cao, X. Xu, C.-X. Deng, T. Finkel, M. Nussenzweig, J.M. Stark, A. Nussenzweig, 53BP1 Inhibits Homologous Recombination in Brca1-Deficient Cells by Blocking Resection of DNA Breaks, *Cell.* 141 (2010) 243–254. <https://doi.org/10.1016/j.cell.2010.03.012>.
- [21] N.A. Wallace, K. Robinson, H.L. Howie, D.A. Galloway, β -HPV 5 and 8 E6 Disrupt Homology Dependent Double Strand Break Repair by Attenuating BRCA1 and BRCA2 Expression and Foci Formation, *PLOS Pathogens.* 11 (2015) e1004687. <https://doi.org/10.1371/journal.ppat.1004687>.
- [22] T. Gheit, Mucosal and Cutaneous Human Papillomavirus Infections and Cancer Biology, *Frontiers in Oncology.* 9 (2019). <https://www.frontiersin.org/article/10.3389/fonc.2019.00355> (accessed February 9, 2022).
- [23] D. Kremsdorf, S. Jablonska, M. Favre, G. Orth, Biochemical characterization of two types of human papillomaviruses associated with epidermodysplasia verruciformis., *J Virol.* 43 (1982) 436–447.
- [24] H. Pfister, Chapter 8: Human Papillomavirus and Skin Cancer, *JNCI Monographs.* 2003 (2003) 52–56. <https://doi.org/10.1093/oxfordjournals.jncimonographs.a003483>.
- [25] L.N. Truong, Y. Li, L.Z. Shi, P.Y.-H. Hwang, J. He, H. Wang, N. Razavian, M.W. Berns, X. Wu, Microhomology-mediated End Joining and Homologous Recombination share the initial end resection step to repair DNA double-strand breaks in mammalian cells, *Proc Natl Acad Sci U S A.* 110 (2013) 7720–7725. <https://doi.org/10.1073/pnas.1213431110>.

- [26] L. Deriano, D.B. Roth, Modernizing the nonhomologous end-joining repertoire: alternative and classical NHEJ share the stage., *Annual Review of Genetics*. 47 (2013) 433–55. <https://doi.org/10.1146/annurev-genet-110711-155540>.
- [27] D. Viariso, K. Müller-Decker, R. Accardi, A. Robitaille, M. Dürst, K. Beer, L. Jansen, C. Flechtenmacher, M. Bozza, R. Harbottle, C. Voegelé, M. Ardin, J. Zavadil, S. Caldeira, L. Gissmann, M. Tommasino, Beta HPV38 oncoproteins act with a hit-and-run mechanism in ultraviolet radiation-induced skin carcinogenesis in mice, *PLoS Pathog*. 14 (2018). <https://doi.org/10.1371/journal.ppat.1006783>.
- [28] S.O. Wendel, N.A. Wallace, Loss of Genome Fidelity: Beta HPVs and the DNA Damage Response, *Frontiers in Microbiology*. 8 (2017). <https://doi.org/10.3389/fmicb.2017.02250>.
- [29] M. Tommasino, HPV and skin carcinogenesis, *Papillomavirus Research*. 7 (2019) 129–131. <https://doi.org/10.1016/j.pvr.2019.04.003>.
- [30] J.E. Leeman, Y. Li, A. Bell, S.S. Hussain, R. Majumdar, X. Rong-Mullins, P. Bleuca, R. Damerla, H. Narang, P.T. Ravindran, N.Y. Lee, N. Riaz, S.N. Powell, D.S. Higginson, Human papillomavirus 16 promotes microhomology-mediated end-joining, *Proc Natl Acad Sci USA*. 116 (2019) 21573–21579. <https://doi.org/10.1073/pnas.1906120116>.
- [31] A.N. Weaver, T.S. Cooper, M. Rodriguez, H.Q. Trummell, J.A. Bonner, E.L. Rosenthal, E.S. Yang, DNA double strand break repair defect and sensitivity to poly ADP-ribose polymerase (PARP) inhibition in human papillomavirus 16-positive head and neck squamous cell carcinoma, *Oncotarget*. 6 (2015). <https://doi.org/10.18632/oncotarget.4863>.

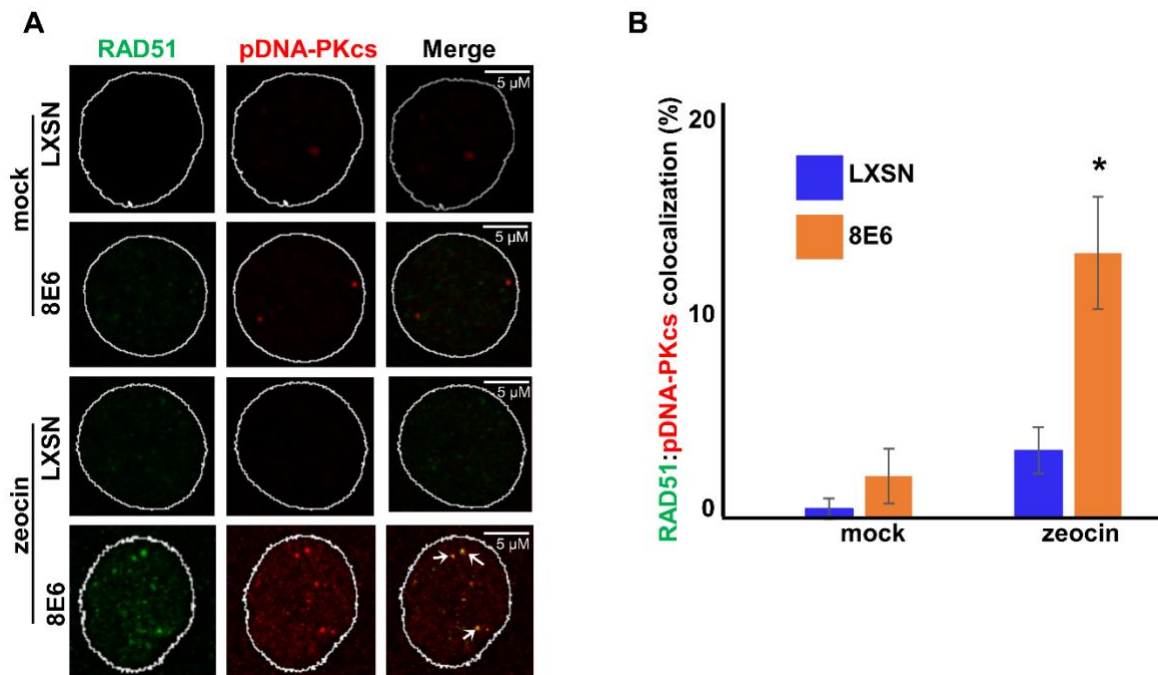


Figure 4-1. 8E6 allows RAD51:pDNA-PKcs colocalization.

(A) Representative images of HFK LXS and HFK 8E6 cells stained for RAD51 (green) and pDNA-PKcs (red) 24 hours after DSB induction by growth in media containing zeocin (10 $\mu\text{g}/\text{mL}$, 10 min) or media containing additional water (solvent for zeocin) as a negative control.

Additional water control is described as “mock” in Figure. White arrows indicate colocalizing RAD51 and pDNA-PKcs foci. (B) Percentage of HFK cells with colocalized RAD51 and pDNA-PKcs foci after mock treatment or zeocin treatment. All values are represented as mean \pm standard error. The statistical significance of differences between cell lines were determined using Student’s t-test. * indicates significant difference between 8E6 and LXSJN with same treatment ($p < 0.05$). At least 150 cells were counted over three independent experiments. Nuclei were determined by DAPI staining. The edge of this staining is shown by a white line depicting the nucleus.

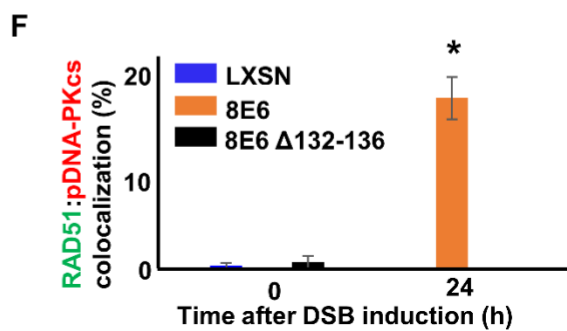
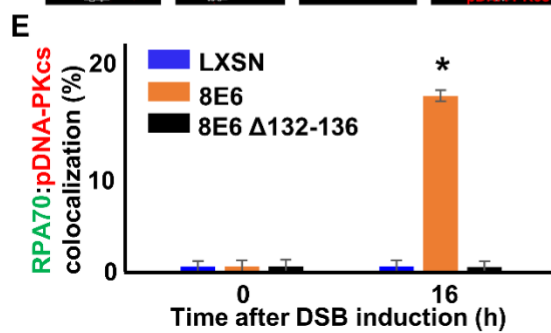
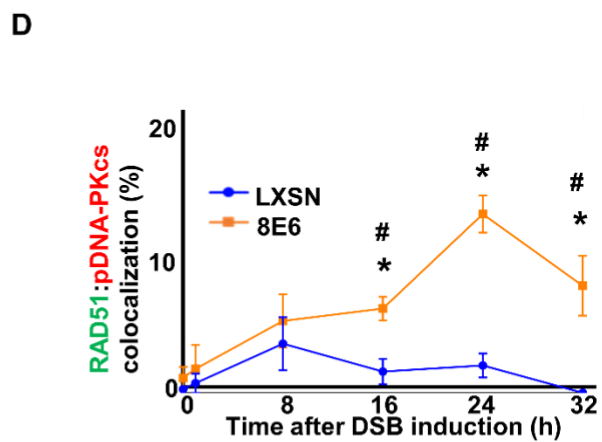
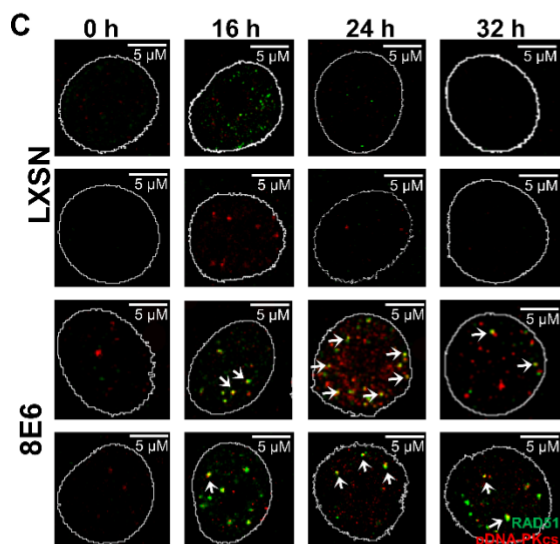
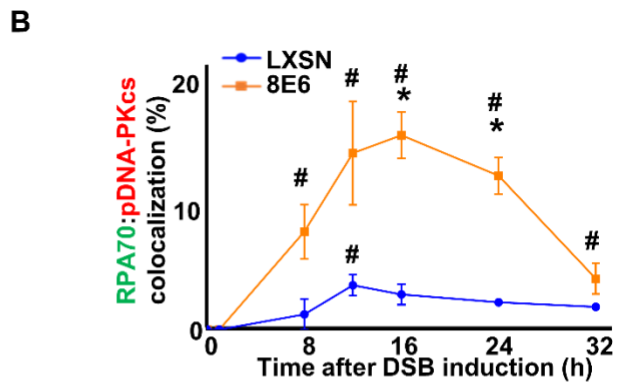
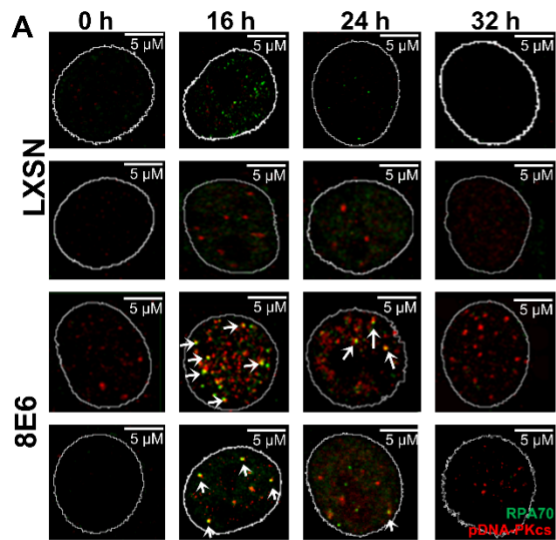


Figure 4-2. By binding p300, 8E6 allows RAD51 and RPA70 foci to colocalize with persistent pDNA-PKcs foci.

(A) Representative images of HFK LXSJ and HFK 8E6 cells stained for RPA70 (green) and pDNA-PKcs (red) following zeocin treatment (10 μ g/mL, 10 min). (B) Percentage of HFK cells with colocalized RPA70 and pDNA-PKcs foci. (C) Representative images of HFK LXSJ and HFK 8E6 cells stained for RAD51 (green) and pDNA-PKcs (red) following zeocin treatment (D) Percentage of HFK cells with colocalized RAD51 and pDNA-PKcs foci. (E) Percentage of primary HFKs with colocalized RPA70 and pDNA-PKcs foci. (F) Percentage of primary HFKs with colocalized RAD51 and pDNA-PKcs foci. White arrow indicates colocalization. All values are represented as mean \pm standard error. The statistical significance of differences between two groups were determined using Student's t-test. * indicates significant difference between 8E6 and LXSJ with same treatment ($p < 0.05$). # indicates a significant difference ($p < 0.05$) between control (solvent) and treated group within each cell line. At least 150 cells were counted over three independent experiments. Nuclei were determined by DAPI staining. The edge of this staining is shown by a white line depicting the nucleus.

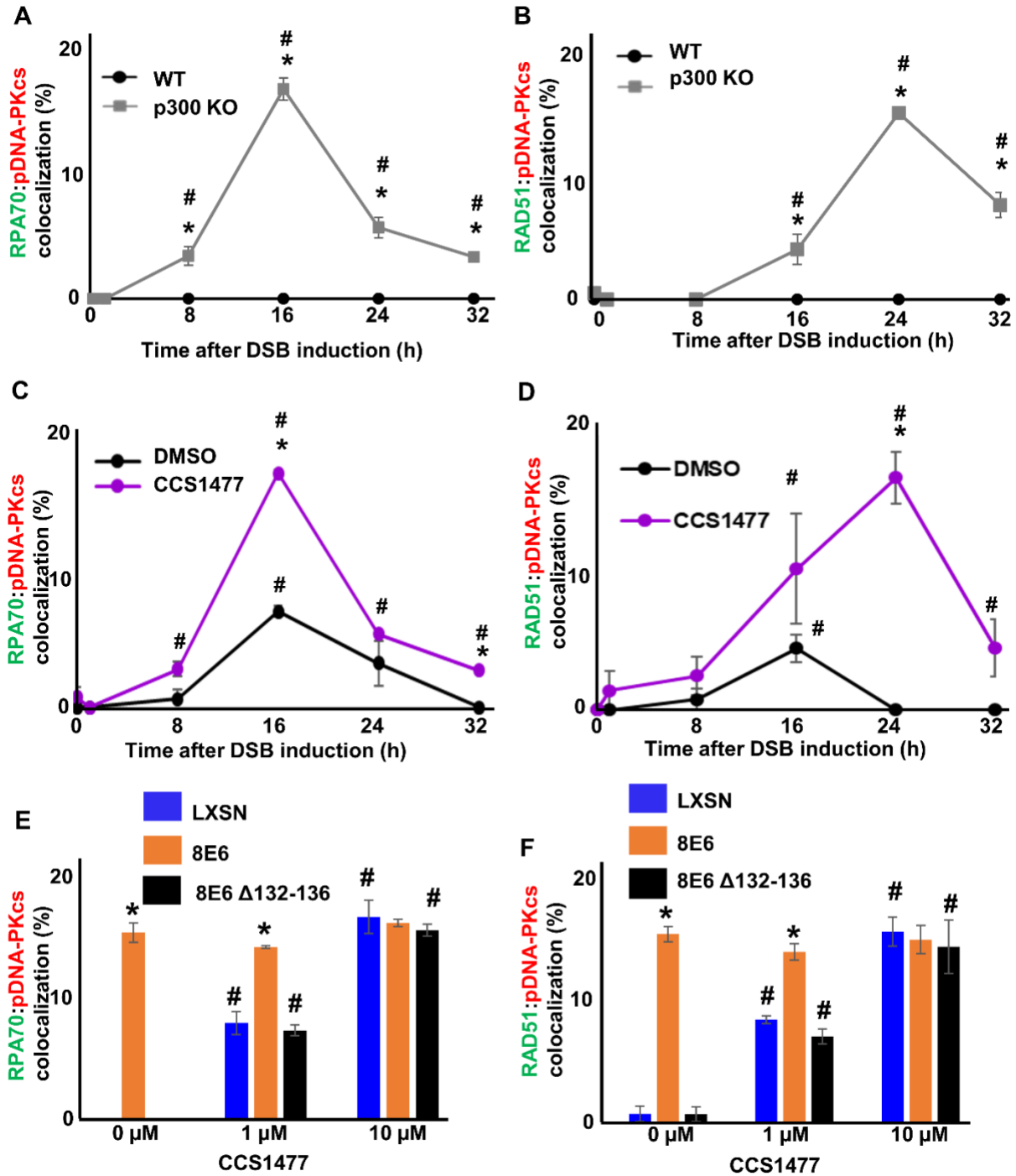


Figure 4-3. p300 reduces co-localization of RAD51 and RPA70 foci with pDNA-PKcs foci. (A-B) Percentage of HFK WT and p300 KO cells with (A) colocalized RPA70 (green) and pDNA-PKcs (red) foci or (B) RAD51 (green) and pDNA-PKcs (red) foci over a 32-hour time course following zeocin exposure (10 μ g/mL, 10 min). (C-D) Percentage of CCS1477 (1 μ M) or

DMSO treated HFK LXSXN cells that contained colocalized (C) RPA70 (green) and pDNA-PKcs (red) or (D) RAD51 (green) and pDNA-PKcs (red) foci following zeocin treatment. (E-F) Percentage of primary HFK cells treated with CCS1477 or DMSO that contained (E) colocalized RPA70 and pDNA-PKcs foci 16-hours following zeocin treatment or (F) RAD51 and pDNA-PKcs foci 24-hours following zeocin treatment. All values are represented as mean \pm standard error. The statistical significance of differences between cell lines or treatments were determined using Student's t-test. * indicates significant difference between two groups (A-D) or LXSXN and 8E6 (E-F) with same treatment ($p < 0.05$). # indicates $p < 0.05$ between control (0 h) and zeocin treated group within each cell line. At least 150 cells were counted over three independent experiments.

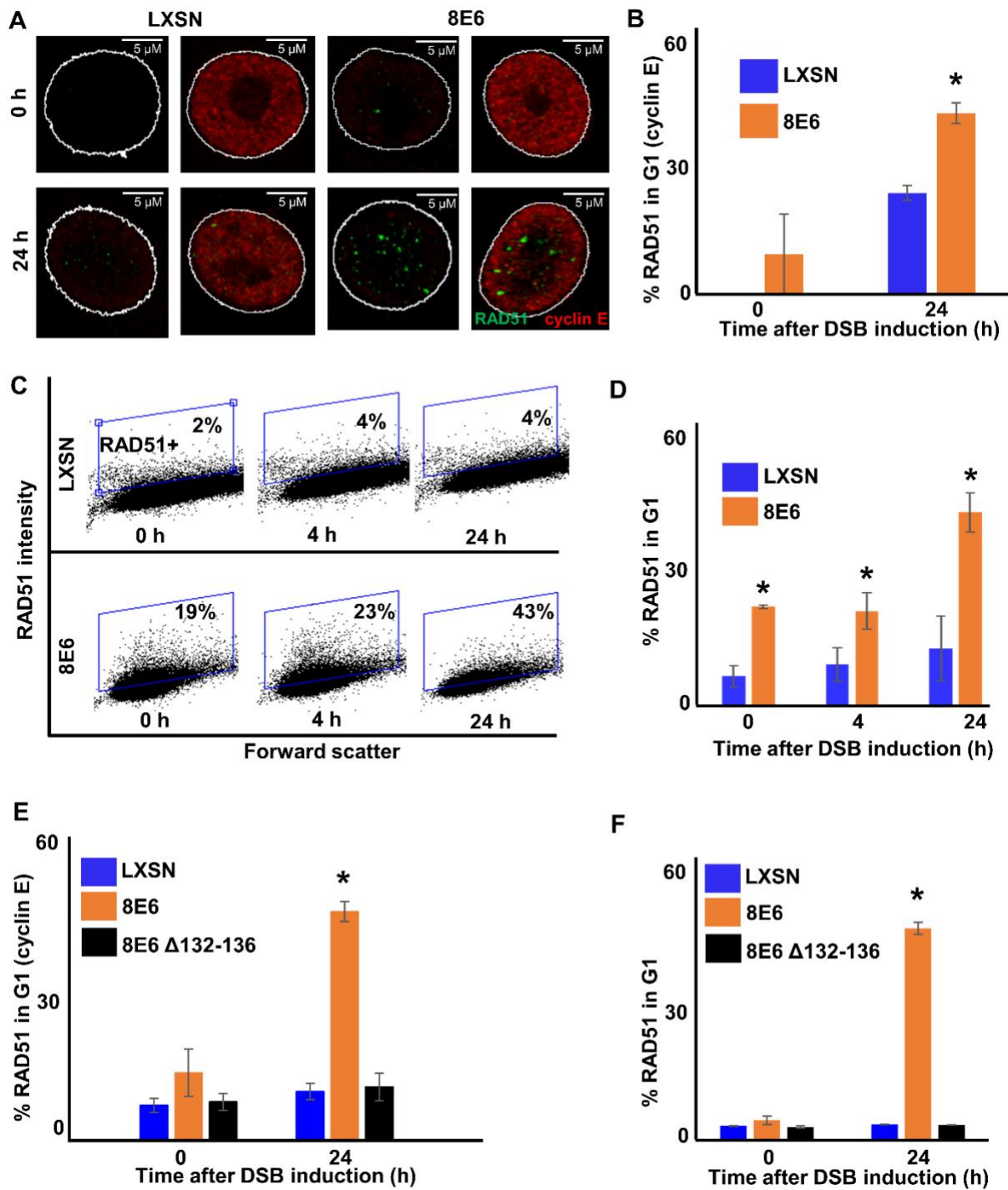


Figure 4-4. 8E6 allows RAD51 foci formation in G1.

(A) Representative cyclin E negative and positive HFK LXSN and HFK 8E6 cells stained for RAD51 (green) and cyclin E (red) 0 and 24 hours following zeocin treatment (10 μg/mL, 10 min). (B) Percentage of RAD51 positive HFK cell in G1 determined by cyclin E staining after

zeocin treatment. (C) Representative images of flow cytometry results of HFK LXS_N and HFK 8E6 cells in G1 stained with RAD51 at three points after zeocin exposure (0, 4, and 24 hours). RAD51 intensity is determined by Alexa 488 conjugated secondary antibody and shown on the y-axis. The gating represents RAD51 positive based off secondary only control. The x-axis shows cells distributed by forward scatter to avoid debris. (D) Percentage of HFK cells in G1 that are positive for RAD51 as determined by flow cytometry. (E-F) Percentage of primary HFKs in G1 that RAD51 staining after zeocin treatment as determined by (E) Cyclin E staining or (F) flow cytometry. All values are represented as mean \pm standard error. The statistical significance of differences between LXS_N and 8E6 cell lines were determined using Student's t-test. * indicates significant difference between 8E6 and LXS_N with same treatment ($p < 0.05$). At least 150 cells were counted over three independent experiments for microscopy. Twenty thousand cells were counted for each of three independent flow cytometry experiments. Nuclei were determined by DAPI staining. The edge of this staining is shown by a white line depicting the nucleus.

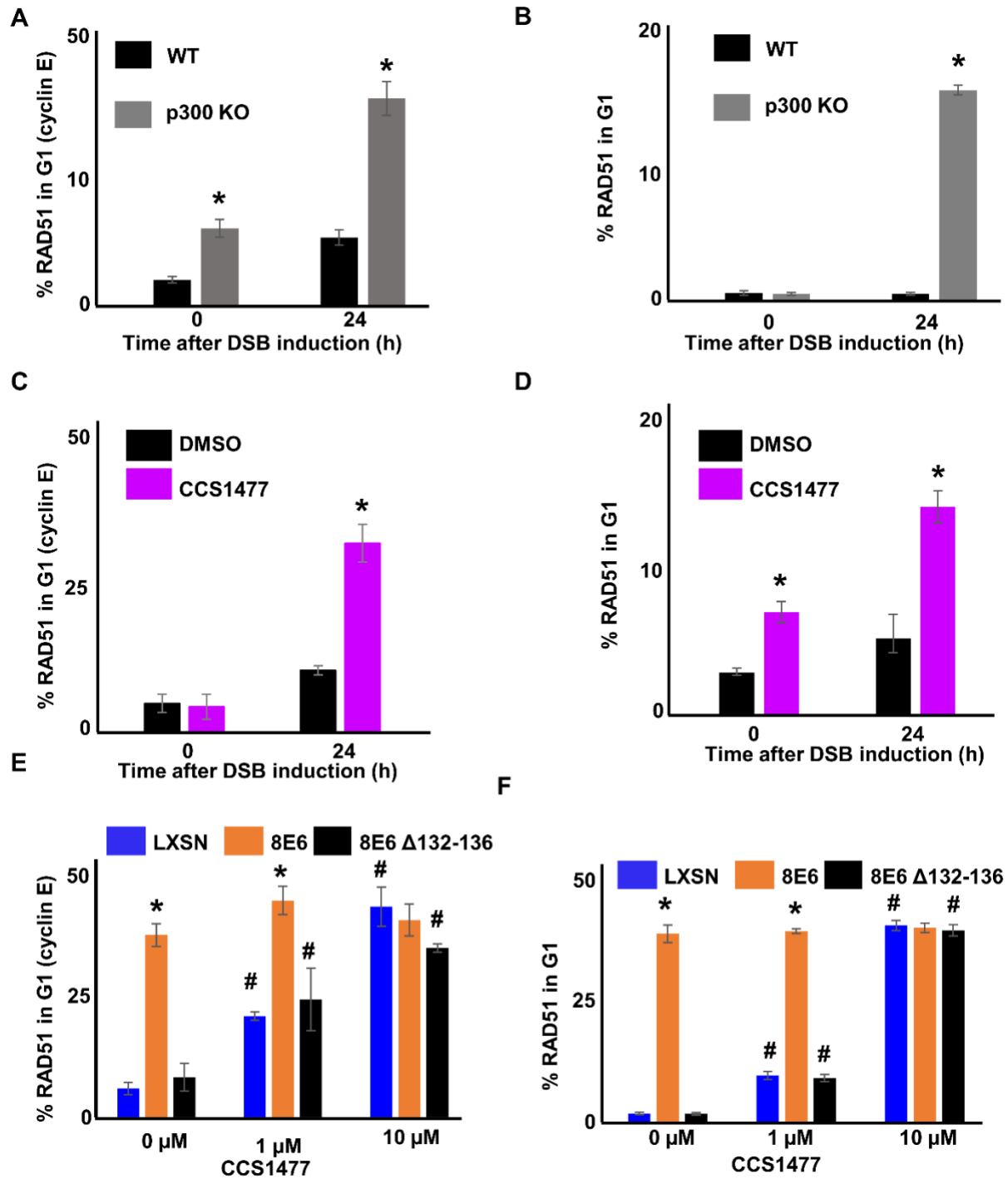


Figure 4-5. p300 restricts RAD51 foci formation in G1.

(A-B) Percentage of HFK WT and HFK p300 KO cells with RAD51 staining in G1 as

determined by (A) Cyclin E staining or (B) flow cytometry after zeocin treatment (10 μg/mL, 10

min). (C-D) Percentage of HFK LXS_N cells treated with DMSO or CCS1477 (1 μM) that had RAD51 staining in G1 as determined by (C) Cyclin E staining or (D) flow cytometry after zeocin treatment. (E-F) Percentage of primary HFK LXS_N cells treated with DMSO or CCS1477 that had RAD51 staining in G1 as determined by (E) Cyclin E staining or (F) flow cytometry after zeocin treatment. All values are represented as mean ± standard error. The statistical significance of differences between cell lines or treatments were determined using Student's t-test. * indicates significant difference between two groups (A-D) or LXS_N and 8E6 (E-F) with same treatment (p < 0.05). # indicates p < 0.05 between control (solvent) and treated group within each cell line. At least 150 cells were counted over three independent experiments for microscopy. Twenty thousand cells were counted for each of three independent flow cytometry experiments.

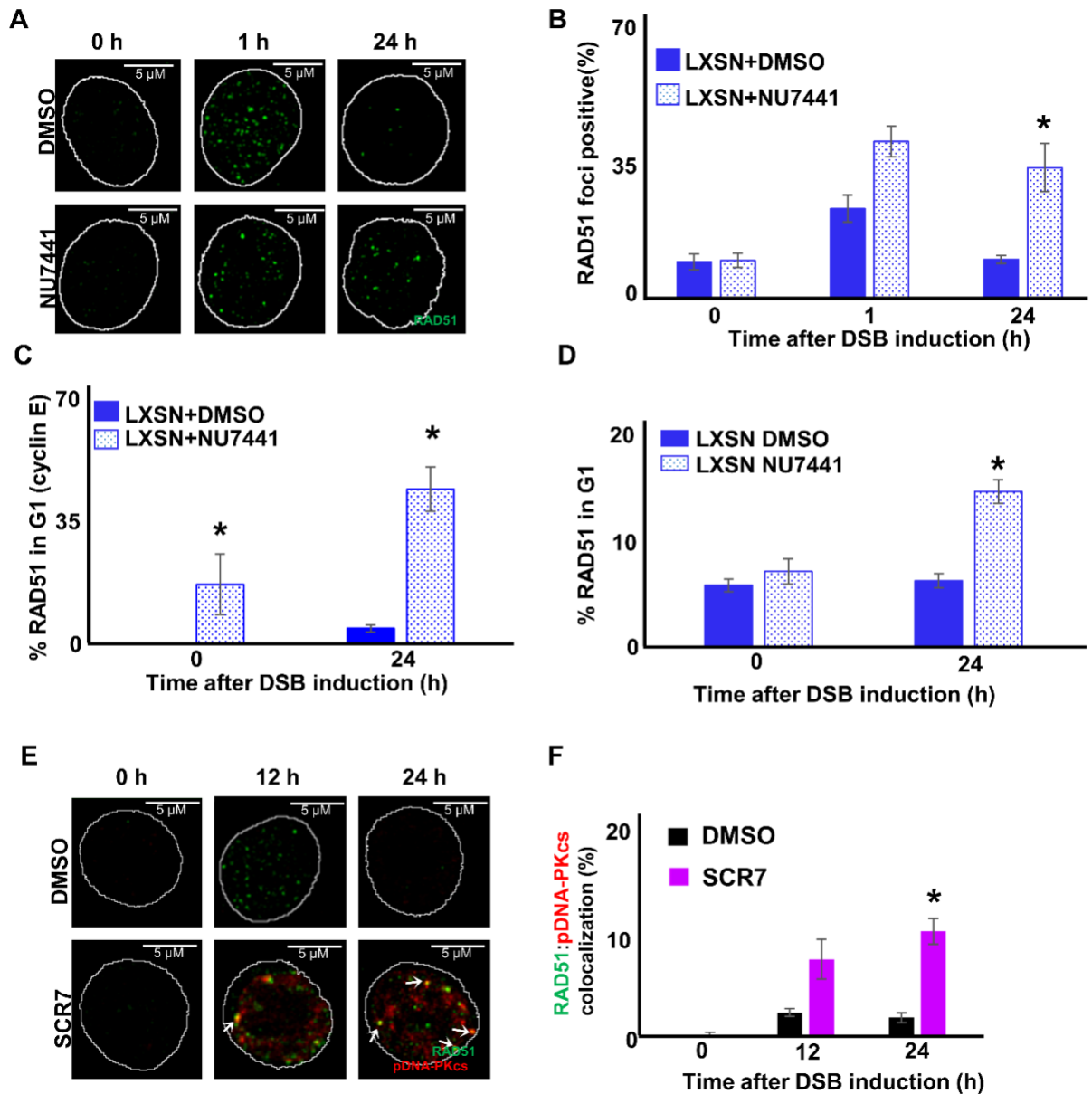


Figure 4-6. DNA-PKcs inhibition increases RAD51 foci in G1.

(A) Representative images of HFK LXSXN cells treated with NU7441 (1 μ M) or DMSO stained for RAD51 (green) following zeocin treatment (10 μ g/mL, 10 min). (B) Percentage of HFK LXSXN cells treated with NU7441 (1 μ M) or DMSO stained with RAD51 foci following zeocin treatment. (C-D) Percentage of HFK LXSXN cells treated with NU7441 (1 μ M) or DMSO stained with RAD51 staining in G1 as determined by (C) cyclin E staining or (D) flow cytometry. (E) Representative images of HFK LXSXN cells treated with ligase IV inhibitor (1 μ M of SCR7) or

DMSO stained for RAD51 (green) and pDNA-PKcs (red) following zeocin treatment. (F). Percentage of HFK LXS cells with colocalized RAD51 and pDNA-PKcs foci after treatment with ligase IV inhibitor or DMSO and exposure to zeocin. White arrow indicates colocalization. All values are represented as mean \pm standard error. The statistical significance of differences between treatments were determined using Student's t-test. * indicates significant difference between control (DMSO) and inhibitor treated groups with same zeocin treatment ($p < 0.05$). At least 150 cells were counted over three independent experiments for microscopy. Twenty thousand cells were counted for each of three independent flow cytometry experiments. Nuclei were determined by DAPI staining. The edge of this staining is shown by a white line depicting the nucleus.

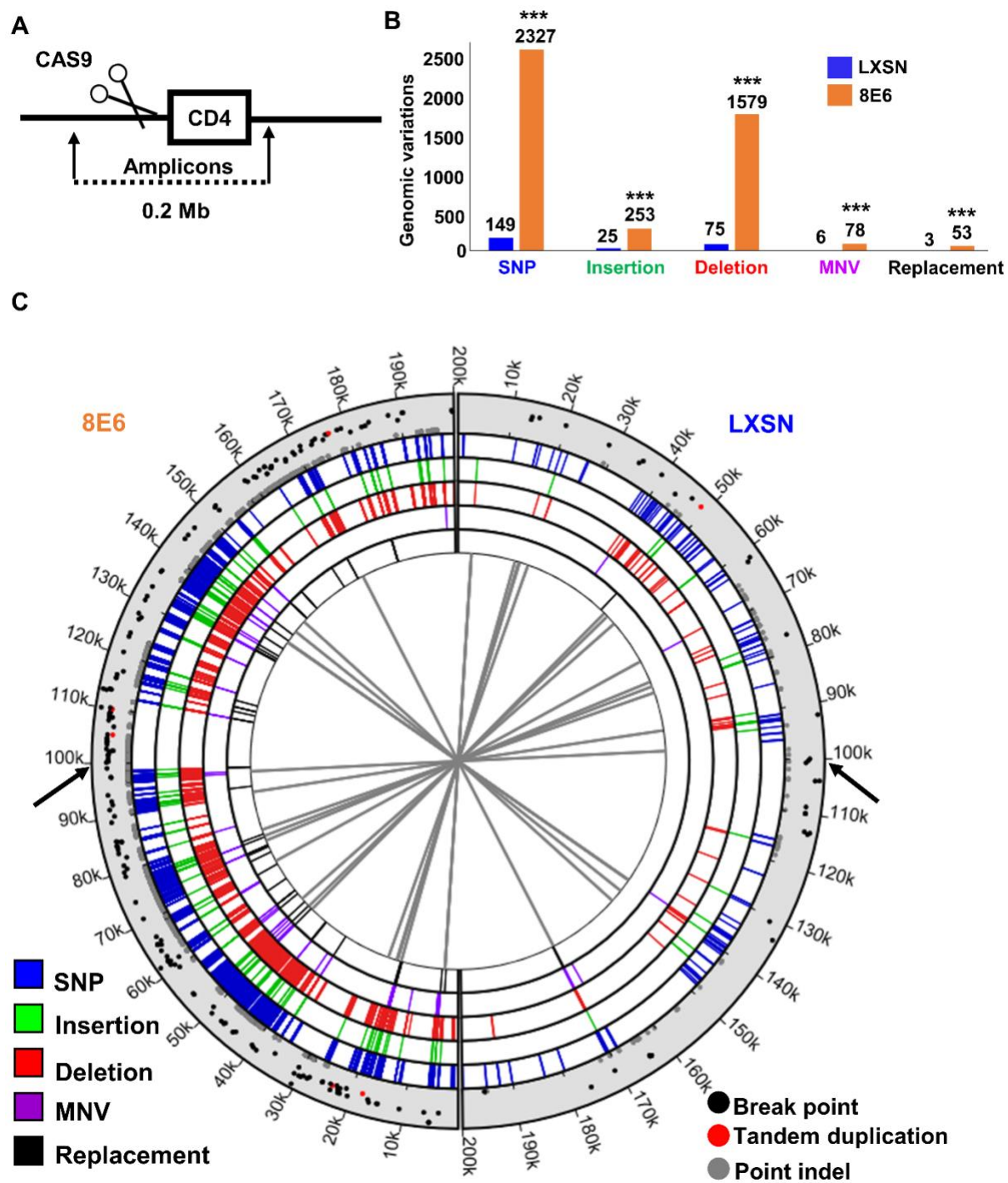


Figure 4-7. β -HPV8E6 increases genomic instability during DSB repair.

(A) Schematic of the placement of CAS9 induced DSB along the sequenced portion of the genome. (B) Genomic variations grouped by types of mutational events in HFK LXSN and HFK

8E6. Each group of genomic variations and total number of variations were compared between HFK LXS and HFK 8E6. (C) Circos plot of DNA mutations in HFK LXS (right side) and HFK 8E6 cells (left side). Black arrows indicate CAS9 cutting sites. The innermost circle displays connections between identical genomic rearrangements. The location of genomic rearrangements colored by types of genomic variations are shown in five concentric circles (blue represents SNP, green represents insertion, red represents deletion, purple represents MNV, and black represents replacement). Scatter plot in the outermost circle displays breakpoints (black), tandem duplications (red), and point indels (grey), in which proximity to the outer edge represents high variant ratio. SNP, single nucleotide polymorphism. MNV, multi-nucleotide variation. Statistical differences between cell lines were measured using a Student's T-test. *** indicates $p < 0.001$.

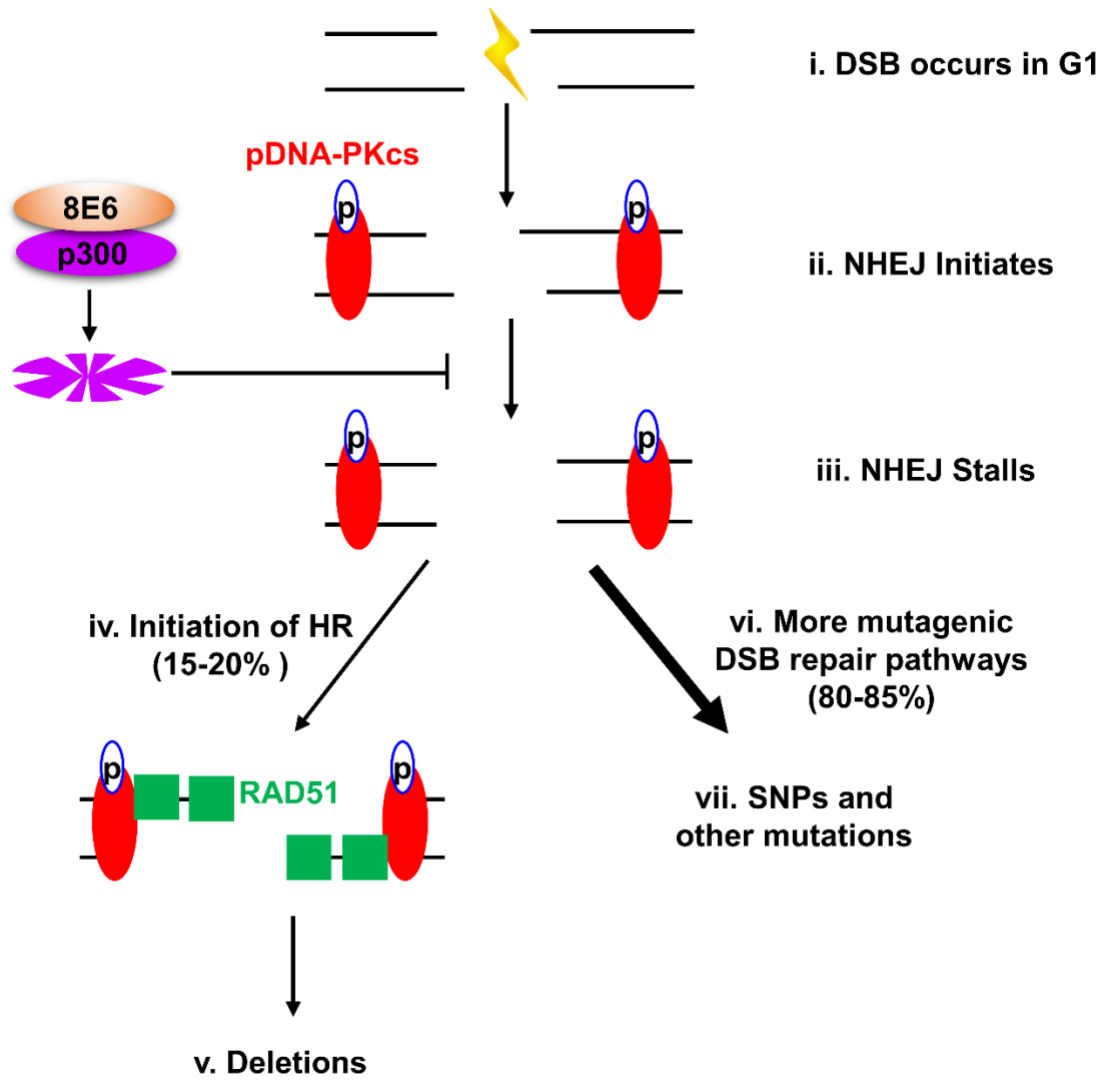
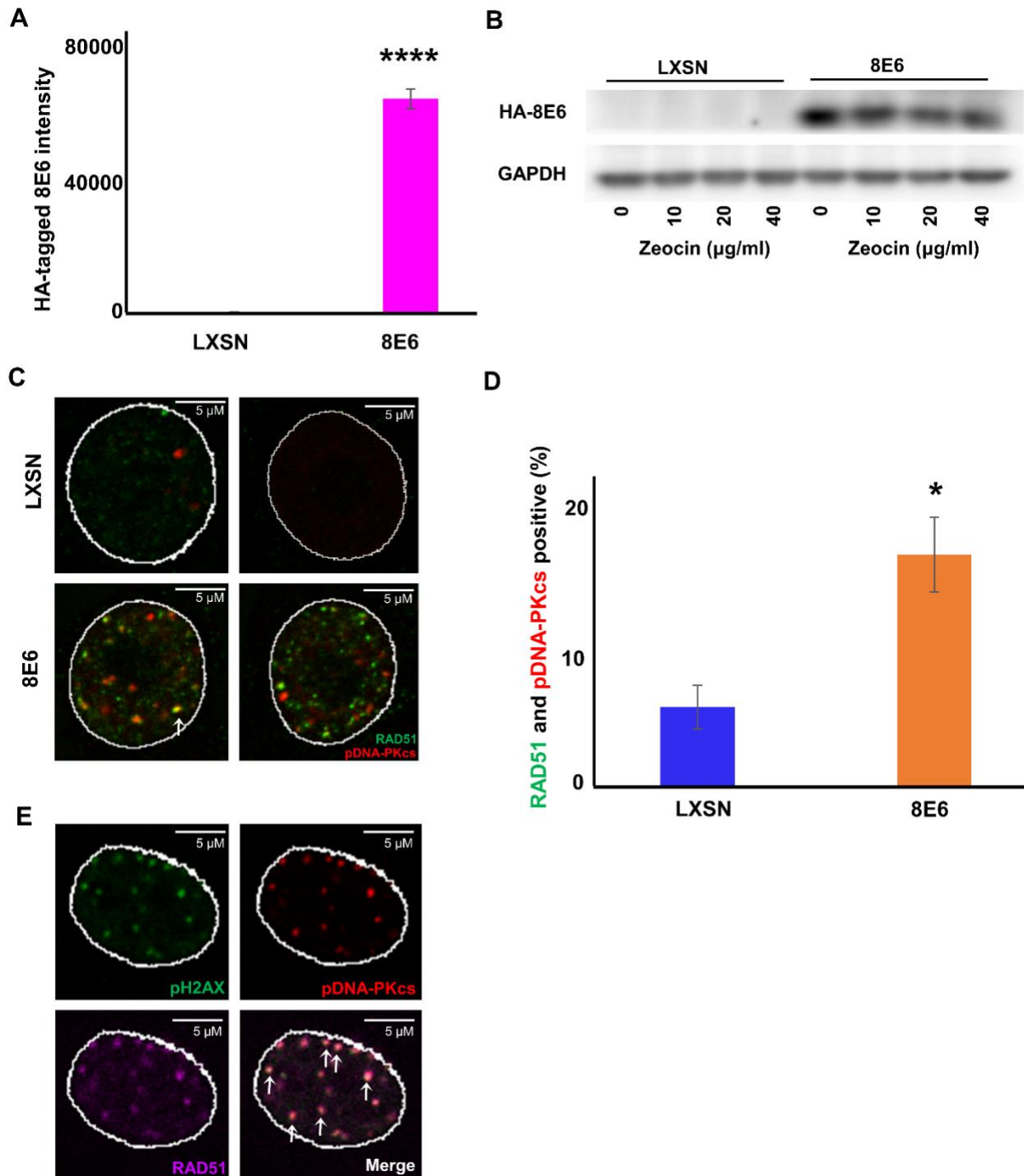


Figure 4-8. Summary figure of DSB repair in G1 phase.

(i) DSB occurs in a cell in G1 phase that is expressing 8E6. (ii) NHEJ initiates. DNA-PKcs is recruited to the lesion where it is auto-phosphorylated. (iii) NHEJ stalls due to 8E6 mediated p300 degradation. This leaves unresolved pDNA-PKcs repair complexes [9]. (iv) HR initiates at the site of failed NHEJ. Single stranded DNA is produced by MRN complex, CtIP, and EXO1 [73]. RPA complexes coat and stabilize the resulting single stranded DNA [39]. RPA70 foci colocalize with pDNA-PKcs indicating that HR-mediated DNA resection occurs after NHEJ fails. Then, RAD51 is recruited to the break site. (v) HR cannot be complete due to the lack of a homologous template and/or 8E6-mediated inhibition of HR [7]. This causes deletions due to antagonist DNA end process by NHEJ and HR and/or by failure to complete HR after resection. (vi) The failure of NHEJ causes cells to use tertiary DSB repair pathways to fix the lesion. (vii) This alternative repair pathway (e.g., Alt-EJ) is error prone and increases other types of mutations (such as SNPs).

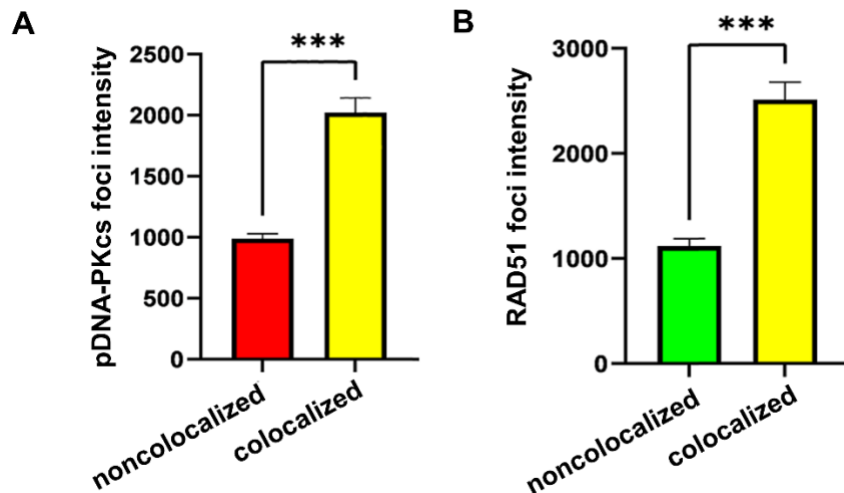
Chapter 4 supplemental figures



S4-1 Fig. 8E6 allows RAD51 and pDNA-PKcs foci formation to occur in the same cell. (A)

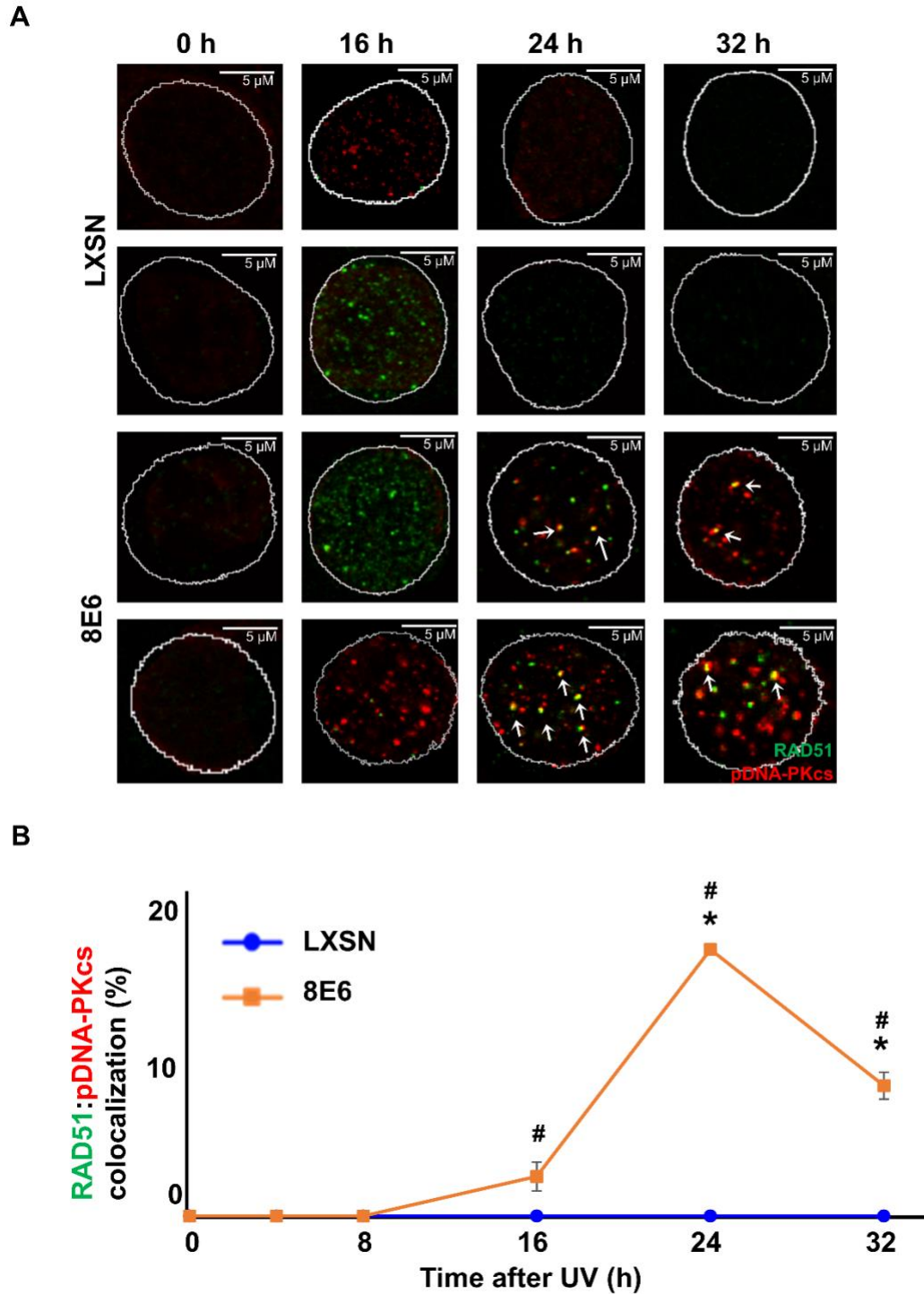
Average intensity of HA staining in HFK LXSN and HFK 8E6 cells measured by

immunofluorescence microscopy (B) Representative immunoblotting of HA-tagged 8E6 (HA-8E6). GAPDH is used as a loading control. (C) Representative images of Rad51 (green) and pDNA-PKcs (red) foci in HFK LXSXN and HFK 8E6 cells 24- hours after zeocin treatment (10 $\mu\text{g}/\text{mL}$, 10min). (D) Percentage of HFK cells with both Rad51 and pDNA- PKcs foci 24-hours after zeocin treatment. (E) Representative images of RAD51, pDNA-PKcs, and pH2AX in N/TERT HFK 8E6 24 hours after zeocin treatment. White arrows indicate colocalization. Statistical significance of the differences between cell lines was determined using Student's t-test. * indicates significant difference between 8E6 and LXSXN (p-value < 0.05). **** indicates p-value < 1.0×10^{-50} . All values are represented as mean \pm standard error. At least 150 cells were counted over three independent experiments. Nuclei were determined by DAPI staining. The edge of this staining is shown by a white line depicting the nucleus.



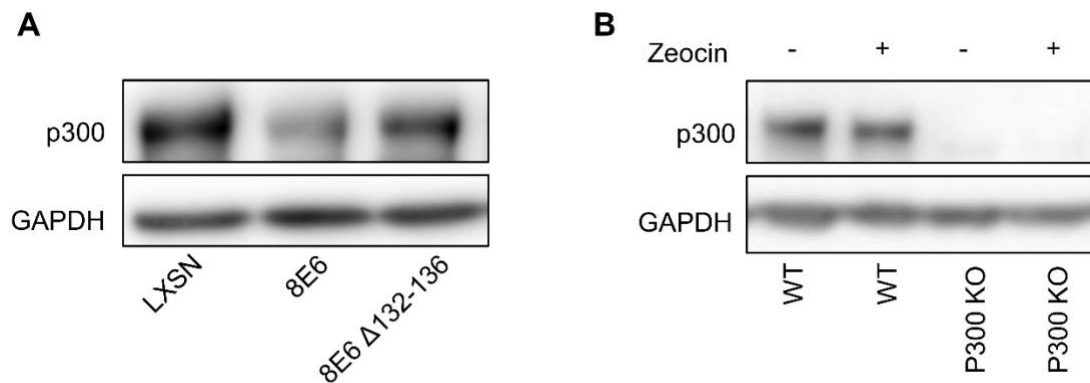
S4-2 Fig. Colocalized foci are larger than non-colocalized foci. (A) pDNAPK intensity (metric of foci size) of non-colocalized and colocalized foci were measured in HFK 8E6 cells 24 hours after zeocin treatment (10 $\mu\text{g}/\text{mL}$, 10 min). (B) RAD51 intensity (metric of foci size) of non-colocalized and colocalized foci were measured in HFK 8E6 cells 24 hours after zeocin treatment. Statistical significance of differences between treatments was determined using

Student's t-test. *** indicates p-value < 0.001 (n=3). All values are represented as mean \pm standard error. At least 150 cells were counted over three independent experiments.

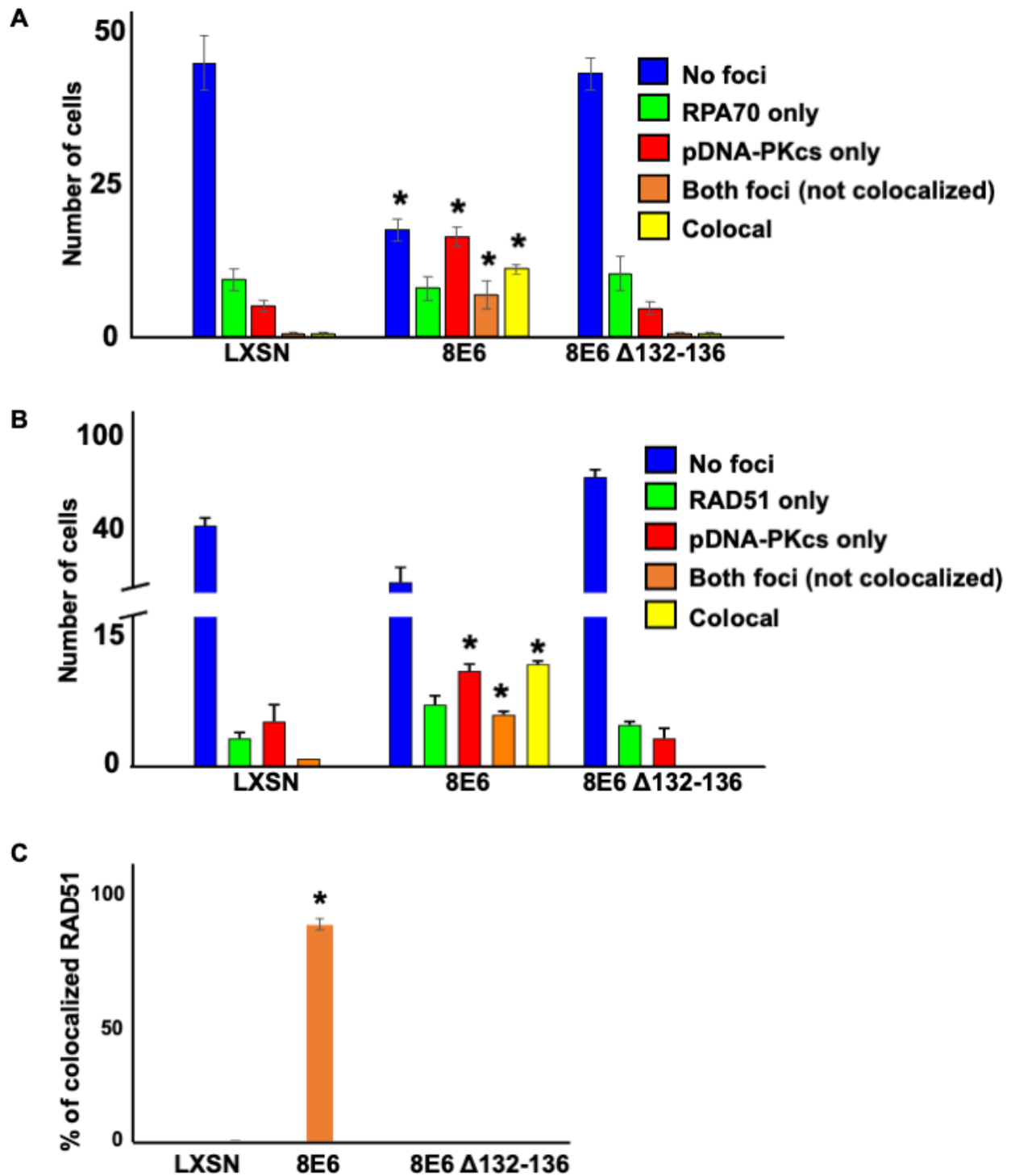


S4-3 Fig. 8E6 increases colocalization of RAD51 and pDNA-PKCs in HFK cells following UV treatment. (A) Representative images of Rad51 (green) and pDNA-PKCs (red) staining in HFK

LXSN and HFK 8E6 following UV (10 mJ/cm²). White arrow indicates colocalization. (B) Percentage of HFK cells with colocalized foci following UV. Statistical significance of differences between treatments was determined using Student's t-test. * indicates significant difference between 8E6 and LXSN (p-value < 0.05). All values are represented as mean ± standard error. # indicates p < 0.05 between control (solvent) and treated group within each cell line. At least 150 cells were counted over three independent experiments. Nuclei were determined by DAPI staining. The edge of this staining is shown by a white line depicting the nucleus.

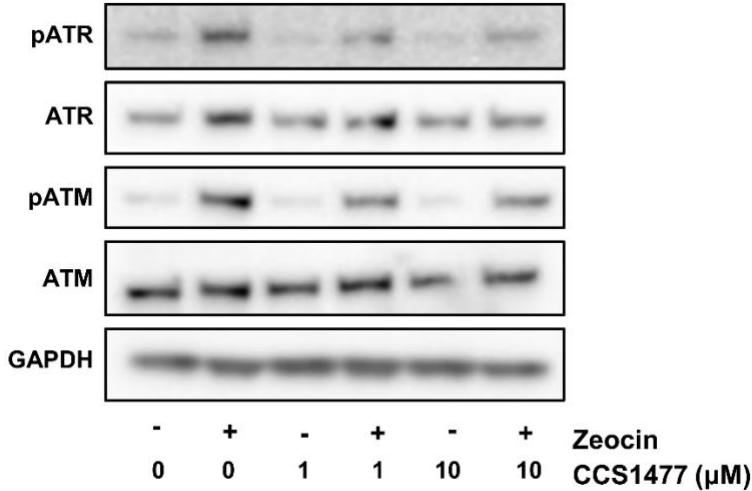


S4-4 Fig. p300 level is detected by immunoblot. (A) Representative immunoblot showing p300 in primary HFK LXSN, HFK 8E6, and 8E6 Δ132-136 cells. GAPDH is used as a loading control. (B) Representative immunoblot showing p300 in HFK WT and HFK p300 knockout (p300 KO) cells 24 hours after zeocin exposure (10 μg/mL, 10min). GAPDH is used as a loading control.

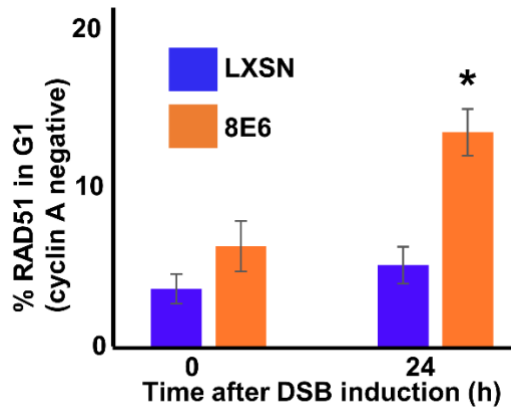


S4-5 Fig. 8E6 increases RPA70:pDNA-PKCs and RAD51:pDNA-PKCs colocalization in primary HFK cells. (A) Average number of cells with no foci, RPA70 alone, pDNA-PKCs alone, both RPA70 and pDNA-PKCs foci (not colocalized), and RPA70:pDNA-PKCs colocalized 16 hours

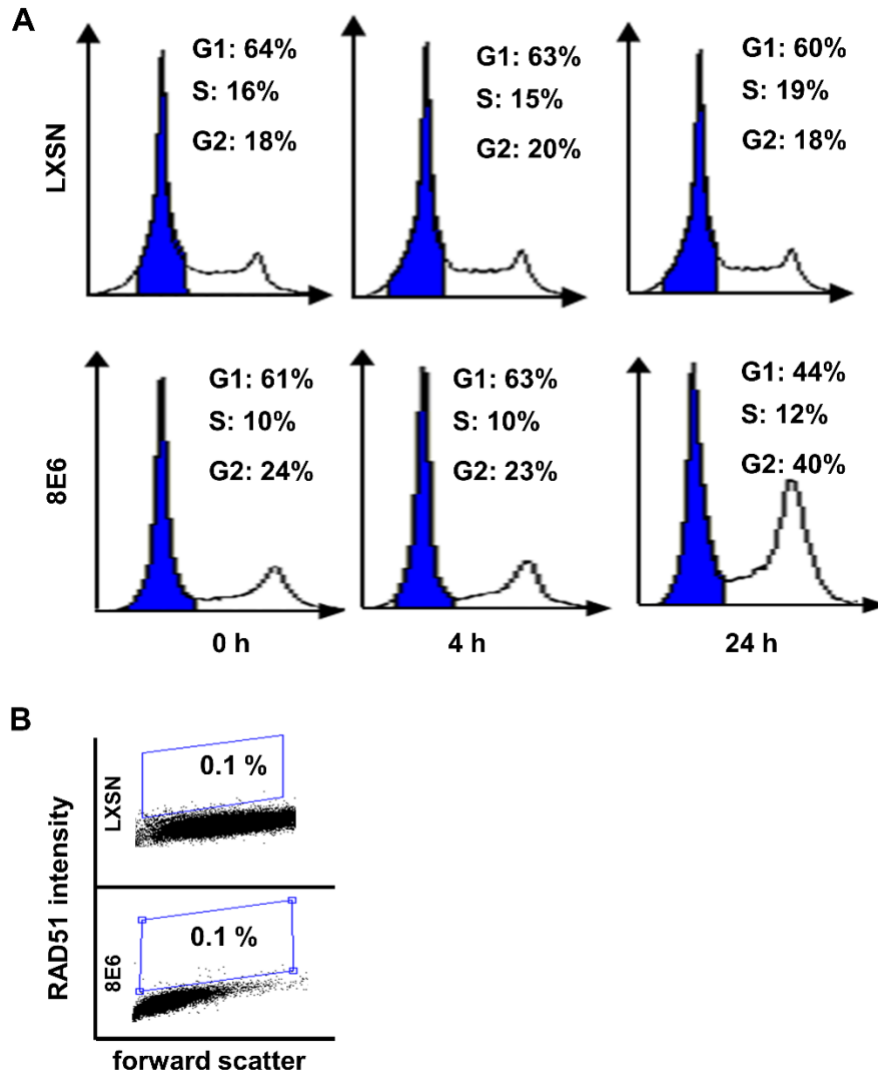
after zeocin treatment (10 $\mu\text{g}/\text{mL}$, 10 min). (B) Average number of cells with no foci, RAD51 alone, pDNA-PKcs alone, both RAD51 and pDNA- PKcs foci (not colocalized), and RAD51:pDNA-PKcs colocalized 24 hours after zeocin treatment. (C) Percentage of RAD51 foci that are colocalized with pDNA-PKcs 24 hours after zeocin treatment. All values are represented as mean \pm standard error. The statistical significance of differences between groups were determined using Student's t-test. * indicates significant difference between 8E6 and LXS (p-value < 0.05). At least 150 cells were counted over three independent experiments.



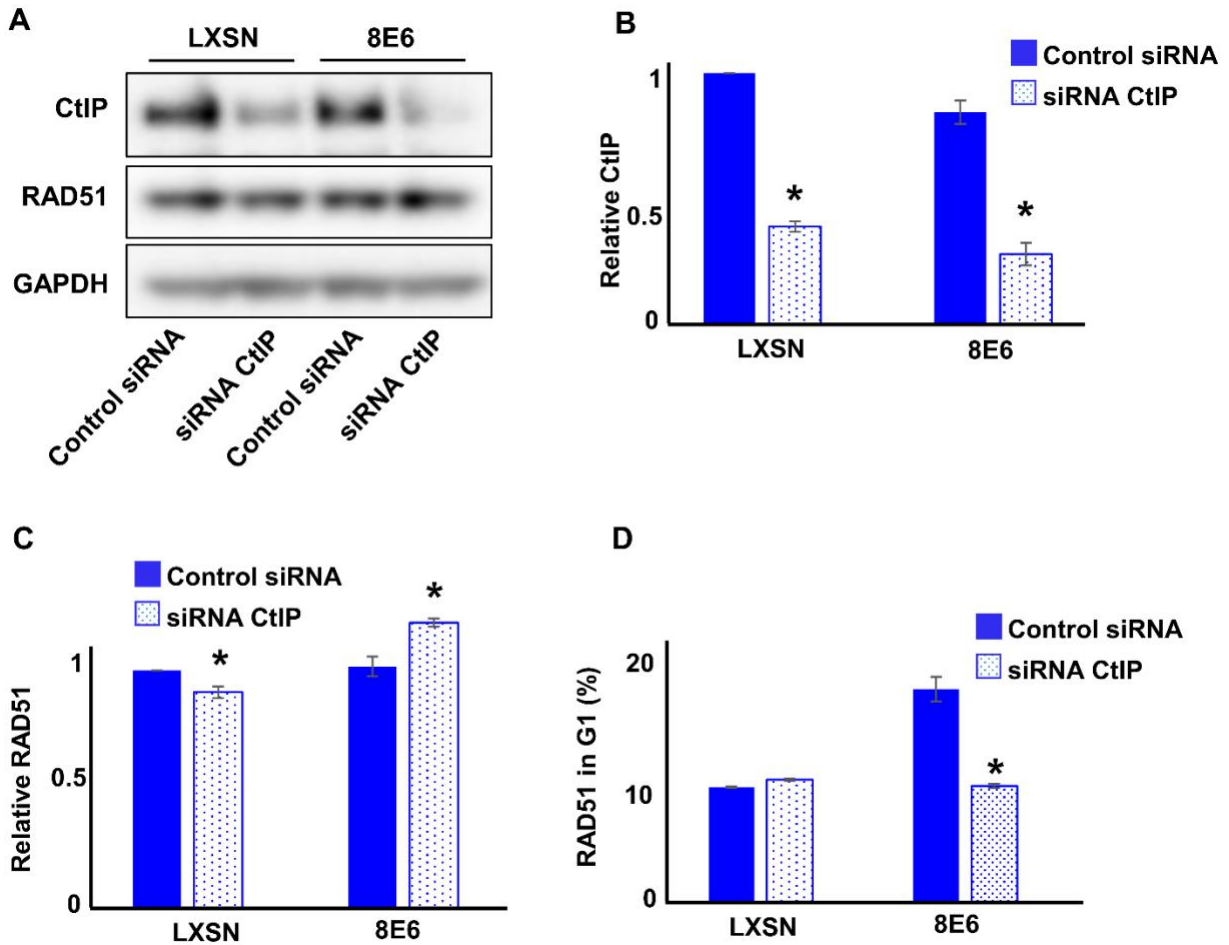
S4-6 Fig. CCS1477 decreases phosphorylated ATR (pATR) and phosphorylated ATM (pATM). Representative immunoblot showing pATR, ATR, pATM, and ATM expression in HFK LXS cells treated with DMSO or CCS1477 (1 μM) 24-hours after zeocin treatment (10 $\mu\text{g}/\text{mL}$, 10min). GAPDH is used as a loading control. This experiment was repeated three times.



S4-7 Fig. 8E6 increases the frequency of cyclin A negative cells with RAD51 staining. Percentage of cyclin A negative HFK cells with RAD51 foci after zeocin treatment (10 $\mu\text{g}/\text{mL}$, 10min). Statistical significance of differences between treatments was determined using Student's t-test. * indicates significant difference between 8E6 and LXS ($p\text{-value} < 0.05$). All values are represented as mean \pm standard error. At least 150 cells were counted over three independent experiments.

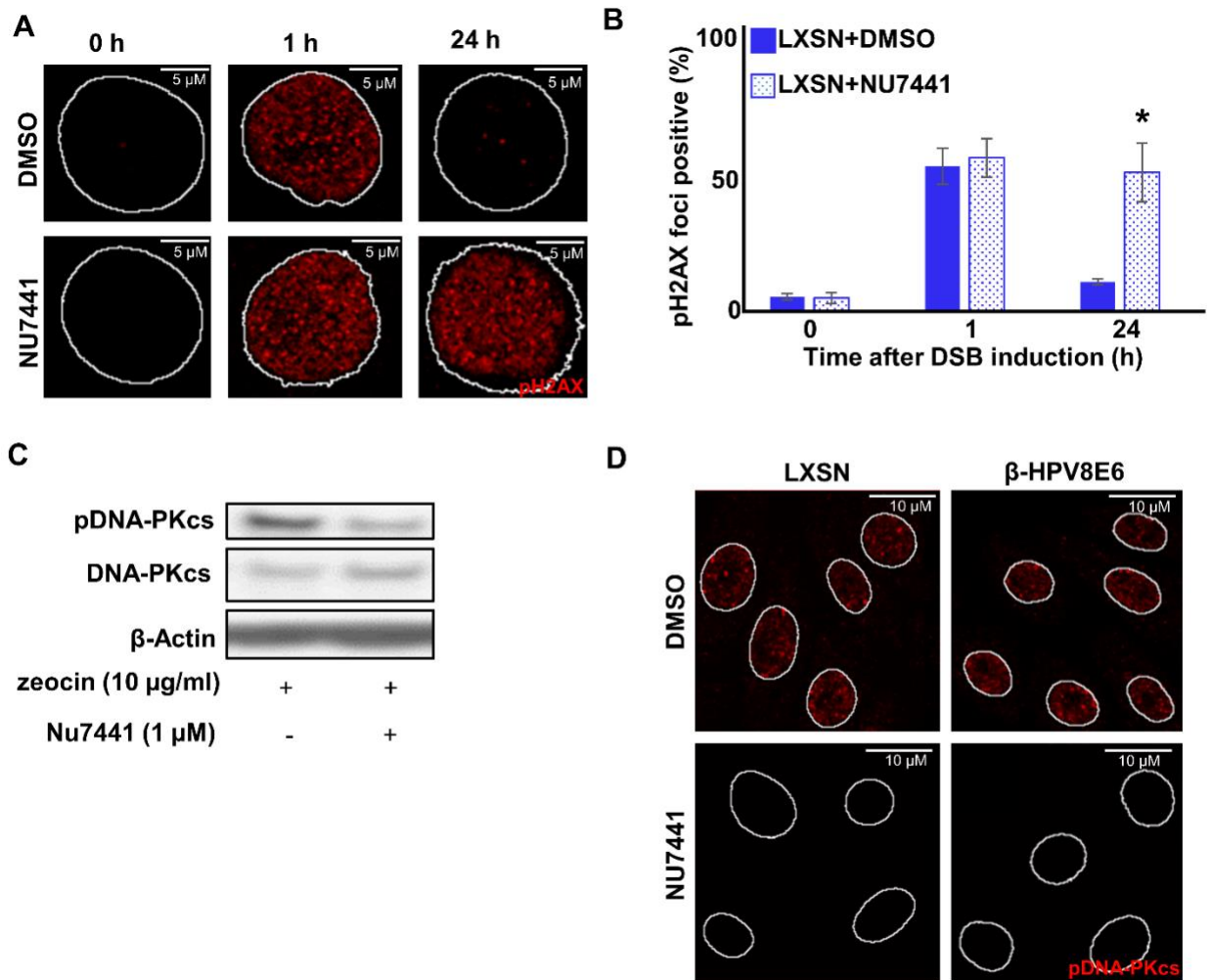


S4-8 Fig. Controls were used to determine RAD51 staining cutoff and G1 gating in HFK cells by flow cytometry. (A) Representative images of cell cycle analysis by flow cytometry following zeocin treatment (10 $\mu\text{g}/\text{mL}$, 10min). DAPI was used to determine DNA content and G1 (blue). (B) Representative images of flow cytometry results of HFK LXSN and HFK 8E6 cells stained with Alexa 488 conjugated secondary antibody and shown on the y-axis. The gating represents RAD51 positive based off secondary only control. The x-axis shows cells distributed by forward scatter to avoid debris. Twenty thousand cells were counted for each of three flow cytometry experiments.



S4-9 Fig. 8E6 requires CtIP to increase the frequency of Rad51 foci formation in G1. (A) Representative immunoblot showing CtIP and RAD51 in U2OS LXSN and U2OS 8E6 cells transfected with control siRNA or siRNA CtIP 24-hours after zeocin treatment (10 μ g/mL, 10min). GAPDH is used as a loading control. (B) Densitometry of CtIP normalized to GAPDH and LXSN with control siRNA (n=3). (C) Densitometry of RAD51 normalized to GAPDH and LXSN with control siRNA (n=3). (D). Percent of Rad51 positive cells in G1 measured by flow cytometry in U2OS LXSN and U2OS 8E6 cells transfected with control siRNA or siRNA CtIP 24-hours after zeocin treatment. Statistical significance of differences between treatments was determined using Student's t-test. * indicates significant difference between control siRNA and

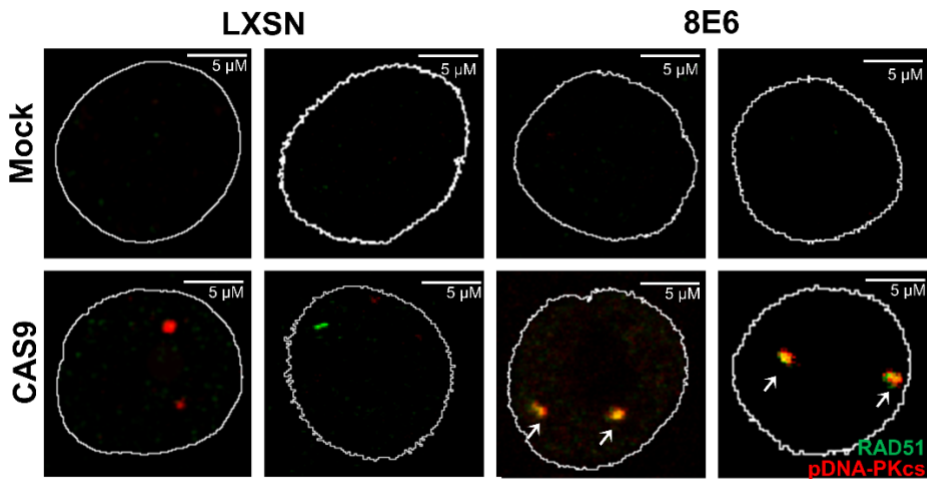
siRNA CtIP treated group ($p < 0.05$, $n=3$). All values are represented as mean \pm standard error. Twenty thousand cells were counted for each of three flow cytometry experiments.



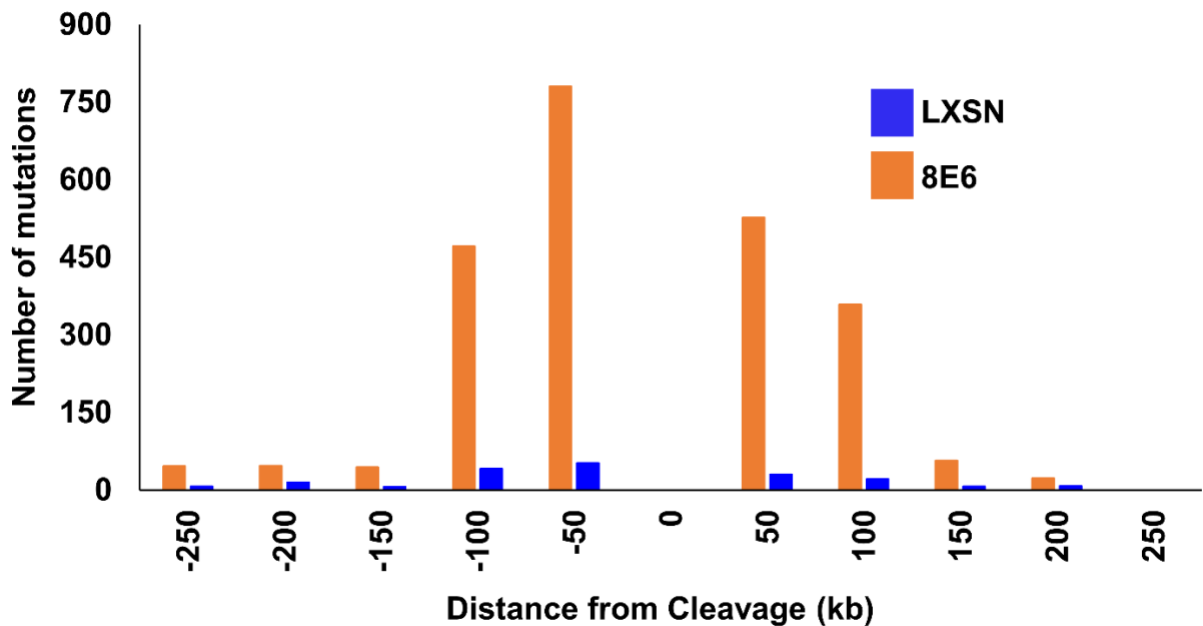
S4-10 Fig. Controls for NU7441 inhibitor of DNA-PKcs (A) Representative images of HFK LXSN cells treated with NU7441 (1 μ M) or DMSO stained for pH2AX S139 (red) following zeocin treatment (10 μ g/mL, 10min). (B) Percentage of HFK LXSN cells with pH2AX S139 foci following zeocin treatment. All values are represented as mean \pm standard error. (C) Representative immunoblots showing pDNA-PKcs and DNA-PKcs abundance in HFK LXSN cells treated with DMSO or NU7441 following zeocin treatment. (D) Representative images of HFK LXSN and HFK 8E6 stained for pDNA-PKcs following DMSO or NU7441 treatment.

Statistical significance of differences between DMSO and NU7441 treated cells was determined using Student's t-test. * indicates significant difference between DMSO and NU7441 treated group (p-value < 0.05). Nuclei were determined by DAPI staining. The edge of this staining is shown by a white line depicting the nucleus. At least 150 cells were counted over three independent experiments. All experiments were repeated in triplicate.

A



B



S4-11 Fig. RAD51/pDNA-PKcs colocalization occurs at CAS9-induced DSBs in 8E6 expressing HFKs. (A) Representative images of Rad51 (green) and pDNA-PKcs (red) staining in HFK LXS and HFK 8E6 cells following DSB induction by CAS9. White arrow indicates colocalization. Nuclei were determined by DAPI staining. The edge of this staining is shown by a white line depicting the nucleus. (B) Genomic variations in HFK LXS and HFK 8E6 are grouped based on the distance from the CAS9 cut site. Each bar represents the total number of variations at the indicated distance from the CAS9-induced DSB.

Chapter 5 - Beta Human papillomavirus 8 E6 promotes alternative end-joining

Changkun Hu¹, Taylor Bugbee¹, Rachel Palinski^{2,3}, Michael McIntosh⁴, Sumita Bhaduri-McIntosh⁵, Nicholas Wallace^{1,*}

1 Division of Biology, Kansas State University, Manhattan, KS 66506, USA.

2 Kansas State Veterinary Diagnostic Laboratory, Kansas State University, Manhattan, KS 66506, USA.

3 Department of Diagnostic Medicine/Pathobiology, Kansas State University, Manhattan, KS 66506, USA.

4 Child Health Research Institute, Department of Pediatrics, University of Florida, Gainesville, FL, USA; Department of Molecular Genetics and Microbiology, University of Florida, Gainesville, FL, USA.

5 Division of Infectious Diseases, Department of Pediatrics, University of Florida, Gainesville, FL, USA; Department of Molecular Genetics and Microbiology, University of Florida, Gainesville, FL, USA

* To whom correspondence should be addressed. Tel: +1 785-532-6014; Fax: +1 785-532-6653; Email: nwallac@ksu.edu

Abstract

Double strand breaks (DSBs) are one of the most lethal DNA lesions in cells. Previous studies show that the E6 protein of beta-human papillomavirus (HPV8 E6) impairs two major DSB repair pathways homologous recombination (HR) and non-homologous end-joining (NHEJ). However, HPV8 E6 delays but does not eliminate DSB repair capability of cells. How DSBs are repaired in cells with HPV8 E6 remains to be studied. We hypothesize that HPV8 E6 promotes a backup DSB repair pathway, alternative end-joining (Alt-EJ). Using CAS9 based Alt-EJ reporters, we show that HPV8 E6 promotes Alt-EJ. Further, using small molecule inhibitors, CRISPR/CAS9 gene knockout, and HPV8 E6 mutant, we find that HPV8 E6 promotes Alt-EJ by binding p300, an acetyltransferase that facilitates DSB repair by HR and NHEJ. Finally, computational analysis shows that HPV8 E6 increases small deletions (2-29 bp) with 2-10 bp microhomology. This study fills the knowledge gap how DSB is repaired in cells with HPV8 E6 and the mutagenic consequences of HPV8 E6 mediated p300 destabilization. Broadly, this study supports the hypothesis that β -HPV promotes cancer formation by increasing genomic instability.

1. Introduction

Beta genus human papillomavirus (β -HPV) is ubiquitous and transiently infects cutaneous epithelia in the general population [1–3]. β -HPVs, including type 8 (HPV8), are

associated with nonmelanoma skin cancer (NMSC) in immunocompromised individuals including people with a rare genetic disorder epidermodysplasia verruciformis and organ transplant recipients [2,4–6]. However, the contribution of β -HPV infections to NMSC in the general population is unclear. Because beta HPV infections are not persistent in immunocompetent people, they are hypothesized to promote cancer formation by making UV induced DNA damage more mutagenic [7–9]. In support of this hypothesis, our group and others have used in vitro and in vivo systems to demonstrate that the E6 protein from HPV8 (8E6) impairs DNA repair [9–11].

The interaction with and destabilization of p300 is a key mechanism by which 8E6 hinders DNA repair [12,13]. P300 is an acetyltransferase that regulates transcription by chromatin remodeling [14–16]. By binding p300, 8E6 decreases the abundance of multiple DNA repair proteins including ATR, ATM, BRCA1, and BRCA2 [11,17,18]. This lowers the activation of ATM and ATR signaling, decreasing the cellular response to UV-damaged DNA [11,19]. The limited ability to repair UV damage increases the frequency with which UV causes replication forks to collapse into double strand breaks (DSBs) in DNA [20,21]. Cells have multiple DSB repair mechanisms. Homologous recombination (HR) is minimally mutagenic, but restricted to in S/G2 phase when the sister chromatids can serve as homologous templates [22,23]. Whenever possible cells use HR to fix DSBs as it allows them to avoid mutations during the repair. When HR is inhibited (by cell cycle position, mutation to repair factors, or artificially), non-homologous end joining (NHEJ) is used to repair DSBs [24]. NHEJ can occur throughout the cell cycle, as it does not require a homologous template. However, because NHEJ generates and ligates blunt ends to fix a DSB, it is more mutagenic than HR [25]. We have shown that 8E6 attenuates both HR and NHEJ by degrading p300 [18,26].

Notably, 8E6 does not block the initiation of NHEJ or HR. NHEJ initiation occurs when DNA-dependent protein kinase catalytic subunit (DNA-PKcs) complexes at DSBs and activates itself by auto-phosphorylation (pDNA-PKcs) [27,28]. This occurs readily in the presence of 8E6. However, 8E6 prevents the resolution of pDNA-PKcs repair complexes and attenuates other downstream steps in NHEJ [26]. Similarly, 8E6 allows the HR pathway to initiate, before hindering the resolution of RAD51 repair complexes [18]. We recently demonstrated that cells respond to 8E6-associated inhibition of NHEJ by trying to complete homologous recombination during G1 [29]. This ultimately leads to persistent RAD51 repair complexes forming during G1.

Thus, currently there is a detailed understanding of how 8E6 causes DSB repair to fail, but less is known about how DSB repair occurs in cells that express 8E6. When NHEJ and HR fail, a mutagenic tertiary repair pathway known as alternative end joining (Alt-EJ) is tasked with completing DSB repair [30]. Here, we use reporter constructs and small molecule inhibitors of DNA repair factors to demonstrate that 8E6 promotes DSB repair by Alt-EJ and that the use of Alt-EJ is indirect result of initiating NHEJ that cannot be completed. Analysis of whole genome sequencing data from cells expressing 8E6 are used to identify mutational signatures associated with Alt-EJ. This observation addresses a key knowledge gap in the field. By promoting DSB repair by Alt-EJ, 8E6 increases the risk of mutations associated with DSBs while allowing cells to avoid the apoptosis that would be associated with an unrepaired DSB. This is consistent with the proposed mechanism by which beta HPV infections are hypothesized to promote NMSC.

2. Material and methods

2.1 Cell culture and Reagents

Immortalized human foreskin keratinocytes (N/TERT HFK) provided by Michael Underbrink (University of Texas Medical Branch) and primary HFK were grown in EpiLife

medium (MEPICF500, Gibco), supplemented with 60 μ M calcium chloride (MEPICF500, Gibco), human keratinocyte growth supplement (MEPICF500, Gibco), and 1% penicillin-streptomycin (PSL02-6X100ML, Caisson). U2OS cells were maintained in DMEM supplemented with 10% FBS and 1% penicillin-streptomycin. Zeocin (J67140-XF, Alfa Aesar) was used to induce DSBs (10 μ g/mL, 10 min). NU7441 (S2638, Selleckchem) was used to inhibit DNA-PKcs phosphorylation (1 μ M) and verify the pDNA-PKcs antibody. SiRNA DNA-PKcs was used to further validate pDNA-PKcs antibody. KU55933 (Sigma-Aldrich, SML1109) was used to validate RAD51 antibody as previously described[31]. CCS1477 (CT-CCS1477, Chemietek) was used to inhibit p300 activity (1 μ M). Alt-EJ plasmids (#113619, #113620, #113625, #113626, Addgene) were used to measure Alt-EJ efficiency.

2.2 Immunofluorescence Microscopy

Cells were seeded onto either 96-well glass-bottom plates and grown overnight. Cells treated with zeocin (10 μ g/mL, 10 min) were fixed with 4% paraformaldehyde. Then, 0.1% Triton-X was used to permeabilize the cells, followed by blocking with 3% bovine serum albumin. Cells were then incubated with the following antibodies: RAD51 (ab1837, Abcam, 1:200), cyclin E (4132S, Cell Signaling), pH2AX S139 (9718S, Cell Signaling), and cyclin A (ab39, Abcam). The cells were washed and stained with the appropriate secondary antibodies: Alexa Fluor 594 (red) goat anti-rabbit (A11012, Thermo Scientific), Alexa Fluor 488 (green) goat anti-mouse (A11001, Thermo Scientific). After washing, the cells were stained with 10 μ M DAPI in PBS and visualized with the Zeiss LSM 770 microscope. Images were analyzed using the ImageJ techniques previously described[32]. Cyclin E intensity was measured for each cell. Average cyclin E intensity of cells grown in media without growth factor for 4 hours was used to define the threshold of cyclin E positive.

2.3 Flow Cytometry

Cells were collected from 6 cm plates, at about 80-90% confluence, by using trypsinization. Cells were washed with cold PBS and fixed with 95% cold ethanol for 10 min at -20 °C. Cells were stained with anti-RAD51 antibody (ab1837, Abcam, 1:100) and Alexa Fluor 488 goat anti-mouse (A11001, Thermo Scientific,). After washing, cells were resuspended in 200 µL PBS and NUCLEAR-ID Red DNA stain (ENZ-52406, Enzo Life Science), and incubated in the dark at room temperature for 30 min. Samples were analyzed by a BD Accuri C6 Plus Flow Cytometer.

2.4 Immunoblotting

After being washed with ice-cold PBS, cells were lysed with RIPA Lysis Buffer (VWRVN653-100ML, VWR Life Science), supplemented with Phosphatase Inhibitor Cocktail 2 (P5726-1ML, Sigma) and Protease Inhibitor Cocktail (B14001, Bimake). The Pierce BCA Protein Assay Kit (89167-794, Thermo Scientific) was used to determine protein concentration. Equal protein lysates were run on Novex 3–8% Tris-acetate 15 Well Mini Gels (EA03785BOX, Invitrogen) and transferred to Immobilon-P membranes (IPVH00010, Fisher Scientific). Membranes were then probed with the following primary antibodies: GAPDH (sc-47724, Santa Cruz Biotechnologies, 1:1000), P300 (sc-48343, Santa Cruz Biotechnologies), CAS9 (65832S, Cell Signaling). After exposure to the matching HRP-conjugated secondary antibody, cells were visualized using SuperSignal West Femto Maximum Sensitivity Substrate (34095, Thermo Scientific).

2.5 Transfection and Alt-EJ assay

HFK cells were plated in 3 mL of complete growth medium in a 6 cm plate. Cells were used at 80-90% confluency. 2 μ g of plasmids were diluted in 200 μ L Xfect transfection reagent (631317, Takara). The mixture was incubated at room temperature for 15 min. The transfection mixture was added to each well drop-wise and incubated for 48 hours at 37 °C. Cells were harvested for flow cytometry analysis.

2.6 Statistical Analysis

All values are represented as mean \pm standard error (SE). Statistical differences between groups were measured by using Student's t-test. p-values in all experiments were considered significant at less than 0.05.

3. Results

3.1 8E6 promotes DSB repair by Alt-EJ.

8E6 delays rather than abrogates DSB repair, but it is unclear how these lesions are repaired as 8E6 hinders the completions of HR and NHEJ. Because Alt-EJ serves as a backup DSB repair mechanism should HR and NHEJ fail, we hypothesized that DSBs were instead repaired by Alt-EJ. To test this, we examined previously described telomerase (N/TERT) immortalized human foreskin keratinocyte (HFK) expressing vector control (HFK LXS_N) and 8E6 (HFK 8E6) [8]. An established reporter cassette where a 46 nt insertion disrupts GFP open reading frame was used to measure Alt-EJ [5,6]. Figure 1A describes how this assay is capable of measuring Alt-EJ that requires resection (imbedded) and Alt-EJ that occurs independent of resection (terminal). Transient transfection of this reporter construct into HFK LXS_N and HFK 8E6 demonstrated that 8E6 increased terminal and imbedded Alt-EJ (Fig. 5-1B-E and S1).

To further confirm that 8E6 promoted Alt-EJ, we examined DSB repair in cells where Alt-EJ was blocked by small molecule inhibitor against PARP-1, an established component of the Alt-EJ pathway (1 μ M of Olaparib) [9]. We confirmed that PARP-1 inhibition blocked Alt-EJ using the reporter system described above (Fig. 5-2A-D and S5-2). DSB were induced by growth in media containing zeocin (10 μ g/mL, 10 min), a radiation mimetic reagent [10]. H2AX phosphorylated at Serine 139 or pH2AX is used as standard DSB marker [11]. PARP-1 inhibition did not significantly alter DSB repair in HFK LXS cells (Fig. 5-2E-F). This is consistent with the established view that most DSB repair occurs via either HR or NHEJ, with Alt-EJ serving as a backup should these pathways fail [12–14]. In contrast, PARP-1 inhibition significantly delayed DSB repair in HFK 8E6 cells.

3.2 DNA-PK inhibition forces 8E6 expressing cells to use Alt-EJ more frequently.

NHEJ initiation blocks DSB repair by other pathways, including Alt-EJ [13–15]. 8E6 does not prevent the initiation of NHEJ as autophosphorylated DNA-PKcs foci form readily in HFK 8E6 cells [16]. Instead, 8E6 blocks the completion of NHEJ. Thus, we hypothesized that preventing HFK 8E6 cells from initiating NHEJ would force them to repair DSBs via Alt-EJ. To test this, we determined the frequency of Alt-EJ in HFK LXS and HFK 8E6 cells in the presence of a small molecule inhibitor of DNA-PKcs (1 μ M of NU7441) to block NHEJ initiation. As expected, DNA-PKcs inhibition increased both imbedded and terminal Alt-EJ in HFK LXS cells (Fig. 5-3 and S5-3). However, the increase in HFK LXS cells did not reach the levels of Alt-EJ in mock treated HFK 8E6 cells. DNA-PKcs inhibition resulted in a further significant increased use of Alt-EJ in HFK 8E6 cells. Together these data support the conclusion that 8E6 promotes the use of Alt-EJ and that the use of the pathway is further enhanced if cells are not allowed to initiate NHEJ.

When HFK 8E6 cells are allowed to initiate NHEJ, many of the pDNA-PKcs repair complexes that form persist for over 24 hours [16]. Homologous recombination factors (e.g., RAD51) are then recruited to these unresolved repair foci [17]. However, HR is ultimately unable to repair the lesions and become persistent. We hypothesized that forcing HFK 8E6 cells to use Alt-EJ by preventing initiation of NHEJ would lead to more efficient DSB repair by allowing them to avoid these abortive attempts at DSB repair. NU7441 (1 μ M) was used to block NHEJ initiation and DSBs were detected using pH2AX. DNA-PKcs inhibition increases DSB persistence in HFK LXSJ (Fig. 5-4A-B). In mock treated HFK 8E6 cells, DSBs were also more persistent. Supporting our hypothesis, DNA-PKcs inhibition made DSB repair more efficient in HFK 8E6 cells (Fig. 5-4A-B).

We next determined the extent that DNA-PKcs inhibition in HFK 8E6 cells resulted in increased resolution of RAD51 foci. As we have previously reported, DNA-PKcs increased the persistence of RAD51 in HFK LXSJ (Fig. 5-4C-D). A similar increase in RAD51 persistence was also seen in mock treated HFK 8E6 cells. However, DNA-PKcs inhibition increased the rate of RAD51 resolution in HFK 8E6 (Fig. 5-4C-D). To determine if inhibition of a later step in the NHEJ pathway also increased the efficiency of DSB repair in HFK 8E6 cells, we used a small molecular inhibitor of ligase IV (1 μ M of SCR7) to block a near terminal step in NHEJ. Ligase IV inhibition delayed DSB in both HFK LXSJ and HFK 8E6 cells (Fig. 5-4E-F). Thus, restoration of DSB repair in HFK 8E6 specifically requires inhibition of an early NHEJ step, rather than inhibition of a later step in the pathway.

3.3. DNA-PKcs inhibition prevents 8E6 from causing RAD51 foci to form during G1.

The persistent RAD51 repair complexes that form in HFK 8E6 cells occur during G1 [17]. These observations and the ones described in Figure 4 led us to hypothesize that blocking NHEJ initiation via DNA-PKcs inhibition will prevent 8E6 from causing RAD51 foci to form in G1. To test this, we detected RAD51 foci and cyclin E (G1 marker) after the induction of DSB by zeocin. DNA-PKcs inhibition increased the frequency of HFK LXS in G1 that contained RAD51 foci (Fig. 5-5A-B). Without DNA-PKcs inhibition, 8E6 increased the frequency of cells in G1 that had RAD51 foci. However, DNA-PKcs inhibition prevented 8E6 from promoting the formation of RAD51 repair complexes during G1. As cyclin E is also expressed during early S phase, this examination was repeated using cyclin A as a marker of cell in S/G2. These experiments confirmed our observations using cyclin E to determine cell cycle position, providing further evidence that DNA-PKcs inhibition prevented 8E6 from promoting the formation of RAD51 foci during G1 (Fig. S5-4). We used flow cytometry as a final determinant of cell cycle position, using NUCLEAR-ID Red DNA staining to select cells in G1 based on DNA content and then determined the frequency with which these cells stained for RAD51 (Fig. S5-5). Consistent with our hypothesis, DNA-PKcs inhibition increased the frequency of RAD51 in G1 in HFK LXS and prevented 8E6 from promoting RAD51 in G1 (Fig. 5-5C-D).

3.4 DNA-PKcs inhibition does not promote HR in cells with 8E6

These data above demonstrate that the attenuation of DSB repair by 8E6 can be overcome by inhibiting DNA-PKcs. DNA-PKcs inhibition also increases the resolution of RAD51, suggesting that DNA-PKcs inhibition may prevent 8E6 from attenuating HR. To test this, we

measured HR efficiency using an established HR reporter, described in Figure 6A [3]. In vector control U2OS cells (LXSN), NU7441 increases HR efficiency (Fig. 5-6B-C). This is consistent with the established idea that NHEJ and HR compete for access to DSBs [18–20]. As previously reported, 8E6 decreased HR efficiency [21]. However, DNA-PKcs inhibition did not prevent 8E6 from hindering HR (Fig. 5-6B-C). Consistent with a p300-dependent mechanism (see next section for more details), results in U2OS cells expressing a mutant 8E6 (8E6 Δ 132-136) that does not bind to p300 were similar to vector control (Fig. 5-6B-C).

3.5 8E6 promotes Alt-EJ by destabilizing p300

8E6 delays DSB repair by binding/destabilizing p300, leading us to hypothesize that the residues of 8E6 that facilitate the interaction with p300 were important for the phenotypes described thus far [18,26,29]. To test this, we examined previously described U2OS cells expressing either a vector control (LXSN), wildtype 8E6, or 8E6 Δ 132-136 [18,26]. U2OS cells are routinely used to probe 8E6 biology because 8E6 retains its ability to alter DNA repair in these cells [18,26]. Consistent with the p300-dependent mechanism, 8E6 Δ 132-136 shows similar Alt-EJ frequency with U2OS LXSN (Fig. 5-7A-B).

The deletion of these residues from 8E6 has been shown to prevent some but not all aspects of 8E6 biology. As a result, we examined p300 knockout N/TERT immortalized HFK cells. p300 knockout lead to increases in both terminal and imbedded Alt-EJ (Fig. 5-7C-D). To further confirm p300-dependence, we used a small molecule inhibitor of p300 (1 μ M of CCS1477) to block p300 activity. Consistently, CCS1477 increased both terminal and imbedded Alt-EJ (Fig. 5-7E-F).

3.6 DNA-PKcs inhibition prevents the formation of RAD51 foci in G1 that is caused by loss of p300.

We next confirmed that the ability of 8E6 to allow RAD51 foci to form in G1 was blocked by DNA-PKcs inhibition in U2OS cells (Fig. 5-8A-B). Consistent with a p300-dependent mechanism, RAD51 foci were more likely to occur in G1 when DNA-PKcs was inhibited in U2OS cells expressing vector control (LXSN) and 8E6 Δ 132-136. Further confirming a p300-dependent mechanism of action, HFK without p300 displayed an increased the frequency of RAD51 staining in G1 that could be overcome by DNA-PKcs inhibition (Fig. 5-8C-D). As a final confirmation of the p300-dependence of this phenotype, we treated N/TERT HFKs with 1 μ M of CCS1477 to block p300 activity. Inhibition of p300 alone increased the frequency of RAD51 staining in G1 as did DNA-PKcs inhibition alone (Fig. 5-8E-F). However, RAD51 staining in G1 was not increased by their dual application.

4. Discussion

It has previously been shown that 8E6 attenuates the two most prominent DSB pathways (HR and NHEJ) [16,21]. However, 8E6 delays rather than abrogates DSB repair, leaving the question of how DSBs are repaired in cells expressing 8E6. Here, we show that 8E6 promotes DSB repair via Alt-EJ. Moreover, HFK 8E6 cells can be further induced to repair DSBs via Alt-EJ by the inhibition of an early step during NHEJ (DNA-PKcs) but not a later step in the pathway (Ligase IV). The increased use of Alt-EJ induced by DNA-PKcs inhibition prevented 8E6 from generating previously described DSB repair defects including the formation of RAD51 foci in G1 and delayed DSB repair. We also show that DNA-PKcs inhibition does not cause an increase in HR. Further, we provide mechanistic insight into these phenomena by showing that 8E6

promotes Alt-EJ via p300 degradation and that DNA-PKcs inhibition can prevent RAD51 foci from forming in G1 because of p300 loss.

Many of the findings in this study are consistent with standing hypothesis about both DSB repair and the potential for β -HPV infections to promote NMSCs [22–24]. For example, our data in vector control (LXSN) cells shows that Alt-EJ is increased when NHEJ is inhibited and that DSB repair is not significantly delayed by inhibition of Alt-EJ. This is consistent with the idea that Alt-EJ is primarily used when there are defects in either HR or NHEJ [14,25,26]. Similarly, by showing that 8E6 promotes Alt-EJ, a mutagenic DSB repair pathway, we provide further evidence in support of the hypothesized “hit and run” mechanism by which β -HPV infections may promote cancer development [27–29]. We also provide novel insights relevant to both fields. Namely, we show that p300 restricts DSB repair by Alt-EJ and that at least some of the DSB repair defects caused by p300 loss or 8E6 expression can be overcome by inhibition of DNA-PKcs. Does DNA-PKcs inhibition represent a feasible approach to block the increased mutagenesis that likely accompany some beta HPV infections and that has been linked to their tumorigenic potential? Or on the contrary, does DNA-PKcs inhibition promote more mutations generated by Alt-EJ?

The promotion of Alt-EJ is not limited to HPV8 as a recent report demonstrated that HPV16 E7 also increases the use of the pathway [30]. Further, this work used a sequencing analysis to reveal a mutational signature consistent with increased Alt-EJ occurring in HPV16 positive head and neck squamous cell carcinoma [30,31]. The ability to promote Alt-EJ seems to have evolved at least twice independently in the HPV family (once in HPV16 E7 and once in HPV8 E6)[30]. Why would these viruses both evolve ways to promote Alt-EJ? Perhaps, this can be linked to their ability to impair HR and/or NHEJ [16,21]. Unrepaired DSBs are highly lethal,

thus there would a strong selective pressure for HPV (a non-lytic virus) to find a way to repair DSBs.

Finally, the data presented here raise exciting possibilities. Do HPV8 infections leave Alt-EJ signatures during natural infections? If so, can Alt-EJ signatures be used to provide evidence that β -HPVs cause mutations present in NMSCs? The ability to identify mutations in NMSC caused by past transient beta HPV infections would provide the long-sought after evidence directly linking these viruses with NMSC in the general population.

Acknowledgments

We appreciate KSU-CVM Confocal Core for our immunofluorescence microscopy, Michael Underbrink for providing the TERT-immortalized HFKs, and Jeremy M. Stark for providing plasmids of the alt-EJ reporter assay. This research was supported by the National Institute of General Medical Sciences (NIGMS) of the National Institutes of Health (NIH, P20GM130448); NIH Research Enhancement Award (NCI R15 CA242057 01A1); US department of defense (CMDRP PRCRP CA160224 (NW)); and Johnson Cancer Research Center of Kansas State University.

References

- [1] P. Brianti, E. De Flammis, S.R. Mercuri, Review of HPV-related diseases and cancers, *New Microbiol.* 40 (2017) 80–85.
- [2] D. Hasche, S.E. Vinzón, F. Rösl, Cutaneous Papillomaviruses and Non-melanoma Skin Cancer: Causal Agents or Innocent Bystanders?, *Front Microbiol.* 9 (2018). <https://doi.org/10.3389/fmicb.2018.00874>.
- [3] A.J. Pierce, R.D. Johnson, L.H. Thompson, M. Jasin, XRCC3 promotes homology-directed repair of DNA damage in mammalian cells, *Genes Dev.* 13 (1999) 2633–2638.
- [4] N. Bennardo, A. Cheng, N. Huang, J.M. Stark, Alternative-NHEJ Is a Mechanistically Distinct Pathway of Mammalian Chromosome Break Repair, *PLoS Genet.* 4 (2008). <https://doi.org/10.1371/journal.pgen.1000110>.

- [5] R. Bhargava, M. Sandhu, S. Muk, G. Lee, N. Vaidehi, J.M. Stark, C-NHEJ without indels is robust and requires synergistic function of distinct XLF domains, *Nat Commun.* 9 (2018) 2484. <https://doi.org/10.1038/s41467-018-04867-5>.
- [6] L.J. Tsai, F.W. Lopezcolorado, R. Bhargava, C. Mendez-Dorantes, E. Jahanshir, J.M. Stark, RNF8 has both KU-dependent and independent roles in chromosomal break repair, *Nucleic Acids Research.* 48 (2020) 6032–6052. <https://doi.org/10.1093/nar/gkaa380>.
- [7] R. Bhargava, F.W. Lopezcolorado, L.J. Tsai, J.M. Stark, The canonical non-homologous end joining factor XLF promotes chromosomal deletion rearrangements in human cells, *J. Biol. Chem.* 295 (2020) 125–137. <https://doi.org/10.1074/jbc.RA119.010421>.
- [8] K.M. Bedard, M.P. Underbrink, H.L. Howie, D.A. Galloway, The E6 Oncoproteins from Human Betapapillomaviruses Differentially Activate Telomerase through an E6AP-Dependent Mechanism and Prolong the Lifespan of Primary Keratinocytes, *J Virol.* 82 (2008) 3894–3902. <https://doi.org/10.1128/JVI.01818-07>.
- [9] A. Kötter, K. Cornils, K. Borgmann, J. Dahm-Daphi, C. Petersen, E. Dikomey, W.Y. Mansour, Inhibition of PARP1-dependent end-joining contributes to Olaparib-mediated radiosensitization in tumor cells, *Mol Oncol.* 8 (2014) 1616–1625. <https://doi.org/10.1016/j.molonc.2014.06.008>.
- [10] M. Tsukuda, K. Miyazaki, DNA fragmentation caused by an overdose of Zeocin, *Journal of Bioscience and Bioengineering.* 116 (2013) 644–646. <https://doi.org/10.1016/j.jbiosc.2013.05.004>.
- [11] E.P. Rogakou, D.R. Pilch, A.H. Orr, V.S. Ivanova, W.M. Bonner, DNA Double-stranded Breaks Induce Histone H2AX Phosphorylation on Serine 139, *Journal of Biological Chemistry.* 273 (1998) 5858–5868. <https://doi.org/10.1074/jbc.273.10.5858>.
- [12] G. Iliakis, T. Murmann, A. Soni, Alternative end-joining repair pathways are the ultimate backup for abrogated classical non-homologous end-joining and homologous recombination repair: Implications for the formation of chromosome translocations, *Mutation Research/Genetic Toxicology and Environmental Mutagenesis.* 793 (2015) 166–175. <https://doi.org/10.1016/j.mrgentox.2015.07.001>.
- [13] J. Patterson-Fortin, A.D. D'Andrea, Exploiting the Microhomology-Mediated End-Joining Pathway in Cancer Therapy, *Cancer Res.* 80 (2020) 4593–4600. <https://doi.org/10.1158/0008-5472.CAN-20-1672>.
- [14] D. Simsek, M. Jasin, Alternative end-joining is suppressed by the canonical NHEJ component Xrcc4–ligase IV during chromosomal translocation formation, *Nature Structural & Molecular Biology.* 17 (2010) 410–416. <https://doi.org/10.1038/nsmb.1773>.
- [15] M. Wang, W. Wu, W. Wu, B. Rosidi, L. Zhang, H. Wang, G. Iliakis, PARP-1 and Ku compete for repair of DNA double strand breaks by distinct NHEJ pathways, *Nucleic Acids Res.* 34 (2006) 6170–6182. <https://doi.org/10.1093/nar/gkl840>.
- [16] C. Hu, T. Bugbee, M. Gamez, N.A. Wallace, Beta Human Papillomavirus 8E6 Attenuates Non-Homologous End Joining by Hindering DNA-PKcs Activity, *Cancers.* 12 (2020) 2356. <https://doi.org/10.3390/cancers12092356>.
- [17] C. Hu, T. Bugbee, D. Dacus, R. Palinski, N.A. Wallace, Beta human papillomavirus 8 E6 allows colocalization of non-homologous end joining and homologous recombination repair factors, *PLOS Pathogens.* 18 (2022) e1010275. <https://doi.org/10.1371/journal.ppat.1010275>.
- [18] A. Orthwein, S.M. Noordermeer, M.D. Wilson, S. Landry, R.I. Enchev, A. Sherker, M. Munro, J. Pinder, J. Salsman, G. Dellaire, B. Xia, M. Peter, D. Durocher, A mechanism for

- the suppression of homologous recombination in G1 cells, *Nature*. 528 (2015) 422–426. <https://doi.org/10.1038/nature16142>.
- [19] J.R. Chapman, M.R.G. Taylor, S.J. Boulton, Playing the End Game: DNA Double-Strand Break Repair Pathway Choice, *Molecular Cell*. 47 (2012) 497–510. <https://doi.org/10.1016/j.molcel.2012.07.029>.
- [20] S.F. Bunting, E. Callén, N. Wong, H.-T. Chen, F. Polato, A. Gunn, A. Bothmer, N. Feldhahn, O. Fernandez-Capetillo, L. Cao, X. Xu, C.-X. Deng, T. Finkel, M. Nussenzweig, J.M. Stark, A. Nussenzweig, 53BP1 Inhibits Homologous Recombination in Brca1-Deficient Cells by Blocking Resection of DNA Breaks, *Cell*. 141 (2010) 243–254. <https://doi.org/10.1016/j.cell.2010.03.012>.
- [21] N.A. Wallace, K. Robinson, H.L. Howie, D.A. Galloway, β -HPV 5 and 8 E6 Disrupt Homology Dependent Double Strand Break Repair by Attenuating BRCA1 and BRCA2 Expression and Foci Formation, *PLOS Pathogens*. 11 (2015) e1004687. <https://doi.org/10.1371/journal.ppat.1004687>.
- [22] T. Gheit, Mucosal and Cutaneous Human Papillomavirus Infections and Cancer Biology, *Frontiers in Oncology*. 9 (2019). <https://www.frontiersin.org/article/10.3389/fonc.2019.00355> (accessed February 9, 2022).
- [23] D. Kremsdorf, S. Jablonska, M. Favre, G. Orth, Biochemical characterization of two types of human papillomaviruses associated with epidermodysplasia verruciformis., *J Virol*. 43 (1982) 436–447.
- [24] H. Pfister, Chapter 8: Human Papillomavirus and Skin Cancer, *JNCI Monographs*. 2003 (2003) 52–56. <https://doi.org/10.1093/oxfordjournals.jncimonographs.a003483>.
- [25] L.N. Truong, Y. Li, L.Z. Shi, P.Y.-H. Hwang, J. He, H. Wang, N. Razavian, M.W. Berns, X. Wu, Microhomology-mediated End Joining and Homologous Recombination share the initial end resection step to repair DNA double-strand breaks in mammalian cells, *Proc Natl Acad Sci U S A*. 110 (2013) 7720–7725. <https://doi.org/10.1073/pnas.1213431110>.
- [26] L. Deriano, D.B. Roth, Modernizing the nonhomologous end-joining repertoire: alternative and classical NHEJ share the stage., *Annual Review of Genetics*. 47 (2013) 433–55. <https://doi.org/10.1146/annurev-genet-110711-155540>.
- [27] D. Viariso, K. Müller-Decker, R. Accardi, A. Robitaille, M. Dürst, K. Beer, L. Jansen, C. Flechtenmacher, M. Bozza, R. Harbottle, C. Voegelé, M. Ardin, J. Zavadil, S. Caldeira, L. Gissmann, M. Tommasino, Beta HPV38 oncoproteins act with a hit-and-run mechanism in ultraviolet radiation-induced skin carcinogenesis in mice, *PLoS Pathog*. 14 (2018). <https://doi.org/10.1371/journal.ppat.1006783>.
- [28] S.O. Wendel, N.A. Wallace, Loss of Genome Fidelity: Beta HPVs and the DNA Damage Response, *Frontiers in Microbiology*. 8 (2017). <https://doi.org/10.3389/fmicb.2017.02250>.
- [29] M. Tommasino, HPV and skin carcinogenesis, *Papillomavirus Research*. 7 (2019) 129–131. <https://doi.org/10.1016/j.pvr.2019.04.003>.
- [30] J.E. Leeman, Y. Li, A. Bell, S.S. Hussain, R. Majumdar, X. Rong-Mullins, P. Blecua, R. Damerla, H. Narang, P.T. Ravindran, N.Y. Lee, N. Riaz, S.N. Powell, D.S. Higginson, Human papillomavirus 16 promotes microhomology-mediated end-joining, *Proc Natl Acad Sci USA*. 116 (2019) 21573–21579. <https://doi.org/10.1073/pnas.1906120116>.
- [31] A.N. Weaver, T.S. Cooper, M. Rodriguez, H.Q. Trummell, J.A. Bonner, E.L. Rosenthal, E.S. Yang, DNA double strand break repair defect and sensitivity to poly ADP-ribose polymerase (PARP) inhibition in human papillomavirus 16-positive head and neck squamous cell carcinoma, *Oncotarget*. 6 (2015). <https://doi.org/10.18632/oncotarget.4863>.

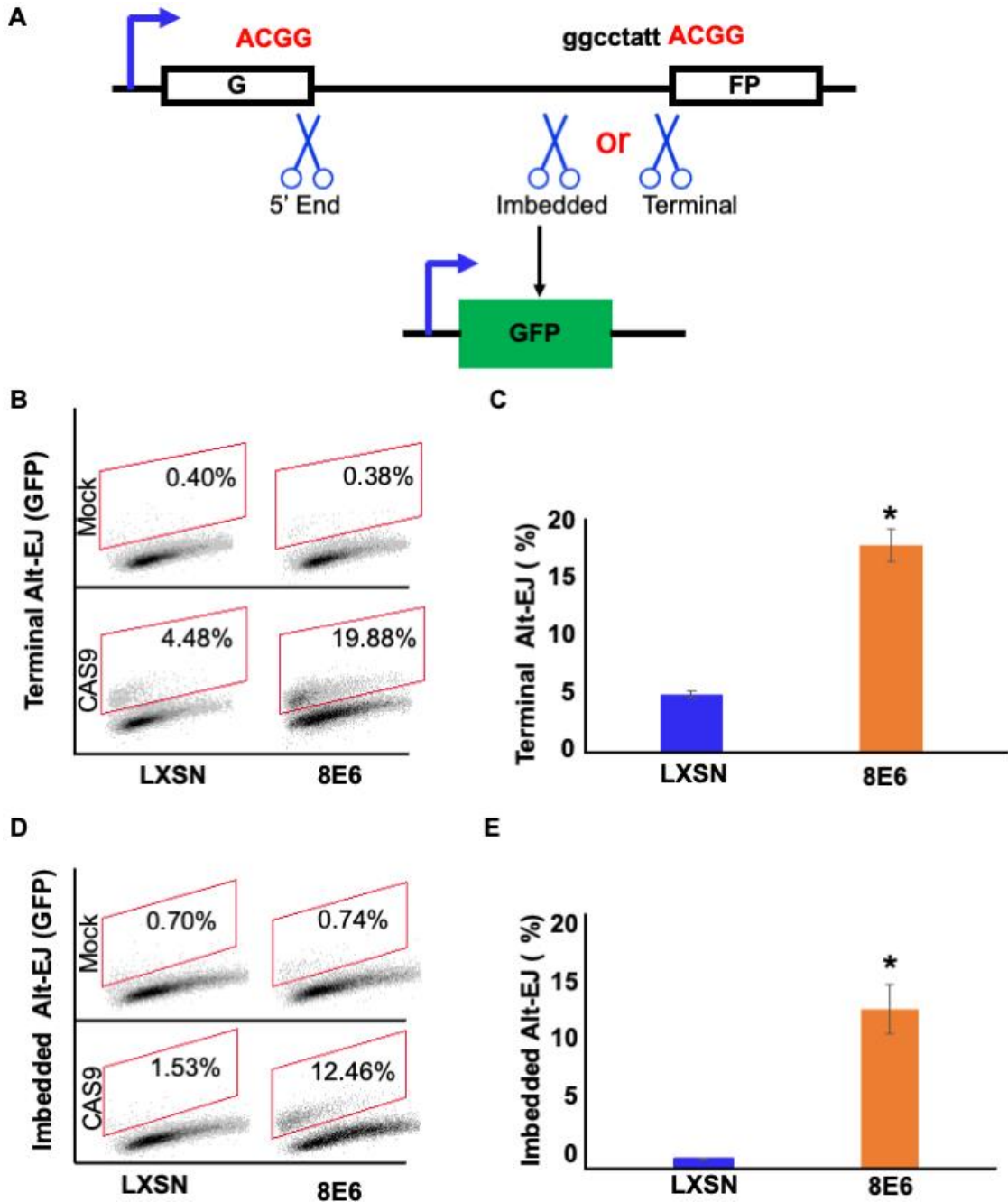


Figure 5-1. 8E6 promotes Alt-EJ frequency.

(A) Schematic of Alt-EJ reporter. GFP is disrupted by a 46 nt insertion. One CAS9 is used to induce an upstream DSB (5' End) and another CAS9 is used to induce a downstream DSB (either Imbedded or Terminal). Following CAS9 expression, a 4 nt microhomology mediated Alt-EJ event can restore GFP expression. (B) Representative images of flow cytometry results of

HFK cells that are GFP positive 24 hours after transfection with Terminal Alt-EJ. The gating represents GFP positive based off mock transfected control. The x-axis shows cells distributed by forward scatter to avoid debris. (C) Percentage of HFK cells that are positive for GFP following transfection with Terminal Alt-EJ determined by flow cytometry. (D) Representative images of flow cytometry results of HFK cells that are GFP positive 24 hours after transfection with Imbedded Alt-EJ. The gating represents GFP positive based off mock transfected control. The x-axis shows cells distributed by forward scatter to avoid debris. (E) Percentage of HFK cells that are positive for GFP following transfection with Imbedded Alt-EJ determined by flow cytometry.

All values are represented as mean \pm standard error. The statistical significance of differences between cell lines were determined using Student's t-test. * indicates significant difference between cell lines ($p < 0.05$). Twenty thousand cells were counted for each of three independent flow cytometry experiments.

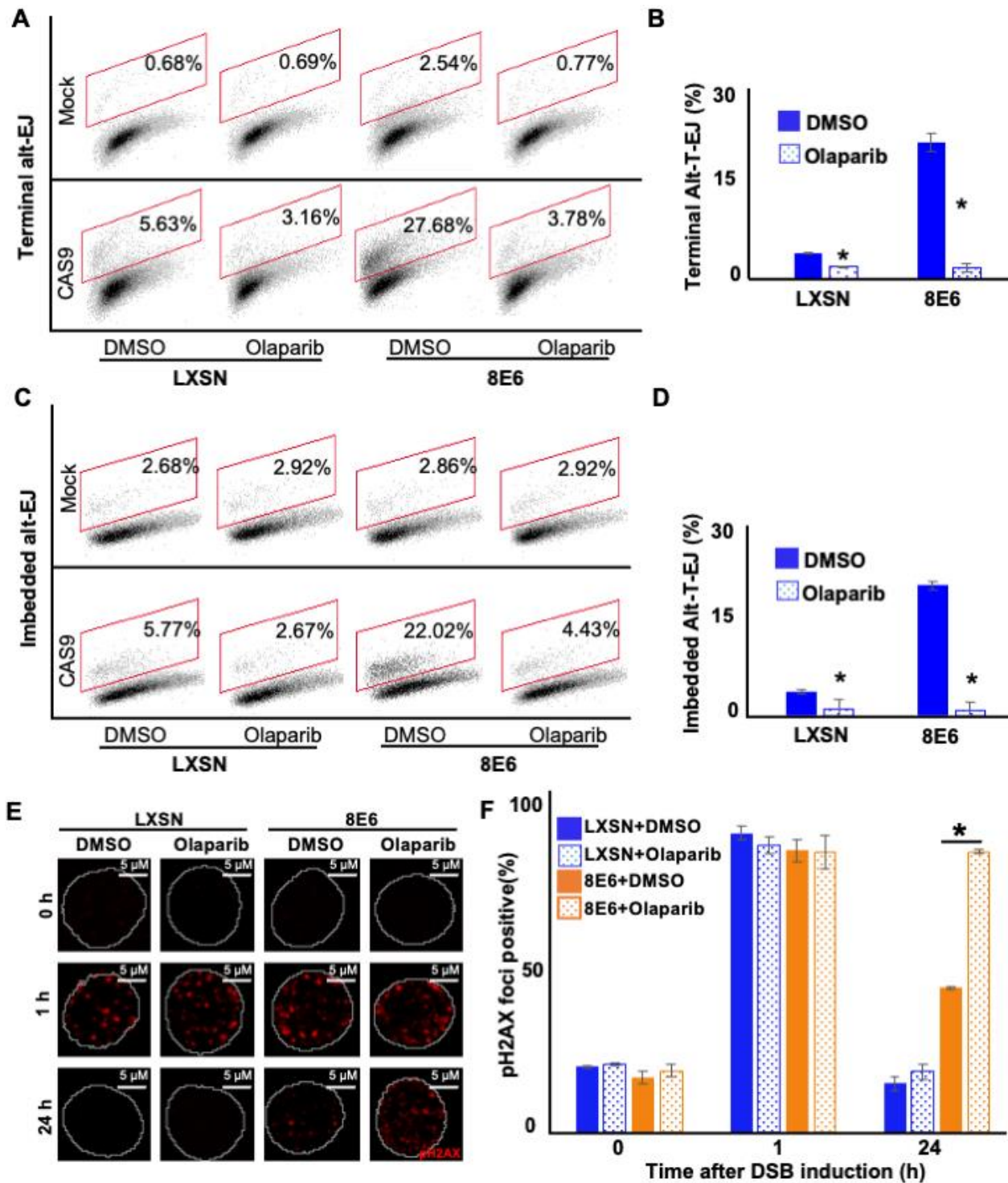


Figure 5-2. Olaparib abrogates Alt-EJ frequency and increases persistent p2AX.

(A) Representative images of flow cytometry results of HFK cells treated with DMSO or olaparib (1 μ M) that are GFP positive 24 hours after transfection with Terminal Alt-EJ. The gating represents GFP positive based off mock transfected control. The x-axis shows cells distributed by forward scatter to avoid debris. (B) Percentage of HFK cells that are positive for

GFP following transfection with Terminal Alt-EJ determined by flow cytometry. (C) Representative images of flow cytometry results of HFK cells treated with DMSO or Olaparib that are GFP positive 24 hours after transfection with Imbedded Alt-EJ. The gating represents GFP positive based off mock transfected control. The x-axis shows cells distributed by forward scatter to avoid debris. (D) Percentage of HFK cells that are positive for GFP following transfection with Imbedded Alt-EJ determined by flow cytometry. (E) Representative images of p^{H2}AX in HFK LXSN and HFK 8E6 treated with DMSO or olaparib (1 μM) following zeocin treatment (10 μg/mL, 10 min). (F) percentage of p^{H2}AX foci positive cells in HFK LXSN and HFK 8E6 treated with DMSO or olaparib following zeocin treatment. All values are represented as mean ± standard error. The statistical significance of differences between treatments were determined using Student's t-test. * indicates significant difference between DMSO and olaparib with same cell line (p < 0.05). Twenty thousand cells were counted for each of three independent flow cytometry experiments.

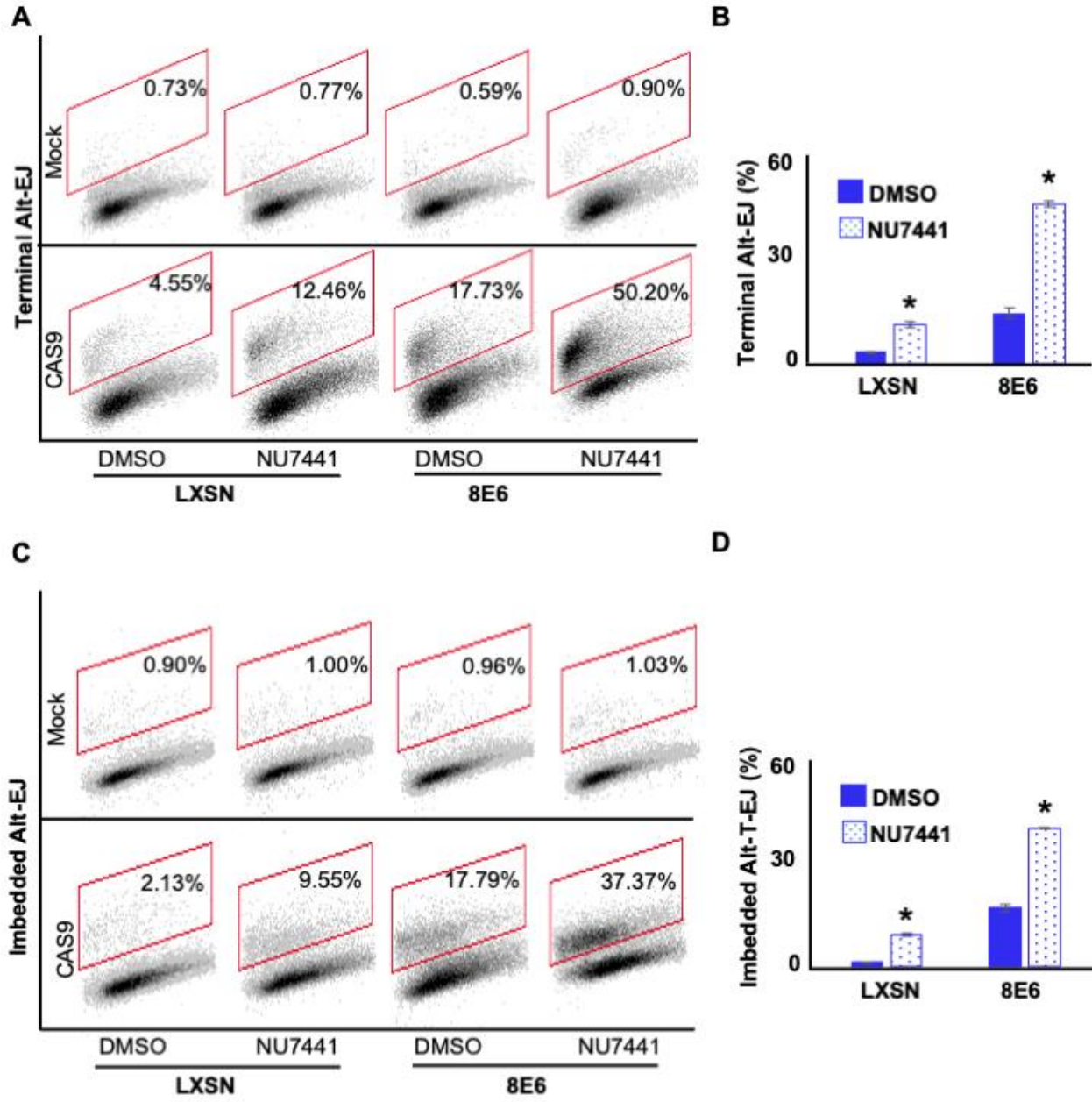


Figure 5-3. NU7441 promotes Alt-EJ.

(A) Representative images of flow cytometry results of HFK cells treated with DMSO or NU7441 (1 μ M) that are GFP positive 24 hours after transfection with Terminal Alt-EJ. The gating represents GFP positive based off mock transfected control. The x-axis shows cells distributed by forward scatter to avoid debris. (B) Percentage of HFK cells that are positive for GFP following transfection with Terminal Alt-EJ determined by flow cytometry. (C) Representative images of flow cytometry results of HFK cells treated with DMSO or NU7441 that are GFP positive 24 hours after transfection with Imbedded Alt-EJ. The gating represents GFP positive based off mock transfected control. The x-axis shows cells distributed by forward scatter to avoid debris. (D) Percentage of HFK cells that are positive for GFP following transfection with Imbedded Alt-EJ determined by flow cytometry. All values are represented as mean \pm standard error. The statistical significance of differences between treatments were determined using Student's t-test. * indicates significant difference between DMSO and NU7441 within the same cell line ($p < 0.05$). Twenty thousand cells were counted for each of three independent flow cytometry experiments.

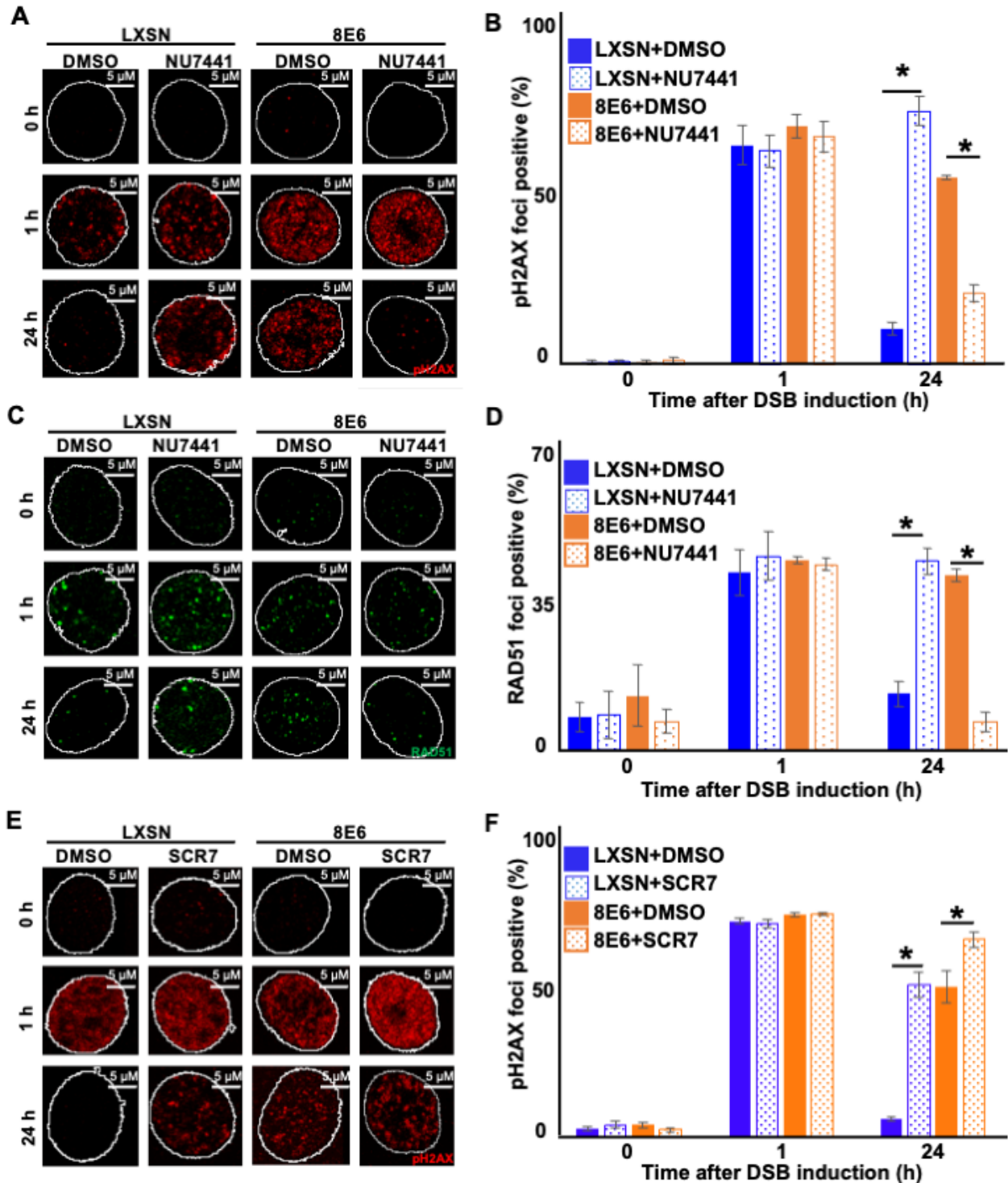


Figure 5-4. Nu7441 increases DSB repair in cells with 8E6.

(A) Representative images of pH2AX in HFK LXSN and HFK 8E6 treated with NU7441 (1 μ M) following zeocin treatment (10 μ g/mL, 10 min). (B) percentage of pH2AX foci positive cells in HFK LXSN and HFK 8E6 treated with NU7441 following zeocin treatment. (C) Representative images of RAD51 in HFK LXSN and HFK 8E6 treated with NU7441 following zeocin treatment. (D) percentage of RAD51 foci positive cells in

HFK LXSN and HFK 8E6 treated with NU7441 following zeocin treatment. (E) Representative images of pH2AX in HFK LXSN and HFK 8E6 treated with SCR7 (1 μ M) following zeocin treatment. (F) percentage of pH2AX foci positive cells in HFK LXSN and HFK 8E6 treated with SCR7 following zeocin treatment. All values are represented as mean \pm standard error. The statistical significance of differences between treatments were determined using Student's t-test. * indicates significant difference between DMSO and inhibitor treated with the same cell line ($p < 0.05$). At least 150 cells were counted over three independent experiments. Nuclei were determined by DAPI staining. The edge of this staining is shown by a white line depicting the nucleus.

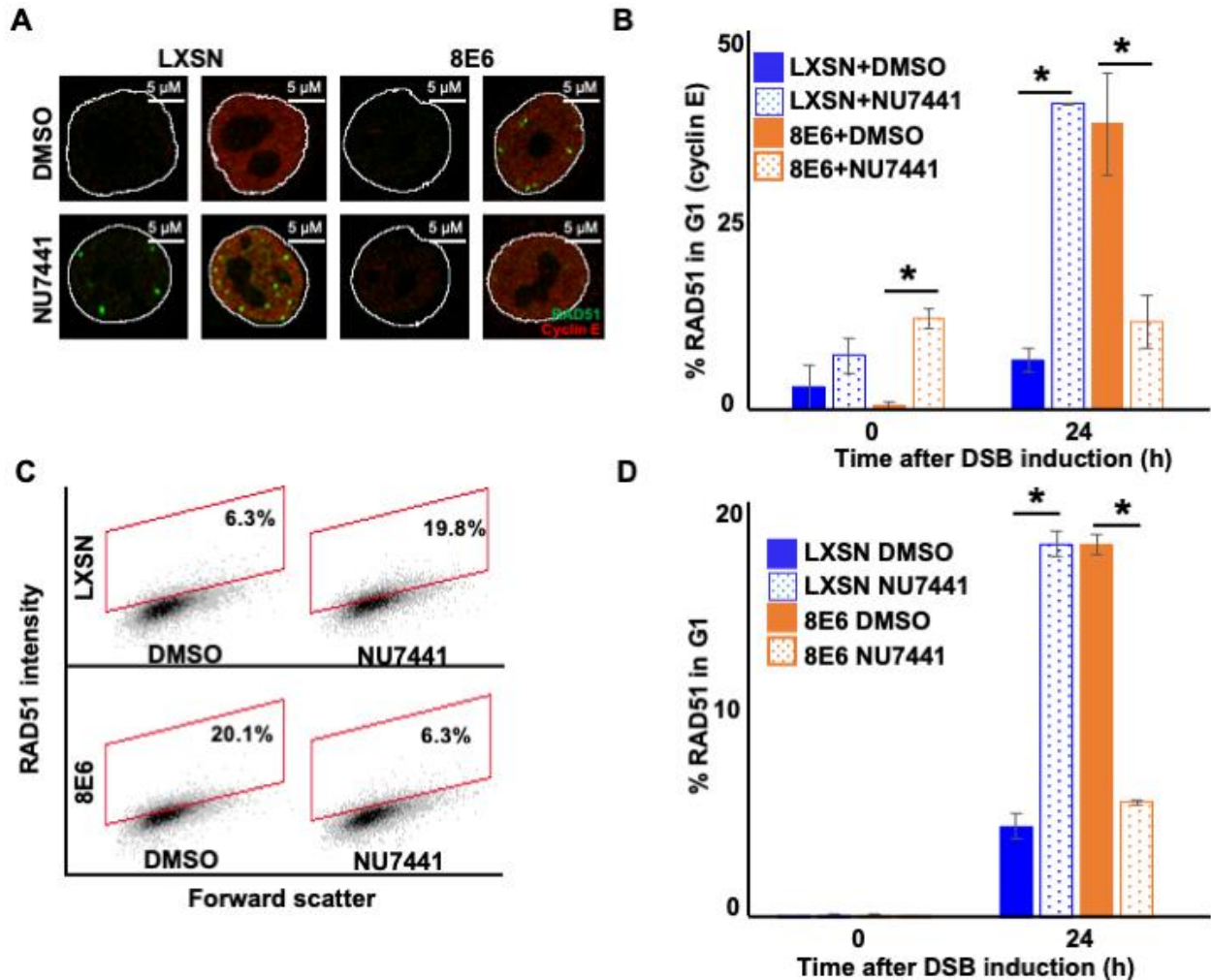


Figure 5-5. NU7441 abrogates RAD51 in G1 induced by 8E6.

(A) Representative cyclin E negative and positive HFK LXSN and HFK 8E6 cells stained for RAD51 (green) and cyclin E (red) treated with DMSO or NU7441 (1 μ M) 24 hours following zeocin treatment (10 μ g/mL, 10 min). (B) Percentage of RAD51 positive HFK cell in G1 determined by cyclin E staining after zeocin treatment. (C) Representative images of flow cytometry results of HFK LXSN and HFK 8E6 cells in G1 stained with RAD51 treated with DMSO or NU7441 24 hours after zeocin treatment. RAD51 intensity is determined by Alexa 488

conjugated secondary antibody and shown on the y-axis. The gating represents RAD51 positive based off secondary only control. The x-axis shows cells distributed by forward scatter to avoid debris. (D) Percentage of HFK cells in G1 that are positive for RAD51 as determined by flow cytometry. Nuclei were determined by DAPI staining. The edge of this staining is shown by a white line depicting the nucleus. All values are represented as mean \pm standard error. The statistical significance of differences between treatments were determined using Student's t-test. * indicates significant difference between DMSO and NU7441 treatment with the same cell line ($p < 0.05$). At least 150 cells were counted over three independent experiments for microscopy. Twenty thousand cells were counted for each of three independent flow cytometry experiments.

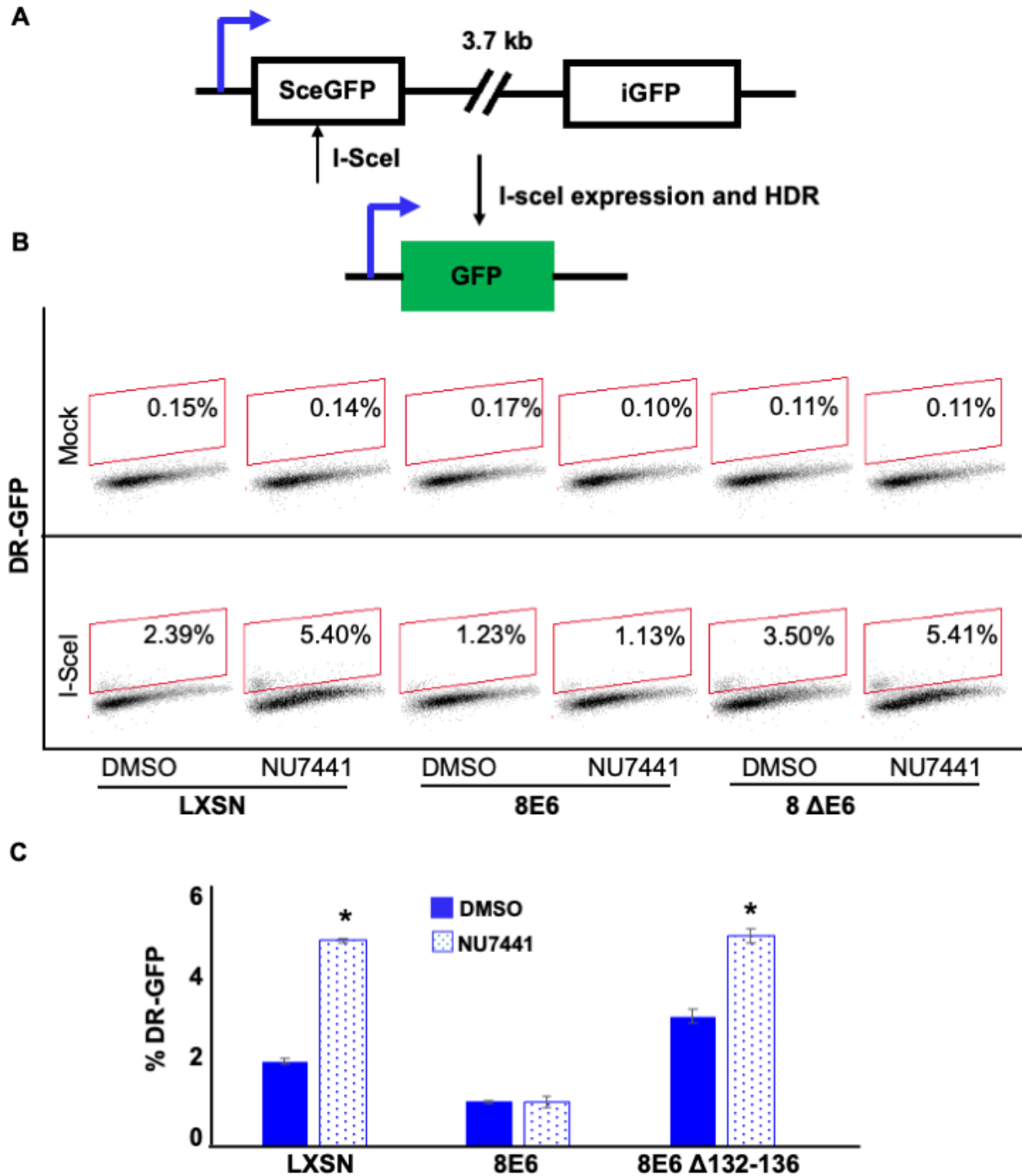


Figure 5-6. NU7441 does not increase HR in cells with 8E6.

(A) Schematic of DR-GFP reporter. GFP open reading frame is disrupted by insertion of ISCE-1 site (SceGFP). Downstream of the reporter is a truncated internal GFP(iGFP) that can be used as a template to remove the ISCE-1 site and restore GFP expression during HR event. (B)

Representative images of flow cytometry results of U2OS cells that are GFP positive treated with

DMSO or NU7441(1 μ M) 24 hours after ISCE-1 transfection. The gating represents GFP positive based off mock transfected control. The x-axis shows cells distributed by forward scatter to avoid debris. (C) Percentage of U2OS cells that are positive for GFP determined by flow cytometry. All values are represented as mean \pm standard error. The statistical significance of differences between treatments were determined using Student's t-test. * indicates significant difference between DMSO and NU7441 with same cell line ($p < 0.05$). Twenty thousand cells were counted for each of three independent flow cytometry experiments.

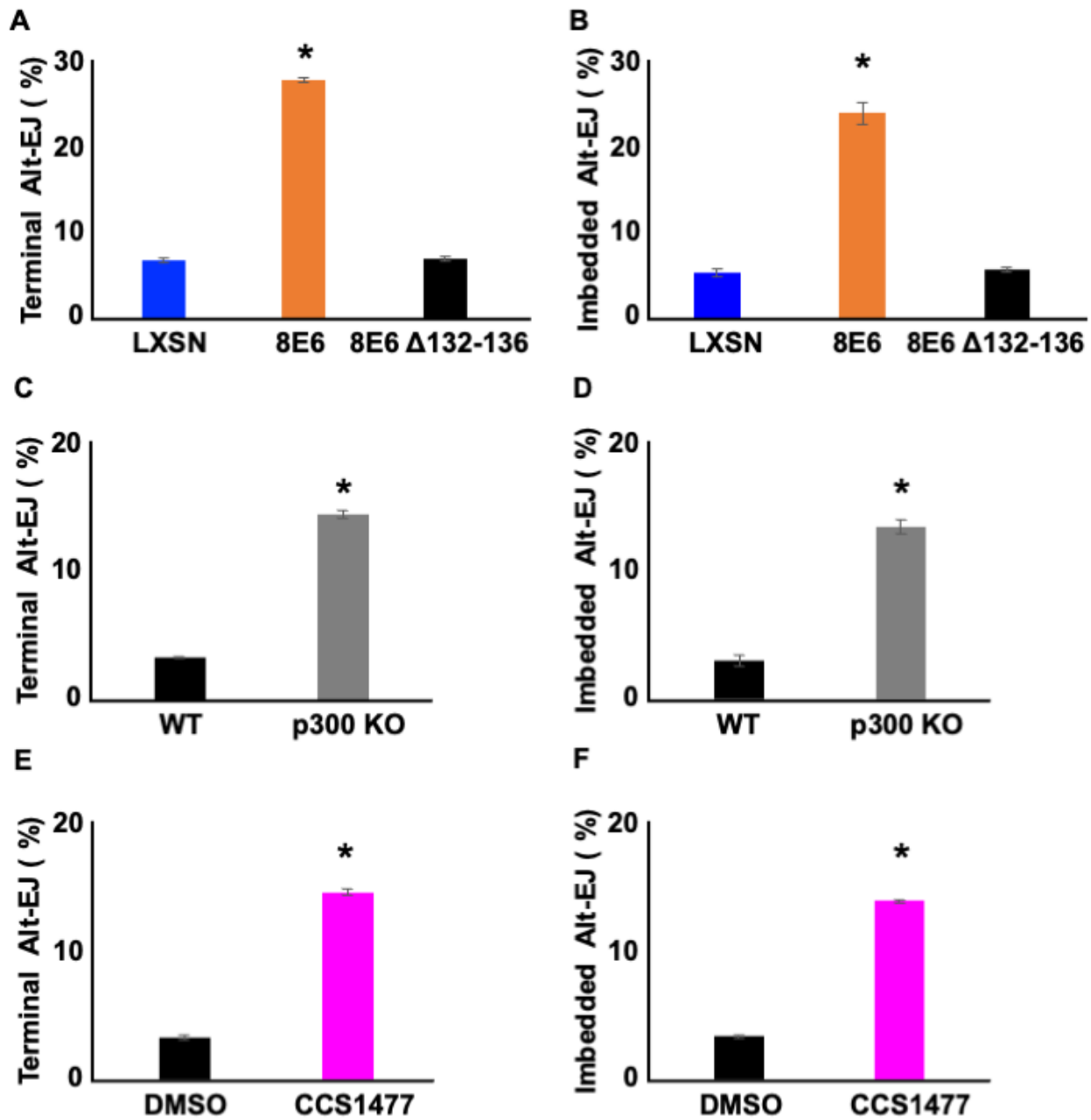


Figure 5-7. Losing p300 activity promotes Alt-EJ frequency.

(A-B) Percentage of U2OS cells that are positive for Alt-EJ following transfection with (A) Terminal or (B) Imbedded determined by flow cytometry. (C-D) Percentage of HFK WT and HFK p300 KO cells that are positive for Alt-EJ following transfection with (C) Terminal or (D) Imbedded determined by flow cytometry. (E-F) Percentage of HFK cells treated with DMSO or CCS1477 (1 μ M) that are positive for Alt-EJ following transfection with (E) Terminal or (F) Imbedded determined by flow cytometry. All values are represented as mean \pm standard error. The statistical significance of differences between cell lines and treatments were determined using Student's t-test. * indicates significant difference between LXSJ and 8E6 (A-B); WT and p300KO (C-D); and DMSO and CCS1477 treatment (E-F) ($p < 0.05$). Twenty thousand cells were counted for each of three independent flow cytometry experiments.

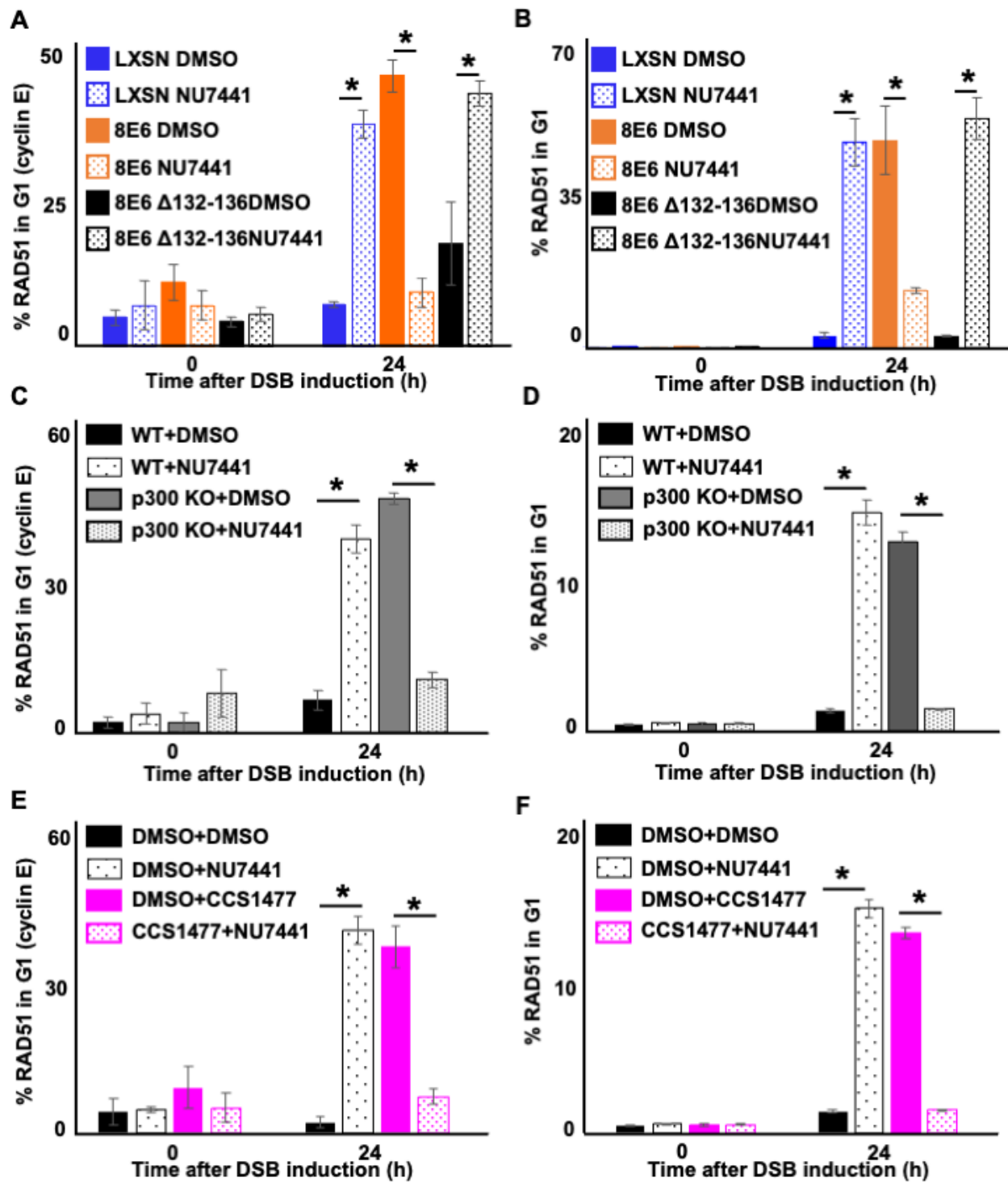


Figure 5-8. NU7441 abrogates RAD51 in G1 induced by losing p300 activity.

(A-B) Percentage of U2OS treated with DMSO or NU7441 (1 μ M) in G1 that RAD51 staining after zeocin treatment (10 μ g/mL, 10 min) as determined by (A) Cyclin E staining or (B) flow cytometry. (C-D) Percentage of HFK cells treated with DMSO or NU7441 in G1 that RAD51 staining after zeocin treatment determined by (C) Cyclin E staining or (D) flow cytometry. (E-F)

Percentage of HFK cells treated with DMSO, CCS1477 (1 μ M), or NU7441 in G1 that RAD51 staining after zeocin treatment determined by (E) Cyclin E staining or (F) flow cytometry. All values are represented as mean \pm standard error. The statistical significance of differences between treatments were determined using Student's t-test. * indicates significant difference between DMSO and NU7441 with same cell line ($p < 0.05$). At least 150 cells were counted over three independent experiments for microscopy. Twenty thousand cells were counted for each of three independent flow cytometry experiments.

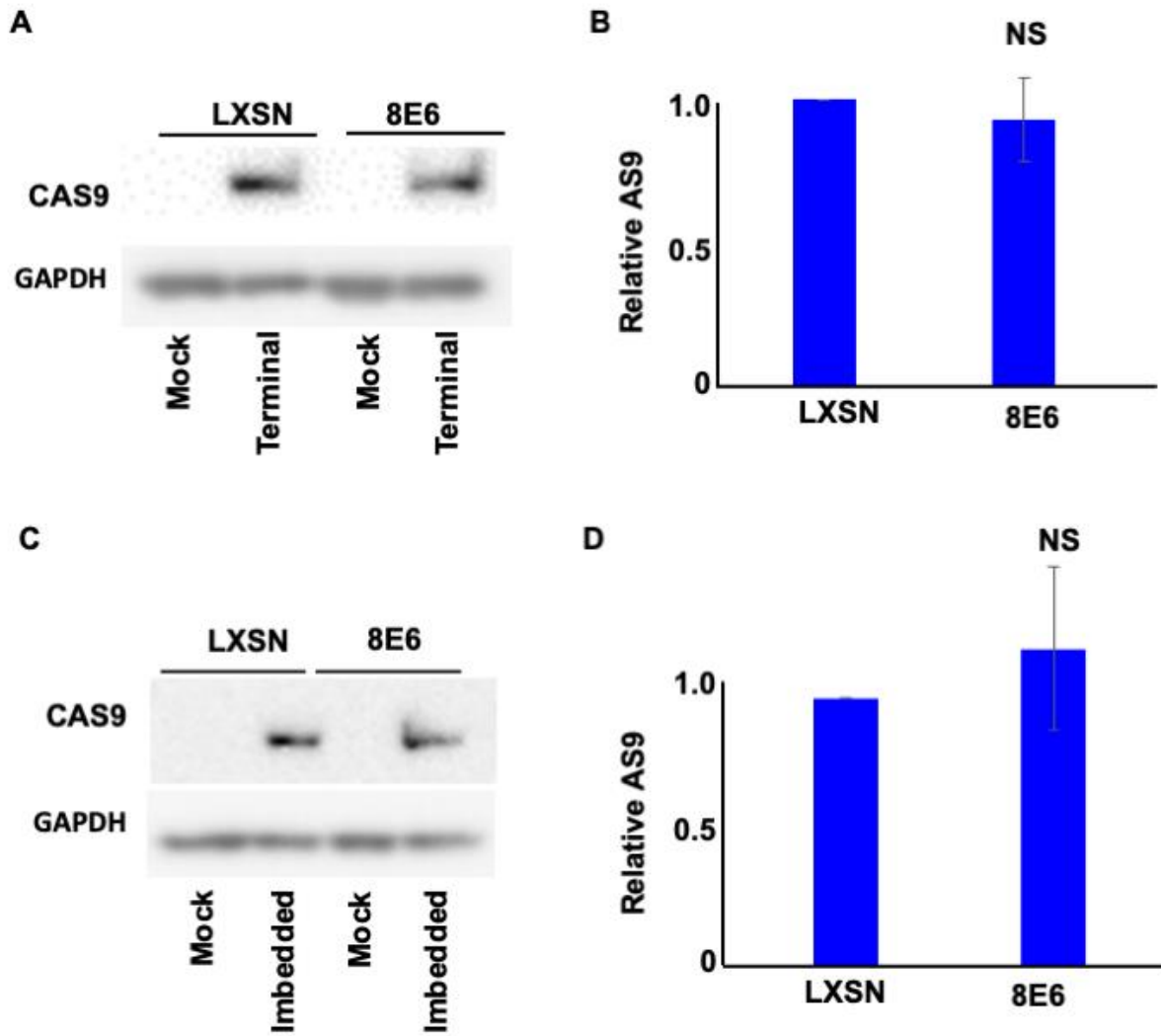


Fig. S5-1. Transfection efficiency represented by CAS9 expression in hTERT HFK. (A) Representative immunoblotting of CAS9 after transfection with Terminal Alt-EJ. GAPDH is used as a loading control. (B) Densitometry of CAS9 level in cells transfected with Terminal Alt-EJ. (C) Representative immunoblotting of CAS9 after transfection with Imbedded Alt-EJ. GAPDH is used as a loading control. (D) Densitometry of CAS9 level in cells transfected with Imbedded Alt-EJ. All values are represented as mean \pm standard error (n=3). The statistical significance of differences between cell lines were determined using Student's t-test. No significant differences were obtained.

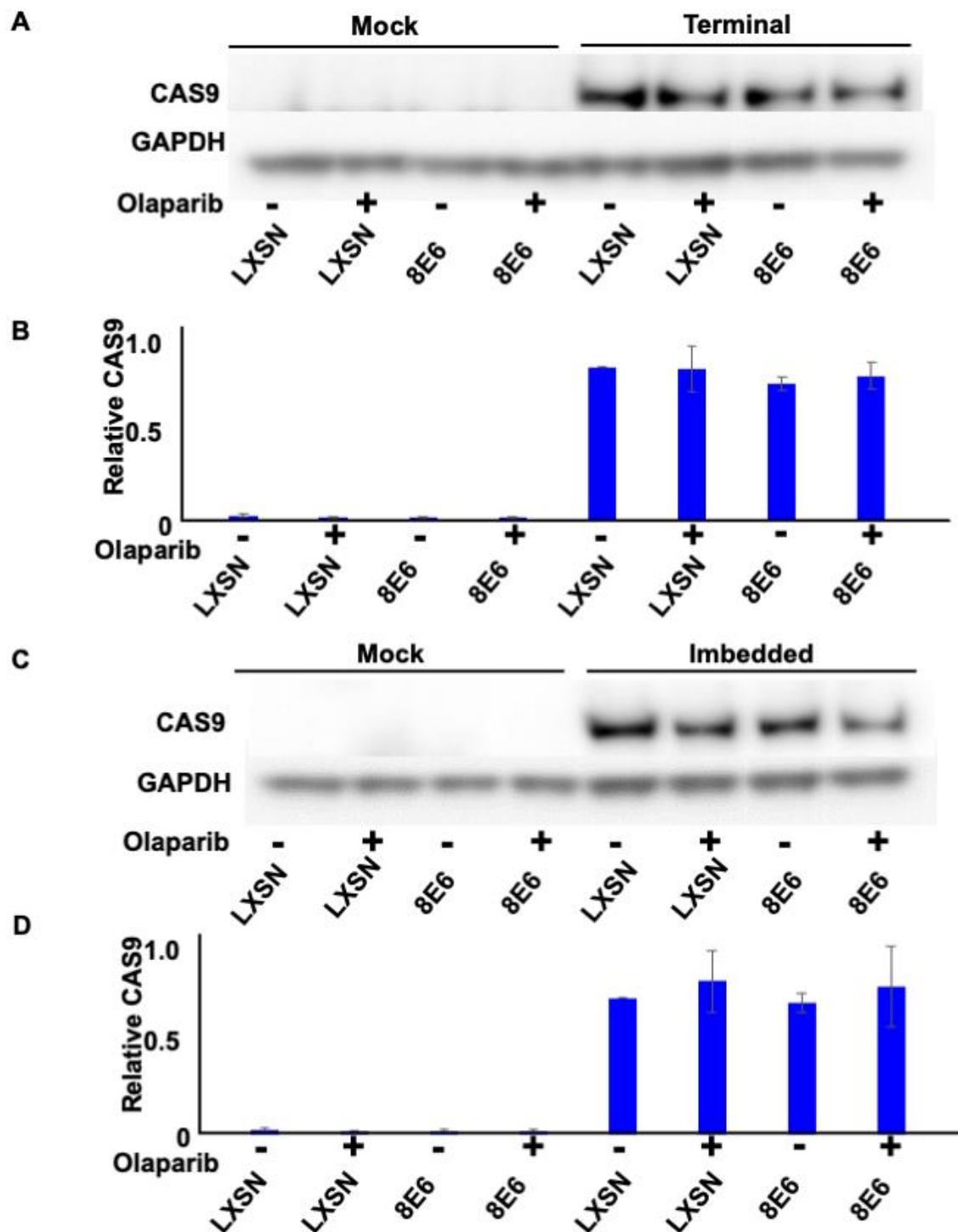


Fig. S5-2. Transfection efficiency represented by CAS9 expression in hTERT HFK. (A) Representative immunoblotting of CAS9 in cells treated with DMSO or olaparib (1 μ M) after transfection with Terminal Alt-EJ. GAPDH is used as a loading control. (B) Densitometry of CAS9 level in cells transfected with Terminal Alt-EJ. (C) Representative immunoblotting of

CAS9 in cells treated with DMSO or olaparib after transfection with Imbedded Alt-EJ. GAPDH is used as a loading control. (D) Densitometry of CAS9 level in cells transfected with Imbedded Alt-EJ. All values are represented as mean \pm standard error (n=3). The statistical significance of differences between cell lines were determined using Student's t-test. No significant differences were obtained.

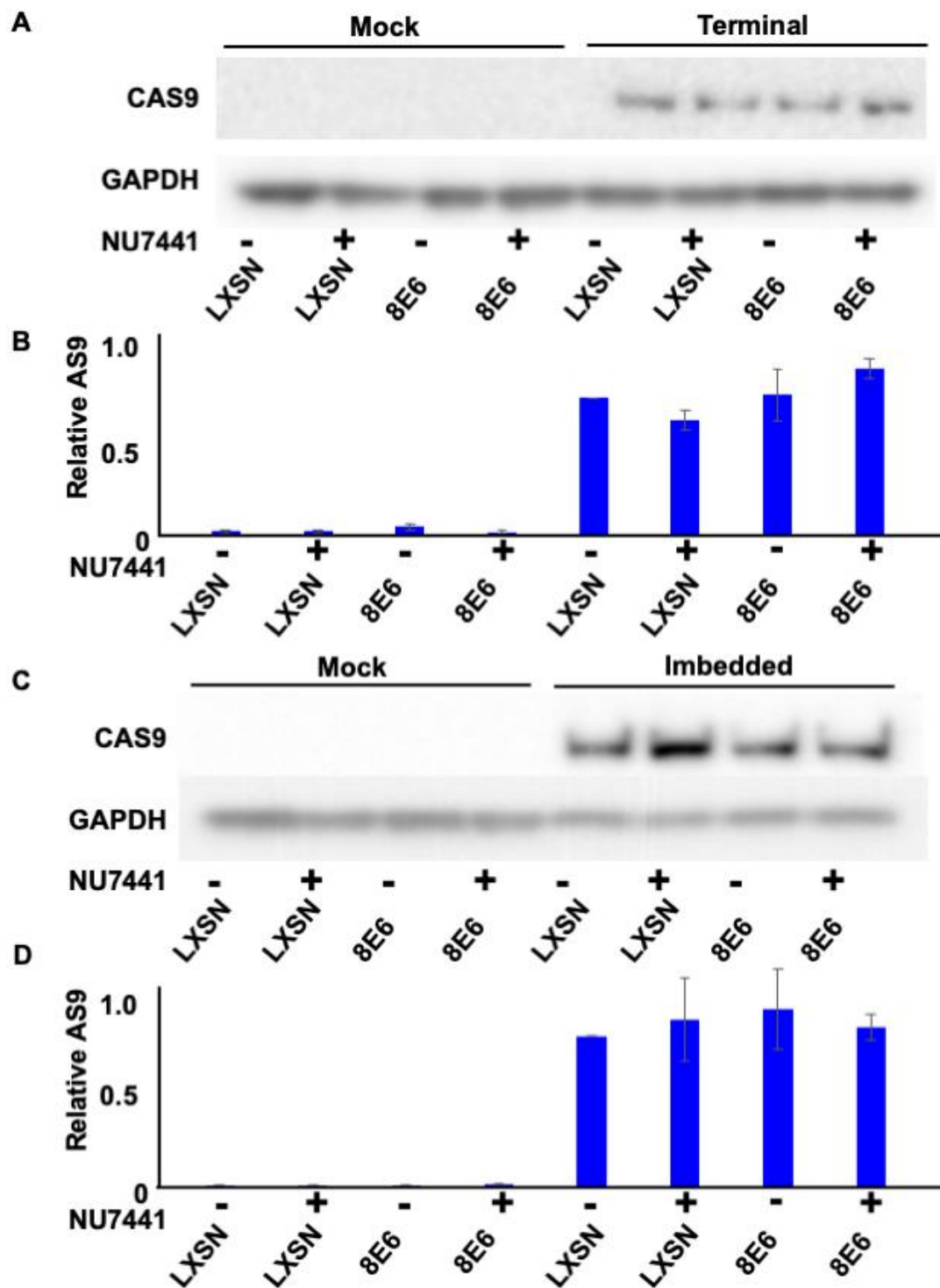


Fig. S5-3. Transfection efficiency represented by CAS9 expression in hTERT HFK. (A) Representative immunoblotting of CAS9 in cells treated with DMSO or NU7441 (1 μ M) after transfection with Terminal Alt-EJ. GAPDH is used as a loading control. (B) Densitometry of

CAS9 level in cells transfected with Terminal Alt-EJ. (C) Representative immunoblotting of CAS9 in cells treated with DMSO or NU7441 (1 μ M) after transfection with Imbedded Alt-EJ. GAPDH is used as a loading control. (D) Densitometry of CAS9 level in cells transfected with Imbedded Alt-EJ. All values are represented as mean \pm standard error (n=3). The statistical significance of differences between cell lines were determined using Student's t-test. No significant differences were obtained.

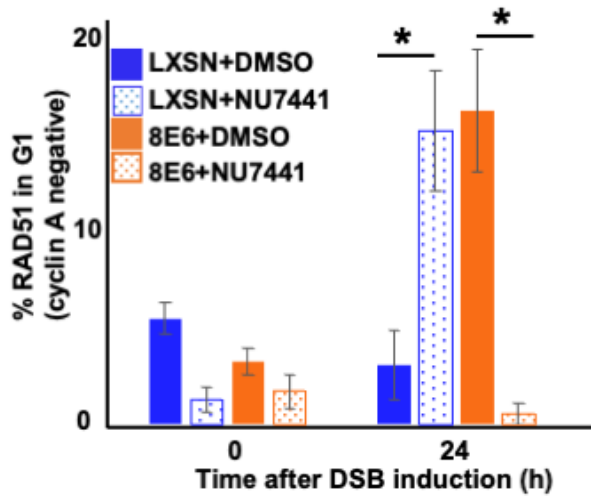


Fig. S5-4. NU7441 abrogates RAD51 in G1 (cyclin A negative) induced by 8E6. Percentage of RAD51 positive HFK cell treated by DMSO or NU7441 (1 μ M) in G1 determined by cyclin A negative after zeocin treatment (10 μ g/mL, 10 min). All values are represented as mean \pm standard error. The statistical significance of differences between treatments were determined using Student's t-test. * indicates significant difference between DMSO and NU7441 treatment with same cell line ($p < 0.05$). At least 150 cells were counted over three independent experiments for microscopy.

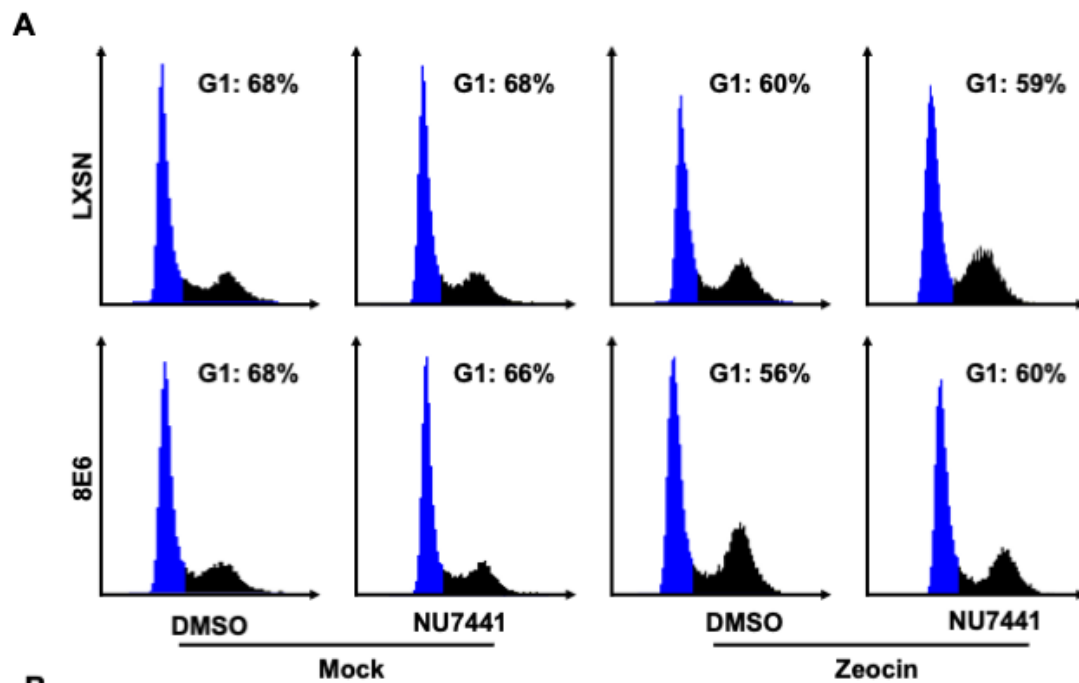


Fig. S5-5. Controls were used to determine RAD51 staining cutoff and G1 gating in HFK cells by flow cytometry. (A) Representative images of cell cycle analysis by flow cytometry following zeocin treatment (10 μ g/mL, 10min). NUCLEAR-ID Red DNA stain was used to determine

DNA content and G1 (blue). (B) Representative images of flow cytometry results of HFK LXSJ and HFK 8E6 cells stained with Alexa 488 conjugated secondary antibody and shown on the y-axis. The gating represents RAD51 positive based off secondary only control. The x-axis shows cells distributed by forward scatter to avoid debris. Twenty thousand cells were counted for each of three flow cytometry experiments.

Chapter 6-Conclusion and future directions

Conclusion

This dissertation supports the hypothesized role of β -HPV infections in NMSC. More broadly, it improves the understanding of cellular mechanisms that protect against genomic instability, a fundamental cause of tumorigenesis. We used standard molecular biological techniques and have developed new techniques to examine the mechanisms by which β -HPV disrupts DNA repair (Chapter 1). The established techniques that were used include primary cell manipulation, next-generation sequencing (NGS), immunofluorescence microscopy (confocal microscopy), transduction with lentivirus, gene knockout with CRISPR-CAS9, gene knockdown with small interfering RNA (siRNA), gel electrophoresis and immunoblotting, DNA repair reporters, flow cytometry, and viability assay with MTT/colony formation. Specifically, we used lentivirus to generate stable primary cell lines expressing HPV E6 protein. We used NGS to identify mutations in cells following DSB repair [33,34]. We used immunofluorescence microscopy (confocal microscopy) to detect the kinetics of the DNA repair complex following DSB induction [35,36]. We used immunoblotting to measure the expression and activation of DNA repair proteins. We used CRISPR-CAS9 to knockout DNA repair gene p300. We used siRNA to knockdown DNA-PKcs. We used GFP-based DSB repair reporters to measure the efficiency of major DSB repair pathways. We used flow cytometry to identify DNA repair factors in different cell cycle stages. Finally, we used MTT and colony formation assays to examine cell viability when treated with small molecule inhibitors. We also developed methods to characterize DNA repair kinetics using confocal microscopy [36]. Moreover, we developed another assay to identify mutations associated with DNA repair at a user-defined genomic locus, which can be widely adapted to studies with transfectable cell lines (Chapter 3) [34].

We hypothesized that 8E6 increases NHEJ because it is known to compete with HR to repair DSBs. However, using immunofluorescence (IF) microscopy we observed that 8E6 slows NHEJ instead of increasing it [37]. Further, 8E6 acts by attenuating DNA-dependent protein kinase (DNA-PK) activity, a critical NHEJ kinase (Chapter 2). This includes reduced DNA-PKcs phosphorylation and the phosphorylation of DNA-PKcs targets. As a result, DNA-PKcs repair complex does not resolve. NHEJ reporter assay confirmed that 8E6 decreases NHEJ.

Because 8E6 impairs two major DSB repair pathways, we hypothesize that 8E6 increases mutations following DSB repair. Further, HR and NHEJ are not thought to occur in the same cell at the same time (Chapter 4). HR is restricted to cells in S/G2 phase when homologous templates are available, while NHEJ occurs primarily during G1. With IF microscopy, we found that 8E6 causes colocalization of HR factors with an NHEJ factor at persistent DSBs. With flow cytometry and IF microscopy we found that 8E6 also causes HR to initiate during G1. The initiation of NHEJ and HR at the same lesion could lead to antagonistic DNA end processing. Further, HR cannot be readily completed in an error-free manner during G1. Both aberrant repair events would cause deletions. With next-generation sequencing of the 200kb surrounding a CAS9-induced DSB, we found that 8E6 caused a 21-fold increase in deletions. Chemical inhibitors of DNA repair provided mechanistic insight by mimicking 8E6-induced dysregulation of DNA repair in a virus-free system. Specifically, inhibition of NHEJ causes RAD51 foci to form in G1 and colocalization of RAD51 with pDNA-PKcs.

DSB repair is delayed but not eliminated by 8E6. We hypothesize that a backup DSB repair pathway, alternative end-joining (Alt-EJ), is used to repair DSBs in cells with 8E6. Also, DSBs are the most deleterious lesions to the cells. In normal cells, a single unrepaired DSB can lead to cell cycle arrest. This conflicts with the β -HPV life cycle that relies on the proliferation of

cells. With flow cytometry, IF microscopy, and GFP-based reporters, we found that 8E6 promotes both DNA resection-dependent and independent Alt-EJ (Chapter 5). Alt-EJ involves microhomology bridging and deletion. Thus, Alt-EJ is a survival strategy but increases mutations. Potential Alt-EJ mutational signatures in cells with β -HPV 8E6 are examined using whole-genome sequencing and computational analysis. These results provide a potential target for the development of cancer treatment.

The most significant contribution of this dissertation to this field is that it characterized how beta-HPV disrupts the repair of the most dangerous DNA damages. Although beta-HPVs have been hypothesized to promote NMSC formation by disrupting DNA repair pathways, how DSB repair occurs in cells with beta-HPV was not clear. This study, for the first time showed that beta-HPV8 E6 impairs a prevalent DSB repair pathway, NHEJ (Chapter 2). More importantly, with cutting edge techniques, this dissertation shows that beta-HPV8 E6 allows two incompatible DSB repair pathways to initiate at the same break site and increases multiple type of mutations (Chapter 3 and 4). Additionally, unpublished data shows that HPV8 E6 promotes an intrinsically mutagenic DSB repair pathway, which fills the knowledge gap how DSB is repaired in cells with beta-HPV E6 (Chapter 5). These results above provide robust evidence supporting the long-established proposal that beta-HPV promotes cancer formation.

Future directions

Although this dissertation shows that β -HPV 8E6 disrupts major DSB repair pathways by decreasing p300 protein, it is unclear how p300 is involved in NHEJ pathway at a molecular level. A previous study showed that p300 plays a role in the recruitment of Ku, an upstream NHEJ protein and subunit of DNA-PK protein [38]. We attempted to detect Ku protein using IF

microscopy but unfortunately, we are not able to detect the repair complex by probing Ku. One possible reason is that Ku is a constitutive gene with pan-nuclear expression [39]. Regardless of the technique hurdle, we did not find a significant difference of the repair complex formation in pDNA-PKcs between control cells and 8E6 expressing cells right after DSB induction.

Our computational analysis based on the cBioportal database showed that p300 is highly associated with cell cycle related gene expression. Since NHEJ and HR are greatly regulated by cell cycle, attenuated NHEJ in cells without p300 could be an outcome of erroneous initiation of HR pathway in G1 phase (Chapter 4). Although our data show that HR initiation is induced by stalled NHEJ, we cannot rule out the possibility that initiation of HR in G1 attenuates NHEJ. To confirmatively test the potential NHEJ/HR pathway switch, live-cell imaging is required to detect repair factors of NHEJ and HR at the same time [40–42]. The challenge to these experiments is labeling DNA repair proteins without altering their function. In addition, labeled NHEJ or HR factors can be added to the cells with transfection, but this could alter NHEJ/HR pathway choice as these two pathways compete with each other by protein abundance and access to DNA binding [43–46].

This dissertation only evaluates the E6 protein of beta-HPV. Whether another putative oncogene beta-HPV E7 affects DSB repair is unclear. Further, it is unknown if the expression of the whole viral genome leads to the same results induced by 8E6 alone. Future research could evaluate whether HPV8 E1, E2, E4, or/and E7 affect DSB repair. Broadly, this dissertation only evaluates HPV type 8. Whether other beta-HPV types affect DSB repair remains to be studied.

To increase the significance, physiologically relevant experiments should be used to study how beta-HPV affects DSB repair. Organotypic raft is well established to study alpha HPV infection but this model is not used as much to study beta-HPV and DNA repair [47,48]. Rodent

cutaneous papillomavirus such as cutaneous MmuPV can be a good model to test if DSB repair is altered in vivo [49,50]. Finally, whole genome sequencing could be used to detect potential mutational signatures caused by beta-HPV in human skin samples. These understanding questions can be investigated using the models and approaches reviewed in Chapter 1.

References

- [1] P. Brianti, E. De Flammineis, S.R. Mercuri, Review of HPV-related diseases and cancers, *New Microbiol.* 40 (2017) 80–85.
- [2] P.M. Howley, H.J. Pfister, Beta Genus Papillomaviruses and Skin Cancer, *Virology.* 0 (2015) 290–296. <https://doi.org/10.1016/j.virol.2015.02.004>.
- [3] D. Hasche, S.E. Vinzón, F. Rösl, Cutaneous Papillomaviruses and Non-melanoma Skin Cancer: Causal Agents or Innocent Bystanders?, *Front Microbiol.* 9 (2018). <https://doi.org/10.3389/fmicb.2018.00874>.
- [4] R.L. Winer, T. Gheit, Q. Feng, J.E. Stern, J. Lin, S. Cherno, M. Tommasino, Prevalence and correlates of beta and gamma human papillomavirus detection in oral samples from mid-adult women, *J Infect Dis.* (n.d.). <https://doi.org/10.1093/infdis/jiy632>.
- [5] G.P. Guy, S.R. Machlin, D.U. Ekwueme, K.R. Yabroff, Prevalence and Costs of Skin Cancer Treatment in the U.S., 2002–2006 and 2007–2011, *Am J Prev Med.* 48 (2015) 183–187. <https://doi.org/10.1016/j.amepre.2014.08.036>.
- [6] A. Antonsson, O. Forslund, H. Ekberg, G. Sterner, B.G. Hansson, The Ubiquity and Impressive Genomic Diversity of Human Skin Papillomaviruses Suggest a Commensalic Nature of These Viruses, *J Virol.* 74 (2000) 11636–11641.
- [7] A.J. Kombe Kombe, B. Li, A. Zahid, H.M. Mengist, G.-A. Bounda, Y. Zhou, T. Jin, Epidemiology and Burden of Human Papillomavirus and Related Diseases, Molecular Pathogenesis, and Vaccine Evaluation, *Frontiers in Public Health.* 8 (2021). <https://www.frontiersin.org/article/10.3389/fpubh.2020.552028> (accessed February 11, 2022).
- [8] J.N. Bouwes Bavinck, M. Feltkamp, L. Struijk, J. ter Schegget, Human Papillomavirus Infection and Skin Cancer Risk in Organ Transplant Recipients, *Journal of Investigative Dermatology Symposium Proceedings.* 6 (2001) 207–211. <https://doi.org/10.1046/j.0022-202x.2001.00048.x>.
- [9] D. Bzhalava, L.S.A. Mühr, C. Lagheden, J. Ekström, O. Forslund, J. Dillner, E. Hultin, Deep sequencing extends the diversity of human papillomaviruses in human skin, *Sci Rep.* 4 (2014) 5807. <https://doi.org/10.1038/srep05807>.
- [10] V. Dell’Oste, B. Azzimonti, M. De Andrea, M. Mondini, E. Zavattaro, G. Leigheb, S.J. Weissenborn, H. Pfister, K.M. Michael, T. Waterboer, M. Pawlita, A. Amantea, S. Landolfo, M. Gariglio, High β -HPV DNA Loads and Strong Seroreactivity Are Present in Epidermodysplasia Verruciformis, *Journal of Investigative Dermatology.* 129 (2009) 1026–1034. <https://doi.org/10.1038/jid.2008.317>.

- [11] J.M. Huibregtse, S.L. Beaudenon, Mechanism of HPV E6 proteins in cellular transformation, *Seminars in Cancer Biology*. 7 (1996) 317–326. <https://doi.org/10.1006/scbi.1996.0041>.
- [12] J.D. Strickley, J.L. Messerschmidt, M.E. Awad, T. Li, T. Hasegawa, D.T. Ha, H.W. Nabeta, P.A. Bevins, K.H. Ngo, M.M. Asgari, R.M. Nazarian, V.A. Neel, A.B. Jenson, J. Joh, S. Demehri, Immunity to commensal papillomaviruses protects against skin cancer, *Nature*. 575 (2019) 519–522. <https://doi.org/10.1038/s41586-019-1719-9>.
- [13] S.O. Wendel, N.A. Wallace, Loss of Genome Fidelity: Beta HPVs and the DNA Damage Response, *Frontiers in Microbiology*. 8 (2017). <https://doi.org/10.3389/fmicb.2017.02250>.
- [14] M. Hufbauer, B. Akgül, Molecular Mechanisms of Human Papillomavirus Induced Skin Carcinogenesis, *Viruses*. 9 (2017) E187. <https://doi.org/10.3390/v9070187>.
- [15] M. Hufbauer, J. Cooke, G.T.J. van der Horst, H. Pfister, A. Storey, B. Akgül, Human papillomavirus mediated inhibition of DNA damage sensing and repair drives skin carcinogenesis, *Mol Cancer*. 14 (2015). <https://doi.org/10.1186/s12943-015-0453-7>.
- [16] A. Köhler, T. Forschner, T. Meyer, C. Ulrich, M. Gottschling, E. Stockfleth, I. Nindl, Multifocal distribution of cutaneous human papillomavirus types in hairs from different skin areas, *Br J Dermatol*. 156 (2007) 1078–1080. <https://doi.org/10.1111/j.1365-2133.2007.07809.x>.
- [17] P.F. Lambert, K. Münger, F. Rösl, D. Hasche, M. Tommasino, Beta human papillomaviruses and skin cancer, *Nature*. 588 (2020) E20–E21. <https://doi.org/10.1038/s41586-020-3023-0>.
- [18] A. Müller-Schiffmann, J. Beckmann, G. Steger, The E6 Protein of the Cutaneous Human Papillomavirus Type 8 Can Stimulate the Viral Early and Late Promoters by Distinct Mechanisms, *J Virol*. 80 (2006) 8718–8728. <https://doi.org/10.1128/JVI.00250-06>.
- [19] L. Sicherer, D.E. Rollison, R.P. Amorrrortu, M. Tommasino, Beta Human Papillomavirus and Associated Diseases, *Acta Cytol*. 63 (2019) 100–108. <https://doi.org/10.1159/000492659>.
- [20] N.A. Wallace, K. Robinson, H.L. Howie, D.A. Galloway, HPV 5 and 8 E6 Abrogate ATR Activity Resulting in Increased Persistence of UVB Induced DNA Damage, *PLoS Pathogens*. 8 (2012) e1002807. <https://doi.org/10.1371/journal.ppat.1002807>.
- [21] J.A. Snow, V. Murthy, D. Dacus, C. Hu, N.A. Wallace, β -HPV 8E6 Attenuates ATM and ATR Signaling in Response to UV Damage, *Pathogens*. 8 (2019). <https://doi.org/10.3390/pathogens8040267>.
- [22] M. Gentile, L. Latonen, M. Laiho, Cell cycle arrest and apoptosis provoked by UV radiation-induced DNA damage are transcriptionally highly divergent responses, *Nucleic Acids Res*. 31 (2003) 4779–4790.
- [23] S. Giampieri, A. Storey, Repair of UV-induced thymine dimers is compromised in cells expressing the E6 protein from human papillomaviruses types 5 and 18, *Br J Cancer*. 90 (2004) 2203–2209. <https://doi.org/10.1038/sj.bjc.6601829>.
- [24] H. He, J. Wang, T. Liu, UV-Induced RPA1 Acetylation Promotes Nucleotide Excision Repair, *Cell Reports*. 20 (2017) 2010–2025. <https://doi.org/10.1016/j.celrep.2017.08.016>.
- [25] G. Giglia-Mari, A. Zotter, W. Vermeulen, DNA Damage Response, *Cold Spring Harb Perspect Biol*. 3 (2011). <https://doi.org/10.1101/cshperspect.a000745>.
- [26] S.P. Jackson, Sensing and repairing DNA double-strand breaks, *Carcinogenesis*. 23 (2002) 687–696. <https://doi.org/10.1093/carcin/23.5.687>.

- [27] N. Arnoult, A. Correia, J. Ma, A. Merlo, S. Garcia-Gomez, M. Maric, M. Tognetti, C.W. Benner, S.J. Boulton, A. Saghatelian, J. Karlseder, Regulation of DNA Repair pathway choice in S/G2 by the NHEJ inhibitor CYREN, *Nature*. 549 (2017) 548–552. <https://doi.org/10.1038/nature24023>.
- [28] N. Dimitrova, Y.-C.M. Chen, D.L. Spector, T. de Lange, 53BP1 promotes non-homologous end joining of telomeres by increasing chromatin mobility, *Nature*. 456 (2008) 524–528. <https://doi.org/10.1038/nature07433>.
- [29] N.A. Wallace, K. Robinson, H.L. Howie, D.A. Galloway, β -HPV 5 and 8 E6 Disrupt Homology Dependent Double Strand Break Repair by Attenuating BRCA1 and BRCA2 Expression and Foci Formation, *PLOS Pathogens*. 11 (2015) e1004687. <https://doi.org/10.1371/journal.ppat.1004687>.
- [30] N. Bennardo, A. Cheng, N. Huang, J.M. Stark, Alternative-NHEJ Is a Mechanistically Distinct Pathway of Mammalian Chromosome Break Repair, *PLoS Genet*. 4 (2008). <https://doi.org/10.1371/journal.pgen.1000110>.
- [31] L. Deriano, D.B. Roth, Modernizing the nonhomologous end-joining repertoire: alternative and classical NHEJ share the stage., *Annual Review of Genetics*. 47 (2013) 433–55. <https://doi.org/10.1146/annurev-genet-110711-155540>.
- [32] J. Patterson-Fortin, A.D. D’Andrea, Exploiting the Microhomology-Mediated End-Joining Pathway in Cancer Therapy, *Cancer Res*. 80 (2020) 4593–4600. <https://doi.org/10.1158/0008-5472.CAN-20-1672>.
- [33] C. Hu, T. Bugbee, D. Dacus, R. Palinski, N.A. Wallace, Beta human papillomavirus 8 E6 allows colocalization of non-homologous end joining and homologous recombination repair factors, *PLOS Pathogens*. 18 (2022) e1010275. <https://doi.org/10.1371/journal.ppat.1010275>.
- [34] C. Hu, T. Doerksen, T. Bugbee, N.A. Wallace, R. Palinski, Using Next Generation Sequencing to Identify Mutations Associated with Repair of a CAS9-induced Double Strand Break Near the CD4 Promoter, *JoVE (Journal of Visualized Experiments)*. (2022) e62583. <https://doi.org/10.3791/62583>.
- [35] C. Hu, T. Bugbee, M. Gamez, N.A. Wallace, Beta Human Papillomavirus 8E6 Attenuates Non-Homologous End Joining by Hindering DNA-PKcs Activity, *Cancers*. 12 (2020) 2356. <https://doi.org/10.3390/cancers12092356>.
- [36] V. Murthy, D. Dacus, M. Gamez, C. Hu, S.O. Wendel, J. Snow, A. Kahn, S.H. Walterhouse, N.A. Wallace, Characterizing DNA Repair Processes at Transient and Long-lasting Double-strand DNA Breaks by Immunofluorescence Microscopy, *JoVE (Journal of Visualized Experiments)*. (2018) e57653. <https://doi.org/10.3791/57653>.
- [37] R. Bhargava, F.W. Lopezcolorado, L.J. Tsai, J.M. Stark, The canonical non-homologous end joining factor XLF promotes chromosomal deletion rearrangements in human cells, *J. Biol. Chem*. 295 (2020) 125–137. <https://doi.org/10.1074/jbc.RA119.010421>.
- [38] H. Ogiwara, A. Ui, A. Otsuka, H. Satoh, I. Yokomi, S. Nakajima, A. Yasui, J. Yokota, T. Kohno, Histone acetylation by CBP and p300 at double-strand break sites facilitates SWI/SNF chromatin remodeling and the recruitment of non-homologous end joining factors, *Oncogene*. 30 (2011) 2135–2146. <https://doi.org/10.1038/onc.2010.592>.
- [39] P. Reynolds, J.A. Anderson, J.V. Harper, M.A. Hill, S.W. Botchway, A.W. Parker, P. O’Neill, The dynamics of Ku70/80 and DNA-PKcs at DSBs induced by ionizing radiation is dependent on the complexity of damage, *Nucleic Acids Res*. 40 (2012) 10821–10831. <https://doi.org/10.1093/nar/gks879>.

- [40] K. Karanam, R. Kafri, A. Loewer, G. Lahav, Quantitative live cell imaging reveals a gradual shift between DNA repair mechanisms and a maximal use of HR in mid-S phase, *Mol Cell*. 47 (2012) 320–329. <https://doi.org/10.1016/j.molcel.2012.05.052>.
- [41] O.D. Shahar, E.V.S. Raghu Ram, E. Shimshoni, S. Hareli, E. Meshorer, M. Goldberg, Live imaging of induced and controlled DNA double-strand break formation reveals extremely low repair by homologous recombination in human cells, *Oncogene*. 31 (2012) 3495–3504. <https://doi.org/10.1038/onc.2011.516>.
- [42] A. Sollazzo, B. Brzozowska, L. Cheng, L. Lundholm, H. Scherthan, A. Wojcik, Live Dynamics of 53BP1 Foci Following Simultaneous Induction of Clustered and Dispersed DNA Damage in U2OS Cells, *International Journal of Molecular Sciences*. 19 (2018) 519. <https://doi.org/10.3390/ijms19020519>.
- [43] H.H.Y. Chang, N.R. Pannunzio, N. Adachi, M.R. Lieber, Non-homologous DNA end joining and alternative pathways to double-strand break repair, *Nature Reviews Molecular Cell Biology*. 18 (2017) 495–506. <https://doi.org/10.1038/nrm.2017.48>.
- [44] J.M. Daley, P. Sung, 53BP1, BRCA1, and the Choice between Recombination and End Joining at DNA Double-Strand Breaks, *Molecular and Cellular Biology*. 34 (2014) 1380–1388. <https://doi.org/10.1128/MCB.01639-13>.
- [45] A.J. Davis, L. Chi, S. So, K.-J. Lee, E. Mori, K. Fattah, J. Yang, D.J. Chen, BRCA1 modulates the autophosphorylation status of DNA-PKcs in S phase of the cell cycle, *Nucleic Acids Res*. 42 (2014) 11487–11501. <https://doi.org/10.1093/nar/gku824>.
- [46] L.P. Ferretti, L. Lafranchi, A.A. Sartori, Controlling DNA-end resection: a new task for CDKs, *Front Genet*. 4 (2013). <https://doi.org/10.3389/fgene.2013.00099>.
- [47] D. Anacker, C. Moody, Generation of organotypic raft cultures from primary human keratinocytes, *J Vis Exp*. (2012) 3668. <https://doi.org/10.3791/3668>.
- [48] M.A. Ozbun, N.A. Patterson, Using organotypic (raft) epithelial tissue cultures for the biosynthesis and isolation of infectious human papillomaviruses, *Curr Protoc Microbiol*. 34 (2014) 14B.3.1-14B.3.18. <https://doi.org/10.1002/9780471729259.mc14b03s34>.
- [49] J.M. Meyers, A. Uberoi, M. Grace, P.F. Lambert, K. Munger, Cutaneous HPV8 and MmuPV1 E6 Proteins Target the NOTCH and TGF- β Tumor Suppressors to Inhibit Differentiation and Sustain Keratinocyte Proliferation, *PLOS Pathogens*. 13 (2017) e1006171. <https://doi.org/10.1371/journal.ppat.1006171>.
- [50] D. Viarisio, A. Robitaille, K. Müller-Decker, C. Flechtenmacher, L. Gissmann, M. Tommasino, Cancer susceptibility of beta HPV49 E6 and E7 transgenic mice to 4-nitroquinoline 1-oxide treatment correlates with mutational signatures of tobacco exposure, *Virology*. 538 (2019) 53–60. <https://doi.org/10.1016/j.virol.2019.09.010>.